AD A279545

# HIGH TEMPERATURE SUPERCONDUCTING FILMS AND MULTILAYERS FOR ELECTRONICS

John R. Gavaler and John Talvacchio
Cryoelectronic, Crystal, and Electro-Optical Technology

Final Report for the Period
February 21, 1991 to February 20, 1994

AFOSR Contract No. F49620-91-C-0034
Research Sponsored by the
Air Force Office of Scientific Research
Air Force Systems Command
United States Air Force

April 19, 1994

Approved for public release, distribution unlimited.

Westinghouse STC
1310 Beulah Road
Pittsburgh, Pennsylvania 15235-5098

SECURITY CLASSIFICATION OF THIS PAGE

# REPORT DOCUMENTATION PAGE

Form Approved OMB No. 0704-0188

| | |
|---|---|
| 1a. REPORT SECURITY CLASSIFICATION: Unclassified | 1b. RESTRICTIVE MARKINGS |
| 2a. SECURITY CLASSIFICATION AUTHORITY: Unclassified | 3. DISTRIBUTION/AVAILABILITY OF REPORT: Approved for public release; distribution unlimited |
| 2b. DECLASSIFICATION/DOWNGRADING SCHEDULE: N/A | |
| 4. PERFORMING ORGANIZATION REPORT NUMBER(S): 94-9SL2-SUPER-R1 | 5. MONITORING ORGANIZATION REPORT NUMBER(S): AFOSR-TR- 94 0307 |
| 6a. NAME OF PERFORMING ORGANIZATION: Westinghouse Science & Technology Center; 6b. OFFICE SYMBOL (If applicable): | 7a. NAME OF MONITORING ORGANIZATION: DCASMA Pittsburgh 53111A |
| 6c. ADDRESS (City, State, and ZIP Code): 1310 Beulah Road, Pittsburgh, Pennsylvania 15235-5098 | 7b. ADDRESS (City, State, and ZIP Code): 1626 William S. Moorhead Federal Building, 1000 Liberty Avenue, Pittsburgh, Pennsylvania 15222 |
| 8a. NAME OF FUNDING/SPONSORING ORGANIZATION: Air Force Office of Scientific Research; 8b. OFFICE SYMBOL (If applicable): NE | 9. PROCUREMENT INSTRUMENT IDENTIFICATION NUMBER: F49620-91-C-0034 |
| 8c. ADDRESS (City, State, and ZIP Code): 110 Duncan Ave Ste B115, Bolling AFB DC 20332-0001 | 10. SOURCE OF FUNDING NUMBERS: PROGRAM ELEMENT NO. 61102F; PROJECT NO. 2305; TASK NO. GS; WORK UNIT ACCESSION NO. |

11. TITLE (Include Security Classification)

HIGH TEMPERATURE SUPERCONDUCTING FILMS AND MULTILAYERS FOR ELECTRONICS

12. PERSONAL AUTHOR(S)

Gavaler, J. R. and Talvacchio, J.

| 13a. TYPE OF REPORT | 13b. TIME COVERED | 14. DATE OF REPORT (Year, Month, Day) | 15. PAGE COUNT |
|---|---|---|---|
| Final | FROM 2-21-91 TO 2-20-94 | 1994 April 19 | 223 |

16. SUPPLEMENTARY NOTATION

| 17. COSATI CODES | | | 18. SUBJECT TERMS (Continue on reverse if necessary and identify by block number) |
|---|---|---|---|
| FIELD | GROUP | SUB-GROUP | superconductors, yttrium, barium, copper, oxides, high, critical, temperature, thin films, tunneling, barriers, sputtering |
| | | | |
| | | | |

19. ABSTRACT (Continue on reverse if necessary and identify by block number)

The overall objective of this program was to develop a materials and fundamental device base for high-transition-temperature superconducting (HTS) electronics capable of operating at > 50K. Progress is reported on four tasks which address problems fundamental to the understanding of the superconducting state in HTS films, the application of HTS films in passive microwave circuits, the realization of HTS digital electronics, and the development of new superconducting devices. Large-area epitaxial YBCO films with low rf losses developed under this program and techniques for depositing them on both sides of single-crystal substrates were used in other Westinghouse and government-funded programs to develop HTS channelized filterbanks, delay lines, UHF antenna matching networks, and low-phase-noise resonators. An understanding was achieved of the role of oxygenation during film growth and the effect of film microstructure on rf losses. For HTS digital circuit fabrication, both active devices step-edge and edge-type YBCO Josephson junctions and trilayer BKBO junctions and passive structures were developed, such as crossovers, vias, and contacts. These capabilities were transferred to other Westinghouse and government-funded programs which demonstrated the first HTS SFQ circuits and SQUIDs with integrated ground planes.

| 20. DISTRIBUTION/AVAILABILITY OF ABSTRACT | 21. ABSTRACT SECURITY CLASSIFICATION |
|---|---|
| ☐ UNCLASSIFIED/UNLIMITED ☒ SAME AS RPT. ☐ DTIC USERS | Unclass |
| 22a. NAME OF RESPONSIBLE INDIVIDUAL: Wunstock | 22b. TELEPHONE (Include Area Code): 202-767-4933; 22c. OFFICE SYMBOL: NE |

DD Form 1473, JUN 86 — Previous editions are obsolete. — SECURITY CLASSIFICATION OF THIS PAGE: Unclassified

Qualified requesters may obtain additional copies from the Defense Documentation Center; all others should apply to the Clearinghouse for Federal Scientific and Technical Information.

Reproduction, translation, publication, use and disposal in whole or in part by or for the United States Government is permitted.

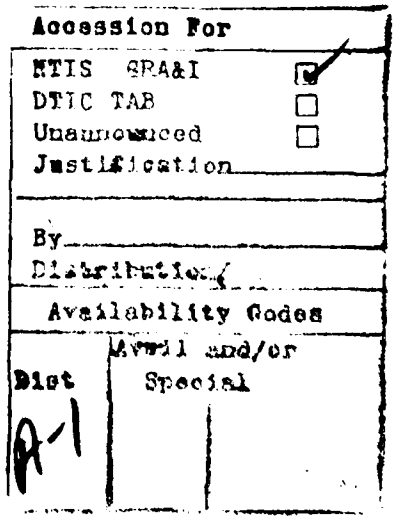

# 1. ANNUAL REPORT: HIGH-TEMPERATURE SUPERCONDUCTING FILMS AND MULTILAYERS FOR ELECTRONICS

February 21, 1991 to February 20, 1994
AFOSR Contract No. F49620-91-C-0034
J. R. Gavaler and J. Talvacchio

## 2. ABSTRACT

The overall objective of this program was to develop a materials and fundamental device base for high-transition-temperature superconducting (HTS) electronics capable of operating at > 50K. Progress is reported on four tasks which address problems fundamental to the understanding of the superconducting state in HTS films, the application of HTS films in passive microwave circuits, the realization of HTS digital electronics, and the development of new superconducting devices. Large-area epitaxial YBCO films with low rf losses developed under this program and techniques for depositing them on both sides of single-crystal substrates were used in other Westinghouse and government-funded programs to develop HTS channelized filterbanks, delay lines, UHF antenna matching networks, and low-phase-noise resonators. An understanding was achieved of the role of oxygenation during film growth and the effect of film microstructure on rf losses. For HTS digital circuit fabrication, both active devices — step-edge and edge-type YBCO Josephson junctions and trilayer BKBO junctions — and passive structures were developed, such as crossovers, vias, and contacts. These capabilities were transferred to other Westinghouse and government-funded programs which demonstrated the first HTS SFQ circuits and SQUIDs with integrated ground planes.

# 3. OBJECTIVES

The objectives of the Westinghouse-AFOSR program were:

1. Search for thin film superconductors with enhanced $T_c$'s and other superconducting properties.
2. Determine the fundamental lower limit of HTS rf surface resistance.
3. Investigate epitaxial multilayers, including Josephson junctions, incorporating deposited insulators and normal conductors with HTS films.
4. Develop materials and processing for alternative HTS devices.

# 4. ACCOMPLISHMENTS

## 4.1 PREAMBLE

The research reported here was performed under a Westinghouse-AFOSR Program which began February 20, 1991. The specific objectives of the program are listed in Section 3 of this report. These objectives are identical to the Tasks of the Work Statement. The overall objective was to investigate the fundamental physics and materials science of superconductors to enhance their properties for application in passive devices based on transmission line structures, active devices based on Josephson junctions, and novel active device structures based on the unique properties of superconductors. In Section 4, an overview is presented of some of the significant accomplishments of this program. More detailed descriptions are available in the published scientific papers that were generated by this program. Copies of these papers are included in the appendices of this report and are listed by title in Section 5. The references in Section 4 refer to this listing.

## 4.2 ENHANCED SUPERCONDUCTING FILM PROPERTIES

The work on this task was focused on two distinct areas. In the first of these, the research was more speculative in that it was motivated by the hoped-for but unproved possibility that there exist even higher-critical-temperature superconductors than those presently known. In the second area the effort was directed toward improving properties of already existing superconducting materials thereby making them more useful in practical device applications.

No enhancements above those presently known were achieved from work done in the search for higher-$T_c$ superconductors. However, work on this task did provide useful data on three of the more important oxide-superconductor systems, namely, $La_{2-x}Sr_xCuO_4$ (LSCO), $Y_1Ba_2Cu_3O_7$ (YBCO), and $Ba_{0.6}K_{0.4}BiO_3$ (BKBO). These data have both theoretical and technological significance.

Considering YBCO first, at the beginning of this program there were still three major unsolved problems associated with the growth of thin films of this compound. These were: (1) the inability to reproducibly grow films with $T_c$'s of >90K, (2) the presence, in many cases, of Cu-O second-phase particles (the so-called "boulders") in the films, and (3) the difficulty in growing films on large-area substrates. As the result of the data obtained in this program, all three of these problems were resolved.[3,4,8,16,19]

It was demonstrated that a degradation of $T_c$ could occur, under otherwise optimum growth conditions, due to a gradual depletion of active oxygen in the sputtering target. It was found that the addition of water vapor to the sputtering gas reversed this process and allowed the deposition of >90K films even when using targets that had hundreds of hours of service. A second cause of degraded $T_c$s in YBCO films was also identified. It was shown that over-doping of YBCO films with oxygen could lower $T_c$ as much as five or six degrees. Therefore, to obtain optimum oxygen content, the temperature, time, and oxygen pressure during annealing needed to be carefully controlled. It was also found that the optimization of the annealing procedure had to be periodically redone as the result of changes in other variables in the growth process including, particularly, the installation of a new sputtering target.

The solution of the boulder problem came from understanding that the source of the boulders was from submicroscopic contamination on the substrate surface. A technique to deflect contaminants from the substrate region during growth by applying a bias voltage to a ring surrounding the substrates was used successfully. Ultimately

the best solution was found to be the maintenance of an ultra-clean environment for the substrates both before and during the deposition process.

To deposit large-area (up to 2" diameter) films a new sputtering system was designed and assembled which did not require bonding the substrate to the holder with silver paste. This procedure had been done here and in other laboratories to achieve the high and uniform substrate temperatures required for the deposition of high quality YBCO films. The silver paste insured good heat conduction between the substrates and holder. In this new system silver paste was unnecessary. Currently large-area films are now routinely being prepared in other research programs which are "boulder-free" and which have excellent superconducting properties.

The phenomenon of oxygen over-doping observed in YBCO films was also found in LSCO films.[15] LSCO films were prepared by off-axis sputtering which had various values of Sr composition, x. The optimum Sr content for superconductivity was determined to be at $x = 0.17$. Films with $x > 0.17$ were found to have the same properties as bulk samples that had been annealed in 100 atm $O_2$. Although the normal-state resistivity decreased as x was increased, $T_c$ also decreased. The resistivity in the a-b plane for films with $x = 0.30$ had the lowest value for normal-state resistivity ever measured for a perovskite material.

An increase in normal-state conductivities with a corresponding decrease in critical temperature, observed in both the YBCO and the LSCO systems is a manifestation of the critical roles played by the chain layers in determining both the normal-state and superconducting properties of oxide superconductors. In a YBCO material that has a relatively low number of oxygen vacancies, i.e. when x is close to zero in the formulation $YBa_2Cu_3O_{7-x}$, it has been suggested that ordering rather than reducing the number of vacancies in the chain layers, may be more important in determining the electrical properties of the material. This possibility is in accord with the phenomenological model of Kresin and Wolf in which it is proposed that the chain

layer is a superconductor due to its proximity to the Cu-O planes. Chains that had interruptions because of vacancies would act as pair breakers.

Regarding the study of BKBO, the interest in this material was due to its having a significantly higher coherence length than the higher-$T_c$ oxides and also because it has a cubic crystal structure, its properties are isotropic. However, similar to the highest-$T_c$ oxide superconductors with anisotropic properties, the necessity for growing epitaxial single crystal films still holds because of the intrinsic weak links that form in oxide films containing high-angle grain boundaries.

Strontium titanate is the only substrate found to date on which single-orientation, epitaxial BKBO films with high $T_c$'s, $J_c$'s, and small x-ray rocking curve widths can be grown, but it is one of the least practical substrate materials due to its poor dielectric properties. By growing $SrTiO_3$(001) buffer layers on $LaAlO_3$ or $NdGaO_3$, single-orientation BKBO(001) films were grown with properties equal to those obtained for films grown directly on $SrTiO_3$ single crystals, $T_c > 26K$ and $\Delta\Omega \approx 0.7°$. (25)

The superconducting phase of $Ba_{1-x}K_xBiO_3$ exists in the range, $0.4 \leq x \leq 0.5$, with the highest $T_c$ occurring for $x \approx 0.4$. The lowest normal-state resistivity (45 μΩ-cm at 30K) and highest resistivity ratio $\rho_{300K}/\rho_{30K} = 1.89$) ever reported for BKBO was found in K-rich films that were prepared for this program.(17)

### 4.3 RF SURFACE RESISTANCE

The research done under this task primarily involved work on YBCO films. This work was directed toward gaining an understanding of the critical factors which degrade rf surface resistance, $R_s$, in YBCO and relatedly in other oxide superconductors. (3,4,8,9,19) Over the course of this program it was found that YBCO films that had optimum $T_c$'s of >90K, could be grown using a wide variety of conditions. However, it was also found that not all of these films had low $R_s$ values.

The effort was therefore focused on identifying the features that caused $R_S$ to be degraded in certain of these films.

Initially all YBCO films that were grown for this program had a large density of second-phase Cu-O particles (the so-called boulders). Later, when boulder-free films were grown it became possible to determine the effect of this defect on $R_S$. Somewhat surprisingly, at 77 K, the presence of boulders had only a marginal effect on surface resistance. For example, in one film in which over 50% of the surface area was covered with boulders, $R_S$ was 0.45 mΩ (at 10 GHz). This compared very favorably to the lowest value measured in boulder-free films at that time of 0.33 mΩ.

It was only at temperatures below 77K where boulders were found to have a significant effect on $R_S$. Considering the two above-mentioned films for illustration, the surface resistance of the boulder-free film was found to decrease continuously with decreasing temperature. At 4.2K, $R_S$ was measured to be 0.060 mΩ. In the case of the film with boulders, $R_S$ remained essentially constant with decreasing temperature down to and including the lowest measurement temperature (4.2K).

Based on data taken on oxygen over-doped films it initially appeared that the excess oxygen content in these films had an extremely deleterious effect on surface resistance. Some over-doped films which had only slightly degraded $T_C$'s of 86-87K were found to have $R_S$ values of >10 mΩ. These films were re-annealed at 450°C under conditions to optimize oxygen content which raised the $T_C$'s to >90K. Despite the significant improvement in $T_C$, however, re-measurement of surface resistances indicated that almost no changes had occurred.

To try to identify the reason for poor surface properties of these films, they and other >90K films that had low $R_S$ values were structurally analyzed. From x-ray diffraction data it was found that all were single phase and had similar lattice parameters. However, it was also found that the films with the higher $R_S$ values tended to have larger rocking curve widths. In addition, measurement of rocking

curve widths of the (309) peaks of YBCO(001) showed that they were clearly split into two peaks, due to a-b twinning, in low-$R_S$ films, but were single peaks with the same overall widths for higher-$R_S$ films.

Based on these data, it can be concluded that very subtle differences in the crystalline quality of YBCO can result in significant difference in rf surface properties. Therefore, variables such as temperature, oxygen pressure, and contamination that greatly influence crystal growth must be carefully controlled during the film deposition process. From results obtained in this program it is clear that even minor fluctuations in these variables, that produce no degradation in $T_c$, can cause greatly degraded rf surface properties.

### 4.4 EPITAXIAL FILMS AND LAYERED STRUCTURES

Thick epitaxial insulating layers are required in the fabrication of a number of devices to permit integration of ground planes and crossovers in active circuits, fabrication of lumped-element capacitors, and implementation of flux transformers. Insulating film requirements were estimated for each of these applications. Epitaxial bilayers and trilayers of YBCO/insulator and YBCO/insulator/YBCO were fabricated with $SrTiO_3$, $LaAlO_3$, and MgO as the insulator.[26] Vertical transport and capacitance measurements were made to obtain values for the resistivity and dielectric constant of the insulator. The highest resistivity was found for $SrTiO_3$ - higher than any value reported in the literature for an epitaxial insulator on an HTS film and sufficiently high for any application. The problem with $SrTiO_3$ is its high real and imaginary dielectric constants which slow and attenuate signals.

A second series of candidate insulating films was evaluated for comparison with $SrTiO_3$. Since $SrTiO_3$ already met requirements for dc resistivity and film morphology, only materials with suitable dielectric constants and loss tangents were considered, including $NdGaO_3$, $CeO_2$, and $Sr_2Al\ TaO_6$ (SAT). Although single crystals could not

be grown due to incongruent melting, a composite sputtering target was purchased to see if SAT could be stabilized in thin-film form. In the cases of $NdGaO_3$ or $CeO_2$, suitable growth conditions were not found for high-resistivity films to grow at a reasonable rate. However, growth conditions were found for deposition of SAT films on YBCO which resulted in smooth films with very high resistivity. Resistivities in the $10^{10}$ Ω-cm range were measured at both room temperature and at 77K.(25) SAT has been reported to have a dielectric constant of 25 and loss tangent of $1 \times 10^{-4}$ so it should be suitable for the many applications where the group velocity in $SrTiO_3$ is too slow or $SrTiO_3$ is too lossy.

A mask set was fabricated which enabled measurements to be made of the properties of epitaxial YBCO and insulator films under the same conditions as when they are incorporated into multilayer HTS circuits. In contrast to the Ar ion milling parameters used in fabricating step-edge grain-boundary or S-N-S Josephson junctions, the edges of each film layer were ion-milled at a shallow angle to avoid the formation of a weak link or a discontinuity in places where the YBCO or insulating film must cover a step. The dc resistivity of the insulator was reduced to from $>10^9$ Ω-cm in planar structures to $10^7$ Ω-cm over a step. This is still adequate for digital circuit applications.(25)

In contrast to $SrTiO_3$ and SAT, conditions could not be found for the growth of smooth $CeO_2$ films on YBCO. However, $CeO_2$ was used successfully as a buffer layer which permitted low-$R_s$ YBCO films to be grown on the R plane (1102) of sapphire. Based on the $R_s$ values of YBCO overlayers, $CeO_2$ buffer layers were superior to any of the other buffer layers for sapphire tested in this program including MgO, La-Sr-Cu-O, $SrTiO_3$, or $LaAlO_3$.

Two of the insulators studied in this program, MgO and $SrTiO_3$, were used to make BKBO junctions. They were selected since they are the two substrate materials which have the closest lattice match to BKBO. The best results for all-BKBO junctions

were obtained with $SrTiO_3$ barriers.[23] The magnitude of the gap voltage indicated that nearly equal contributions were made by the base and counterelectrodes.

## 4.5 MATERIALS AND PROCESSING FOR HTS DEVICES

Several different configurations for YBCO Josephson junctions are under development at Westinghouse.[1,17,23,25,26] One of the configurations investigated during this program is a step-edge S-N-S junction in which a thin YBCO film is made discontinuous by covering a sharp step in the substrate which is high compared to the film thickness. The YBCO banks are then connected by a much thicker normal metal. The yield of these junctions was remarkably high when gold, deposited in situ, was used as the normal metal layer. Modulation of the Josephson current was observed up to 82K.

Two normal-metal alternatives to Au were investigated: Ag-Au alloys and epitaxial layers of over-doped $La_{2-x}Sr_xCuO_4$.[15,18] Films of LSCO with x = 0.3 were developed as part of Task 1 which were not superconducting but which have a lower normal-state resistivity at 40-80K than superconducting LSCO (x = 0.17). A disadvantage of using higher-resistivity normal-metal barriers is that the barrier length must be shorter to maintain the same Josephson current since the normal-metal coherence length is proportional to the inverse square root of the resistivity. In the step-edge junctions, it was not clear whether the length scale of the separation between YBCO banks was approximately the step height or some smaller distance. Since typical step heights were 10 times the LSCO coherence lengths and no Josephson coupling was observed for these junctions, the height of the step was apparently a good approximation for the separation between YBCO banks. Alloys of Ag and Au represented an intermediate resistivity. The resistivity of these junctions were higher than for Au barriers but the junctions were less reproducible. Since reproducibility is a

greater concern than $I_cR_n$ product, Au barriers were used for most junction experiments.

A systematic study was performed on the effects of step heights and step angles on junction characteristics and reproducibility. Steps were made in either $NdGaO_3$ substrates or $SrTiO_3$ insulating films. All steps were made by Ar ion milling using a deposited Nb milling mask. Cross-sectional SEM micrographs were obtained both for uncoated steps and steps covered with a YBCO/Au bilayer. The milling angle was found to be the critical variable affecting junction performance. Using a new 15 cm ion miller with a cold rf discharge operated at 150 eV, step angles were well-controlled and measured to be 10° greater than the milling angles in a range of angles from normal incidence. When samples were not rotated during milling, the range was 0° to 45°. With rotation, the range was 0° to 20°. Outside these ranges, the step profiles were pathological.

The optimum milling angle for junction reproducibility was approximately 15°. Junctions made on such steps had RSJ-like characteristics. Although the junction resistance, $R_n$, was independent of angle, the Josephson critical current, $I_c$, increased as the angle increased. At high angles, $I_c$ and $I_cR_n$ were large but the I-V curves were indicative of flux flow and the other indicators of Josephson coupling, Shapiro steps and SQUID voltage modulation, were less pronounced. The 15° junctions had a spread in critical current of ±30% across a wafer. Much broader distributions were obtained if YBCO films contained CuO precipitates which nucleated preferentially at the step.

A second junction configuration under investigation as part of this program required a-axis-oriented YBCO films in a traditional (with respect to low-$T_c$ superconductors) sandwich structure. The a-axis orientation permits the maximum value of the anisotropic coherence length to determine junction properties. Growth conditions were found for preparing a-axis films by off-axis sputtering. The optimum deposition temperature was 580°C for a-axis films. As discussed in Section 4.1 of this

report, the addition of water vapor into the sputtering gas, was used to maintain high $T_c$. However, water vapor was also found to promote c-axis instead of a-axis growth and therefore was left out of the sputter gas mixture when growing a-axis films.

The $LaAlO_3$(001) wafers used for the growth of a-axis films were cut and polished to ±1° of the [001] direction. The a-axis films which were grown on the particular wafers which were cut to within 0.5° of the [001] direction, grew epitaxially with four in-plane directions for the c-axis, each separated from the next by 90°. A-axis films deposited on $LaAlO_3$ wafers miscut by >0.5°, also grew epitaxially but with a single in-plane direction for the c-axis either parallel to the [100] or [010] direction of the substrate. The preferred direction of these two was the one closer to the gradient of the miscut. Bridges were patterned in several films with a preferred in-plane direction for the c axis. The resistivity measured for currents flowing in the c direction was semiconductor-like (negative temperature coefficient) with a value comparable to measurements made in this direction in YBCO single crystals. The resistivity for currents flowing in a bridge perpendicular to the c-axis on the same sample had the metallic temperature dependence characteristic of current flow in the a-b plane.

Trilayers of YBCO/PrBCO/YBCO were grown under the same conditions used for single-layer a-axis films. The trilayers grew epitaxially with a preferred in-plane direction for the c-axis in each layer. Previous work under this program and in other laboratories either used c-axis films for these trilayers or used a-axis films containing high-angle (90°) grain boundaries arising from the four directions for the c-axis.

The epitaxial insulators developed under Task 3 have dielectric constants which are satisfactory for digital circuits or SQUID sensor circuits but too high for some other applications.[9,25] In the case of multi-chip modules, low dielectric constants, $\varepsilon \approx 6$, are required. In the case of crossovers in analog microwave circuits, the crosstalk between lines due to capacitive coupling is minimized by reducing $\varepsilon$. The lowest dielectric constant obtainable requires the development of air-bridge crossovers. Some efforts

reported by other laboratories used Au air bridges deposited on polyimide supports but the rf surface resistance is too high in Au. In this program, a mask set was fabricated to permit YBCO film layers to cross using air bridges. The design used an epitaxial $SrTiO_3$ insulating layer to support the growth of the top YBCO film. A highly differential wet-chemical etch for $SrTiO_3$ was used to remove the insulator.

Another unique requirement for insulators is presented by HTS multi-chip modules (MCMs). The major fabrication issues for HTS MCMs are deposition of a very thick (1.5-2 μm) low-ε insulator, and patterning of very long, 2 μm-wide, lines in YBCO films grown on top of the thick insulator. Both problems were addressed in this program. The best epitaxial insulator available at present for this application is MgO since it has the lowest dielectric constant. Films of MgO 1.5 μm thick were grown by electron-beam evaporation on suitable substrates for epitaxial growth. Although electron diffraction measurements confirmed that the MgO was epitaxial, x-ray rocking curve widths were much greater than for typical thin insulators (≈0.3 μm). Long and narrow lines, 6 cm × 4 μm wide, were patterned in YBCO films deposited on $LaAlO_3$ substrates with no degradation in film quality.

### 4.6 OTHER ACCOMPLISHMENTS

In support of the work described above, a file of reprints and preprints on high-$T_c$ superconductivity started in 1987 was maintained. The updated list of papers was entered into a computer and keywords were assigned to them to aid in retrieval. The entire database has been made available to the research community through the computer facilities at High-$T_c$ Update. Annual updates to the database have been published in the Journal of Superconductivity.[5] During 1992, the database was transferred to the University of South Carolina where it will be updated in the future.

The year 1992 marked the completion of a three-year, $4M upgrade of facilities, funded by Westinghouse, which are dedicated to superconducting electronics. This

program had the benefit of new equipment for the deposition, patterning, and characterization of superconducting films and circuits. The number of vacuum deposition systems dedicated to HTS film structures was increased from two at the start of the program to seven by the end of 1992. The most recently installed system incorporated experience in growing YBCO-based structures gained in this program into a fully-automated production system capable of sequentially coating both sides of two 2-inch or one 4-inch substrate with multilayers composed of YBCO and appropriate epitaxial insulators or conductors. The most important new equipment in the superconducting electronics clean room (which has been doubled in area) is a dedicated ion miller with capability for up to a 6"-diameter wafer. The most significant new characterization tool is a state-of-the-art four-circle x-ray diffractometer.

To obtain optimum use of the unique material and measurement capabilities developed under this and previous AFOSR-Westinghouse programs, collaborations with other research institutions were continued and expanded. These collaborations were made with researchers whose work fell within the overall objectives of this program. A table of technical collaborations which were active during the program is shown in Section 7 of this report.

# 5. PUBLICATIONS


1. M. G. Forrester, J. Talvacchio, J. R. Gavaler, M. Rooks, and J. Lindquist, "Fabrication and Characterization of $YBa_2Cu_3O_7$/Au/$YBa_2Cu_3O_7$ Josephson Junctions," IEEE Trans. Magn. 27(2), 3098 (1991).
2. H.-P. Baum, B. K. Sarma, M. Levy, J. R. Gavaler, and A. Hohler, "SAW Measurements on a Nb Film and an $YBa_2Cu_3O_7$ Film," IEEE Trans. Magn. 27(2), 1280 (1991).
3. J. Talvacchio, M. G. Forrester, J. R. Gavaler, and T. T. Braggins, "Large-Area YBCO Films for Microwave Applications," IEEE Trans. Magn. 27(2), 978 (1991).
4. J. R. Gavaler, J. Talvacchio, T. T. Braggins, and J. Greggi, "Critical Parameters in Single Target Sputtering of YBCO," J. Appl. Phys. 70, 4383 (1991).
5. J. Talvacchio, "High-$T_c$ Superconductivity in 1990," published as a Special Issue of the Journal of Superconductivity 4(2), 75-169 (1991).
6. D. H. Kim, K. E. Gray, R. T. Kampwirth, J. C. Smith, D. S. Richeson, T. J. Marks, J. H. Kang, J. Talvacchio, and M. Eddy, "Effect of Cu-O Layer Spacing on the Magnetic Field Induced Resistive Broadening of high-Temperature Superconductors," Physica C 177, 431 (1991).
7. H. Buhay, S. Sinharoy, M. H. Francombe, W. H. Kaser, J. Talvacchio, B. K. Park, N. J. Doyle, D. R. Lampe, and M. Polinsky, "Pulsed Laser Deposition of Oriented Bismuth Titanate Films for Integrated Electronic Applications," J. Ferroelectrics (1991); reprinted in Integrated Ferroelectrics (Gordon and Breach, 1992) pp. 213-222.
8. T. T. Braggins, J. R. Gavaler, and J. Talvacchio, "In-Situ Deposition of YBaCuO Films on Both Sides of Two-Inch-Diameter Wafers by Off-Axis Sputtering," Proc. ICMC, Advances in Cryogenic Engineering (Materials), Vol. 38, (Plenum, New York, 1991), pp. 1013-1018.
9. J. Talvacchio, S. H. Talisa, and G. R. Wagner, "High-$T_c$ Film Development for Electronic Applications," Microwave Journal, 105 (June, 1991).

10. D. H. Kim, D. J. Miller, J. C. Smith, R. A. Holoboff, J. H. Kang, and J. Talvacchio, "The Effects of Microstructure on Flux Pinning in Epitaxial $YBa_2Cu_3O_7$ Films," Phys. Rev. B 44, 7607 (1991).

11. G. L. Belenky, S, M. Green, A. Roytburd, C. J. Lobb, S. J. Hagen, R. L. Greene, M. G. Forrester, and J. Talvacchio, "Effect of Stress along the a-b Plane on the $J_c$ and $T_c$ of $YBa_2Cu_3O_7$ Thin Films," Phys. Rev. B 44(10), 10117 (1991).

12. M. M. Driscoll, J. T. Haynes, S. Horwitz, R. A. Jelen, R. W. Weinert, J. R. Gavaler, J. Talvacchio, G. R. Wagner, K. A. Zaki, and X.-P. Lang, "Cooled, Ultra-high Q, Sapphire Dielectric Resonators for Low Noise Microwave Signal Generation," Proc. 45th IEEE Symposium on Frequency Control, 700 (1991); IEEE Trans. Ultrasonics, Ferroelectrics, and Frequency Control (1992).

13. D. H. Kim, K. E. Gray, and J. H. Kang, "Josephson Tunneling for Magnetic Fields perpendicular to Discreet Nb Junctions: Implications to the Irreversibility Crossover in High-Temperature Superconductors," accepted for Phys. Rev. B (1992).

14. J. Owliaei, S. Sridhar, and J. Talvacchio, "Field-Dependent Crossover in the Vortex Response at Microwave Frequencies in $YBa_2Cu_3O_7$ Films," Phys. Rev. Lett. 69(23), 3366 (1992).

15. F. Gao, D. B. Romero, D. B. Tanner, J. Talvacchio, and M. G. Forrester, "Infrored Properties of Epitaxial $La_{2-x}Sr_xCuO_4$ Thin Films in the Normal and Superconducting States," Phys. Rev. B 47(2) (1992).

16. J. R. Gavaler and J. Talvacchio, "YBCO-Based Multilayer Structures on Large-Area Substrates," in Layered Superconductors: Fabrication, Properties, and Applications, ed. by D.T. Shaw, C. C. Tsuei, T. R. Schneider, and Y. Shihara (Materials Research Society, Vol. 275, 1992).

17. B. A. Baumert and J. Talvacchio, "Artificial Barriers for Ba-K-Bi-O Tunnel Junctions," IEEE Trans. Appl. Superconductivity 3(1), 1576 (1993).

18. D. B. Tanner, F. Gao, M. Quijada, D. B. Romero, J. P. Rice, D. M. Ginsberg, J. Talvacchio, M. G. Forrester, L. Forro, D. Mandrus, L. Mihaly, G. L. Carr, and G. P. Williams, "Optical Conductivity of the High-$T_c$'s: Search for the Energy Gap," J. Phys. Chem. Solids 53(12), 1611 (1992).

19. T. T. Braggins, J. R. Gavaler, and J. Talvacchio, "In-Situ Deposition of YBaCuO Films on Both Sides of Two-Inch-Diameter Wafers by Off-Axis Sputtering," Microwave Journal 35(8), 106 (1992).

20. T. Gong, L. X. Zheng, W. Xiong, W. Kula, R. Sobolewski, J. P. Zheng, H. S. Kwok, and J. R. Gavaler, "Femtosecond Spectroscopy of Y-Ba-Cu-O Thin Films," Proceedings of the Conference on Superconductivity and Its Applications, Buffalo, NY (1993).

21. H.-J. Chen, S. Sridhar, and J. Talvacchio, "Dynamics of Vortex-Anti- vortex Pairs at Microwave Frequencies in $YBa_2Cu_3O_7$ Films," submitted to Phys. Rev. Lett. (1993).

22. W. Xiong, W. Kula, R. Sobolewski, and J. R. Gavaler, "Superconducting Properties of Laser-Annealed Lines Fabricated in Oxygen Deficient Y-Ba-Cu-O Thin Films," Proceedings of the Conference on Superconductivity and Its Applications, Buffalo, NY (1993).

23. B. A. Baumert, J. Talvacchio, and M. G. Forrester, "$SrTiO_3$ Buffer Layers and Tunnel Barriers for Ba-K-Bi-O Junctions," Appl. Phys. Lett. 62(17), 2137 (1993).

24. R. Sobolewski, W. Xiong, W. Kula, and J. R. Gavaler, "Laser Patterning of YBCO Thin-Film Devices and Circuits," Appl. Phys. Lett. 64(5), 643 (1994).

25. A. Davidson, J. Talvacchio, M. G. Forrester, and J. R. Gavaler, "Superconductive Electronics with High Transition Temperature Films," Proc. ICMC, Advances in Cryogenic Engineering (Materials), Vol. 39, (Plenum, New York, 1993); reprinted in Microwaves & RF (1994).

26. M. G. Forrester, A. Davidson, J. Talvacchio, and J. R. Gavaler, "Inductance Measurements in Multilevel High-$T_c$ Step-Edge Grain Boundary SQUIDs," submitted to Appl. Phys. Lett. (1994).

# 6. PERSONNEL

J. R. Gavaler*

J. Talvacchio*

A. Davidson

M. G. Forrester

R. L. Grassel

J. Greggi

J. H. Kang

D. L. Meier

G. R. Wagner

B. A. Baumert (Carnegie Mellon University)

J. D. McCambridge (Yale University)

M. McGaughey (Penn State University)

G. Skofronick (Penn State University)

* Principal Co-Investigators

## COUPLING ACTIVITIES

(Speaker's name is underlined.)

1. "The Effect of Uniaxial Strain on $J_C$ and $T_C$ of thin YBaCuO Films," G. L. Belenky, S. M. Green, S. J. Hagen, R. L. Greene, M. G. Forrester, and J. Talvacchio, Contributed presentation to the American Physical Society March Mtg., March 1991.
2. "Heterostructures Formed with High Temperature Superconductors," J. Talvacchio, Invited presentation to the Materials Research Society Spring Meeting, Anaheim, April 1991.
3. "Superconducting Materials and Electronics Research at Westinghouse STC," M. G. Forrester, University of Maryland Physics Dept. Colloquium, April 1991.
4. "Pulsed Laser Deposition of Oriented Bismuth Titanate Films for Integrated Electronic Applications," H. Buhay, S. Sinharoy, M. H. Francombe, W. H. Kaser, J. Talvacchio, B. K. Park, N. J. Doyle, D. R. Lampe, and M. Polinsky, Contributed presentation to the 3rd International Conf. on Integrated Ferroelectrics, Colorado Springs, April 1991.
5. "Electronic Applications of Superc ductors," J. Talvacchio, Invited presentation to the Pittsburgh Chapter of the IEEE Magnetics Soc., Pittsburgh, May 1991.
6. "In-Situ Deposition of YBaCuO Films on Both Sides of Two-Inch-Diameter Wafers by Off-Axis Sputtering," T. T. Braggins, J. R. Gavaler, and J. Talvacchio, Contributed presentation to the International Cryogenics Materials Conf., Huntsville, June 1991.
7. "Present and Projected Performance of High-Temperature Superconducting Filters," S. H. Talisa, M. A. Janocko, J. Talvacchio, and C. Moskowitz, Contributed presentation to the IEEE Microwave Symposium (MTT-S), Boston, June 1991.
8. "Sputtered YBCO Film Structures for Microstrip and S-N-S Devices," J. Talvacchio, Invited presentation to the Third Annual DARPA HTSC Workshop, Seattle, October 1991.
9. "Cooled, Ultra-high Q, Sapphire Dielectric Resonators for Low Noise Microwave Signal Generation," M. M. Driscoll, J. T. Haynes, S. Horwitz, R. A. Jelen, R. W.

Weinert, J. R. Gavaler, J. Talvacchio, G. R. Wagner, K. A. Zaki, and X.-P. Lang, Invited presentation to the 3rd DARPA HTSC Workshop, October 1991.

10. "Current Status of Single-Target Sputtering of YBCO," J. R. Gavaler, Invited presentation to the Fall Meeting of the Materials Research Society, Boston, December 1992.

11. "Surface Properties and Microstructure of Sputtered Ba-K-Bi-O Films," B. A. Baumert and J. Talvacchio, Contributed presentation to the Fall Meeting of the Materials Research Society, Boston, December 1992.

12. "Pulsed Laser Deposition and Characterization of Epitaxial Bi-Ti-O/YBCO 'Ferroic-Superconductor' Structures," H. Buhay, S. Sinharoy, J. Talvacchio, W. H. Kasner, N. J. Doyle, and M. H. Francombe, Contributed presentation to the Fall Meeting of the Materials Research Society, Boston, December 1992.

13. "Requirements for Substrates and Deposited Insulators Used in Analog and Digital HTS Circuits," J. Talvacchio, Invited presentation to the Workshop on Substrate Materials for High Temperature Superconductors, Williamsburg, February 1992.

14. "Barriers for Ba-K-Bi-O Tunnel Junctions," J. Talvacchio and B. A. Baumert, Contributed presentation to the APS March Meeting, Indianapolis, March 1992.

15. "Effect of Substrate-Induced Microstructure on Transport Properties in Epitaxial $YBa_2Cu_3O_7$ and $Tl_2Ba_2CaCu_2O_X$ Films," D. H. Kim, D. J. Miller, J. D. Hettinger, J. Sharping, R. A. Holoboff, R. T. Kampwirth, J. H. Kang, J. Talvacchio, and M. Eddy, Contributed presentation to the APS March Meeting, Indianapolis, March 1992.

16. "High-$T_c$ Step-Edge SNS Junctions and SQUIDs," J. D. McCambridge, J. Talvacchio, and M. G. Forrester, Contributed presentation to the APS March Meeting, Indianapolis, March 1992.

17. "Infrared conductivity of Epitaxial $La_{2-x}Sr_xCuO_4$ Thin Films in the Normal and Superconducting States," F. Gao, D. B. Tanner, J. Talvacchio, and M. G. Forrester, Contributed presentation to the APS March Meeting, Indianapolis, March 1992.

18. "YBCO-Based Multilayer Structures on Large-Area Substrates," J. R. Gavaler and J. Talvacchio, Contributed presentation to the MRS Spring Meeting, San Francisco, April 1992.

19. "Development of a Digital Integrated Circuit Process Based on Step-edge YBCO/Au S-N-S Junctions," M. G. Forrester, J. D. McCambridge, J. Talvacchio, J. H. Kang, J. X. Przybysz, D. L. Miller, and J. R. Gavaler, Contributed presentation to the Applied Superconductivity Conference, Chicago, August 1992.

20. "Artificial Barriers for Ba-K-Bi-O Tunnel Junctions," B. A. Baumert and J. Talvacchio, Contributed presentation to the Applied Superconductivity Conference, Chicago, August 1992.

21. "Epitaxial Insulating Thin films for High-Tc Superconducting Electronics," J. Talvacchio, M. G. Forrester, J. R. Gavaler, and S. H. Talisa, Contributed presentation to the Applied Superconductivity Conference, Chicago, August 1992.

22. "Role of Oxygen in Optimizing Surface Resistance in YBCO Films," J. R. Gavaler, J. Talvacchio, S. H. Talisa, and G. B. Draper, Contributed presentation to the Applied Superconductivity Conference, Chicago, August 1992.

23. "Optimizing YBCO Step-Edge S-N-S Junctions for Digital Electronics," J. D. McCambridge, M. G. Forrester, and J. Talvacchio, Contributed presentation to the Applied Superconductivity Conference, Chicago, August 1992.

24. "Requirements for Thin Films Used in High-Speed Analog and Digital HTS Circuits," J. Talvacchio, Invited presentation to the First International Workshop on MOCVD of High-Temperature Superconductors, Chicago, August 1992.

25. "Relationship of Microstructure to rf Surface Resistance in YBCO," J. Talvacchio, J. R. Gavaler, S. H. Talisa, and R. W. Weinert, Contributed presentation to the APS March Meeting, Seattle, March 1993.

26. "Post-Growth Annealing conditions for In-Situ Sputtered YBCO Films," J. R. Gavaler and J. Talvacchio, Contributed presentation to the APS March Meeting, Seattle, March 1993.

27. "Low-Frequency Noise Peaks due to the Motion of Vortices in Epitaxial YBCO Films," D-H. Kim, K. E. Gray, P. G. Landis, J. E. Sharping, J.-H. Kang, and J. Talvacchio, Contributed presentation to the APS March Meeting, Seattle, March 1993.

28. "Insulator Properties in Multi-Level HTS Circuits," J. Talvacchio, M. G. Forrester, G. J. Faychak, and J. H. Uphoff, Contributed presentation to the Materials Research Society Spring Meeting, San Francisco, April 1993.

29. "Heteroepitaxy in the Ba-K-Bi-O/$SrTiO_3$ System," B. A. Baumert, J. Talvacchio, and M. G. Forrester, Contributed presentation to the Materials Research Society Spring Meeting, San Francisco, April 1993.

30. "Multilayer HTS for GHz A/D Converters," M. G. Forrester, A. Davidson, J. X. Przybysz, J. Talvacchio, J. R. Gavaler, and J. Greggi, Contributed presentation to the Workshop on Superconductive Digital Electronics, Maine, October 1993.

31. "Applications of High-$T_c$ Superconductors in Signal Processing," J. Talvacchio, University of Pittsburgh Elecrical Engineering Department Seminar, October 1993.

32. "Ex-Situ Processing of Multi-Level HTS Structures," J. Talvacchio, M. G. Forrester, J. R. Gavaler, D. L. Meier, and A. Davidson, Contributed presentation to the Materials Research Society Fall Meeting, Boston, November 1993.

33. B. A. Baumert and J. Talvacchio, "Heteroepitaxial Barriers for Ba-K-Bi-O Tunnel Junctions," Contributed presentation to the Materials Research Society Fall Meeting, Boston, November 1993.

34. "Josephson Junctions: Physics, Materials, Circuits, and Applications," J. Talvacchio, Guest Lecture, joint Carnegie Mellon University and University of Pittsburgh graduate course on superconductivity, Pittsburgh, November 1993.

35. "Progress in Thin Film Applications of High-$T_c$ Superconductors," J. Talvacchio, Discussion Leader at the Gordon Research Conference on Superconductivity, Oxnard, January 1994.

36. "Superconductor Properties for Cryogenic Radar Subsystems," J. Talvacchio, S. H. Talisa, R. W. Weinert, M. G. Forrester, J. R. Gavaler, A. Davidson, D. L. Meier, M. A. Janocko, J. X. Przybysz, D. L. Miller, J. H. Kang, and G. R. Wagner, Contributed presentation to the Gordon Research Conference on Superconductivity, Oxnard, January 1994.

37. J. Talvacchio, D. L. Meier, S. H. Talisa, R. W. Weinert, J. R. Gavaler, and R. L. Grassel, "Surface Studies of YBCO Films during Processing of Microwave Circuits," Contributed presentation to the March Meeting of the American Physical Society, Pittsburgh, March 1994.

38. "Integration of Step-Edge Junctions in an HTS Flash A?D Converter," J. Talvacchio, M. G. Forrester, A. Davidson, J. R. Gavaler, and J. X. Przybysz, Invited presentation to the Materials Research Society Spring Meeting, San Francisco, April 1994.

39. "Epitaxial Oxide Film Requirements for HTS Electronics," J. Talvacchio, Invited presentation to the 2nd International Workshop on MOCVD of High-Temperature Superconductors, San Francisco, April 1994.

## OUTSIDE COLLABORATIONS

| Institution / Collaborator | Effort / Special Requirements |
|---|---|
| Argonne National Laboratory<br>Dr. K. E. Gray | Properties of bicrystal jcts<br>- YBCO grain-boundary jcts grown on bicrystals |
| Jet Propulsion Laboratory<br>Dr. B. D. Hunt | Comparison of sputtering and laser ablation<br>- SNS edge junctions |
| Northwestern Universtiy<br>Prof. B. Wessels | BSCCO flux-flow devices/integration with YBCO<br>- low-flux-pinning BSCCO films |
| USAF Wright Laboratory<br>Dr. R. R. Biggers | Growth mechanism and surfaces of YBCO films<br>- YBCO films grown on vicinal substrates |
| Argonne National Laboratory<br>Dr. D. H. Kim | Vortex dynamics in superconductors<br>- epitaxial YBCO and NbN patterned films |
| University of Maryland<br>Prof. C. J. Lobb | Strain effects in YBCO<br>- patterned YBCO bridges |
| NIST (Boulder)<br>Dr. A. Roshko | Scanning tunneling microscopy<br>- YBCO and BKBO films with measured $R_S$ |
| Carnegie Mellon University<br>Prof. M. E. McHenry | Flux pinning and creep in BKBO<br>- Epitaxial BKBO films |
| University of Florida<br>Prof. D. Tanner | Infrared reflection and absorption<br>- single crystal LSCO films |
| Yale University<br>Prof. D. E. Prober | S-N-S Josephson junction development<br>- in-situ S-N interface formation |
| CVC Products, Inc.<br>Dr. P. Ballentine | rf surface resistance measurements<br>- 2" dia. YBCO films |
| Northeastern University<br>Prof. C. Vittoria | Calibration of new $R_S$ meas. technique<br>- YBCO with measured $R_S$ |
| Penn State University<br>Prof. A. M. Carim | Microstructure of a-axis YBCO structures<br>- a-axis YBCO/PrBCO/YBCO trilayers |

| Institution/Collaborator | Effort / Special Requirements |
|---|---|
| Northeastern University<br>Prof. S. Sridhar | Magnetic field phase diagram mapped with $R_S$<br>- YBCO with measured $R_S$ |
| Carnegie Mellon University<br>Prof. N. S. VanderVen | Low-field microwave absorption<br>- Low-$R_S$ YBCO films |
| EMCORE Corp.<br>Dr. C. Chern | rf surface resistance measurements<br>- YBCO films grown by MOCVD |
| University of Alberta<br>Prof. J. Jung | Mapping of critical current density<br>- Patterned YBCO films |
| University of Maryland<br>Prof. T. Venkatesan | Epitaxial insulator films<br>- YBCO/insulator/YBCO structures |
| University of Rochester<br>Dr. R. Sobolewski | Laser-patterning of YBCO films<br>- Single-phase YBCO films |
| Purdue University<br>Prof. M. W. McElfresh | Vortex dynamics in YBCO<br>- Patterned a-axis YBCO films |

# 8. PATENTS

1. "Thin-Film Growth of Thallium-Based Superconductor," N. B. Singh and J. Talvacchio, Disclosure No. RDS-91-027, disclosed April 1991.
2. "Sputtering Method for Forming Superconductive Films Using Water Vapor Addition," J. R. Gavaler and T. T. Braggins, U. S. Patent #5,126,318, issued June 30, 1992.

# APPENDICES

Reprints of publications listed in Section 5 and abstracts of papers in preparation based on work performed under this program. Appendix numbers refer to the list in Section 5.

# FABRICATION AND CHARACTERIZATION OF $YBa_2Cu_3O_7$/Au/$YBa_2Cu_3O_7$ JOSEPHSON JUNCTIONS

M. G. Forrester, J. Talvacchio,* and J. R. Gavaler*
Westinghouse Science & Technology Center
1310 Beulah Road
Pittsburgh, PA 15235

M. Rooks
National Nanofabrication Facility
Cornell University
Ithaca, NY

J. Lindquist
FEI Company
Beaverton, OR

**APPENDIX 1**

## Abstract

We have fabricated all-high-$T_c$ Josephson junctions in a planar S-N-S geometry, by bridging narrow gaps (≈ 0.1 - 0.2 μm) in epitaxial $YBa_2Cu_3O_7$ (YBCO) films with Au. The resulting devices exhibit a variety of non-hysteretic I-V characteristics, with $I_cR_N$ of order 0.1 to 10 mV, and exhibit Shapiro steps under microwave irradiation, and weak periodic modulation of the critical current with applied magnetic field. The transport properties of the junctions appear to be dominated by the Au/YBCO interfaces rather than by the Au itself.

## Introduction

The development of an integrated circuit technology based on high temperature superconductors (HTS) requires the controlled fabrication of Josephson junctions. Current low temperature superconducting (LTS) circuit technology is based on S-I-S tunnel junctions, typically of the type Nb/$AlO_x$/Nb, whose reproducibility and controllability has made possible the fabrication of complex circuits, and whose hysteretic I-V characteristics suggest various logic schemes relying on the zero-voltage and gap-voltage states to define logical "0" and "1".[1]

At present there is no HTS tunnel junction technology, due to the materials problems associated with the growth of a homogenous barrier compatible with the high-temperature deposition conditions for *in-situ* HTS films. This has led to an interest in the fabrication of non-hysteretic S-N-S junctions, as an interim basis for electronic circuits, using logic schemes which do not require hysteretic junctions. Such junctions may additionally replace grain-boundary weak links currently used in many HTS SQUID's. The first such junction reported was a planar YBCO/Au/YBCO bridge fabricated from a post-annealed YBCO film using electron-beam lithography to define the 1 μm junction length, and which exhibited a critical current up to 16 K.[2] Subsequent developments have emphasized an *in-situ* trilayer approach, using, for example, $PrBa_2Cu_3O_7$ as the normal barrier.[3] While the latter approach, which more closely parallels LTS Nb technology, is ultimately preferable, further materials development is needed to reduce the density of defects, such as micro-shorts, which currently dominate the electrical characteristics of such devices.

Here we report preliminary results on the fabrication of planar junctions, with lengths, d, as short as 0.1 μm, which exhibit Josephson effects up to 70 K.

* Supported in part by AFOSR contract no. F49620-88-C-0039.
Manuscript received September 24, 1990.

## Sample Fabrication

Our YBCO films were deposited by off-axis dc magnetron sputtering from a stoichiometric target, onto substrates of (100) and (110) $SrTiO_3$. The deposited films were epitaxial, with (001) orientation on (100) substrates and (103)/(013) orientation on (110) substrates. Thicknesses used varied from ≈ 50 to 200 nm. Films typically exhibited transition temperatures in the 88-92 K range, room-temperature resistivity of 300 μΩ-cm, and critical currents in excess of $10^6$ A/$cm^2$ at 77 K. Further details of the film properties and deposition conditions have been reported elsewhere.[4]

After the post-deposition cool-down the YBCO films were coated, *in-situ*, with 50 to 100 nm sputtered Au, to

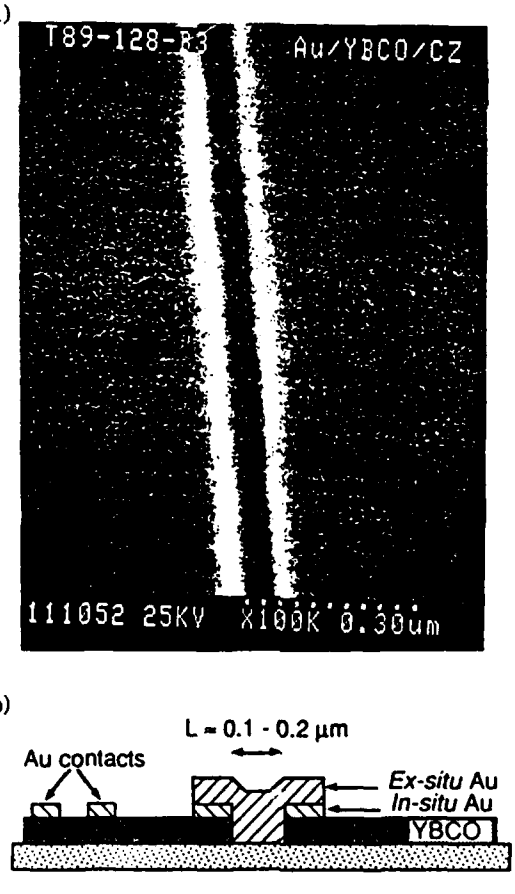


Figure 1. (a) Micrograph of a ≈ 0.1 μm-wide slot in a Au/YBCO bilayer, formed by electron-beam lithography and broad-beam ion milling. (b) Schematic diagram of completed planar junction.

0018-9464/91/0300-3098$01.00 © 1991 IEEE

protect the top surface of the YBCO during subsequent processing.

Fabrication by Electron-Beam Lithography

A film of a slow-milling material, such as $Si_3N_4$ or Ti, was deposited on the Au/YBCO bilayers to serve as an ion-milling mask for patterning of the YBCO. The resulting trilayer was coated with a layer of PMMA resist. After exposure of the narrow slots by 50 keV electrons the resist pattern was transferred into the masking layer by reactive ion etching (RIE), and then into the Au/YBCO by 500 eV Ar ion milling. Although the actual devices were not isolated at this point, various test patterns included on each chip enabled us to check that the milled slots were electrically open ($> 10^4\ \Omega$). Figure 1a shows an example of a 0.1 μm slot defined in this manner.

After removal of the remaining mask layer, photolithographic processing and ion milling were used to isolate the junctions and their individual four-point current and voltage leads, and to define the junction width, w, of 10 μm. The sample was then coated with ≈ 200 nm of sputtered Au (ρ ~ 1 μΩ-cm at room temperature), and the Au selectively patterned by RIE to define the junctions and their contact pads. Some samples were annealed at 600 °C in flowing $O_2$ to improve the Au/YBCO contact. Figure 1b shows a schematic diagram of a completed junction.

Samples were wire-bonded into a 32-lead sapphire chip carrier for electrical measurements.

Fabrication by FIB etching

A more direct approach to junction fabrication is to use a focussed ion beam (FIB) to etch the submicron slots directly, without the use of masking layers and resists. We have used a 30 keV Ga ion beam, with a nominal FWHM of 60 nm, which produced slots of approximately 0.2 μm at the film's top surface. Test samples were again checked for electrical open circuit to ensure complete etching, and etch time and current were chosen so as to over-etch somewhat, to avoid shorts due to defects such as surface particles on the YBCO.[4] The side walls of the etched slots appeared less steep than those produced by e-beam lithography and broad-beam ion milling, possible because of the approximately gaussian shape of the beam resulting in partial etching of the film by the beam "tails." Further reductions in linewidth are expected by use of a slightly smaller aperture, and shorter etching times.

Subsequent processing of the FIB samples was identical to the e-beam approach.

Measured characteristics

Figure 2 shows a set of I-V characteristics as a function of temperature for an e-beam-fabricated junction with a length of approximately 0.1 μm, on $SrTiO_3$ (100). At low temperatures the measured behavior is not unlike the RSJ model prediction (in the absence of thermal fluctuations) of $V = R(I^2 - I_c^2)^{1/2}$. However, for increasing temperatures the characteristic broadens much more than predicted by the thermal fluctuation model of Ambegaokar and Halperin.[5]

Figure 3 shows a set of dV/dI vs. I curves, at 42 K,

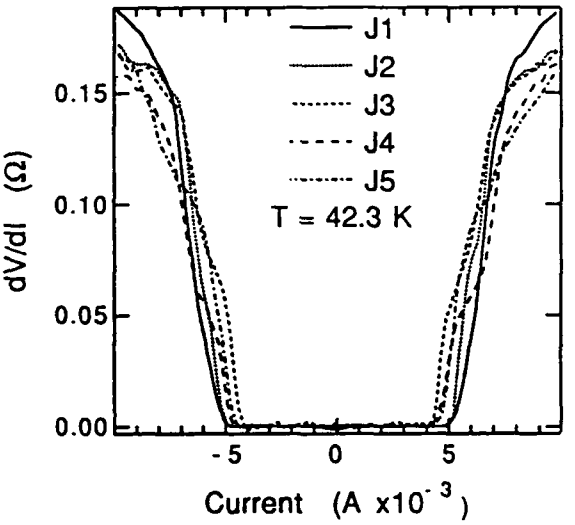


Figure 3. Differential resistance vs. current for five FIB-fabricated junctions on one chip.

for five junctions on a FIB-fabricated sample, on $SrTiO_3$ (100), which was annealed according to the procedure discussed above. The nominal junction length was 0.2 μm. The similarity of the characteristics is encouraging, suggesting that the junctions are reasonably homogeneous and reproducible within a chip.

Figure 4 shows the measured critical current $I_c$, determined by an arbitrary voltage criterion of 5 μV, for

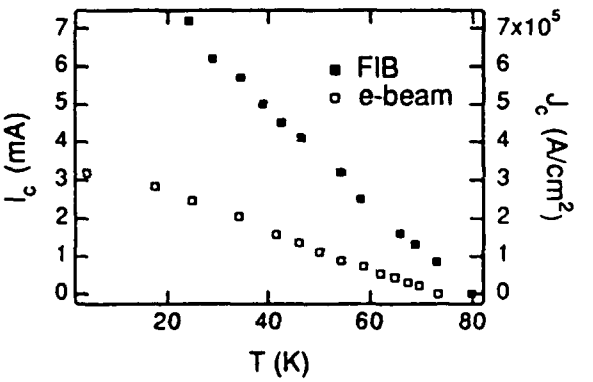


Figure 4. Critical currents for the e-beam junction of Fig. 2, and junction J5 of Fig. 3.

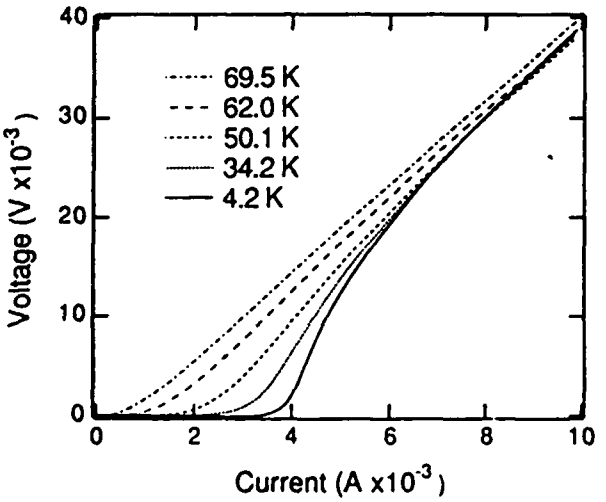


Figure 2. Current -voltage characteristics for a ≈ 0.1 μm long e-beam-fabricated YBCO/Au/YBCO junction.

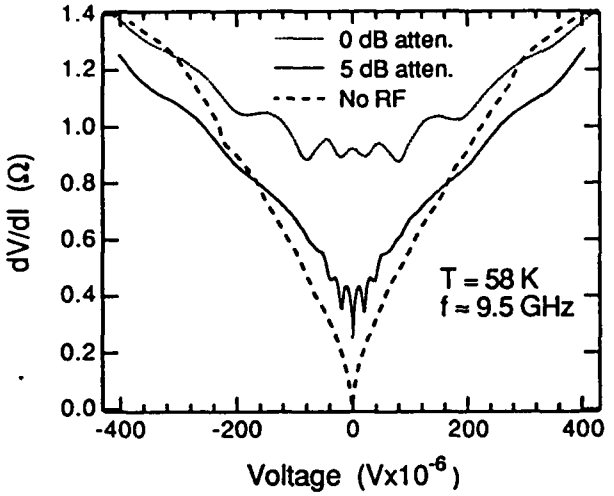


Figure 5. Differential resistance vs. voltage for the e-beam junction of Fig. 2, showing rounded Shapiro steps induced by 9.5 GHz radiation. The "0 dB" and "5 dB" curves are displaced vertically by 0.5 Ω and 0.25 Ω, respectively, for clarity.

the sample of Figs. 2 and 3. The annealed FIB-fabricated sample, despite its greater length, exhibited a larger critical current than the unannealed e-beam junction of Fig. 2, as well as a lower resistance (≈ 0.1 Ω, compared to 4 Ω), consistent with an improvement in the quality of the Au/YBCO interfaces upon annealing.

The response of the sample of Fig. 2 to f = 9.5 GHz radiation is shown in Fig. 5, at a temperature of 58.5 K. Radiation was weakly coupled in through a half-wave antenna approximately 5 mm above the sample. The characteristics exhibit weak Shapiro steps at voltages V=nhf/2e. Above approximately 67 K the steps washed out completely due to thermal fluctuations, while below about 38 K there was apparently insufficient microwave power to produce steps.

Measurements of dV/dI vs. applied magnetic field, at a fixed bias current above $I_c$, for a 0.1 × 10 μm junction are shown in Figure 6, for a temperature of 56 K. The data show an extremely weak periodic modulation, with maxima in dV/dI (corresponding to minima in $I_c$) occurring with a period of approximately 7 gauss. The expected period, ΔB, is given by the relation

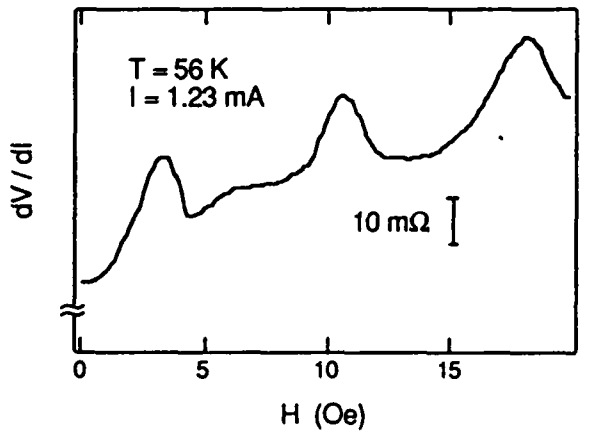


Figure 6. Weak periodic modulation of the sample differential resistance, at a fixed bias current above $I_c$, as a function of magnetic field, reflecting periodic modulation of the junction critical current.

$$\Delta B = \frac{\Phi_0}{w\,(d + 2\lambda)}\,, \qquad (1)$$

where λ is the penetration depth of the YBCO and $\Phi_0$ is the flux quantum. Using $w$ = 10 μm, $d$ = 10 μm, and λ = 0.15 μm yields ΔB = 5 gauss, in reasonable agreement with the measured value. The weak modulation depth may be partially due to the sample being in a self-field-limited regime, $w > 2\lambda_J$, where the current flows witnin a characteristic width $\lambda_J$ of each edge of the junction, and partially to inhomogeneous coupling across the width of the junction. The Josephson penetration depth, in SI units, is given by

$$\lambda_J^2 = \frac{\hbar}{2eJ_c\,\mu_0(2\lambda + d)}\,, \qquad (2)$$

where $J_c$ is the critical current density. Applying this expression straightforwardly to the junction of Fig. 6, which had $J_c \approx 7.5 \times 10^4$ A/cm$^2$ at 56 K, yields $\lambda_J \approx 0.9$ μm, so that w (10 μm) >> 2 $\lambda_J$.

## Discussion

The results presented above give unambiguous evidence of Josephson behavior in these planar junctions. However, the nature of the junctions is far from clear, and almost certainly does not represent true S-N-S behavior. For example, the resistance of the junctions, ~ 0.1 - 1 Ω, is much greater than the ~ mΩ expected for the resistance of the Au alone, and must be dominated by the Au/YBCO interfaces, suggesting that the actual devices have an S-I-N-I-S character. In fact, the measured resistances are consistent with a specific contact resistance of the order $10^{-8}$ to $10^{-9}$ Ω-cm$^2$, which is quite typical of measured Au/YBCO contact resistances.

The approximately linear temperature dependence of the measured critical current also disagrees with the $I_c \propto \exp(-d/\xi_N(T))$ form expected for an S-N-S junction, and is also, at least close to $T_c$, consistent with S-I-N-I-S behavior.

It is also unclear which surface of the YBCO provides the strongest superconducting proximity effect coupling through the Au — the milled side walls, or the top surface which is protected by *in-situ* Au. In principle this will depend on the growth orientation of the film, with c-axis films potentially having stronger coupling through the side walls, and a-axis through the top surface. The effective length, d, for a junction fabricated from an a-axis film would then be somewhat larger than the slot width, by some geometrical factor. The results here were obtained with c-axis films.

The use of a-axis films may ultimately be preferable, because it will likely be easier to reproducibly control the YBCO/*in-situ* Au interface than that formed with the *ex-situ* Au at the side walls.

## Summary and Conclusions

We have fabricated Josephson junctions with a planar S-N-S geometry, with lengths as short as 0.1 μm, which exhibit Josephson effects to 70 K. The measured characteristics are consistent with a S-I-N-I-S device geometry, with the junction resistance being dominated by the Au/YBCO interfaces.

The intra-chip consistency of some of the measured junctions is encouraging, indicating that the characteristics are not dominated by small numbers of isolated defects such as shorts. However the chip-to-chip reproducibility needs improvement.

Because of their relatively high $I_cR_N$ products, the junctions show promise for use in circuits based on flux quantum logic schemes, which do not require hysteretic junctions,[6] as well as for SQUID applications.

## Acknowledgments

We are pleased to acknowledge A. Foley and J. Uphoff for building the measurement apparatus, and the staff of the National Nanofabrication Facility and FEI Company for assistance with sample fabrication.

## References

1. See, for example, Y. Tarutani, M. Hirano, and U. Kawabe, "Niobium-Based Integrated Circuit Technologies," *Proc. of the IEEE*, Vol. 77, 1164, 1989.

2. P. M. Mankiewich, D. B. Schwartz, R. E. Howard, L. D. Jackel, B. L. Straughn, E. G. Burkhardt, and A. H. Dayem, "Fabrication and Characterization of an YBa2Cu3O7/Au/YBa2Cu3O7 S-N-S Microbridge," in *Proceedings of the 5th International Workshop on Future Electron Devices*, Miyagi-Zao, 1988, p. 157.

3. C. T. Rogers, A. Inam, M. S. Hegde, B. Dutta, X. D. Wu, and T. Venkatessan, "Fabrication of Heteroepitaxial $YBa_2Cu_3O_{7-x}$–$PrBa_2Cu_3C_{7-x}$–$YBa_2Cu_3O_{7-x}$ Josephson Devices Grown by Laser Deposition," *Appl. Phys. Lett.* 55, 2032, 1989.

4. J. R. Gavaler and J. Talvacchio, "Optimization of $T_c$ and $J_c$ in Sputtered YBCO Films," *Physica B* 165, 1513, 1990, and J. Talvacchio, M. G. Forrester, J. R. Gavaler, and T. T. Braggins, "YBCO and LSCO Films Grown by Off-Axis Sputtering," to appear in *Science and Technology of Thin-Film Superconductors II*, edited by R. McConnell and S. A. Wolf, Plenum, New York, 1990.

5. V. Ambegaokar and B. I. Halperin, "Voltage Due to Thermal Noise in the dc Josephson Effect," *Phys. Rev. Letters*, 22, 1364, 1969.

6. V. K. Kaplunenko, M. I. Khabipov, V. P. Koshelets, K. K. Likharev, O. A. Mukhanov, V. K. Semenov, I. L. Serpuchenko, and A. N. Vystavkin, "Experimental Study of the RSFQ Logic Elements," IEEE Trans. on Magnetics, Vol. 25, no. 2, 861-864, 1989.

# SAW MEASUREMENTS ON A Nb FILM AND AN $YBa_2Cu_3O_7$ FILM

H.-P. Baum, B. K. Sarma and M. Levy
University of Wisconsin-Milwaukee
Milwaukee, WI 53201

J. Gavaler
Westinghouse R & D Center
Pittsburgh, PA 15235

A. Hohler
Institut für Angewandte Physik
Henrich-Buff-Ring 16, D-6300 Giessen, FRG

**APPENDIX 2**

Abstract

Surface acoustic wave attenuation measurements have been performed in a screen room on a superconducting film of Nb at 659 MHz and on a high $T_c$ film of $YBa_2Cu_3O_7$ at 168 MHz. The attenuation in the Nb film is due to electron-phonon interaction and follows a BCS curve in the superconducting state. The measured change in attenuation was 0.8 dB/cm giving an electron mean free path which is about twice as large as the value obtained from the sheet resistivity of this Nb film. The sheet resistivity of the $YBa_2Cu_3O_7$ film was 45 $\Omega/\square$, and the observed change in attenuation at $T_c = 87$ K was 0.18 dB/cm. A percolation model is proposed for describing the behavior of both the attenuation and the sheet resistivity in the superconducting state. This model is also used to determine the minimum resistance of $YBa_2Cu_3O_7$ along the *ab* plane. It is found to be 12.5 $\mu\Omega$cm.

## 1. Introduction

There are two ways to produce an interaction between a metallic film deposited on a piezoelectric substrate and a surface acoustic wave SAW travelling through the substrate. In one, the mechanical deformation of the substrate is transmitted to the superimposed film so that there is acousto mechanical coupling between the two. In the other, the polarization fields produced in the piezoelectric substrate induce electrical currents on the superimposed film so that there is acousto electrical coupling between the two. In both cases, the complex elastic constants of the SAW are affected. There are both changes in velocity and attenuation of the SAW that can be produced by the interactions. Obviously, it is possible to make measurements in regimes where both mechanisms contribute to the interaction equally, which would make it difficult to separate the contributions of each effect. In this paper we shall present measurements on two superconducting films in which either one or the other mechanism is the principal source for the interaction. The acousto mechanical interaction gives rise to electron-phonon attenuation in a Nb film measured at 659 MHz, while the acoustic electric interaction is quenched by the transition to the superconducting state in an $YBa_2Cu_3O_7$ film at 168 MHz. Fortunately in both cases it is possible to exclude the effects of the other interaction. This is because in the limits in which these measurements are made, $ql_e << 1$ and $\omega\tau_s << 1$ electron phonon interaction in the normal state is proportional to the electrical conductivity while the acousto electric effect is proportional to the sheet electrical resistivity. In the above, $q$ is the SAW wavevector $2\pi/\lambda$ where $\lambda$ is the SAW wavelength and $l_e$ is the electron mean free path; and, $\omega$ is the angular frequency, and $\tau_s$ is the acousto electric relaxation time, $\omega\tau_s = v_o(\epsilon+\epsilon_o)R_\square$ where $v_o$ is the SAW velocity, $\epsilon$, and $\epsilon_o$ are the permittivity of the substrate and free space respectively, and $R_\square$ is the sheet resistivity of the film. Both sets of measurements were performed in an electromagnetic screen room. This improved the signal to noise ratio, so that SAW attenuation changes from the normal to the superconducting state of 0.8 dB/cm and 0.18 dB/cm could be measured on the Nb film and the $YBa_2Cu_3O_7$ film respectively. Thus, sensitivities of 0.02 dB could be achieved in the screen room.

## 2. Electron Phonon Interaction in Nb Film

A quasi single crystal film was deposited on a $LiNbO_3$ substrate in ultrahigh vacuum with ultrapure material.[1] The thickness of the film is 3000Å and its resistivity ratio is 2.7. The midpoint of the superconducting transition is 8.6 K. The width of the transition from normal value to zero value is 0.28 K. Figure 1 shows a plot of the normalized attenuation data $\alpha_s/\alpha_n$ versus the reduced temperature $T/T_c$. Here $\alpha_s$ and $\alpha_n$ are the attenuation in the superconducting and normal states respectively, and $T_c$ is the superconducting transition temperature.

In a bulk superconductor the attenuation for both longitudinal and transverse waves[2] is given by

$$\frac{\alpha_s}{\alpha_n} = \frac{2}{e^{\Delta/k_BT}+1} \qquad (1)$$

where $\Delta$ is the temperature dependent superconducting energy gap and $k_B$ is Boltzmann's constant. Since SAW travelling through a thin film superimposed on a substrate can be decomposed into independent longitudinal and shear motions,[3] the ratio of $\alpha_s/\alpha_n$ can also be given by equation 1. The solid line in Figure 1 is plotted by using the BCS[4] temperature dependent superconducting energy gap in equation 1 with the BCS value for $2\Delta(0) = 3.52\ kT_c$. It appears that this yields a good fit to the data within the sensitivity of the attenuation measurements. Although the films are quasi crystalline, the resistivity ratio is such that crystalline anisotropies should be smeared out by the shortness of the mean free path, producing essentially a simple spherical Fermi surface which, according to Anderson's[5] model, should result in a BCS value for $2\Delta(0)$. This is a result that is confirmed by our data.

We shall now turn our attention to estimating the value of the electron mean free path. The SAW ultrasonic attenuation coefficient due to electron phonon interaction in a thin film on

Manuscript received September 24, 1990.

0018-9464/91/0300-1280$01.00 © 1991 IEEE

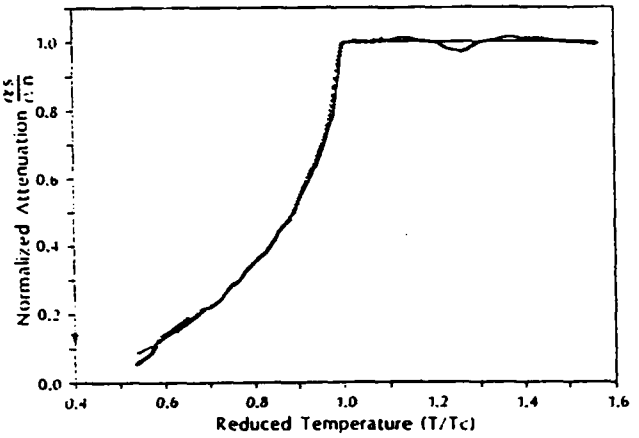


Figure 1 Normalized attenuation versus reduced temperature for 659 MHz SAW on Nb film (+ symbols). The solid line is the BCS curve for $2\Delta(0) = 3.52 k_B T_c$.

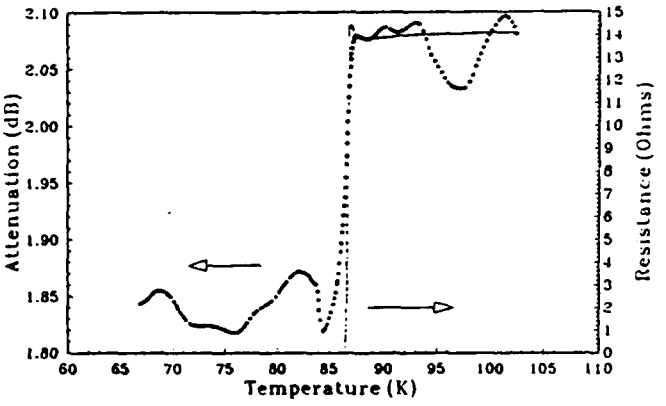


Figure 2 SAW attenuation data (solid dots) and four wire resistance (solid line) simultaneously obtained as a function of temperature for an $Y_1B_2Cu_3O_{7-\delta}$ film whose sheet resistivity is 45 $\Omega/\square$ and with a value of $L \simeq 10$. (See text.)

a substrate is given by[3]

$$\alpha_n = \frac{N m v_F^2 \tau q^3 h}{\rho_s v} F(\nu)$$

or

$$l_e = \frac{\alpha_n \rho_s v}{N m v_F q^3 h F(\nu)} \qquad (2)$$

where, for niobium, $N = 5.56 \times 10^{22}$ elns/cm$^3$; $m$ = free electron mass; $v_F$ = Fermi velocity = $1.37 \times 10^8$ cm/sec, $\tau_e$ = electron relaxation time; $q = 1.3 \times 10^4$ cm$^{-1}$, $h$ = film thickness = 3000Å, $\rho_s$ = mass density of YZ-$LiNbO_3$ substrate = 4.65 gm/cm$^3$; $v$ = SAW velocity under film = $3 \times 10^5$ cm/sec; $\nu = 0.39$, Poisson's ratio; and $\alpha_n = 0.8$ dB/cm = 0.092 Np/cm. $F(\nu)$ is a function of Poisson's ratio which according to Fig. 4 in reference 2, after making a factor of 3 correction suggested by a comparison of Fig. 4 in ref. 6 with Fig. 6 in ref. 7, is equal to 0.022 for $\sigma = 0.39$ which yields an acoustically determined electron mean free path $l_e = v_F \tau_e \simeq 1050$Å. We may also find the electron mean free path from the normal state value of the electrical resistivity of our film $\rho_e = 1.94\,\mu\Omega$·cm. Using $l_e = m v_F / N e^2 \rho_e$, we find $l_e = 450$Å for the resistivity determined electron mean free path. Either of these values for $l_e$ gives $q l_e < 0.14$ which is consistent with our assumption that $q l_e < 1$.

## 3. Acousto-electric Interaction in $YBa_2Cu_3O_7$ Film

A highly textured film of $YBa_2Cu_3O_7$ was d.c. magnetron sputtered[9] onto a Y-cut Z-propagate $LiNbO_3$ substrate at the University of Giessen, West Germany. The film was about 3000Å thick and has a sheet resistivity $R_\square = 45\Omega$ as measured with four wires. The SAW attenuation at 168 MHz and the four wire resistance are shown in Fig. 2 in the temperature range from 65 K to 105 K. It is evident that the behavior of the attenuation in the superconducting state is very different from the BCS behavior displayed in Fig. 1. The attenuation in Fig. 2 drops sharply at the transition. As mentioned in the introduction the noise level is about ±0.02 dB. The change in attenuation at the transition is about 0.18 dB/cm. The resistive transition starts at T = 86.0, and we surmise that this is the temperature at which the individual grains become superconducting $T_g$. The film as a whole becomes superconducting at $T_c$ = 86.4 K. In the limit where $\omega\tau_e << 1$ the attenuation due to the acousto electric effect is given by[9]

$$\alpha = \frac{\omega K^2}{2}(\epsilon + \epsilon_o) R_\square$$

where $K^2$ = electromechanical coupling constant = 0.048 and $\epsilon = 50\epsilon_o$ for $LiNbO_3$ and $R_\square = 45\Omega$. Therefore $\alpha = 9.4 \times 10^{-13} \omega R_\square = 0.045$ dB/cm. This value is about four times smaller than the observed attenuation.

According to the percolation model proposed in reference 10 and modified in ref. 11, it is possible not only to explain this difference but also the width in both the attenuation and resistance curves in the superconducting states. Moreover it is also possible to deduce the minimum value of the normal resistivity of the individual grains of $YBa_2Cu_3O_7$.

In the percolation model, it is assumed that the film is composed of individual grains that are connected by tunneling junctions, which are represented by resistances distributed in a square network. The junction resistances are assumed to be given by $r = r_0 e^{\xi}$, where $\xi$ is a random variable related to the intergrain distance and which is assumed to have a uniform distribution which results in a hyperbolic distribution function for the junction resistances $W_n(r) = 1/(r \ln r_2/r_1)$, $W_n(r)$ being zero for $r < r_1$ or $> r_2$. Thus $r_2$ is the maximum resistance of the network and $r_1$ is the minimum resistance of the network. Therefore, it can be inferred that $r_1$ is the resistance of the individual grains. According to the Ambegaokar, Halperin and Langer (AHL)[12] model, the sheet resistivity of this network is obtained when the critical percolation fraction of these resistors, $p_c$, is occupied, after starting to fill the network from the lowest valued resistors up.

For a square network $p_c = \frac{1}{2}$ and the assumed distribution function yields $R_\square = \sqrt{r_1 r_2}$. Now this would be the sheet resistivity of an infinite network, which is the $R_\square$ sampled by a dc electrical current. However, a surface acoustic wave samples a smaller network, and the authors in ref. 10 suggest that the dimensions of this network are comparable to the SAW wavelength, more specifically $L' = \frac{\lambda}{2\pi} = 3.5\mu m$. Thus the SAW are measuring the average sheet resistivity $R_\square^L$ of square sub-networks whose dimensions are L on a side where $L$ is the

ratio of $L'$ to the average grain size. A scanning electron micrograph of the $Y_1Ba_2Cu_3O_{7-\delta}$ film indicates that the grain size of the crystallites is about $0.35\mu m$ which is comparable to the film thickness. Therefore there are about 10 grains on a side of the squares sampled by the SAW, or ten junction resistances. Thus the SAW take a different percolation average of the resistors than the electrical resistance measurement does. If we assume that the randomly distributed resistors in these sub-networks have a Gaussian distribution $\phi_L$ for their critical percolation fractions $p_L$, then

$$\phi_L = \frac{1}{\sqrt{2\pi}\,\sigma_L}\exp\left[-\frac{(p_L-\bar{p}_L)^2}{2\sigma_L^2}\right]$$

The width of this distribution is

$$\sigma_L = BL^{-3/4}$$

where $B \simeq 1$. The average of $p_L$ is set equal to $p_c$, the critical percolation fraction of the whole system, and, $L \simeq 10$. Thus $\sigma_L \simeq 0.178$.

Since the average of the normal resistance $R_n(L)$ over all sub-networks is proportional to the observed $\alpha_{obs}$ and since $R_n$ is proportional to the Adler acousto electric attenuation $\alpha_{ae}$ one can invert equation 20 of ref. 10 to write another relation for the width of the distribution

$$\sigma_L = \frac{1}{ln(r_2/r_1)}\left[2\,ln\left(\frac{\alpha_{obs}}{\alpha_{ae}}\right)\right]^{\frac{1}{2}}$$

in which $r_1$ is the minimum resistance of all the resistors in the network, taken as the grain resistance. Now since $\alpha_{obs}/\alpha_{ae} \simeq 4$, and $\sqrt{r_1 r_2} = 45\Omega$ we find that $r_1 = 0.417\Omega$. And finally if we assume that $r_1$ measures the resistance of a grain of pure material, the resistivity of pure $YBa_2Cu_3O_7$ is given by $\rho = r_1\, t_{Film} = 12.5\,\mu\Omega$cm, where $t_{film}$ = thickness of film. This value is at least a factor of two lower than the lowest value that has been obtained for the resistivity of a single crystal along the $ab$ plane.

Now we turn our attention to the behavior of the attenuation and resistivity in the superconducting state. We assume that the resistors in the network become zero resistance superconducting Josephson junctions when the temperature is such that their normal state value is smaller than $r_j(T)$ given by

$$r_j(T) = \frac{\pi\hbar\,\Delta(T)}{4e^2\gamma k_B T}\tanh\left[\frac{\Delta(T)}{2k_BT}\right]$$

As before $\Delta(T)$ is the BCS gap function, with $\Delta(0) = \gamma k_B T_c = 1.76\,k_B T_c$; $e$ is the electronic charge and $\hbar$ is Planck's constant.

We shall first discuss the attenuation behavior. The individual sub-networks will become superconducting when the temperature is such that the resistance of their critical percolation fraction of Josephson resistors has gone to zero. A mean field approximation is used to calculate their resistance above this temperature.

A binary distribution is assumed

$$W_s(r) = p(T)\delta(r-0) + (1-p(T))\delta(r-R_n)$$

where $p(T)$ is the fraction of resistors that have gone to zero at $T$. The average value of the nonzero resistors is set equal to $R_n$. And, $R(T)/R_n = 1-(p(T)/p_c)$. Following the procedure in ref. 10, we find

$$\frac{\alpha(T)}{\alpha_n} = \frac{1}{\sqrt{2\pi}\,\sigma_L}\int_0^{1-p(T)}\frac{x}{x+p}\exp\left\{-\frac{(x+p-p_c)^2}{2\sigma_L^2}\right\}dx \quad (3)$$

where $\bar{p}_c = p_c + \sigma_L^2\, ln(\frac{r_2}{r_1})$. The results of performing the integration in equation 3 numerically are superimposed on the attenuation data in Figure 3. The fit appears to be good. The temperature scale has been expanded to better show the data around the transition temperature.

We now turn our attention to the resistivity. Since the dc resistance measurement samples the full network, Schmidt *et al.* have found that a binary distribution function does not provide as good a fit as one that takes into account the full distribution given by

$$W_s(r) = p(T)\delta(r) + [1-p(T)]W_n(r)$$

A mean field approximation then gives[11]

$$\frac{R(T)}{R_n} = \left(\frac{r_2}{r_1}\right)^{p_2}\left[\frac{(\frac{r_2}{r_1})^{1-p_1}-1}{(\frac{r_2}{r_1})^{p_1}-1}\right] \quad (4)$$

where $p_1 = \frac{1}{2-2p(T)}$ and $p_2 = p(T)p_1$. The results of calculating $R(T)$ according to equation 4 are shown, together with the data, in Fig. 4. Again, the fit to the data appears to be good.

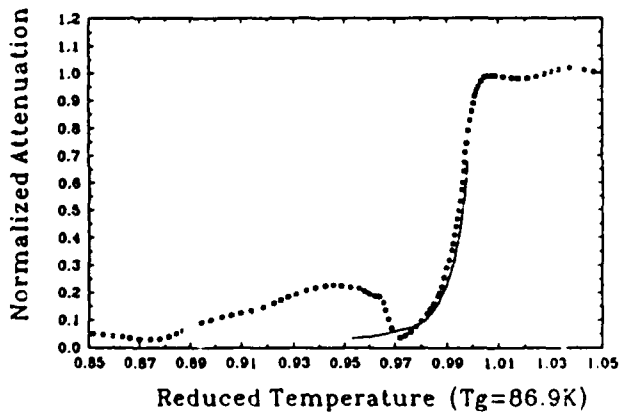


Figure 3 Comparison of normalized attenuation data with results (solid line) obtained from percolation model.

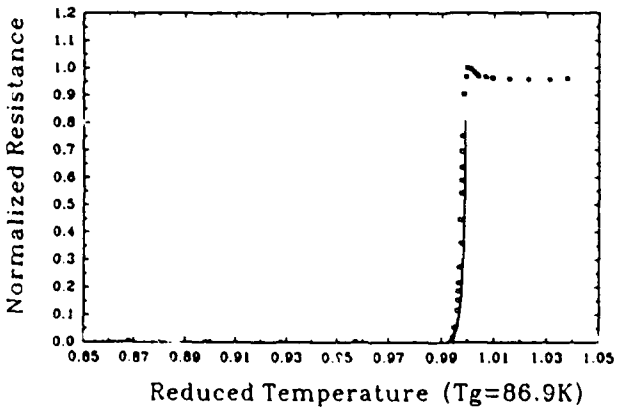


Figure 4 Comparison of normalized sheet resistivity with results (solid line) obtained from percolation model.

## 4. Discussion and Summary

We have presented SAW measurements on a Nb film and a $YBa_2Cu_3O_7$ film. Electron phonon interaction was the source of the attenuation mechanism in the Nb film. A BCS decrease in attenuation was observed below $T_c$, which was fit with a zero temperature energy gap of 3.52 $k_BT_c$. The change in attenuation from the normal state to the superconducting state was used to determine the electron mean free path, whose value was about twice as large as that found from the electrical resistivity measurements. This is not an unexpected result if the film has textured domains, because then the electrical resistivity will have an additional contribution due to the interface resistance between the domains. This same resistance does not contribute to the ultrasonic attenuation since the latter is proportional to the electron mean free path and therefore the longest mean free path, the one within the domains, will make the major contribution to the attenuation.

A percolation model was used to analyze both the acousto electric SAW attenuation and the sheet resistivity of a $YBa_2Cu_3O_7$ film. This model gave a reasonably good fit to the temperature dependence of both sets of data in the superconducting state. More importantly, a comparison of the sheet resistivity with the change in attenuation between the normal and superconducting states yielded a value for the resistivity of pure $YBa_2Cu_3O_7$ crystals along the *ab* plane. This value of 12.5$\mu\Omega$cm is about a factor of two better than what has been reported in the literature at present. Therefore, we believe that SAW attenuation measurements in textured films can provide important information about the quality of the material being investigated.

The research at UWM was supported by the Office of Naval Research.

## References

1. A. I. Braginski, J. R. Gavaler and K. Schulze, "Formation of A15 Phase in Epitaxial and Polycrystalline Nb-Sn Diffusion Couples", *Advances in Cryogenic Engineering Materials* Vol. 32, pp. 585-592 (Ed. R. P. Reed and A. F. Clark, Plenum Press, New York, 1986).

2. M. Levy, "Ultrasonic Attenuation in Superconductors for $ql < 1$", *Phys. Rev.* 131, 1497-1500 (1963).

3. M. Tachiki, H. Salvo, Jr., D. A. Robinson and M. Levy, "Ultrasonic Mean Free Path in a Granular Aluminum Film", *Solid State Comm.* 17, 653-656 (1975).

4. J. Bardeen, L. N. Cooper and J. R. Schrieffer, "Theory of Superconductivity", *Phys. Rev.* 108, 1175-1204 (1957).

5. P. W. Anderson, "Theory of Dirty Superconductors", *J. of Phys. and Chem. of Solids* 11, 26-30 (1959).

6. Harry L. Salvo, Jr., "Surface Acoustic Wave Investigation of a $Nb_3Ge$ Film", Ph.D. Thesis, University of Wisconsin-Milwaukee, 1979 (unpublished).

7. D. R. Snider, H. P. Fredricksen and S. C. Schneider, "Surface Acoutic Wave Attenuation by a Thin Film", *J. Appl. Phys.* 52(5), 3215-3222 (1981).

8. A. Hohler, D. Guggi, H. Neeb and C. Heiden, "Fully Textured Growth of $Y_1Ba_2Cu_3O_{7-\delta}$ Films by Sputtering on $LiNbO_3$ Substrates", *Appl. Phys. Lett.* 54(11), 1066-1067 (1989).

9. R. Adler, "Simple Theory of Acoustic Amplification" *IEEE Trans. Sonics and Ultrasonics*, SU 18, 115-118 (1971).

10. M. Levy, J. Schmidt, A. Schenstrom, M. Revzen, A. Ron, B. Shapiro and C. G. Kuper, "Ultrasonic Attenuation and the Resistive Transition in a Superconducting Granular Lead Film", *Phys. Rev.* B43, 1508-1513 (1986).

11. J. Schmidt, M. Levy and A. F. Hebard, "Ultrasonic Investigation of Granular Superconducting Films", *Phys. Rev.* (to be published).

12. V. Ambegaokar, B. I. Halperin and J. S. Langer, "Hopping Conductivity in a Disordered System" *Phys. Rev.* B24, 2612-2620 (1971).

# LARGE-AREA YBCO FILMS FOR MICROWAVE APPLICATIONS*

**APPENDIX 3**

J. Talvacchio, M. G. Forrester, J. R. Gavaler, and T. T. Braggins
Westinghouse Science & Technology Center
Pittsburgh, PA 15235

## Abstract

We have developed techniques for the in-situ deposition of epitaxial YBCO films on two-inch diameter wafers of $LaAlO_3$(001) or $\alpha$-$Al_2O_3$(1$\bar{1}$02) with a Sr-doped $La_2CuO_4$(001) (LSCO) buffer layer. The inductively-measured transition temperature varied within the values of 91.1 ± 0.5K across the surface of the $LaAlO_3$ wafer, and 90.7 ± 0.4K across the buffered sapphire wafer. The epitaxial LSCO buffer layer acted not only as a barrier to diffusion of Al into the YBCO films, but improved the YBCO(005) x-ray rocking curve widths from 4° for films grown on bare sapphire to 1.2° for films on the LSCO-buffered sapphire. The typical buffer-layer thickness was 40 nm although layers as thin as 4 nm appeared to be equally effective. The transport critical current density was greater than $10^6$ A/cm$^2$ at 77 K for films on buffered sapphire. At 8.8 GHz and 4.2K, the rf surface resistance was lower than that of gold, indicating that the films on sapphire will be useful in large-area UHF applications.

## Introduction

In a recent review of materials issues in the fabrication of microwave devices from high temperature superconductors (HTS),[1] the requirement that was common to all applications was a low rf surface resistance, $R_s$. Each microwave component considered individually also required either a larger area, lower dielectric constant, or lower dielectric loss than is available from $LaAlO_3$ substrates, the best substrate alternative at present. In a practical subsystem, integration of components places an additional demand on the size and uniformity of high-quality HTS films.

Sapphire substrates for YBCO films have received a great deal of attention since they fulfill the requirements of large size, low dielectric constant, and low dielectric loss, with good mechanical properties. However, since sapphire has a poor lattice match to YBCO and Al diffuses into YBCO readily at high (≥750°C) temperature, epitaxial buffer layers have been used as a diffusion barrier and to grade the lattice parameter. Buffer layers of MgO(100),[2-4] $SrTiO_3$(100),[5] and $LaAlO_3$(100)[6] have been investigated to date – all deposited on the (1$\bar{1}$02) face of sapphire (R-plane). These buffer layer materials share the fact that – in bulk, single-crystal form – they are the popular substrates for HTS film growth.

In this paper, we describe the properties of epitaxial YBCO films grown on sapphire with a new buffer layer material, Sr-doped $La_2CuO_4$ (LSCO). The YBCO film properties are compared with those of films grown on $LaAlO_3$. The uniformity of film properties is presented for YBCO grown on two-inch diameter substrates of each type.

The use of bulk $La_2CuO_4$ as a substrate material for YBCO films has been reported just once where YBCO was screen-printed on a polycrystalline $La_2CuO_4$ ceramic to produce a poor-quality film.[7] In our work, the $La_{2-x}Sr_xCuO_4$ buffer layers had $x \simeq 0.2$, a c-axis growth orientation, and the a and b axes were aligned with the sapphire substrate in the plane of the film.

* Supported in part by AFOSR
Contract No. F49620-88-C-0043.
Manuscript received September 24, 1990.

In the a-b plane, there is a close lattice match between LSCO and YBCO. The lattice constant of LSCO is nearly independent of x. LSCO is tetragonal with $a_o$ = $b_o$ = 0.3797 nm at the YBCO deposition temperature of ~700°C. At this temperature, YBCO is also tetragonal with an a-b lattice constant +2.4% larger than LSCO. There is a similar mismatch of +2.0% between YBCO and $LaAlO_3$.

## Film Deposition

Both LSCO and YBCO films were deposited by 90° off-axis dc magnetron sputtering from single, stoichiometric targets. The sputter gas was typically 150 mtorr Ar and 50 mtorr $O_2$. Our results with this technique and the effects of varying the sputter-gas composition were published previously.[8] The optimum deposition temperature for LSCO was 620-680°C. The YBCO was deposited at 680-720°C. The details of the deposition-chamber configuration were also published.[9] The functions of the deposition system which were specifically used in this work were the capabilities of mounting a two-inch wafer on the 5.7 cm diameter circular substrate holder and rotating the holder about its symmetry axis. Silver paint was used for both mechanical and thermal anchoring of the substrates whether a series of small chips or a single large wafer was used. After deposition, the chamber was filled to 20 torr $O_2$ and the samples were first cooled to 400°C for a 15-20 min soak and then to room temperature.

## Electrical Properties

Data on the critical temperature, $T_c$, critical current density, $J_c$, and rf surface resistance for our YBCO films deposited on $LaAlO_3$ substrates by off-axis sputtering were published in Ref. 9. Examples of $T_c$ and $J_c$ for YBCO grown on LSCO-buffered sapphire substrates are shown in Fig. 1 and Fig. 2. The normal-state resistivity of the sample in Fig. 1 was characteristic of samples placed at the outer 5 mm edge of the substrate holder during growth. These samples had resistivity values at room temperature approximately 25% higher than the $\rho$(300K) ≃ 250 μΩ-cm obtained over the rest of the sample holder, presumably due to a lower substrate

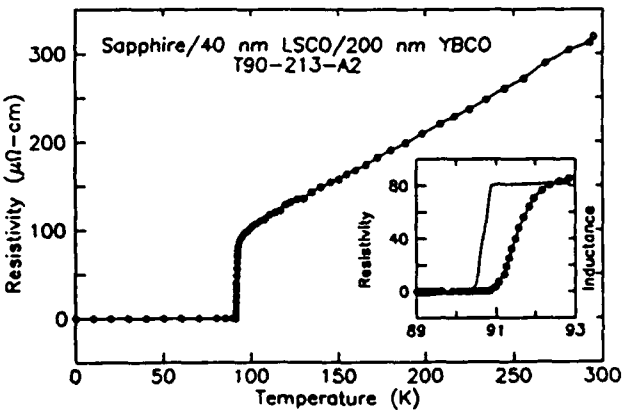


Figure 1. Resistivity for a YBCO(001) film grown on LSCO-buffered sapphire. The inset figure compares the resistive transition (open circles) to the transition measured by the change of inductance of a coil placed against the film (solid line).

0018-9464/91/0300-0978$01.00 © 1991 IEEE

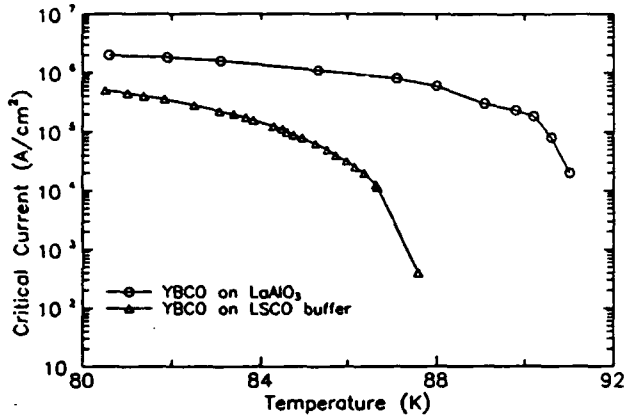


Figure 2. Transport critical current density measured in self-field plotted as a function of temperature for YBCO films deposited on $LaAlO_3$ and LSCO-buffered sapphire. The $T_c$'s (R=0) for these films were 91.2K and 88K, respectively. In both cases, the film was patterned into a 25 $\mu$m wide bridge with voltage taps spaced 1 mm apart. There was no change in $T_c$ from patterning the films in a phosphoric acid etch. A 5 $\mu$V criterion ($\rho < 10^{-8}$ $\Omega$-cm for $J_c > 10^4$ A/cm$^2$) was used to define $J_c$. The film on sapphire had $J_c > 10^6$ A/cm$^2$ for temperatures less than 78K.

temperature. The temperature dependence of the resistivity was independent of sample position with $\rho$(T>100K) extrapolating to zero resistivity at zero kelvin and superconducting transition widths of ~1K. The ac susceptibility transition (inset in Fig. 1) was typically 1K wide and occurred at 0.5 to 1K lower temperature than the resistive transition.

The critical current density data in Fig. 2 represents the highest such data obtained for our YBCO films grown on $LaAlO_3$ and sapphire. Few such measurements have been made since the dc current-carrying capacity is not directly related to the suitability of films for microwave applications. However, the dc critical current at T > 77K was an indicator of film homogeneity that generally correlated with the widths of the resistive and inductive superconducting transitions. Fig. 2 shows that YBCO films on both types of substrates had $J_c = 10^5$ A/cm$^2$ within a few kelvin of the superconducting transition, and $J_c > 10^6$ A/cm$^2$ at 77K.

The rf surface resistance of YBCO on buffered sapphire (LSCO 30 nm thick) was measured at 4.2K by two different techniques, an 8.8 GHz all-YBCO microstrip resonator and a 4 GHz stripline resonator with a Nb resonator bar.[1] In both cases, the film served as a ground plane with the substrate turned so it was inside the resonator. In both cases, $R_s$ was lower than that of Au. The calculation of $R_s$ from the measured Q was more straightforward for the stripline resonator (although the unloaded Q was always assumed to equal the loaded Q). The measured Q was 5.7k for YBCO on sapphire corresponding to $R_s$ = 6 m$\Omega$, and Q was 3.8k for Au corresponding to $R_s$ = 8 m$\Omega$. In contrast, $R_s$ for our YBCO on $LaAlO_3$ was < 1 m$\Omega$ at 77K and 10 GHz. Since $R_s$ scales with frequency as $f^2$ for (most) YBCO, and is proportional to $f^{1/2}$ for a normal metal, the $R_s$ of YBCO on sapphire represents a substantial improvement over Au at UHF despite its marginal improvement at X-band.

Substantially better $R_s$ results at 4.2K have been reported for YBCO grown on $SrTiO_3$-buffered sapphire.[5] In those measurements, rf currents were concentrated at the free surface of the film rather than the substrate interface. Both LSCO and $SrTiO_3$ are lossy materials in the vicinity of 77K which can lower the effective surface resistance of YBCO in the types of rf measurements we performed. However, by keeping the buffer layer thin, rf losses can be made negligible. Although the typical LSCO buffer layer thickness used in this study was 40 nm, YBCO films grown on buffer layers as thin as 4 nm appeared to be equivalent to YBCO on the thicker buffer layers.

The LSCO buffer layers grown by off-axis sputtering were significant by themselves.[9] They were grown epitaxially on $SrTiO_3$ and $LaAlO_3$ substrates in addition to sapphire. Typical $T_c$'s (R=0) for LSCO films on these substrates were 30K, 27K, and 21K, respectively. The highest $T_c$'s obtained, 31K, were the highest reported for films in this materials system.[10] A transport critical current density of $7\times10^4$ A/cm$^2$ at 4.2K was the highest reported for this material.

## Structural Properties

X-ray diffractometer data for an LSCO film on sapphire and a YBCO film on buffered sapphire are shown in Fig. 3. In both cases, the c-axis orientation exhibited in the figure was representative of all of the films. LSCO deposited on the A-plane of sapphire [$\alpha$-$Al_2O_3(11\bar{2}0)$] was also highly oriented with roughly equal fractions of a-axis and c-axis orientation and no (103) x-ray peak, the largest peak observed in powder patterns.

The diffraction data in Fig. 3 proved only that the films were highly oriented in the growth direction. Fig. 4 contains RHEED patterns obtained from the surfaces of a LSCO film on sapphire and a YBCO film grown on buffered sapphire. The RHEED patterns showed that the films were also highly oriented in the

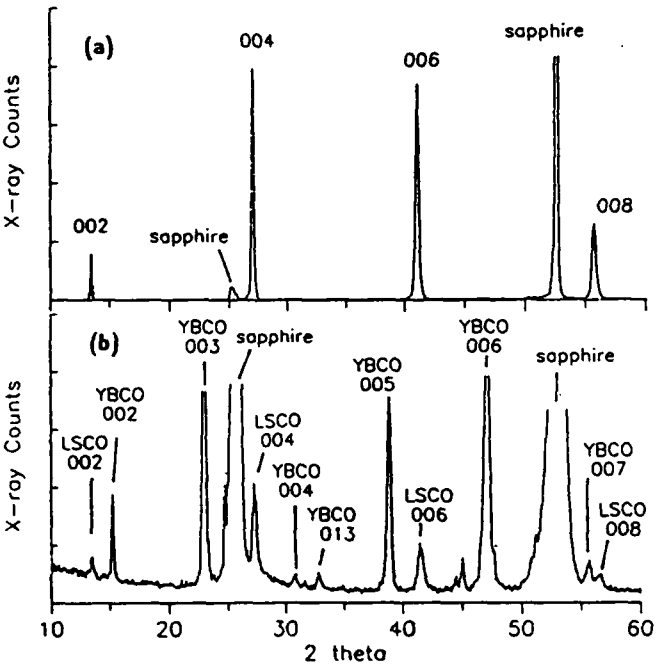


Figure 3. X-ray diffraction data for (a) a 300 nm thick LSCO(001) film grown on $\alpha$-$Al_2O_3(1\bar{1}02)$, and (b) a 100 nm thick YBCO(001) film grown on a 30 nm LSCO buffer layer on sapphire. The LSCO film in each case had an exclusively c-axis orientation. The YBCO film in (b) had a predominantly c-axis orientation. Small YBCO(013) and YBCO(200) diffraction peaks indicated the presence of some misaligned grains.

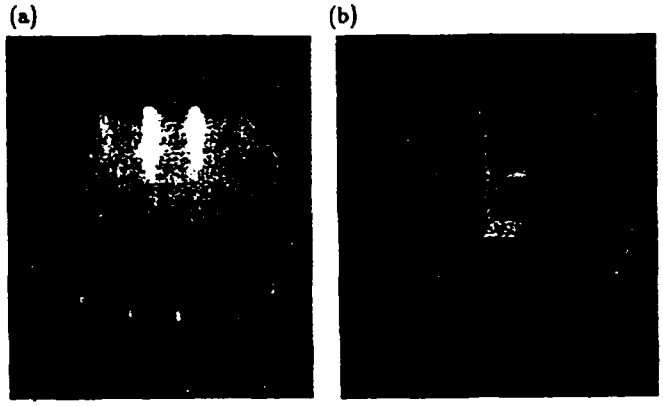


Figure 4. Ex-situ 9 kV RHEED patterns from the surfaces of (a) a LSCO(001) film on sapphire, and (b) a YBCO(001) film grown on LSCO-buffered sapphire, showing that the films grew epitaxially. In both cases the electron beam was parallel to [010] directions in the films.

a-b plane, that is, that they grew epitaxially. Both RHEED patterns in Fig. 4 were obtained after the films were briefly exposed to the atmosphere during a transfer from one vacuum system to another. The LSCO RHEED pattern was recorded after cleaning the surface by heating the sample to 500°C in 20 torr $O_2$ in the RHEED vacuum chamber. The YBCO pattern was recorded without surface cleaning.

Although the RHEED patterns in Fig. 4 were readily obtained, LEED patterns could not be obtained for either LSCO grown on sapphire or YBCO grown on buffered sapphire. LEED patterns were obtained for both LSCO and YBCO grown on $LaAlO_3$ or $SrTiO_3$ substrates indicating greater crystalline order in these films than in the ones grown on sapphire.

A quantitative comparison of the crystalline order of epitaxial YBCO deposited on various substrates is

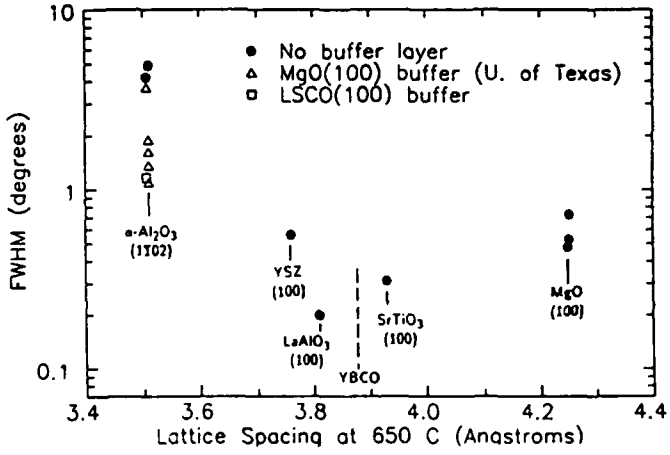


Figure 5. X-ray rocking curve widths for the (005) peak of epitaxial YBCO films grown on various substrates. The data is seen to correlate with the difference between the lattice constant of YBCO and that of the substrate at the deposition temperature of 700°C. For sapphire and yttria-stabilized zirconia (YSZ), the lattice spacing is the length of a diagonal in the two-dimensional surface lattice that lies parallel to a <100> direction in the YBCO film. The data on MgO-buffered sapphire is from Ref. 11.

presented in Fig. 5 where the YBCO(005) x-ray rocking curve width (full width at half maximum) is plotted as a function of the substrate lattice constant at 700°C. The lattice constant of YBCO is shown as a dashed line. The narrowest rocking curves were measured for films grown on substrates with the smallest lattice mismatch with YBCO.

The rocking curve width was also dependent on the film thickness. Most of the YBCO films in Fig. 5 were 100 nm thick. The exceptions were the films on bare sapphire (400-500 nm) and MgO-buffered sapphire (120-300 nm) from Ref. 11. The rocking curve width of the 100 nm thick YBCO film on LSCO-buffered sapphire was just 1.17° – substantially smaller than for YBCO on bare sapphire – but still large compared with YBCO on $LaAlO_3$ or $SrTiO_3$.

We speculate that $R_s$ for YBCO on sapphire will not be reduced unless the rocking curve width is reduced. One possible route is to increase the buffer layer thickness. The rocking curve widths of the (006) peak of 800 nm thick LSCO films were 0.68°, 0.18°, and 0.28° for sapphire, $LaAlO_3$, and $SrTiO_3$ substrates, respectively. For such thick buffer layers to be practical, the Sr content should be reduced or eliminated to have an insulator instead of a normal conductor at 77K. Surface roughness is not a limitation on buffer layer thickness. Even the 800 nm thick LSCO films were very smooth. The appearance of multiple Laue zones in the RHEED pattern in Fig. 4(a) gives a clear indication of this smoothness.

## Film Uniformity

Fig. 6 shows the transition temperature and indicates the location on the substrate holder of five YBCO films grown on $LaALO_3$ chips without rotating the holder. The resistive transition was defined by R=0. The inductive transition was defined as the temperature where 50% of the change in susceptibility had occurred. The transitions were all qualitatively like the one shown in Fig. 1. The variation in $T_c$ across the substrate holder was less than 1K. The excellent uniformity displayed in Fig. 6 is similar to results obtained in Refs. 9 and 12 with individual chips placed on a stationary two-inch diameter holder.

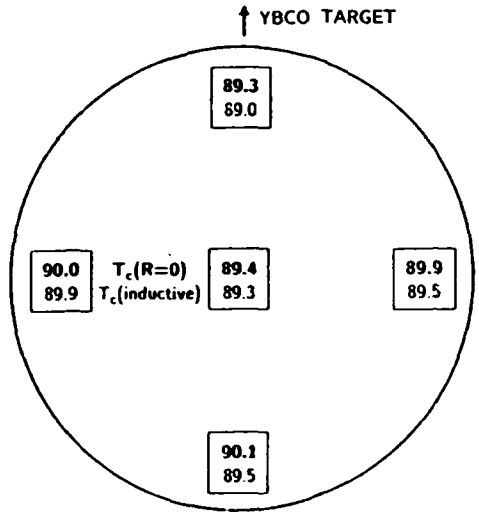


Figure 6. The resistive and inductive transition temperatures of YBCO films on five $LaAlO_3$ chips spaced across a two-inch diameter area and coated without rotating the substrate holder. The variation in $T_c$ was less than 1K.

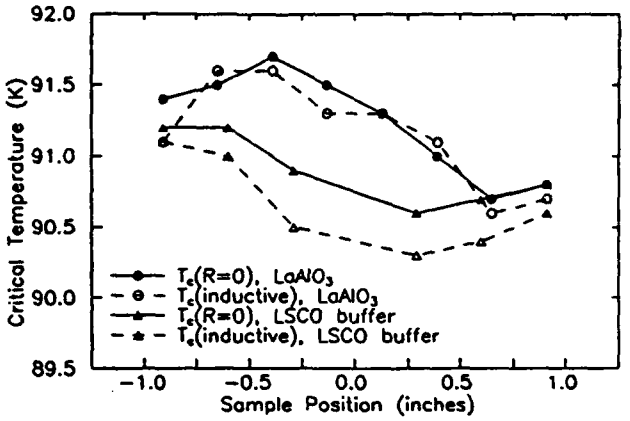


Figure 7. Resistive and inductive transition temperatures measured on a series of chips cut from two-inch diameter, YBCO-coated $LaAlO_3$ and buffered sapphire wafers and plotted as a function of distance from the center of the wafer.

In Fig. 7, the resistive and indcutive transition temperatures are plotted as a function of distance from the center of a two-inch diameter wafer of $LaAlO_3$ or LSCO-buffered sapphire. The YBCO films were deposited before dicing the wafer and the substrate holder was rotated during deposition. The film on $LaAlO_3$ was 150 nm ±10% thick everywhere on the wafer. The variation of ±10% was due to the difficulty in measuring accurate film thicknesses on heavily-twinned $LaAlO_3$. The inductively-measured transition temperature varied within the values of 91.1 ± 0.5K across the surface of the $LaAlO_3$ wafer, and 90.7 ± 0.4K across the buffered sapphire wafer. Assuming a constant film thickness across the wafer, the room-temperature resistivity was in the range of 260 ± 20 μΩ-cm over all but the outer 5 mm of the wafer for both types of wafers. The outer 5 mm ring had a resistivity approximately 25% higher at all temperatures.

## Conclusions

- LSCO(001) films as thin as 40 angstroms grown epitaxially on R-plane sapphire are effective buffer layers for growth of YBCO. It is not clear at this point whether LSCO is superior to $SrTiO_3$ or MgO buffer layers. It has an *a priori* advantage over MgO in having a closer lattice match to YBCO.

- Although $T_c$ and $J_c$ are high for YBCO on buffered sapphire, $R_s$ is only low enough for practical applications at UHF. However, the need for large substrates is particularly acute in UHF applications since device size is often determined by wavelength.

- Rocking curve widths show that YBCO is not as well aligned on buffered sapphire as on single-crystal perovskite substrates. The mosaic spread in the growth direction and in the plane of YBCO films is perhaps the most important parameter in determining rf surface resistance. The YBCO(005) x-ray rocking curve width improved from 4° for films grown on bare sapphire to 1.2° for films on the LSCO-buffered sapphire.

- Excellent uniformity has been obtained for growth of YBCO on 2-inch diameter $LaAlO_3$ and sapphire wafers. The capability of producing films on this scale not only increases the possible size of microwave components but permits them to be integrated on a single wafer.

## Acknowledgments

The authors acknowledge the assistance of J. H. Uphoff, J. C. Brown, S. J. Pieseski, and C. L. Jones with film patterning and dc measurements; G. R. Wagner, S. H. Talisa, B. R. McAvoy, D. H. Watt, and G. B. Draper with the measurements of surface resistance; N. J. Doyle and A. M. Stewart with x-ray measurements; and T. J. Mullen with EDS measurements. We also acknowledge the collaboration with A. B. Berezin and A. L. de Lozanne of the University of Texas which helped us to compare LSCO with MgO buffer layers.

## References

1. J. Talvacchio and G. R. Wagner, "High-$T_c$ Film Development for Electronic Applications," in Superconductivity Applications for Infrared and Microwave Devices, SPIE Proc. Vol. 1292, Bellingham, Washington, 1990.

2. E. J. Tomlinson, Z. H. Barber, G. W.Morris, R. E. Somekh, and J. E. Evetts, "Optimization of Thin-Film $YBa_2Cu_3O_7$ Deposition by DC Sputtering onto Sapphire Substrates," *IEEE Trans. Magn.* 25, 2530-2533, 1989.

3. J. Talvacchio, G. R. Wagner, and H. C. Pohl, "$YBa_2Cu_3O_7$ Films Grown on Epitaxial MgO Buffer Layers on Sapphire," *Physica C* 162-164, 659-660, 1989.

4. A. B. Berezin, C. W. Yuan, and A. L. de Lozanne, "$Y_1Ba_2Cu_3O_{7-x}$ Thin Films Grown on Sapphire with Epitaxial MgO Buffer Layers," *Appl. Phys. Lett.* 57, 90-92, 1990.

5. K. Char, N. Newman, S. M. Garrison, R. W. Barton, R. C. Taber, S. S. Laderman, and R. D. Jacowitz, "Microwave Surface Resistance of Epitaxial YBCO Thin Films on Sapphire," *Appl. Phys. Lett.* 57, 409-411, 1990.

6. A. E. Lee, C. E. Platt, J. R. Burch, R. W. Simon, J. P. Goral, and M. M. Al-Jassim, "Epitaxially-Grown Sputtered $LaAlO_3$ Films," submitted to *Appl. Phys. Lett.*, 1990.

7. U. V. Varadaraju, G. V. Subba Rao, K. D. Chandrasekaran, and A. Baradarajan, "Superconductivity Behaviour in Screen-Printed $YBa_2Cu_3O_7$ Films," *Thin Solid Films* 164, 119-121, 1988.

8. J. R. Gavaler and J. Talvacchio, "Optimization of $T_c$ and $J_c$ in Sputtered YBCO Films," *Physica B* 165-166, 1513-1514, 1990.

9. J. Talvacchio, M. G. Forrester, J. R. Gavaler, and T. T. Braggins, "YBCO and LSCO Films Grown by Off-Axis Sputtering," in Science and Technology of Thin Film Superconductors II, edited by R. McConnell and S. A. Wolf, Plenum, New York, 1990.

10. M. Suzuki, "Hall Coefficients and Optical Properties of $La_{2-x}Sr_xCuO_4$ Single-Crystal Thin Films," *Phys. Rev. B* 39, 2312-2317 1989.

11. A. B. Berezin, C. W. Yuan, and A. L. de Lozanne, "YYBCO Thin Films on Sapphire with an Epitaxial MgO Buffer," submitted to *IEEE Trans. Magn.*, 1990.

12. N. Newman, K. Char, S. M. Garrison, R. W. Barton, R. C. Taber, C. B. Eom, T. H. Geballe, and B. Wilkens, "YBCO Superconducting Films with Low Microwave Surface Resistance over Large Areas," *Appl. Phys. Lett.* 57, 520-522, 1990.

# Critical parameters in the single-target sputtering of $YBa_2Cu_3O_7$

J. R. Gavaler, J. Talvacchio, T. T. Braggins, M. G. Forrester, and J. Greggi
*Westinghouse Science and Technology Center, 1310 Beulah Road, Pittsburgh, Pennsylvania 15235*

(Received 2 May 1991; accepted for publication 16 July 1991)

**APPENDIX 4**

The critical parameters in the single-target magnetron sputtering of $YBa_2Cu_3O_7$ have been identified and sufficiently optimized to allow the reproducible deposition of films with $T_c$'s of $>90$ K and $J_c$'s of $\geq 10^6$ A/cm$^2$ at 77 K. It was found that during film growth the bombardment of the $YBa_2Cu_3O_7$ by energetic particles must be minimized and also a stronger oxidizing agent than molecular oxygen must be present to obtain films with these properties. Otherwise, films are deposited that, by x-ray diffraction and energy dispersive x-ray spectroscopy analyses, are indistinguishable from the highest-$T_c$ 1:2:3 stoichiometric material but which have critical temperatures of $<90$ K. Films need not have 1:2:3 overall stoichiometry to have optimum superconducting properties. In such cases the excess elements are present as second-phase particles.

## I. INTRODUCTION

Among the high-$T_c$ oxide superconductors, the most studied and at the present time the most important for electronic applications is $YBa_2Cu_3O_7$ (YBCO). A variety of techniques has been reported for preparing this compound in thin-film form. One of the most successful of these has been single-target sputtering. In the past few years there have been several papers describing the preparation and properties of YBCO films made by this technique. (See Refs. 1–5 for examples of reports on single-target sputtering). In these papers, however, there are significant differences reported in the properties of the sputtered YBCO films. Also, there is presently no consensus regarding the optimum experimental procedures for depositing the highest-quality films. This perhaps should not be surprising since in sputtering there are very many experimental variables that can and often do influence film quality. These variables tend to be closely interdependent, which can make their identification and optimization a very difficult problem. In this paper we report on what we believe to be the most important variables in the single-target sputtering of YBCO. We also report on the conditions that we have found for depositing YBCO with optimum superconducting properties. Some of the data discussed in this paper have been reported previously in a preliminary or abbreviated form.[6,7]

## II. EXPERIMENTAL PROCEDURE

All of the sputtering experiments were done in a nonbaked vacuum chamber that had a base pressure in the low $10^{-6}$-Torr range. Films were deposited from a rf magnetron sputter gun manufactured by US, Inc. This gun was used with either rf or dc power. Two types of pressed and sintered sputtering targets were used, either orthorhombic or tetragonal $YBa_2Cu_3O_x$. In both cases the dimensions were 2 in. diameter and a 0.25 in. thick. Two target-substrate configurations were investigated. These are illustrated in Fig. 1. The substrate holder used was a 5.7-cm-diam nickel block mounted on a manipulator that could be positioned in either of the two orientations shown in this figure. The substrates were single-crystal $SrTiO_3$ (100) and (110), $LaAlO_3$ (100), MgO (100), and $R$-plane sapphire. The nickel block temperature was determined by a thermocouple located in a well in the back of the block. The relationship of this temperature to the substrate surface temperature was determined using an infrared pyrometer. The accuracy of the surface temperature reported here is estimated to be $\pm 20$ °C. The sputtering gases were oxygen, argon, and water vapor mixed in various combinations. The sputtering gas was continuously pumped from the system during the deposition process. Following deposition, the films were annealed *in situ* in pure oxygen for 20 min at 400 °C and then allowed to cool to room temperature before being removed from the system. An oxygen pressure of 25 Torr was found to be adequate for this low-temperature annealing. The use of higher pressures produced no improvement in film properties.

Film compositions were determined by energy dispersive x-ray spectroscopy (EDS). The accuracy and reproducibility of the EDS analyses were approximately $\pm 2$ at. %. Structural analyses were by x-ray diffraction, transmission electron microscopy (TEM), and scanning electron microscopy (SEM). $T_c$'s were measured both resistively, using the standard van der Pauw method, and also inductively. $J_c$'s were determined by passing current through a 25-$\mu$m-wide by 1-mm-long bridge and observing the onset of resistance. A 1-$\mu$V microvolt criterion was used to define $J_c$ which is equivalent to $< 10^{-10}\ \Omega$ cm over most of the temperature range employed.

## III. RESULTS AND DISCUSSION

A major difficulty in reporting data on any sputtering process is the large number of interdependent parameters that can and often do influence the quality of the deposited films. To try to minimize this problem, we will begin our discussion by listing a specific (but not unique) set of conditions that was found to produce high-quality YBCO films. Starting from this base point we will then report on the effect of changing each of the individual parameters. This starting set of conditions is shown in Table I. Under

 0021-8979/91/084383-09$03.00 © 1991 American Institute of Physics 

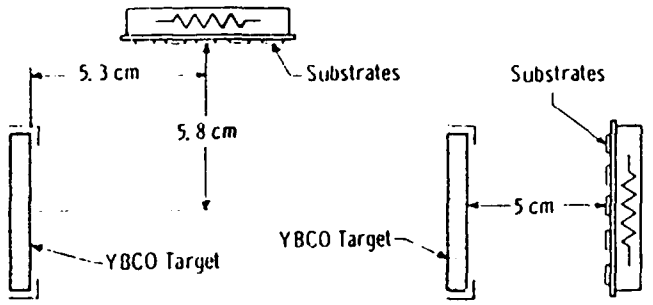


FIG. 1. Schematic drawing illustrating the off-axis (left-hand side) and the parallel (right-hand side) target-substrate configurations employed in this work.

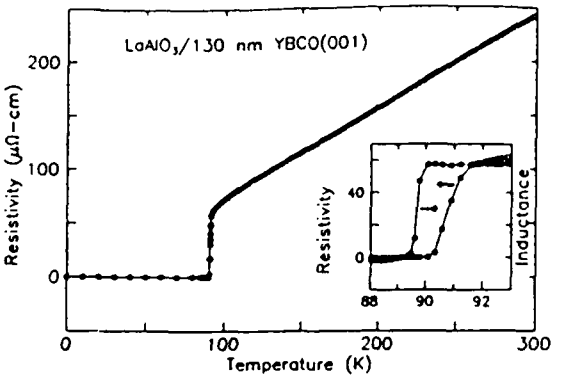


FIG. 2. The resistive ($R = 0$) and inductive critical temperatures of a 130-nm YBCO film made under the conditions listed in Table I.

these conditions the deposition rate was a ~20 nm/h. The deposited films were found to be *c*-axis oriented with a lattice parameter of 1.170 nm. TEM analysis indicated that the in-plane orientation was the same throughout the ~1-$mm^2$ area that was scanned indicating that the film had grown epitaxially.

The critical temperature and the critical current density of films grown under the above conditions are shown in Figs. 2 and 3. The properties of films down to a thickness of ~20 nm were similar. At thicknesses of ~10 and ~7.5 nm, values as high as 85 and 75 K, respectively, were obtained. Films of this quality were deposited over the entire area of the substrate holder.

We will now consider the effect of changing each of the sputtering parameters listed in Table I. Unless specifically noted otherwise, all of the conditions will be those shown in the table with the exception of the variable being investigated.

### A. Target-substrate configuration

Although eventually $T_c$'s of >90 K were obtained with both of the two substrate-target configurations studied, initially when using the conditions listed in Table I, with the exception of the substrate-target configuration that was changed to the parallel orientation (see Fig. 1), we obtained films with $T_c$'s of only ~75 K. EDS analyses of these films showed that they had the same 1:2:3 cation stoichiometry as those grown in the off-axis configuration. From x-ray data the films were also found to have grown with *c*-type epitaxy and had lattice parameters similar to the >90-K off-axis films. X-ray data for a representative 90-K film and a 75-K film are shown in Fig. 4. These data are for films grown on MgO substrates which exhibited superconducting properties similar to those on $LaAlO_3$. $T_c$'s of 90 K were ultimately achieved in films grown in the parallel orientation by increasing the sputtering gas pressure to over 400 mTorr. A detailed description of the effect of the sputtering gas on superconducting properties will be given in the section dealing with that variable.

Very early in the development of sputtering as a means for preparing YBCO films it was reported[8] that the presence of negative oxygen ions in the plasma could produce backsputtering from the depositing films. Since Cu and Ba tended to backsputter preferentially, early YBCO films often did not have 1:2:3 stoichiometry. This lack of proper cation stoichiometry was given as the reason why these films had poor superconducting properties. Solutions to this problem were accomplished by increasing the sputtering gas pressure and by changing the target-substrate orientation.[1-5] Both of these two techniques lower the energies of the particles bombarding the substrate and prevent the preferential backsputtering of Cu and Ba. The present results show, however, that even when particle bombardment is minimized sufficiently that proper cation

TABLE I. Set of sputtering conditions for preparing high-quality YBCO films.

| | |
|---|---|
| Target-substrate configuration | 90° off-axis |
| Power mode | dc |
| Sputtering target | newly fabricated pressed and sintered orthorhombic structure YBCO |
| Gas composition | argon/oxygen |
| Gas pressure | 250 mTorr argon, 50 mTorr oxygen |
| Substrate temperature | 670 °C |
| Substrate material | single-crystal $LaAlO_3$ |
| Sputtering voltage | 175 V |
| Sputtering current | 0.3 A |

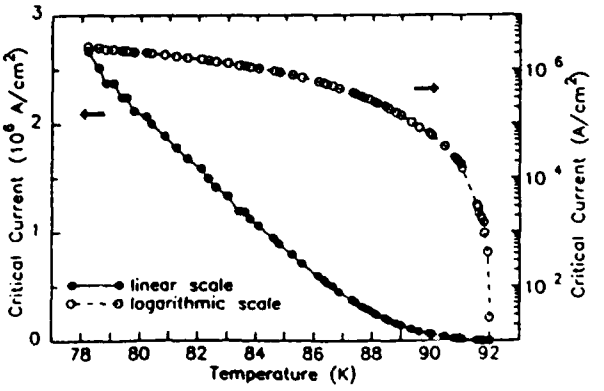


FIG. 3. Critical current density vs temperature data for a 150-nm YBCO film made under the conditions listed in Table I.

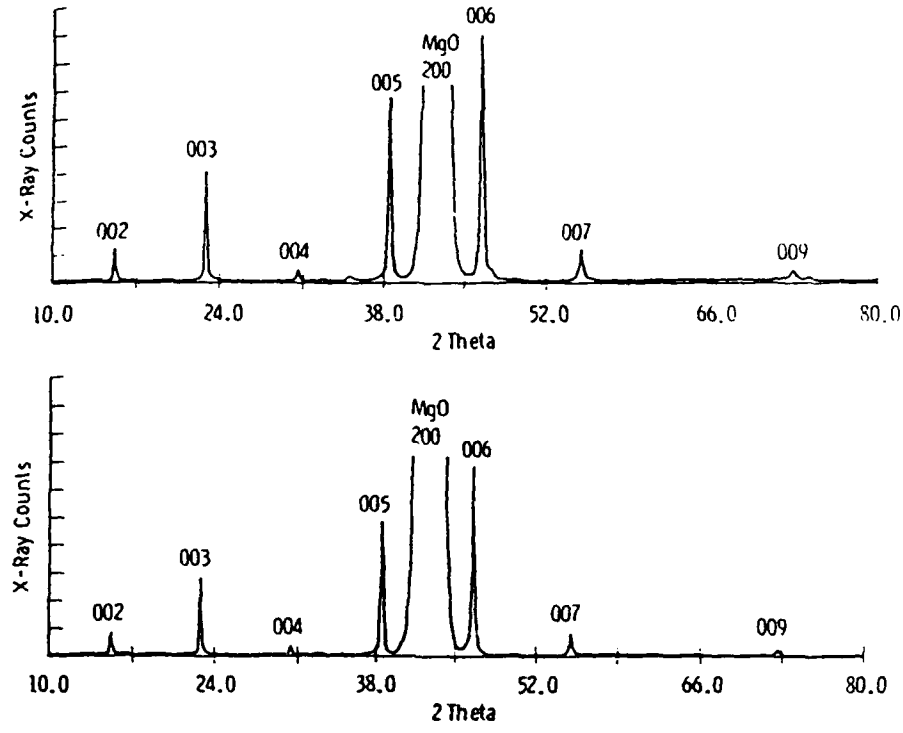


FIG. 4. X-ray-diffraction data on a film grown under conditions of Table I (lower trace) and data on another film deposited under the same conditions except that a parallel substrate-target configuration was used (upper trace). The *c*-axis epitaxy and lattice parameters (1.170 nm) of the two films are the same despite a difference in $T_c$ of 15 K.

stoichiometry is maintained, films can be produced which still have inferior properties.

Another example of material which was found to have 1:2:3 stoichiometry but which did not have optimum properties is films deposited near the outside periphery of the substrate holder when using the parallel orientation. Whereas in the off-axis configuration, under the conditions of Table I, ~90-K films were obtained over the entire 2-in.-diam area of the substrate holder, similarly high $T_c$'s were obtained, when using the parallel configuration and a total gas pressure of 400 mTorr, only in the center approximately 1-in. area. Films outside this center region had $T_c$'s ~15 K lower. All of the films, regardless of location, had 1:2:3 stoichiometry and there was no correlation between $T_c$'s and the lattice parameters of the *c*-axis films. Initially, it was thought that the small temperature difference between the center and outside of the substrate holder might be responsible for the degraded properties in the films positioned near the outside perimeter of the holder. From optical pyrometry it appeared that this temperature difference was about 20 °C. This possibility was eliminated, however, by positioning the block so that the outside perimeter, i.e., the coldest part, was directly opposite the center axis of the target. In this configuration the highest $T_c$'s now were in the films near the edge and the lowest were those in the center. Finally, to insure that the differences in critical temperatures were not due to some subtle differences in the low-temperature postannealing process, representative films were *ex situ* annealed at 400 °C for 4 h in 1 atm of oxygen. No changes in $T_c$'s were observed.

It is clear from the above data that under certain conditions the bombardment of the depositing films during sputtering can be minimized sufficiently to eliminate cation backsputtering but not sufficiently to allow the formation of the highest-$T_c$ YBCO phase. In such cases a structure is formed which, based on our diffraction data, closely resembles the now well-known orthorhombic YBCO structure but which has a lower critical temperature. There are two plausible explanations for the formation of this lower-$T_c$ structure. It is possible that the >90-K YBCO phase is sufficiently unstable that even a relatively mild particle bombardment inhibits its formation. In such a case, some lower-energy structure would be formed. Another possible hypothesis is that even a mild particle bombardment can cause the backsputtering of some reacting species that may be critical to the formation of the highest-$T_c$ structure, thus inhibiting its formation. We will renew the discussion of these hypotheses in the context of other experimental results.

### B. dc versus rf sputtering

We have successfully sputtered YBCO films with similarly high critical temperature and current values using either rf or dc power. However, problems of reproducibility were encountered when using rf sputtering in the parallel configuration. In this case where the target and substrates are positioned closer to each other than in the off-axis configuration, one could sometimes observe an intense plasma surrounding the substrates. When this was not observed, the quality of the films was high, comparable to that achieved with dc sputtering. When the substrates were within this type of plasma, the superconducting properties were degraded, the $T_c$'s occasionally being depressed to as low as 65 K. Once again, similar to the data reported above, based on x-ray-diffraction and EDS analyses, the composition, the structure, and lattice parameters of all of the films were essentially the same despite the differences in $T_c$. We are not certain regarding the reason for the random

differences in the size and intensity of the plasma in the vicinity of the substrates when using rf power. In dc sputtering the plasma tended to be smaller and localized near the target and an intense plasma was never observed close to the substrates.

The data on the rf-deposited films are of interest since they provide another indication of the deleterious effect of particle bombardment on the formation of >90-K YBCO phase. These data, however, provide no further insight regarding the mechanism by which this occurs.

### C. Sputtering targets

In Table I it is noted that a new sputtering target was used to deposit the YBCO films whose properties are shown in Figs. 2 and 3. We have observed that as the sputtering time from a target increased, the character of the sputtering process and the property of the films gradually changed. Maintaining the conditions listed in Table I over a period of hundreds of hours the sputtering voltage would slowly drop to 100 V and less and the deposition rate would go down to ~10 nm/h. Also, and most important, the superconducting properties of the films would gradually degrade. Instead of the 90-K $T_c$'s obtained initially, the critical temperatures would drop to 85 K and less. This problem required the frequent replacement of targets in order to produce films with optimum $T_c$'s. Target replacement was usually done when the voltage had dropped to ~120 V. At this value the critical temperatures of films were still typically above 85 K. Once again, similar to previous results, x-ray analyses showed that both the high- and lower-$T_c$ films were $c$-axis oriented with similar lattice parameters, and from EDS analyses, the compositions of all the films were at or near to 1:2:3 stoichiometry.

We have also found that, under the conditions of Table I, a nonsuperconducting (tetragonal structure) target, particularly when new, would produce films with very depressed properties. In one extreme case, films deposited from a new tetragonal target had $T_c$'s of only ~50 K. Replacing this target with a new superconducting (orthorhombic target) immediately produced films with $T_c$'s of 90 K. EDS and x-ray-diffraction analyses again could not distinguish between the 50- and the 90-K films. The lattice parameters of two representative films from this set of experiments were 1.1718 and 1.1726 nm. Significantly, the film with the larger parameter was sputtered from the orthorhombic target and had the higher critical temperature while the lower-$T_c$ film from the tetragonal target had the smaller parameter. This is, of course, the opposite of what one would expect if both films had the standard orthorhombic YBCO structure and the depressed $T_c$ in one of the films was due to an oxygen deficiency.

We believe that these results on the influence of the target on film properties provide an important insight toward understanding the YBCO growth process. The data reported above on films deposited in the parallel configuration at 300 mTorr indicated that the depressed $T_c$'s, in those 1:2:3 stoichiometric films, were due to particle bombardment of the films during the growth process that prevented the formation of the orthorhombic 90-K phase. From those data, however, it was not possible to determine whether the bombardment destabilized the 90-K phase causing a lower-energy lower-$T_c$ 1:2:3 structure to form, or whether backsputtering due to the bombardment prevented some reactive species, which is critical for the YBCO to form, from staying at the substrate surface. This latter possibility would also inhibit the formation of the highest-$T_c$ YBCO phase. In the present set of experiments, since the sputtering voltages for the two targets were found to be similar, it is reasonable to assume that the level of particle bombardment of the substrates in the two cases is also similar. Therefore the low critical temperatures only in the films from the tetragonal target cannot be ascribed to the destabilizing effect of particle bombardment on the YBCO structure. Based on this conclusion, it would appear that there is indeed some critical reactive species that is required to form YBCO and in these experiments it was available in sufficient quantity only in the orthorhombic target. This unknown species is, undoubtedly, activated oxygen. These data thus indicate that molecular oxygen, which was available in large quantity in the sputtering gas in both experiments, is not sufficiently reactive to permit the formation of the 90-K YBCO phase.

This explanation is consistent with the observed deterioration of film properties with target usage even though the cation compositions of the degraded films remain unchanged.

### D. Sputtering gas

We have already commented on the criticality of gas pressure for achieving optimum superconducting properties when sputtering in the parallel configuration. Using this configuration, and having a gas pressure similar to that listed in Table I, produced films with depressed $T_c$'s. It was necessary to raise the pressure to over 400 mTorr in order to deposit films with properties similar to those of Table I. Although employing a total sputtering gas pressure below ~400 mTorr caused the above-mentioned decrease in critical temperature, it required pressures less than 300 mTorr before films were deposited which did not have 1:2:3 stoichiometry. As would be expected, such films were not superconducting.

We found that gas pressure had an analogous effect when using the off-axis configuration. Decreasing the pressure to 100 mTorr still allowed the deposition of optimum quality films. However, at approximately 50 mTorr, degradation in film properties was observed although cation stoichiometry remained unchanged. Films made at 25 mTorr were found not to be superconducting and their stoichiometry was far removed from 1:2:3. It should be noted that undue attention should not be payed to the absolute pressures reported here since these values are somewhat dependent on such things as chamber geometry and the location of the pressure gauge.

We will consider next the effect of changing gas composition on superconducting properties. We have found that increasing the oxygen:argon ratio of the sputtering gas had no deleterious effect on either the $T_c$ or the $J_c$ of YBCO films. In fact, films with $T_c$'s greater than 90 K

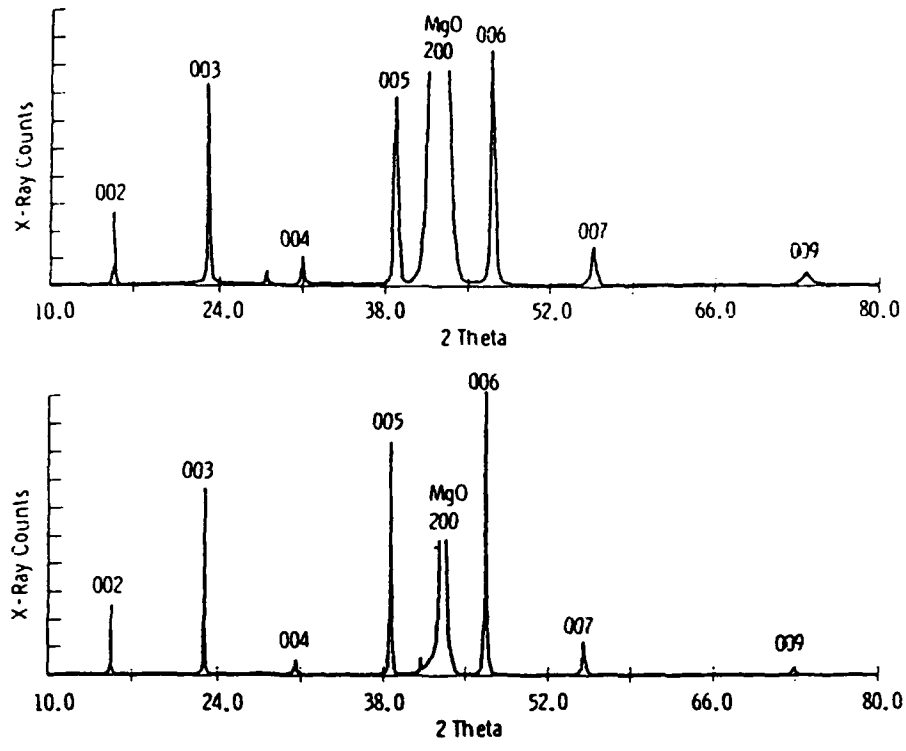


FIG. 5. The upper trace shows an x-ray-diffraction pattern of a film sputtered in oxygen from a degraded target. The films contains a *c*-axis nonsuperconducting Y-Ba-Cu-O structure with a lattice parameter of 1.1629. The lower trace is the pattern for a film prepared under the same conditions but after a long sputtering time. The $T_c$ is now 85 K and the lattice parameter is 1.1692.

were sputtered in pure oxygen in both target-substrate configurations. Maintaining the same pressure but substituting up to 90% of the oxygen with argon also produced films with similarly high critical temperatures. X-ray analyses of films made with and without argon showed the same type of *c*-axis growth illustrated in Fig. 4. However, EDS analyses indicated that films sputtered in pure oxygen tended to have a slightly Y-rich composition ($\sim Y_{21}Ba_{28}Cu_{51}O_x$). TEM analyses showed that the excess yttrium was present as the 2:1:1 phase. We assume that if sputtered long enough in oxygen the surface cation composition of the target would eventually change allowing the deposition of films with 1:2:3 stoichiometry. However, even when this type of slightly Y-rich film was obtained, the critical current densities as well as critical temperature were still high, similar to those shown in Figs. 2 and 3.

Although sputtering even in pure oxygen produced no deleterious effect on superconducting properties, increasing the argon:oxygen ratio to approximately 10 or higher, caused a very sharp degradation in superconducting properties with time. When sputtering was done in argon alone, after only a few hours a noticeable drop in film quality began to be observed. Continuing sputtering in pure argon eventually produced films that were very yttrium rich, $Y_{42}Ba_{33}Cu_{25}O_x$, and were not superconducting. It is important to emphasize, however, that although ultimately the films had this composition and were not superconducting, the very first films had close to optimum properties despite the absence of molecular oxygen in the sputtering gas.

After degrading a new orthorhombic target by sputtering from it for many hours in pure argon we found that it could be almost completely regenerated by sputtering in pure oxygen. Using the parallel configuration films were sputtered in oxygen from a degraded target. Initially films were deposited that had the same very Y-rich composition as those made in argon. After about 12 h of sputtering, however, the above-mentioned slightly Y-rich composition typical for films sputtered in pure oxygen from a new target was obtained. From x-ray analyses these films were now *c*-axis oriented but they had unusually small lattice parameters of 1.1629 nm. They were not superconducting down to 4.2 K. Further sputtering produced films that continued to have the same cation stoichiometry and *c*-axis epitaxy but which had gradually larger lattice parameters. Ultimately the lattice parameters reached 1.1692 nm and the $T_c$'s reached ~85 K. Further sputtering produced no more changes. Figure 5 shows x-ray data for one of the *c*-axis nonsuperconducting films and for an 85-K film.

These results provide additional and even stronger evidence for the critical importance of the target on the properties of sputtered films. By sputtering in pure argon a target was produced that, when later used with pure oxygen as the sputtering gas, deposited films with proper cation stoichiometry and *c*-axis epitaxy but which were not superconducting. In this case, the very low lattice parameters of this *c*-type structure clearly indicates that it was not the orthorhombic YBCO phase.

### E. Substrate temperature

We have found that raising the substrate temperature to 750 °C produced no significant changes in the superconducting properties of the sputtered films. No investigation of higher temperatures were attempted due to limitations of our substrate heater. Lowering the substrate temperature below 670 °C, however, produced two important effects. Gradually more *a*-axis orientation was observed in the films deposited on the $LaAlO_3$ substrates and also there

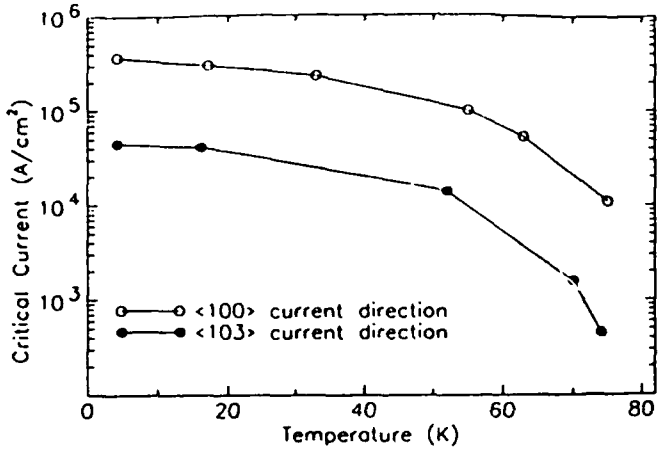


FIG. 6. Critical current density of YBCO film sputtered on a (110) $SrTiO_3$ substrate. The lower curve is with the current in the (103) direction and the upper curve, in the (100) direction.

was a gradual decrease in critical temperature. Films deposited at 600 °C under conditions listed in Table I had over 90% *a*-axis growth; however, they had very low $T_c$'s of <80 K. Similar results were obtained regardless of target-substrate configuration. We were eventually able to obtain superconducting films with $T_c$'s as high as 85 K on $LaAlO_3$ at 600 °C by adding water vapor to the sputtering gas. In experiments on the affect of residual gases on film growth, we have found that water vapor is a very effective oxidizing agent for the growth of YBCO in sputtered films. More detailed results on the use of water vapor will be discussed in the section dealing with residual gases.

### F. Substrate materials

Among the substrates studied, only the films deposited on sapphire did not have optimum $T_c$'s of at least 90 K. The maximum critical temperatures for YBCO on sapphire were ~87 K. These values were obtained only in films deposited at ~750 °C. However even in this case where the $T_c$ was close to the optimum values obtained with the other substrates, the $J_c$'s were greatly depressed. With the exception of those deposited on sapphire the $J_c$'s of YBCO films that had *c*-axis orientation all were similarly high. These include films deposited on (100) MgO, (100) $SrTiO_3$, as well as those on $LaAlO_3$. In the case of $LaAlO_3$, predominantly *c*-axis growth occurred only at temperatures of 670 °C and higher. Below 670 °C, progressively more of the YBCO showed *a*-axis growth as the temperature was decreased. As expected for *a*-axis YBCO, these films had lower critical currents than those with *c*-axis epitaxy. Lower $J_c$'s were also obtained on films deposited on (110) $SrTiO_3$ substrates. In this case the orientation of the YBCO was a mixture of (103) and $(10\bar{3})$. The critical current densities of these films were anisotropic, as seen in Fig. 6.

### G. Residual gases

Although many of the YBCO sputtering experiments reported in the literature were done in nonbaked vacuum systems, there has been little information published on the effect of residual gas impurities on the properties of the films. We have analyzed the gases in our sputtering system after the substrate was heated to 670 °C but prior to the introduction of the sputtering gas. The predominant residual gases were found to be water vapor, nitrogen, argon, and hydrocarbons, in that order. To assess the effect of these gases on $T_c$, we performed successive growth experiments in which ~10 mTorr of water vapor, nitrogen, or methane was added to the sputtering gases. In the case of nitrogen and methane no significant effect, either positive or negative, was observed. However with water vapor this was not the case. As previously discussed, we have found that as sputtering time of a target increased, film quality gradually deteriorated. For example, films that were sputtered from a target that had been used for over 100 h had $T_c$'s of only ~85 K. It was found that when 10 mTorr of water vapor was added to the sputtering gas, $T_c$'s of ~90 K were again obtained reproducibly. Similar high $T_c$'s were obtained when water vapor was added when sputtering from a new tetragonal nonsuperconducting target. As also previously described, without water vapor the superconducting properties from this type of target were invariably depressed.

It was also found that the addition of water vapor allowed the deposition of high-$T_c$ film over a larger surface area than previously could be done. This was particularly noticeable when using the parallel target-substrate configuration. Finally, it was found that with the addition of water vapor, high-$T_c$ films could be deposited at a significantly lower temperature than previously possible. Without the addition of water vapor, the minimum temperature for sputtering high-quality YBCO films was ~670 °C. At lower temperatures the critical temperature degraded and below 600 °C films were usually not even superconducting. By adding water vapor, $T_c$'s as high as 87 K could be obtained in *c*-axis films that were deposited at 590 °C on MgO substrates. Films deposited on $LaAlO_3$ at this temperature showed over 90% *a*-axis growth and had maximum $T_c$'s of 85 K. Experiments were done in which as much as 150 mTorr of water vapor was added to the sputtering gas. The $T_c$'s of these films were still ~90 K.

Another benefit from the use of water vapor was decreasing the importance of having a uniform temperature over an entire substrate area in order to obtain films with uniform properties. The diminution of this requirement eliminated the need to bond the substrates to the heater with silver paste which had been done to obtain good temperature uniformity, particularly when large-area substrates were used. Experiments were performed using the off-axis target-substrate configuration in which the substrate holder, as shown in Fig. 1, was inverted. The distance and the angle between the target and substrates were kept the same. Using this arrangement the substrates were simply positioned on the holder without any bonding or clamping. Under these conditions, when 15 mTorr of water vapor was added to the sputtering gas, up to 2-in.-diam films were reproducibly deposited that had $T_c$'s of > 90 K over their entire surface area. Because bonding the sub-

strates to the heater was not a necessity, it was also possible to deposit 90-K films on both sides of a single substrate. More detailed accounts of these large-area and two-sided deposition experiments will be published elsewhere.[9]

### H. Sputtering voltage and current

As was described in the section dealing with targets an apparent correlation was observed between the higher sputtering voltages that were obtained when using a new target and the high critical temperatures obtained. We have found that adding water vapor to the sputtering gas produced an increase in the sputtering voltage. When using a well-eroded target the voltage would return to values similar to those observed when the target was new. The improved $T_c$'s of the film deposited under these conditions lent credence to a correlation between high sputtering voltages and high $T_c$'s. This was investigated further by studying the effect of another gas, $N_2O$, which similar to water vapor also produced a higher sputtering voltage. In these experiments, however, the deposited films showed no improvement in superconducting properties. This result thus refutes any simple correlation between sputtering voltage and $T_c$.

With respect to sputtering current, no observable effect on film quality was found within the narrow range of values studied, i.e., between 0.2 and 1 A. Occasionally at the higher currents used, the plasma would become unstable and all of the power would become concentrated at one point on the target surface. This tended to happen more often when using dc power and when water vapor was added to the sputtering gas. Films sputtered during such periods of instability would invariably be very copper rich. Interestingly, even in these cases the $T_c$'s of the films would remain high.

### I. Defects in sputtered YBCO films

Using transmission electron microscopy we have analyzed in detail the chemical and structural properties of some representative films deposited on the various substrates (not including sapphire) to try to identify the major defects in these films. In all cases, regardless of substrate material or film orientation, dislocations and/or twinning at the interface due to mismatch between the YBCO and the substrate were observed. These defects are intrinsic to the epitaxial growth process. An example is shown in Fig. 7. Considering films that had $c$-axis epitaxy, the second most common defects found were second-phase particles, either Cu-O or the 2:1:1 phase. As would be expected, very heavy concentrations of such second-phase particles were found in films that, from EDS, did not have the 1:2:3 composition. Most commonly, however, their amount was sufficiently low that their presence could not be detected by the EDS analyses. A TEM photograph of these defects is shown in Fig. 8. Although many films have been grown which are essentially particle free (Fig. 9), we still occasionally observe second-phase particles in films that were deposited under what were believed to be optimum conditions. We have some evidence that indicates that the Cu-O particles nucleate on structural or chemical imperfections on the substrate surface. Figure 10 shows a photomicrograph of Cu-O particles on a $LaAlO_3$ substrate. As can be noted some are in a straight line, implying that they may

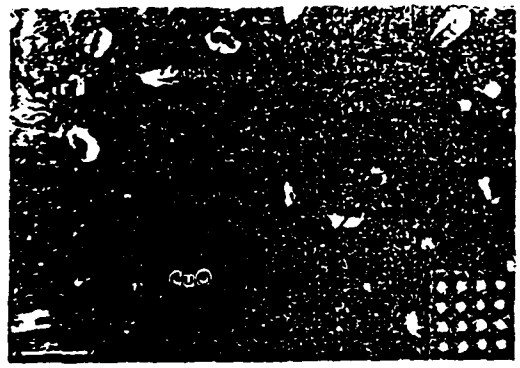


FIG. 8. TEM photomicrograph of (001) YBCO on (100) MgO, deposited in the parallel configuration, and Y rich by EDS analysis. The large dark feature is a Cu-O particle protruding well above the film surface. The smaller light particles are the 2:1:1 phase which are buried in the film.


FIG. 7. A planar TEM photomicrograph of the interface region between a (001) YBCO film and a (100) MgO substrate. The well-defined features (examples indicated by arrows) are interfacial dislocations and/or twins, resulting from lattice mismatch. The distinctness of these features is an indication of good epitaxy.

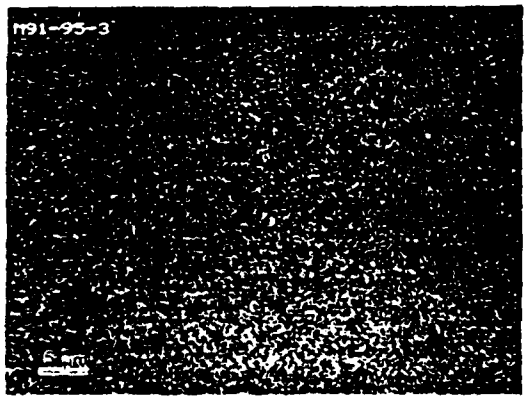


FIG. 9. SEM photomicrograph of an YBCO film which is free of second phase particles. The feature shown was found to permit focusing.

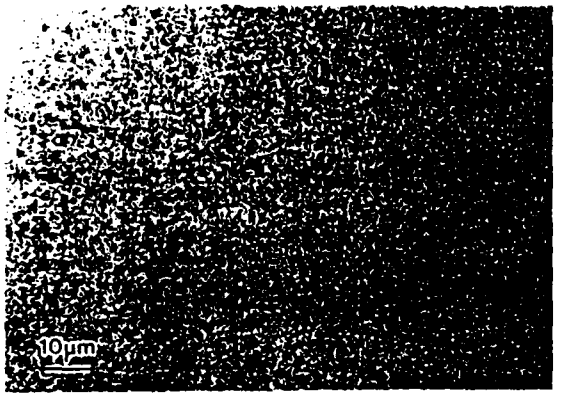


FIG. 10. Optical photomicrograph of an YBCO film showing a relatively dense concentration of Cu-O particles that are sometimes obtained on our sputtered films. Some of the particles are on a straight line implying that they may have nucleated from scratches on the substrate surface.

FIG. 11. TEM photomicrograph of an YBCO film on (110) $SrTiO_3$. The film consists of $\sim 200 \times 500$-nm$^2$ faceted domains, with $(103)/(10\bar{3})$ orientation. It is not certain whether the voids between the domains are intrinsic or a result of the TEM specimen preparation. The substrate directions are indicated by the arrows on the picture.

have originated on scratches on the substrate surface. We have also observed from TEM cross sections that such particles can also nucleate well above the substrate surface. The sputtering target itself apparently can be a source of particles since their concentration is invariably greater when a new target is installed in the system.

We have observed very large concentrations of Cu-O particles in cases where there were intermittent plasma instabilities during film deposition. This was found to occur most often when using dc sputtering and when water vapor was added to the sputtering gas. In the absence of this type of plasma instability the addition of water vapor had no effect on second-phase particle density.

Another structural defect that has been found, in what are desired to be pure *c*-axis films, is *a*-axis growth. In films deposited on $LaAlO_3$ substrates increasingly larger amounts of *a*-axis growth are obtained when the deposition temperature is lowered below 670 °C. However, even above 670 °C, *a*-axis YBCO is found in films thicker than $\sim 400$ nm.

A particular defect associated with *a*-axis films is a "checkerboard" type of structure in which there are two sets of *a*-axis domains that are oriented at a 90° angle with respect to each other. Another defect structure specifically associated with films grown on (110) $SrTiO_3$ is shown in Fig. 11. The $T_c$'s of these films are similar to *c*-axis films, however, the $J_c$'s are significantly less. The currents densities are also anisotropic as shown in Fig. 6.

## IV. SUMMARY AND CONCLUSIONS

We have accumulated extensive data which indicate that it is not a critical requirement for sputtering high-quality YBCO ($T_c > 90$ K and $J_c > 10^6$ A/cm$^2$ at 77 K) to have an overall 1:2:3 cation composition. We have many examples of multiphase films that are yttrium and/or copper rich but which still contain the YBCO orthorhombic phase with such properties. It is only when the amount of the second phases becomes a significant volume fraction of the film that there is any deterioration in superconductivity. A corollary to this is that single-phase *c*-axis films that have 1:2:3 cation stoichiometry can have greatly depressed superconducting properties. We also have many examples of this type of film. In essence, our data show that regardless whether the Y, Ba, and Cu atoms are present in the exact proportion at the substrate surface, the high-$T_c$ YBCO phase will form if other conditions are correct.

We have performed experiments that indicate that the high-$T_c$ orthorhombic YBCO phase is sufficiently unstable that even a relatively low-energy particle bombardment of the substrate, insufficient to affect cation stoichiometry, can still prevent its formation. We believe that the bombardment of the substrates in such a case causes the backsputtering of a reactive species which is critical for the formation of the YBCO phase. Since the cation stoichiometry of the films in these experiments was correct and molecular oxygen was already present in the sputtering gas, this species could only be activated oxygen. Evidence showing that this active oxygen originates from the target was provided by the results from different types of sputtering targets. Films with the same cation composition were deposited from an orthorhombic superconducting target and from an nonsuperconducting tetragonal target. However, the $T_c$'s of the films from the latter target were markedly lower. These data strongly indicate that molecular oxygen, which was present in large quantity in both of these growth experiments, was not sufficiently reactive to form the highest-$T_c$ YBCO phase. We believe that this phase was grown only when activated oxygen apparently present in greater quantity in the orthorhombic target was available to participate in the reaction. In its absence a lower-energy Y-Ba-Cu-O structure was formed that is both compositionally and structurally similar to the orthorhombic YBCO phase but which has degraded superconducting properties.

The credibility of this conclusion is reinforced from the data on films deposited from a new superconducting target that was sputtered many hours in pure argon to purposely degrade its surface. Significantly, the very first films deposited in pure argon were found to have close to optimum

properties despite the absence of molecular oxygen in the sputtering gas. However after many hours of sputtering the films were not superconducting. Sputtering in pure argon, we believe, reduced the amount of the active oxygen in the target. Using this degraded target, a epitaxial $c$-axis structure was subsequently prepared by sputtering in pure oxygen. This structure, however, was not superconducting and had a lattice parameter much lower than that found in the superconducting orthorhombic YBCO phase. After further sputtering in oxygen the films from this degraded target gradually improved until finally reaching maximum $T_c$'s of $\sim 85$ K. Significantly, this is approximately the same slightly degraded $T_c$ that is obtained after many hours of sputtering from a new orthorhombic target under optimum conditions. From these experiments we conclude that the main function of the molecular oxygen in the sputtering process is to oxidize the sputtering target, thus providing a continual source of active oxygen necessary for the formation of superconducting YBCO. This reoxidation process, however, is apparently not adequate to completely replenish the active oxygen that is present in a newly fabricated target.

The conclusion that molecular oxygen does not directly participate in the growth of the high-$T_c$ orthorhombic phase and that a stronger oxidizing agent must be present in order for this phase to form is contrary to current understanding of the YBCO film growth process. It has been known for some time that the addition of some form of active oxygen was required in order to deposit YBCO films with optimum properties when using evaporation.[10,11] However the need to do this is generally ascribed to the inability of introducing high enough pressures of molecular oxygen during the evaporation process. Our data imply that molecular oxygen is an inadequate oxidizing agent for the formation of YBCO (at the temperatures discussed in this report) regardless of its pressure. If this conclusion is indeed correct, it will require the reevaluation of any data showing correlations between orthorhombic phase formation and the partial pressure of molecular oxygen.[12] This would be particularly true for growth experiments in which the amount of water vapor present was either unknown or unspecified. The improved film quality obtained when water vapor was added to the sputtering gas provides evidence that water is a better oxidizing agent than molecular oxygen and is sufficiently reactive to permit the formation of the highest-$T_c$ YBCO phase. Whether the water vapor contributes directly to the growth of YBCO by reacting with the deposited film or indirectly by reoxidizing the sputtering target more effectively than molecular oxygen is not known at this time.

We now have a sufficient understanding of the YBCO single-target sputtering process to permit the reproducible deposition of epitaxial single-crystal films of controlled orientations which have excellent superconducting properties. There is, however, one important problem that remains. We still on occasion observe second-phase Cu-O particles in films which are grown under what are believed to be optimum conditions. We have data that indicate that these particles can nucleate from contamination or as a result of plasma instabilities. Such instabilities were found to more likely occur when water vapor was added to the sputtering gas and when using dc power. Films deposited under these conditions in some cases had very heavy concentrations of Cu-O particles. In the absence of plasma instabilities the addition of water vapor had no direct influence on the amount of second-phase particles.

We believe that the majority of second-phase particles, when present in the relatively low concentrations usually found in our films occur primarily due to contamination either from the substrates, from the hardware in the immediate deposition area, or from the sputtering target. It has already been demonstrated that in certain microwave applications the use of films having the relatively small concentrations of particles discussed here, cause no deleterious effects. The use of such films to construct Josephson junctions, however, could produce problems. Further work toward totally eliminating this type of defect is thus warranted.

## ACKNOWLEDGMENTS

We gratefully thank A. M. Stewart (x-ray diffraction), T. J. Mullen (EDS), J. H. Uphoff (film deposition), C. L. Jones ($J_c$ patterning), and K. Blackham (TEM specimen preparation), for their valuable contributions to this work. Supported in part by the Air Force Office of Scientific Research Contract No. F49620-88-C-0034.

[1] R. L. Sandstrom, W. J. Gallagher, T. R. Dinger, R. H. Koch, R. B. Laibowitz, A. W. Kleinsasser, R. J. Gambino, B. Bumble, and M. F. Chisholm, Appl. Phys. Lett. 53, 444 (1988).
[2] H. C. Li, G. Linker, F. Ratzel, R. Smithey, and J. Geerk, Appl. Phys. Lett. 52, 1098 (1988).
[3] N. Terada, H. Ihara, M. Jo, M. Hirabayashi, Y. Kimura, K. Matsutani, K. Hirata, E. Ohno, R. Sugise, and F. Kawashima, Jpn. J. Appl. Phys. 27, L639 (1988).
[4] U. Poppe, J. Schubert, R. R. Arons, W. Evers, C. H. Freiburg, W. Reichert, K. Schmidt, W. Sybertz, and K. Urban, Solid State Commun. 66, 661 (1988).
[5] C. B. Eom, J. Z. Sun, K. Yamamoto, A. F. Marshall, K. E. Luther, T. H. Geballe, and S. S. Laderman, Appl. Phys. Lett. 55, 595 (1989).
[6] J. R. Gavaler and J. Talvacchio, Physica B 165–166, 1513 (1990).
[7] J. Talvacchio, M. G. Forrester, J. R. Gavaler, and T. T. Braggins, in *Science and Technology of Thin Film Superconductors II*, edited by R. McConnell and S. A. Wolf (Plenum, New York, 1990).
[8] S. M. Rossnagel and J. J. Cuomo, in *Thin Film Processing and Characterization of High-Temperature Superconductors*, edited by J. M. E. Harper, R. J. Colton, and L. C. Feldman (American Institute of Physics, New York, 1988), p. 106.
[9] T. T. Braggins, J. R. Gavaler, and J. Talvacchio (unpublished).
[10] J. Kwo, M. Hong, D. J. Trevor, R. M. Fleming, A. E. White, J. P. Mannaerts, R. C. Farrow, A. R. Kortan, and K. T. Short, Physica C 162–164, 623 (1989).
[11] D. D. Berkley, B. R. Johnson, N. Anand, K. M. Beauchamp, L. E. Conroy, A. M. Goldman, J. Maps, K. Mauersberger, M. L. Mecartney, J. Morton, M. Tuominen, and Y. J. Zhang, Appl. Phys. Lett. 53, 1973 (1988).
[12] R. H. Hammond and R. Bormann, Physica C 162–164, 703 (1989).

# HIGH-$T_c$ SUPERCONDUCTIVITY IN 1990

John Talvacchio
Cryogenic Electronics

March 5, 1991

*Published in the Journal of Superconductivity, Vol. 4, No. 2, pp. 75-169 (1991)*

## TABLE OF CONTENTS

# 1. INTRODUCTION

This document is a 1990 supplement to the Bibliography of High-$T_c$ Superconductivity published in two parts in the Journal of Superconductivity: Vol. 2(1), 1-210 (1989) and Vol. 3(1), 1-153 (1990). Together with the previous reference lists covering 1987-88 and 1989, respectively, the Bibliography of High-$T_c$ Superconductivity spans the entire (brief) history of HTS.

The bibliography is becoming more narrowly focussed on applied superconductivity with each annual update. Fundamental research papers are included when they either have a direct relationship to applications or when they appear to be representative of a body of work. The number of papers added to the bibliography decreased from 4610 in 1987-88 to 2578 in 1989 and 1302 in 1990, although the total number of papers published in high-$T_c$ superconductivity has remained fairly constant throughout this period.

Section 2 of this document lists the two-letter keywords available for assignment to each reference. Section 3 is an index based on these keywords. The index identifies the first author's last name and a paper number corresponding to the complete source information listed in Section 5. The index in Section 4 is based on the chemical elements. The source information in Section 5 is ordered alphabetically by the first author's last name. The references include preprints and papers published during 1990. The first keyword assigned to each reference indicates the month in which it was entered into the database (e.g. .05. for May, 1990).

The entire database containing source information for all 8500 references and search software for IBM compatible or Macintosh computers can be downloaded from Ames Laboratory at Iowa State University. Instructions are contained in the March 1, 1990 issue of High-$T_c$ Update (Vol. 5, No. 5).

I wish to acknowledge the efforts of Mrs. M. B. Cross who has maintained the file cabinet of papers and the reference list. This work was supported in part by AFOSR Contract No. F49620-88-C-0039.

John Talvacchio
Westinghouse STC

# 2. LIST OF KEYWORDS

## General Index



## Chemical Element Index

Physica C 177 (1991) 431–437
North-Holland

**APPENDIX 6**

# Effect of Cu–O layer spacing on the magnetic field induced resistive broadening of high-temperature superconductors

D.H. Kim, K.E. Gray, R.T. Kampwirth and J.C. Smith
*Materials Science Division and Science and Technology Center for Superconductivity, Argonne National Laboratory, Argonne, IL 60439, USA*

D.S. Richeson and T.J. Marks
*Department of Chemistry and Science and Technology Center for Superconductivity, Northwestern University, Evanston, IL 60208, USA*

J.H. Kang and J. Talvacchio
*Westinghouse Science and Technology Center, Pittsburgh, PA 15235, USA*

M. Eddy
*Superconducting Technologies, Inc., Santa Barbara, CA 93111, USA*

Received 2 April 1991

For $H \| c$-axis, the magnetic field induced broadening of the resistive transitions of high-$T_c$ superconductors (HTS) is shown to depend strongly on the Cu–O layer spacing. For the highly anisotropic HTS, we show experimental evidence that *flux motion* results from a thermally activated crossover from three dimensional (3D) vortex *lines* to 2D independent *pancake-like* vortices in the Cu–O layers, which is intrinsic to the material and occurs when $k_B T$ exceeds the Josephson coupling energy of these layers. At low temperatures, however, thermally activated conventional depinning (which can be sample dependent) or melting in the uncoupled 2D Cu–O layers is also required for flux motion. For $YBa_2Cu_3O_7$, this dimensional crossover does not occur *below* $H_{c2}$, presumably because the conducting Cu–O chains short-circuit the Josephson interlayer coupling, leading to better superconducting properties in a magnetic field. These results show that strong interlayer coupling is a key to finding good alternatives.

High-temperature superconductors (HTS) are known to exhibit [1–3] anomalous magnetic field induced broadening of their resistive transitions, which generally increases with anisotropy [4]. This effect places limitations on the value of the materials for moderate to high-field applications. For the applied field, $H$, *parallel* to the superconducting Cu–O layers, i.e., $H \perp c$-axis, the broadening is not as large as for $H$ parallel to the $c$-axis ($H \| c$), and because of the absence of a Lorentz-force dependence [3] together with the anticipated intrinsic pinning of the insulating region between layers, an explanation other than flux motion has been proposed [5]. For $H \| c$, the lack of intrinsic pinning implies that the much greater broadening is due to thermally activated flux motion [6–8]. This broadening is characterized below by an $H^*(T)$, which depends on the voltage criterion of the measurement, and can be related to the magnetic irreversibility line, which is similarly dependent on the measurement time. For the highly anisotropic Bi- and Tl-based HTS, we present experimental evidence that the flux motion associated with this broadening occurs as a result of a dimensional crossover from three dimensional (3D) vortex *lines* to 2D independent *pancake-like* vortices [9], which reside in well-coupled adjacent Cu–O bi- or tri-multilayers. This decoupling of vortices renders the sparse pinning sites in individual Cu–O multilayers much less effective. However, at low reduced temperatures, $t \equiv T/T_c$, the 2D vortex lattice

0921-4534/91/$03.50 © 1991 – Elsevier Science Publishers B.V. (North-Holland)

is sufficiently stiff that these pinning sites are again effective and the value of $H^*$, which is larger than the predicted 3D to 2D crossover, can be described by including either conventional depinning [6,10] or melting [11] in the uncoupled 2D Cu–O layers. At zero temperature, $H^*$ necessarily approaches the upper-critical field, $H_{c2}(0)$.

Combining this low-temperature behavior with interlayer vortex coupling by the Josephson tunneling model, the $H^*(t)$ data are fit convincingly, with parameters which are in substantial agreement with available measurements or reasonable expectations, for the highly anisotropic $Tl_2Ba_2CaCu_2O_x$ (Tl-2212), $TlBa_2CaCu_2O_x$ (Tl-1212), $TlBa_2Ca_2Cu_3O_x$ (Tl-1223), $Bi_2Sr_2CaCu_2O_x$ (Bi-2212) materials. These data are shown to depend only on the insulator width between Cu–O multilayers, $d_i$. The *fitted values* of the $c$-axis resistivities, $\rho_c$, depend approximately exponentially on $d_i$, with a reasonable tunneling barrier height, to further substantiate use of a Josephson tunneling model. For the significantly less anisotropic $YBa_2Cu_3O_7$ (Y-1237), this model predicts that 3D to 2D decoupling will not occur for $H < H_{c2}(T)$ because of the much better interlayer coupling, i.e., smaller $\rho_c$, and we cannot fit $H^*$ with reasonable parameters.

A number of different samples were prepared for the work reported here. Films of Y-1237, grown in-situ by DC magnetron sputtering from a stoichiometric target onto rotating (100) $LaAlO_3$ substrates, were shown by transmission electron microscopy to be epitaxial and $c$-axis oriented, exhibiting zero resistance in zero field at $T_c = 89$ K. Polycrystalline Tl-1212 and Tl-1223 films, prepared on (100) YSZ substrates by a MOCVD technique [12], exhibited $T_c$ of 72 and 104 K and contained 5–10% of Tl-2212 and Tl-1212 impurity phases, respectively. Polycrystalline Tl-2212 films, prepared [13] on (100) MgO by DC magnetron sputtering from a three-gun source followed by post-annealing, exhibited $T_c$ from 100 to 104 K. Additional films of Tl-2212, prepared by laser ablation onto (100) $SrTiO_3$ substrates followed by a postanneal, exhibited $T_c$ of 100 K and were confirmed by electron channeling to be epitaxial. All films were found to be highly $c$-axis oriented by X-ray diffraction. Single crystals of Bi-2212 were grown using a flux method with $T_c = 80$ K.

The thermally activated flux motion was characterized experimentally by the resistive transitions, $\rho(T, H)$, which were uniformly measured at a current density of $\sim 10$ A/cm$^2$, such that $\rho(T, H^*)/\rho_n = 10^{-5}$, where $\rho_n$ is the extrapolated normal-state resistivity at $T_c$ (e.g., see fig. 4 of ref. [5]). Higher current densities lead to larger values of $H^*$. These $H^*$ are plotted in fig. 1 against $1 - t$ for many samples of five HTS materials, including literature [1,2,14] values. For the Bi- and Tl-systems, the data on the magnetically measured irreversibility line are inadequate to compare to $H^*$, and our thermally activated model implies that agreement between these would depend on having equivalent sensitivities for internal electric fields in each measurement. Magnetic measurements of irreversibility often have a considerably greater sensitivity and thus obtain a smaller $H^*$. The equivalence [15,16] of these is demonstrated explicitly for Y-1237 in fig. 1, although the good agreement could be due to the existence of a vortex-glass phase transition [7], rather than equal sensitivities.

Figure 1 also shows that $H^*$ is fairly independent of sample quality (e.g., epitaxial or polycrystalline film, single crystals, minor amounts of second-phase

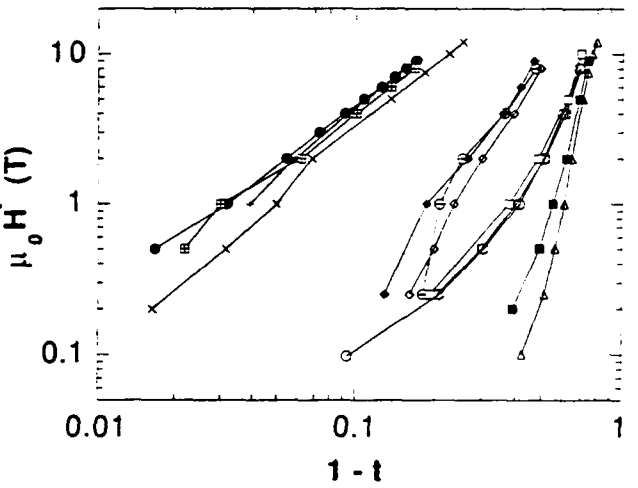


Fig. 1. The resistive broadenings for various HTS are characterized by the measured $\mu_0 H^*$ vs. $1 - t$. The four distinct groups differ by their layer spacings, $d_i$. $YBa_2Cu_3O_7$ single crystals: ref. [16] (solid circles); ref. [14] (pluses); ref. [2] (crosses); $YBa_2Cu_3O_7$ epitaxial film (squares with plus). $TlBa_2CaCu_2O_x$ MOCVD film (circles with plus); $TlBa_2Ca_2Cu_3O_x$ MOCVD films (solid and open diamonds). $Tl_2Ba_2CaCu_2O_x$ epitaxial film (open circles); $Tl_2Ba_2CaCu_2O_x$ sputtered films (open squares). $Bi_2Sr_2CaCu_2O_x$ single crystals: ref. [1] (solid triangles); (open triangles).

material, etc.), at least with our uniform criteria. Note however that the current density for the Bi-2212 crystal of ref. [1] was not reported. For Tl-2212, the data for two *polycrystalline* and one *epitaxial* film coincide quite well, even though the measured $J_c$ of the epitaxial films is $\sim 10$ times larger for all $H$ and $T$. Deviations of the low-field data for Tl-1212 and Tl-1223 are likely an artifact due to minor impurity phases which nonetheless caused double transitions *in that field range*. Note that the shape of $\rho(T, H)$ can vary from sample to sample perhaps due to the differences in their morphology. For example, the resistively determined $H^*$ for Y-1237 shown in fig. 1 bunch together, even though the single-crystal data exhibited a kink near the foot of the transition [2,15] which is not found in our epitaxial films.

Literature values [17] of the $c$-axis distances of the internal structure of the five compounds studied here are presented in table 1. The interlayer (insulator) spacing between Cu–O bi- or tri-layers is $d_i$ and the overall repeat distance of the Cu–O multilayers is $s$. It is clear that the four distinct groups in fig. 1 can be identified by the common $d_i$ values for the members of each group. Thus, the magnitude of the resistive broadening is shown to depend on the *distance between* adjacent Cu–O *multi*layers rather than the *repeat distance*, $s$, or the number, or thickness, $d_s$, of closely coupled Cu–O planes in the multilayer (see e.g., the Tl-1212 and Tl-1223 data). In support of this, assume that $H^*$ increases with $s$: then table 1 would imply a larger $H^*$ for Tl-1223 relative to Tl-2212, but the data indicate the opposite. Note also that for polycrystalline $Tl_2Ba_2Ca_2Cu_3O_x$ (for which $d_i = 11.55$ Å) the $H^*$ data [18] agree with our Tl-2212 and for $t < 0.5$ but fall significantly below it as $T$ increases towards $T_c$. This smaller $H^*$ is likely due to weak-linked intergranular coupling and underscores another important observation of this work: the $H^*$ of weak-linked samples can fall below the intrinsic value, but no amount of perfection can result in significantly larger $H^*$ (unless greater and/or more effective pinning can be introduced in virtually *every* Cu–O multilayer, which may deteriorate $T_c$).

We now present a model for understanding these data. An important step was the recognition that weak coupling between superconducting Cu–O layers, implied by a high degree of anisotropy, allows for *thermally activated* decoupling of the magnetic field induced pancake-like [9] vortices in adjacent Cu–O layers, for $H \| c$. The resulting independent motion of vortices in adjacent layers, i.e., two-dimensional (2D) behavior, greatly reduces the effectiveness of pinning (e.g., by point defects in the Cu–O layers), when compared to extended, 3D vortex lines. However, even in the 2D regime, *any* finite pinning strength in the individual Cu–O multilayers can become effective at sufficiently low temperatures, thereby increasing $H^*$ above the dimensional crossover value. Since the experimental data indicate a weak dependence of $H^*$ on sample quality even at low temperatures (for fields up to $\sim 10$ T), the most likely low-temperature processes, which will be considered below, are intrinsic flux-lattice melting or depinning from universal pinning sites, such as oxygen vacancies in the Cu–O layers. In the latter case, we envision enough elasticity in the flux lattice that individual vortices can be thermally depinned after which *another* vortex falls into the vacant potential well. Our uncertainty about the low-temperature mechanism, means we cannot rule out that improved pinning may increase $H^*$ at low temperatures.

The dimensional crossover occurs when the cou-

**Table 1**
**Parameters for the highly anisotropic HTS. Structural data come from the literature and $T_c$ is measured directly. The fits provide $H_{c2}(0)$, $\rho_c$ and $\alpha B_c(0)^2$, while the rest are derived from formulas assuming $\alpha = 1$**

| Sample | $s$ (Å) | $d_i$ (Å) | $d_s$ (Å) | $T_c$ (K) | $\mu_0 H_{c2}(0)$ (T) | $\rho_c$ (Ω cm) | $\alpha B_c(0)^2/2\mu_0$ (J/cm$^3$) | $B_c(0)$ (T) | $\kappa$ | $\mu_0 H_{c1}(0)$ (T) | $\xi_{ab}(0)$ (Å) | $\lambda_{ab}(0)$ (Å) |
|---|---|---|---|---|---|---|---|---|---|---|---|---|
| Tl-1212 | 12.75 | 9.57 | 3.18 | 72 | 80 | 1.8 | 0.11 | 0.53 | 110 | 0.0165 | 20 | 2100 |
| Tl-1223A | 15.87 | 9.59 | 6.28 | 104 | 110 | 2 | 0.13 | 0.56 | 140 | 0.0141 | 17 | 2400 |
| Tl-2212 | 14.7 | 11.55 | 3.15 | 100 | 60 | 8 | 0.087 | 0.47 | 91 | 0.0164 | 23 | 2100 |
| Bi-2212A | 15.45 | 12.29 | 3.16 | 80 | 40 | 34 | 0.049 | 0.35 | 81 | 0.0135 | 28 | 2300 |
| Bi-2212B | 15.45 | 12.29 | 3.16 | 79 | 40 | 84 | 0.047 | 0.34 | 82 | 0.0130 | 28 | 2300 |

pling energy between adjacent Cu–O multilayers, $E_c(H, T)$, is $\sim k_B T$. Previously, electromagnetic coupling of vortices was considered [9], but the relevant $E_c$ was found [9] to be too small to explain the *relatively* narrow resistive transition in Y-1237, and it could hardly account for the vast differences found in Y-1237 and the highly anisotropic Bi-2212 and Tl-2212. On the other hand, the magnitude of the Josephson coupling energy, $E_{cj}$, for the *phase* of the superconducting order parameter [19], exhibits the right range of values in the highly anisotropic HTS because $\rho_c$ is so large. For Josephson tunneling through an insulating barrier *in zero magnetic field*,

$$E_{cj} = \frac{\hbar I_{cj}(T)}{e} = \frac{\pi\hbar\Delta(T)}{2e^2 R_N} \tanh\left(\frac{\Delta(T)}{2k_B T}\right), \qquad (1)$$

where $I_{cj}$ is the Josephson critical current, $R_N$ is the normal-state resistance of the junction and $\Delta(T)$ is the temperature-dependent energy gap. *For finite fields*, eq. (1) must include [20] a term $(1-b)$ in $E_{cj}$, where $b \equiv H/H_{c2}$, to account for the spatial average of the magnitude of the order parameter over the flux-line lattice. For Josephson coupling of a vortex to *both* neighboring Cu–O layers, $E_c = 2E_{cj}$, and the relevant junction area is that of one vortex, $\Phi_0/H$, so that $R_N = \rho_c s\mu_0 H/\Phi_0$. From standard tunneling theory [21] and experiment [22], $R_N$ or $\rho_c$ should be proportional to $\exp(-d_i/d_0)$, where $d_i$ is the insulator thickness and $d_0 = \hbar/\sqrt{8m\Phi}$ accounts for the tunneling barrier height, $\Phi$. Below $T_c$ we assume $R_N$ is independent of $T$ and $H$. The resulting 3D to 2D dimensional crossover is shown as the thinner solid line in fig. 2 for reasonably weak coupling with $[\pi\hbar\Phi_0/e^2\rho_c s\mu_0 H_{c2}(0)][\Delta(0)/k_B T_c] = 0.05$, i.e., high anisotropy.

Flux-lattice melting in 2D occurs when $k_B T = E_m$, where [11]

$$E_m = \frac{AC_{66}\Phi_0 d_s}{2\pi\mu_0 H}, \qquad (2)$$

where $A$ is of order one, $d_s$ is the superconducting Cu–O bi- or tri-layer thickness ($\sim$3–6 Å) and the shear modulus has been determined by Brandt [23] to be

$$C_{66} = \frac{B_c^2}{2\mu_0} b(1-0.29b)(1-b)^2, \qquad (3)$$

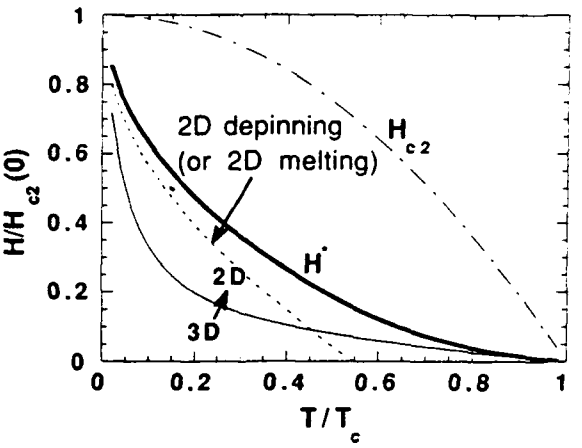


Fig. 2. These curves represent characteristic fields for the thermally activated 3D to 2D crossover (solid), flux depinning (dashed) and the combined effect of both (heavy solid line). The temperature dependence of $H_{c2}(T)/H_{c2}(0) = 1-t^2$ is also shown (dot-dashed line).

where $B_c$ is the thermodynamic critical field. Alternatively, the energy associated with depinning is given by that fraction, $\alpha$, of the loss in superconducting condensation energy of a vortex line, which is compensated by a particular pinning site [10]:

$$E_p = \alpha\pi\xi_{ab}^2 d_s \frac{B_c^2}{2\mu_0}(1-b)^2. \qquad (4)$$

For both $B_c(t)$ and $H_{c2}(t)$ we assume the clean-limit temperature dependence of $1-t^2$, which has some justification from measurements [24] in Y-1237. In that case, the ratio of these is weakly dependent on $b$ and $t$, i.e., $E_p/E_m = 2\pi\alpha(1+t)/A(1-0.29b)$. Thus both terms give reasonable fits to the data when combined with the Josephson tunneling model and it is not possible to choose between them based on the present data and analysis. An example of the thermally activated depinning crossover is also shown in fig. 2 as a dashed line for $\alpha\Phi_0 d_s B_c(0)^2/4k_B T_c\mu_0^2 H_{c2}(0) = 0.5$. It should be noted that $E_p = k_B T$ always has a solution with $b = H^*/H_{c2} = 0$ at a finite $T < T_c$. This can be seen from eq. (4) and the same is true for $E_m$. However, extending these solutions into the 3D regime at low fields would be incorrect since it would not describe vortex *line* interactions, whereas the distinction between 2D and 3D should be valid even at the lowest temperatures. For vortices to move in a transport measurement, they must be free, by overcoming *both* energy barriers, so

we solve $k_B T = E_p(H, T) + 2E_{cj}(H, T)$, as shown by the heavy solid line in fig. 2 to fit to $H^*$.

The data of fig. 1 are thus fit using three parameters: $H_{c2}$, $\rho_c$, which is related to the strength of Josephson coupling; and $\alpha B_c^2/2\mu_0$, which is related to the pinning strength (or a similar parameter for a melting transition). Assuming the BCS value of 1.76 for $\Delta(0)k_B T_c$, these fits are shown in fig. 3 and the resulting parameters are given in table 1 together with other *derived* ones. The values of $B_c(0)$ assume that $\alpha = 1$, $\kappa$ is given by $\mu_0 H_{c2}(0)/\sqrt{2}B_c(0)$, and $H_{c1}(0)$ is $B_c(0)\ln(\kappa)/\sqrt{2}\kappa$. The coherence lengths are given by $\xi_{ab}(0) = \sqrt{\Phi_0/2\pi\mu_0 H_{c2}(0)}$ and $\lambda_{ab}(0) = \kappa\xi_{ab}(0)$. An important further prediction of coupling by Josephson tunneling is an exponential dependence of $\rho_c$ on $d_i$, and the data are shown in fig. 4 for the Tl- and Bi-based HTS material. While these data do not fall on one straight line, we anticipate the possibility of different tunneling barrier heights or tunneling effective masses, at least between Bi–O and Tl–O insulating layers. Nevertheless, the best fit gives a reasonable value of $d_0 = 1$ Å and a barrier height of 0.8 eV, assuming a free electron mass. Values of $d_0 =$ 1–1.6 Å are typically found in artificial or natural oxide tunneling barriers [21,22].

The derived parameters presented in table 1 should be viewed with some caution because of our arbitrary, but uniform, criterion for $H^*$, uncertainty over the proper low-temperature model of flux dynamics and our untested, but reasonable, clean-limit assumption that $B_c(t)$ and $H_{c2}(t)$ are proportional to $1 - t^2$. In addition, in some cases the data do not span a sufficient field range to tie down the parameters of the fits precisely. Nonetheless, the parameters are reasonable. In particular, the penetration lengths $\lambda_{ab}(0)$, and $B_c(0)$ are close to expectations based on measured values for $YBa_2Cu_3O_7$ of [24] 140 nm and [25] ~0.8 T, respectively. For Bi-2212, recent muon spin-resonance experiments [26] have concluded that $\mu_0 H_{c2}(0) = 44$ T, $\kappa \sim 100$ and $\lambda_{ab} \sim 250$ nm, in good agreement with table 1.

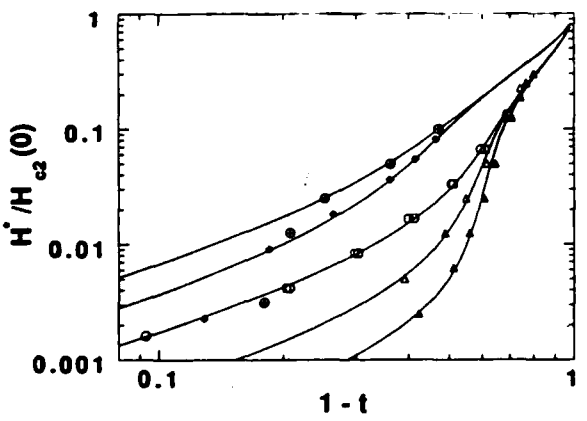


Fig. 3. The solid lines are fits of the $H^*$ data for the highly anisotropic HTS to the model described in the text. From top: $TlBa_2CaCu_2O_x$; $TlBa_2Ca_2Cu_3O_x$; several films of $Tl_2Ba_2CaCu_2O_x$; and two $Bi_2Sr_2CaCu_2O_x$ single crystals.

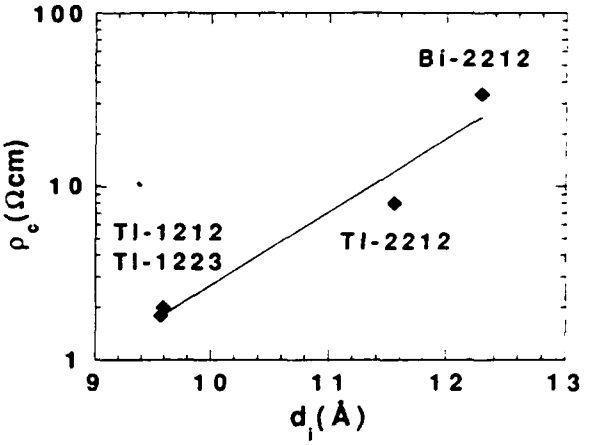


Fig. 4. The *c*-axis resistivity obtained from the fits of fig. 3 plotted against $d_i$ to demonstrate the approximate exponential dependence expected for Josephson tunneling between Cu–O layers.

A further prediction of this model is that *dimensional crossover*, is independent of the pinning strength, whereas the low-temperature $H^*$ and, particularly $J_c$, can be enhanced by improved flux pinning: evidence for this is found in the Tl-2212 films reported above, proton-irradiated Y-1237 crystals [16], an alpha-irradiated Bi-2212 single crystal [4] and neutron irradiated Tl-2223 polycrystals [27]. These studies report small changes at low temperatures in the "irreversibility line" or resistive tail, but large differences in $J_c$.

The data for Y-1237 could not be fit to the model with a reasonable value of $\rho_c$: a possible explanation is that the electrically conducting [28] Cu–O chains short-circuit the tunneling between adjacent Cu–O bilayers in Y-1237, yielding a much lower anisotropy and $\rho_c$. Thus for the smaller experimental $\rho_c$ for Y-1237, the model does not predict a dimensional crossover below $H_c(T)$ and our model does not treat the dynamics of 3D vortex lines. Information based largely on the current–voltage characteristics, $I(V)$,

tends to support [29] a picture of a vortex glass transition for Y-1237. For Tl-2212, the $I(V)$ for a similar range of parameter space *do not* support [5] such a vortex glass model.

In summary, we have shown experimental evidence to suggest that the *flux motion* associated with the magnetic field induced broadening of the resistive transitions of highly anisotropic HTS for $H \| c$ is determined by an intrinsic dimensional crossover from 3D vortex lines to 2D vortex pancakes. In addition, our observation of an exponential dependence on the interlayer (insulator) spacing for various HTS materials is consistent with Josephson tunneling being the relevant coupling between the Cu–O bi- or tri-layers. However, at sufficiently low temperatures, pinning is effective in the 2D regime and thus $H^*$ increases above the dimensional-crossover value and may be sample dependent. For $YBa_2Cu_3O_7$, the dimensional crossover is not predicted to occur *below* $H_{c2}$ presumably because the conducting Cu–O chains short-circuit the Josephson interlayer coupling. These results explain why $YBa_2Cu_3O_7$ has the best superconducting properties in a magnetic field and also shows that small layer spacing is a key to find good alternatives. For the present, Tl-1223 seems to be the best choice, because of the higher $T_c$ relative to either Tl-1212 or Y-1237.

## Acknowledgements

The authors thank Jeff Hettinger and Dick Klemm for discussions and Donglu Shi for the Bi-2212 single crystals. This work is partially supported by the US Department of Energy, Division of Basic Energy Sciences–Materials Sciences, Conservation and Renewable Energy as part of a program to develop electric power technology, and the Superconductivity Pilot Center through the Division of Advanced Utility Concepts, under contract #W-31-109-ENG-38 and the National Science Foundation (DMR 88-09854) through the Science and Technology Center for Superconductivity and the AFOSR. JCS acknowledges support from the Argonne Division of Educational Programs.

## References

[1] T.T.M. Palstra, B. Batlogg, L.F. Schneemeyer and J.V. Waszczak, Phys. Rev. Lett. 61 (1988) 1662.
[2] T.T.M. Palstra, B. Batlogg, R.B. van Dover, L.F. Schneemeyer and J.V. Waszczak, Appl. Phys. Lett. 54 (1989) 763.
[3] K.C. Woo, K.E. Gray, R.T. Kampwirth, J.H. Kang, S.J. Stein, R. East and D.M. McKay, Phys. Rev. Lett. 63 (1989) 1877.
[4] T.T.M. Palstra, B. Batlogg, L.F. Schneemeyer and J.V. Waszczak, Phys. Rev. B 43 (1991) 3756.
[5] D.H. Kim, K.E. Gray, R.T. Kampwirth and D.M. McKay, Phys. Rev. B 42 (1990) 6249.
[6] P.H. Kes, J. Aarts, J. van den Berg, C.J. van der Beek and J.A. Mydosh, Supercond. Sci. Technol 1 (1989) 242.
[7] M.P.A. Fisher, Phys. Rev. Lett. 62 (1989) 1415.
[8] D.R. Nelson, Phys. Rev. Lett. 60 (1988) 1973.
[9] J.R. Clem, Phys. Rev. B 43 (1991) 7837.
[10] K.E. Gray, R.T. Kampwirth, J.M. Murduck and D.W. Capone II, Physica C 152 (1988) 445.
[11] J.M. Kosterlitz and D.J. Thouless, J. Phys. C 6 (1973) 1181; B.A. Huberman and S. Doniach, Phys. Rev. Lett. 43 (1979) 950.
[12] G. Malandrino, D.S. Richeson, T.J. Marks, D.C. DeGroot, J.L. Schindler and C.R. Kannewurf, Appl. Phys. Lett. 54 (1989) 763.
[13] J.H. Kang, R.T. Kampwirth and K.E. Gray, Phys. Lett. A 131 (1988) 208.
[14] W.K. Kwok, private communication.
[15] Y. Xu, M. Suenaga, Y. Gao, J.E. Crow and N.D. Spencer, Phys. Rev. B 42 (1990) 8756.
[16] L. Civale, A.D. Marwick, M.W. McElfresh, T.K. Worthington, A.P. Malozemoff, F.H. Holtzberg, J.R. Thompson and M.A. Kirk, Phys. Rev. Lett. 65 (1990) 1164.
[17] D.E. Cox, C.C. Torardi, M.A. Subramanian, J. Gopalakrishnan and A.W. Sleight, Phys. Rev. B 38 (1988) 6624;
D.P. Matheis and R.L. Snyder, Powder Diffraction 5 (1990) 8;
M.A. Beno, L. Soderholm, D.W. Capone II, D.G. Hinks, J.D. Jorgensen, J.D. Grace, I.K. Schuller, C.U. Segre and K. Zhang, Appl. Phys. Lett. 51 (1987) 57.
[18] Y. Wolfus, Y. Yeshurun and I. Felner, Phys. Rev. B 39 (1989) 11690.
[19] V. Ambegaokar and A. Baratoff, Phys. Rev. Lett. 10 (1963) 486.
[20] D.H. Kim, K.E. Gray, R.T. Kampwirth, K.C. Woo, D.M. McKay and J. Stein, Phys. Rev. B 41 (1990) 11642.
[21] See e.g. E.L. Wolf, Principles of Electron Tunneling Spectroscopy (Oxford, NY, 1985).
[22] K.E. Gray, Solid State Commun. 13 (1973) 1787.
[23] E.H. Brandt, Phys. Status Solidi B 77 (1976) 551.
[24] U. Welp, W.K. Kwok, G.W. Crabtree, K.G. Vandervoort and J.Z. Liu, Phys. Rev. Lett. 62 (1989) 1908;
A. Umezawa, G.W. Crabtree, U. Welp, W.K. Kwok, K.G. Vandervoort and J.Z. Liu, Phys. Rev. B 42 (1990) 8744.

[25] L. Krusin-Elbaum, R.L. Greene, F. Holtzberg, A.P. Malozemoff and Y. Yeshurun, Phys. Rev. Lett. 62 (1989) 217.

[26] D.R. Harshman, R.N. Kleinman, M. Inui, G.P. Espinosa, D.B. Mitzi, A. Kapitulnik, D.L. Williams, Bull. Am. Phys. Soc. 36 (1991) 470.

[27] M.P. Maley, P.H. Kes, G.J. Vogt, D.S. Phillips and M.E. McHenry, Bull. Am. Phys. Soc. 36 (1991) 984.

[28] U. Welp, S. Fleshler, W.K. Kwok, J. Downey, Y. Fang, G.W. Crabtree and J.Z. Liu, Phys. Rev. B 42 (1991) 10189.

[29] R.H. Koch, V. Foglietti, W.J. Gallagher, G. Koren, A. Gupta and M.P.A. Fisher, Phys. Rev. Lett. 63 (1989) 1511; P.L. Gammel, L.F. Schneemeyer and D.J. Bishop, Phys. Rev. Lett. 66 (1991) 953.

*Integrated Ferroelectrics*, 1992, Vol. 1, pp. 213–222
Reprints available directly from the publisher
Photocopying permitted by license only

© 1992 Gordon and Breach Science Publishers S.A.
Printed in the United States of America

**APPENDIX 7**

# PULSED LASER DEPOSITION (PLD) OF ORIENTED BISMUTH TITANATE FILMS FOR INTEGRATED ELECTRONIC APPLICATIONS

H. BUHAY, S. SINHAROY, M. H. FRANCOMBE, W. H. KASNER,
J. TALVACCHIO, B. K. PARK, AND N. J. DOYLE
Westinghouse Science & Technology Center
1310 Beulah Road, Pittsburgh, PA 15235

D. R. LAMPE AND M. POLINSKY
Westinghouse Advanced Technology Division
Nursery and Winterson Roads, Baltimore, MD 21203

*(Received April 3, 1991)*

Abstract In this paper we describe recent successes of growth of epitaxial bismuth titanate (BTO) films by pulsed laser deposition (PLD) suitable for electro-optic and electrical switching device structures, and fabrication of an improved gate structure for a ferroelectric memory FET (FEMFET). TEM and x-ray results indicate that excellent crystalline quality BTO films were achieved on $LaAlO_3$. Polarization switching was demonstrated for BTO capacitors with epitaxial superconducting $YBa_2Cu_3O_7$ as the lower electrode. Using an $SiO_2$ buffer layer, a BTO/Si structure was fabricated and direct charge modulation in the Si by polarization reversal in the BTO was demonstrated.

## INTRODUCTION

Since the growth of stoichiometric[1] and epitaxial[2] films of ferroelectric bismuth titanate, $Bi_4Ti_3O_{12}$ (BTO), by rf sputtering was demonstrated in these laboratories, it has become apparent that films of this material offer several important and unique application opportunities in integrated electronics. These potential applications derive from an unusual combination of several useful properties, such as high electro-optic contrast switching effects under low address fields, demonstrated feasibility of direct integration in silicon FET's as a gate dielectric, and the capability of high specific capacitance associated with low dielectric loss.

The unique electro-optic switching behaviour of BTO crystals has already been duplicated in sputtered epitaxial films to achieve an X-Y addressed display.[3] For this purpose, single-domain film

structures were required with the spontaneous polarization and optic axis lying in the plane of the film. Similarly, experimental Si-based memory structures were successfully fabricated in which switching between the "zero" and "one" states was produced by reversing the ferroelectric polarization in the BTO gate dielectric of an FET.[4] Finally, high-value (0.3 $\mu F/cm^2$ ) and low-loss (tan $\delta$ = 0.005) capacitors were fabricated on metallized silicon substrates at growth temperatures of about 550°C.

Despite these early successes with sputtered films of BTO, serious growth problems were often encountered due to the low deposition rates available, to the $Bi_2O_3$-rich composition needed in the target, and to the influence of ion bombardment at the substrate. These effects led to particle formation in the films,[1] cracking of epitaxial layers and interdiffusion with the substrate material.[4] In particular, the the interdiffusion with Si surfaces produced tunneling barriers which promoted anomalous, injection-dominated switching in ferroelectric FET memories (FEMFETs).

Recent studies by Buhay et al.[5,6] and also by Ramesh et al.[7] have demonstrated that high-quality films of BTO can be grown on a variety of substrates, and epitaxially on MgO, by pulsed laser deposition (PLD), using approaches similar to those developed for growth of oxide superconductor layers. We have shown that, unlike the situation with sputtering, stoichiometric targets can be used to yield particle-free films of excellent structural and electrical quality, displaying essentially bulk ferroelectric properties. Moreover, growth could be achieved at high rates and low substrate temperatures under conditions compatible with the processing needs of semiconductor integrated circuits. In the present paper we describe recent extensions of the PLD method to epitaxial growth of BTO films suitable for electro-optic and electrical switching device structures, and to fabrication of improved gate dielectrics for FEMFET arrays.

## EXPERIMENTAL

Film deposition was carried out using a Lumonics HyperEx-460 industrial laser operating on the KrF transition at 248 nm at pulse energies up to 300 mJ, with pulse durations of 20-30 nsec and repetition rates up to 65 Hz. The films were prepared, as previously

described,[5,6] with an estimated laser fluence, on the stoichiometric BTO ceramic target, of 2 $J/cm^2$, laser pulse rate of 10 Hz, and oxygen flowing at a pressure of 200 mTorr. For these conditions, and for nominal substrate temperatures used in the range 500-700°C, films were grown to a typical thickness of 1 micron, at a rate of about 30 nm/min. Structural characterization was performed using X-ray diffractometry and rocking curve measurements, X-ray oscillation and Weissenberg patterns, electron diffraction and transmission electron microscopy (TEM). The composition of the layers was evaluated using electron microprobe techniques. Capacitance and conductance measurements were made over the frequency range 10-500 kHz using a Boonton bridge, and ferroelectric hysteresis studies were carried out with a modified Sawyer-Tower circuit.

The epitaxial BTO films studied here included BTO/$LaAlO_3$(001), bi-layer structures of the type BTO/YBCO/$LaAlO_3$(001) and BTO/YBCO/YSZ(100) and tri-layer structures of the type BTO/$SrTiO_3$/YBCO/$LaAlO_3$(001) and BTO/$SrTiO_3$/YBCO/YSZ(001). MIS structures involving BTO deposits on thin (100-200A) buffer layers of $CaF_2$ and $SiO_2$ on (001)Si were also prepared for electrical C-V measurements. In the bi- and tri-layer structures the epitaxial films of YBCO ($YBa_2Cu_3O_7$) and $SrTiO_3$ were pre-deposited in a separate vacuum system by rf magnetron sputtering. In the case of silicon substrates, $CaF_2$ and $SiO_2$ were pre-deposited by vacuum sublimation and thermal oxidation respectively.

## RESULTS

### Epitaxial Structures on (001)$LaAlO_3$ and Zirconia (YSZ) Substrates

$LaAlO_3$(001) substrates provide an excellent lattice match to the paraelectric (high-temperature) tetragonal (001) face of BTO (~1% compared to 2% for $SrTiO_3$ and 10% for MgO). BTO films were grown at nominal substrate temperatures of 600, 675, and 750°C. Examination by X-ray diffractometry indicated in each case primarily the ferroelectric orthorhombic phase with a very strong c-axis (normal) crystal orientation. X-ray Weissenberg patterns confirmed a well-oriented epitaxial structure with BTO(001) // $LaAlO_3$(001), and with a-b twinning in the (001) plane of the substrate, i.e. BTO[100] and [010] // $LaAlO_3$[110] (see Figure 1). X-ray rocking curve studies

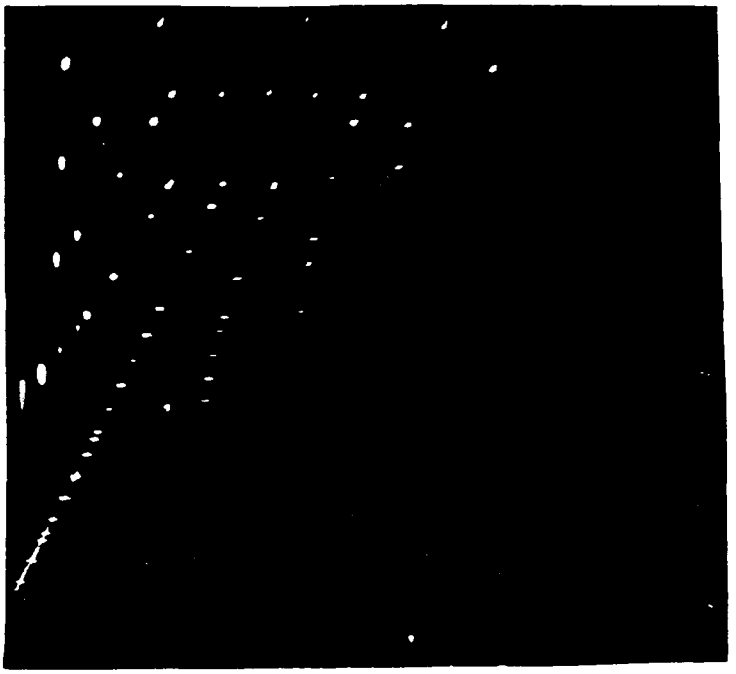

FIGURE 1 X-ray Weissenberg pattern of BTO film grown at 750°C on $LaAlO_3$(100).

yielded FWHM values depending sensitively on growth temperature Increasing the growth temperature from 600 through 675 to 750°C produces a dramatic improvement in film quality, with the corresponding FWHM widths changing as shown in Figure 2.

TEM studies performed on the 750°C sample gave confirmation of the twinned structure (Figure 3). Small area diffraction (SAD) measured in the twinned areas (different contrast regions in Figure 3a and 3b) showed the orientations of the a-b axes differ by 90° rotation and the twin boundaries are parallel to the film axes. Two types of boundaries observed were: (a) straight boundaries (Figure 3a) probably associated with formation of twins directly at the growth temperature near the Curie point (Tc) transition, and (b) curved boundaries (Figure 3b) tentatively attributed to formation of ferroelectric domains on cooling below Tc. These results suggest that the true film growth temperature may differ from that measured at the heater surface by as much as 60-80°C. However, single domain film structures of quality adequate for optical waveguide modulators can probably be achieved by growing further above the Tc transition.

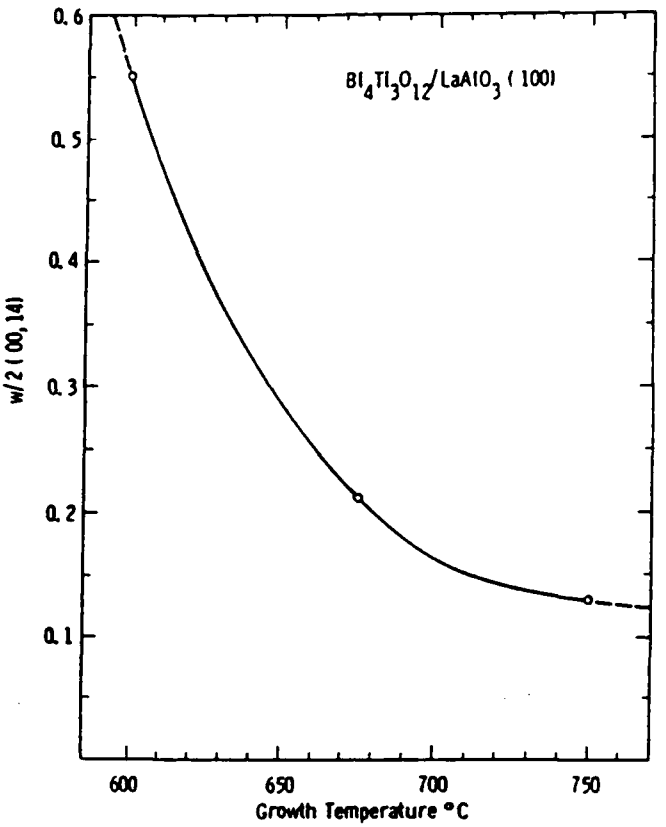


FIGURE 2 FWHM of X-ray rocking curve about (0014) versus temperature for BTO film of Figure 1.

Good-quality epitaxy of BTO was also obtained in the various bi- and tri-layer, (001) oriented samples on $LaAlO_3$ and yttria-stabilized $ZrO_2$. In each case, the BTO c-axis was normal to the substrate plane. In the case of the structures with YBCO, a narrow temperature window was established for BTO growth which led to ferroelectric behaviour without degradation of the superconducting transition at 90K in the YBCO. Using gold top electrodes, hysteresis loops of the type shown in Figure 4 were displayed. The measured polarization at partial saturation (4.3 $\mu C/cm^2$) agrees well with the bulk crystal value parallel to the c-axis, but the coercive field (200-300 kV/cm) is anomalously high. These structures provide a unique example of highly-ordered, lattice-matched electrode/ ferroelectric interfaces, which should possess high stability and reduced fatigue, for example, in semiconductor memory configuration.


(a)


(b)

FIGURE 3 TEMs of same BTO film of Figures 1 and 2: (a) straight twin boundaries; (b) curved twin boundaries.

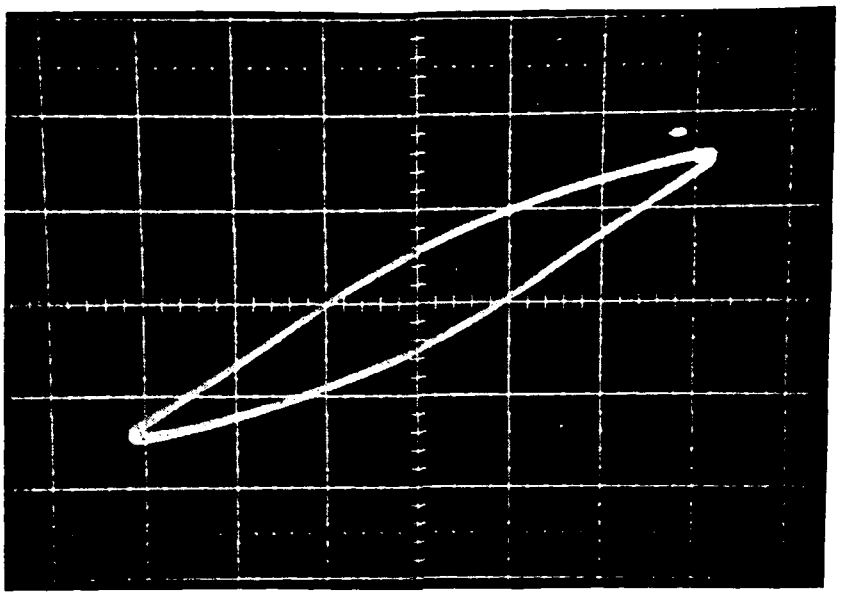

FIGURE 4 Hysteresis loop measured at 2 kHz for BTO/$SrTiO_3$/YBCO/YSZ structure. Scale: Vertical, 3.5 $\mu C/cm^2$ per large division; Horizontal, 310 kV/cm per large division.

MIS Structures on Silicon

These structures were explored with the aim of establishing whether PLD films of BTO on Si (with or without dielectric buffer layers) might exhibit switching behaviour free from the charge injection effects encountered previously with sputter-deposited BTO layers. BTO structures prepared by PLD without such buffer layers were in fact found to display injection effects, and will not be discussed further here. The results for BTO structures using $CaF_2$ or $SiO_2$ as a buffer layer are discussed further below. The BTO/$CaF_2$ dielectric structure was deposited on a standard VHSIC CMOS wafer (4-8 Ohm-cm $p^-$Si epi-layer grown on 0.005-0.02 Ohm-cm $p^{++}$Si substrate). The BTO/$SiO_2$ structure was deposited on a gridded (6 $\mu$m wide $N^+$ lines spaced 60 $\mu$m apart) standard wafer. In both cases a mercury probe having an area of $0.64 \times 10^{-3}$ $cm^2$ was used as the top electrode. The BTO/$CaF_2$ and BTO/$SiO_2$ test structures and C-V plots are shown in Figures 5 and 6 respectively.

The test structure of Figure 5 was intended to simulate a FEMFET that is incorporated in a P-well CMOS VLSIC memory, i.e., an N-channel FEMFET. Thus, as the gate voltage sweeps from +5 volts to -5 volts in the C-V hysteresis curve of Figure 5, the capacitance of the gate dielectric stack increases as the depletion-region "inversion charge

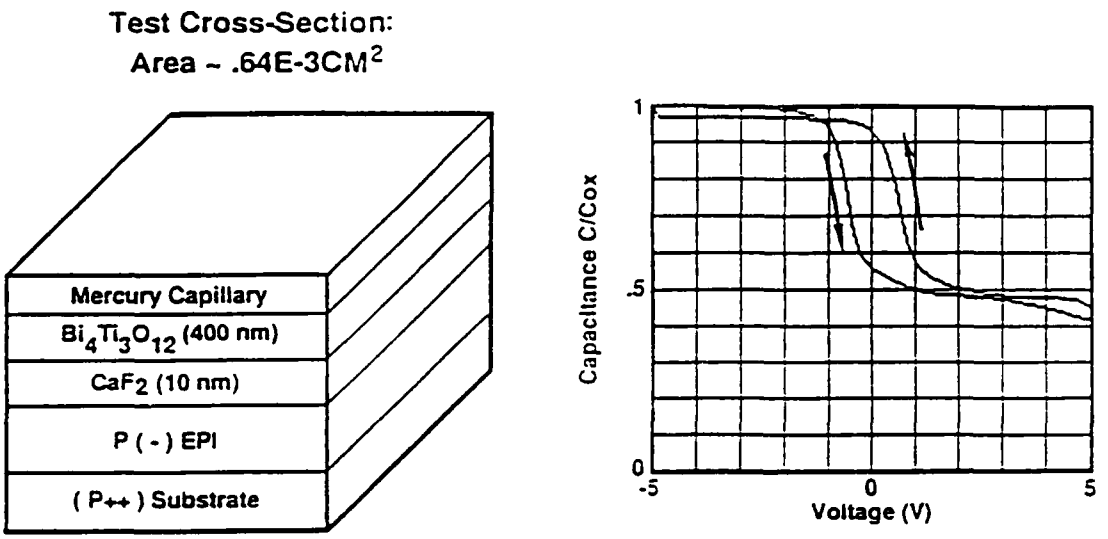


FIGURE 5 Test structure and C-V hysteresis result for a $CaF_2$-buffered BTO film on a standard VHSIC CMOS Si wafer.

layer" becomes an "accumulation charge layer", with the disappearance of the series depletion-region capacitance at approximately the threshold voltage. The shift of the threshold from enhancement mode toward depletion mode in response to negative programming ($V_{gate}$ = -5 volts) indicates positive charge trapped near the semiconductor-gate-dielectric interface rather than a negative sheet of charge that would arise if the negative gate reoriented the ferroelectric dipoles to the positive end adjacent to the negative gate. Thus, the polarity of the threshold shift of the C-V plot (arrow directions shown in Figure 5) for the BTO/$CaF_2$ structure is consistent with the interpretation that charge is being injected from the Si surface into traps near the BTO/$CaF_2$ interface (injection type on/off switching).

The test structure of Figure 6 includes more of the FEMFET (namely, the NMOST source/drain implants) to greatly facilitate both pulsed and endurance C-V measurements. Consequently, in the C-V plot of Figure 6, the lower apparent capacitance is shunted back to its higher value by an inversion layer whose source of electrons is the source/drain grid implant that is shorted to the substrate. Only during the transition from an accumulation layer (arising from a negative gate bias) to the inversion layer (associated with a positive gate bias) does the gate capacitance drop to a minimum value at a gate voltage near the effective threshold voltage. Thus, from the gridded-

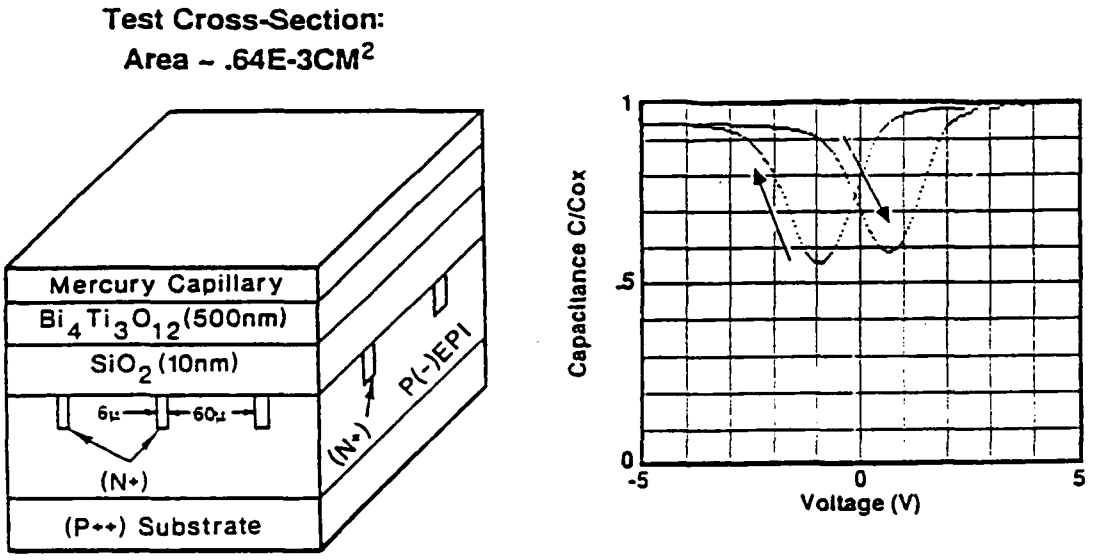


FIGURE 6 Test structure and C-V hysteresis result for a $SiO_2$-buffered BTO film on a gridded wafer.

wafer C-V hysteresis curve of Figure 6, the negative memory-gate programming gives the enhancement mode (normally OFF) while the positive memory gate programming gives the depletion mode (normally ON). The polarity of the threshold shift of the C-V plot (arrow directions shown in Figure 6) for the BTO/$SiO_2$ structure is opposite of that in Figure 5 and is indicative of ferroelectric switching. That is, for 5-volt programming, the reversible ferroelectric polarization dominated when charge tunnelling and trapping was inhibited by the good quality $SiO_2$ buffer layer. The $CaF_2$ buffer layer, however, permitted so much charge tunnelling and trapping that it completely dominated over any likely ferroelectric polarization switching. The faster BTO ferroelectric switching is the desired goal for NDRO FERRAM operation.

## SUMMARY

Pulsed laser deposition has been used, in conjunction with a stoichiometric target, to deposit a variety of BTO epitaxial structures on (001) crystal substrates of $LaAlO_3$ and YSZ. By controlling the growth temperature, it was possible to form high-quality BTO capacitors with epitaxial superconducting YBCO as the lower electrode, and to demonstrate polarization switching. Using

$SiO_2$ buffer layers, BTO/Si MIS structures also were grown, and the feasibility of direct charge modulation in the Si by polarization reversal in the BTO was demonstrated.

ACKNOWLEDGEMENTS

The authors would like to thank B. A. Fleischmann, V. A. Toth, B. A. Blankenship, and J. Uphoff for preparing the BTO films and electrodes for ferroelectric hysteresis measurements and characterization of the superconducting films. We appreciate assistance in interpreting the x-ray and TEM results provided by W. J. Takei and J. Greggi. J. T. acknowledges support from AFOSR contract F-49260-88-C-0039 for preparation of the epi YBCO films and buffer layers.

REFERENCES

1. W. J. Takei, N. P. Formigoni and M. H. Francombe, J. Vac. Sci. Tech. 7, 442 (1970).

2. W. J. Takei, S. Y. Wu and M. H. Francombe, J. Crystal Growth 28, 188 (1975).

3. S. Y. Wu, W. J. Takei and M. H. Francombe, Ferroelectrics 10, 209 (1976).

4. S. Y. Wu, IEEE Trans. Electron Devices ED-21, 499 (1974).

5. H. Buhay, S. Sinharoy, W. H. Kasner, M. H. Francombe, D. R. Lampe and E. Stepke, Proc. 7th Int. Symp. Appl. Ferroelectrics (1990).

6. H. Buhay, S. Sinharoy, W. H. Kasner, N. H. Francombe, D. R. Lampe and E. Stepke, Appl. Phys. Lett. 58, 1470 (1991).

7. R. Ramesh, K. Luther, B. Wilkens, D. L. Hart, E. Wang, A. Inam, X. D. Wu and T. Venkatesan, Appl. Phys. Lett. 57, 1505 (1990).

*accepted for publication*
*in Proc. 1991 ICMC*
Advances in Cryogenic Engineering
(Materials), Vol. 38

**APPENDIX 8**

# IN-SITU DEPOSITION OF YBaCuO FILMS ON BOTH SIDES OF TWO-INCH DIAMETER WAFERS BY OFF-AXIS SPUTTERING*

T. T. Braggins, J. R. Gavaler, and J. Talvacchio

Westinghouse Science and Technology Center
1310 Beulah Road
Pittsburgh, PA 15235

## ABSTRACT

$YBa_2Cu_3O_7$ thin films have been magnetron sputtered in the off-axis geometry from stoichiometric targets on $LaAlO_3$ substrates resulting in in-situ superconducting films with resistive and inductive $T_c$s of about 90 K. Double-sided sputter deposition on two-inch diameter, radiantly heated substrates performed sequentially on each side is reported for the first time. Of particular importance for microwave device applications is the attainment of low surface resistances in the range of 0.3 to 0.7 mΩ at 77 K and 10 GHz for double-sided films.

## INTRODUCTION

One of the first applications of high temperature superconductors (HTS) is the development of passive microwave components. Much of the work has focused on thin films of the HTS $YBa_2Cu_3O_7$ (YBCO) deposited on lattice-matched substrates. Except for the most demanding applications where very low loss sapphire substrates are required, $LaAlO_3$ is the preferred substrate owing to its close lattice match, moderately low loss and reasonable dielectric constant.[1] In previously published work, we have shown that highly c-axis oriented YBCO films with excellent transition temperatures, $T_c$, and surface resistances, $R_s$, at microwave frequencies could be deposited over large (2-in. dia.) areas using a technique in which silver paste was used to attach the wafer to the sample block.[2] Although this method provides good thermal contact and uniformity, it precludes using the back side of the wafer for a second YBCO layer and, because of the fragility of $LaAlO_3$, results in intolerable wafer breakage for large area samples.

For several types of microwave components, e.g. microstrip filters, the proximity of a superconducting ground plane is highly desirable – leading to the necessity of developing techniques for the deposition of YBCO films on both sides of a substrate. The alternative of using stacked single-sided films can lead to mechanical problems, air-gaps causing excessive loss and

*Supported in part by AFOSR Contract No. F49620-91-C-0034.

difficulties with proper grounding of the superconducting ground plane. Additionally, ever larger diameter (2 to 4 in.) substrates will become increasingly important for components which must be critically matched as well as the economic advantage of fabricating many dies per processing cycle. In this paper we will describe the techniques we have developed for double-sided deposition of high quality YBCO films on 2-in. dia. substrates and the characterization of these films. To the best of our knowledge this is the first report of sputter deposition of YBCO films on both surfaces of a substrate with the only other report of double-sided deposition having been performed by a MOCVD process.[3]

## EXPERIMENTAL METHOD

The experimental techniques which are used for the in-situ growth of YBCO films by off-axis sputtering have been reported previously.[2] For this work the geometry (relative position of source and sample) is unchanged except that a sputter-down rather than sputter-up configuration is used as illustrated in Figure 1. This is so because the samples are rested on a quartz plate which covers an approximately 3-in. dia. kanthal heater. The sample is stationary during film deposition. Twenty large-area wafers have been processed in this configuration. Sputtering is performed from a 2-in. dia. stoichiometric YBCO target using 110 watts of rf power in a continuously pumped gaseous atmosphere consisting approximately of 200 mtorr argon, 50 mtorr oxygen and 20 mtorr water vapor. Reasonable variation of the gas composition is not critical;[4] however, we have found that small additions of water vapor are beneficial yielding consistently >90 K superconducting transition temperatures.[4] The sample temperature during deposition, determined by infrared pyrometry, is 670°C with an estimated accuracy of ±20°C. Under these conditions a deposition rate of 20 nm/hr is obtained. Following growth the sample is cooled in 25 torr $O_2$ to 400°C where it is held for 20 min. prior to cooling to room temperature. For double-sided depositions the chamber is opened, the sample is turned over and the process repeated.

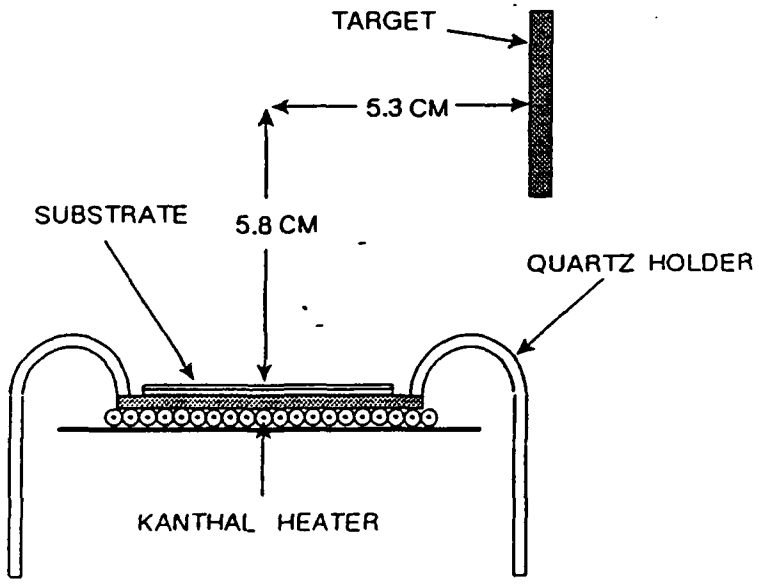


Fig. 1. Sputter-down configuration for off-axis sputtering used for double-sided deposition on 2-in. diameter wafers.

The critical temperature was measured both resistively, using the standard Van der Pauw technique, and as a change of inductance for a copper coil placed against the film and driven at 100 kHz. Resistive $T_c$ was determined at the temperature the resistance goes to zero while the inductive $T_c$ was determined by the transition midpoint. Microwave surface resistances are measured using a parallel plate resonator following the technique developed by Taber.[5] The sample geometry consists of two 1/4x1/2 in. samples separated by .0005 in. teflon film. The RF leads are loosely coupled to the resonator so that the loaded and unloaded Q's can be assumed equal. Values of $R_s$ are normalized from the resonant frequency of approximately 8.5 GHz to 10 GHz assuming an $f^2$ dependence for the surface resistance.

## EXPERIMENTAL RESULTS

YBCO films deposited on $LaAlO_3$ substrates are highly c-axis oriented. A very small a-axis component is observed as seen in Figure 2 where the x-ray diffraction patterns of the front surface (side A) and back surface (side B) of a double-sided film are compared. (Note the logarithmic scale in Figure 2.) These films exhibit amongst the smallest a-axis content we have observed and is an improvement over the smaller area, single sided films we have reported on previously.

Resistive and inductive transition temperatures have been measured on double-sided films where representative results are shown in Figures 3a and 3b for side A and side B of a 2-in. dia. film, respectively. The inductive transition is shown in the inset curves of the figures and is seen to follow

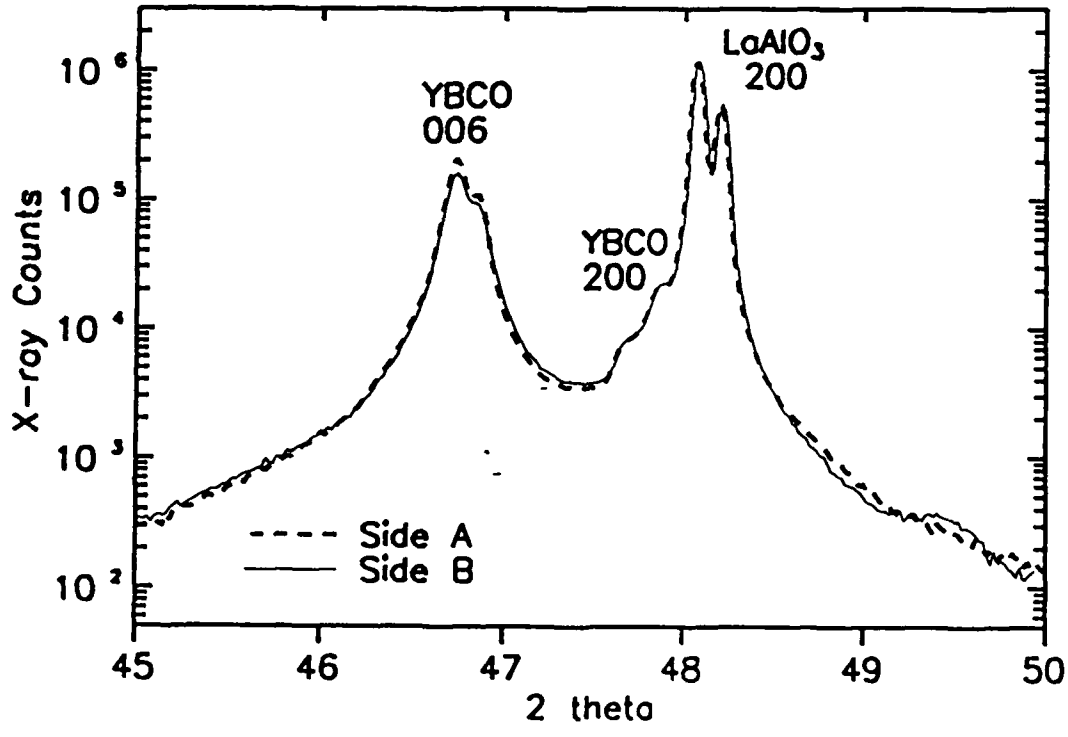


Fig. 2. X-ray diffraction pattern for side A and side B of a double-sided film showing very small a-axis (200) contribution.

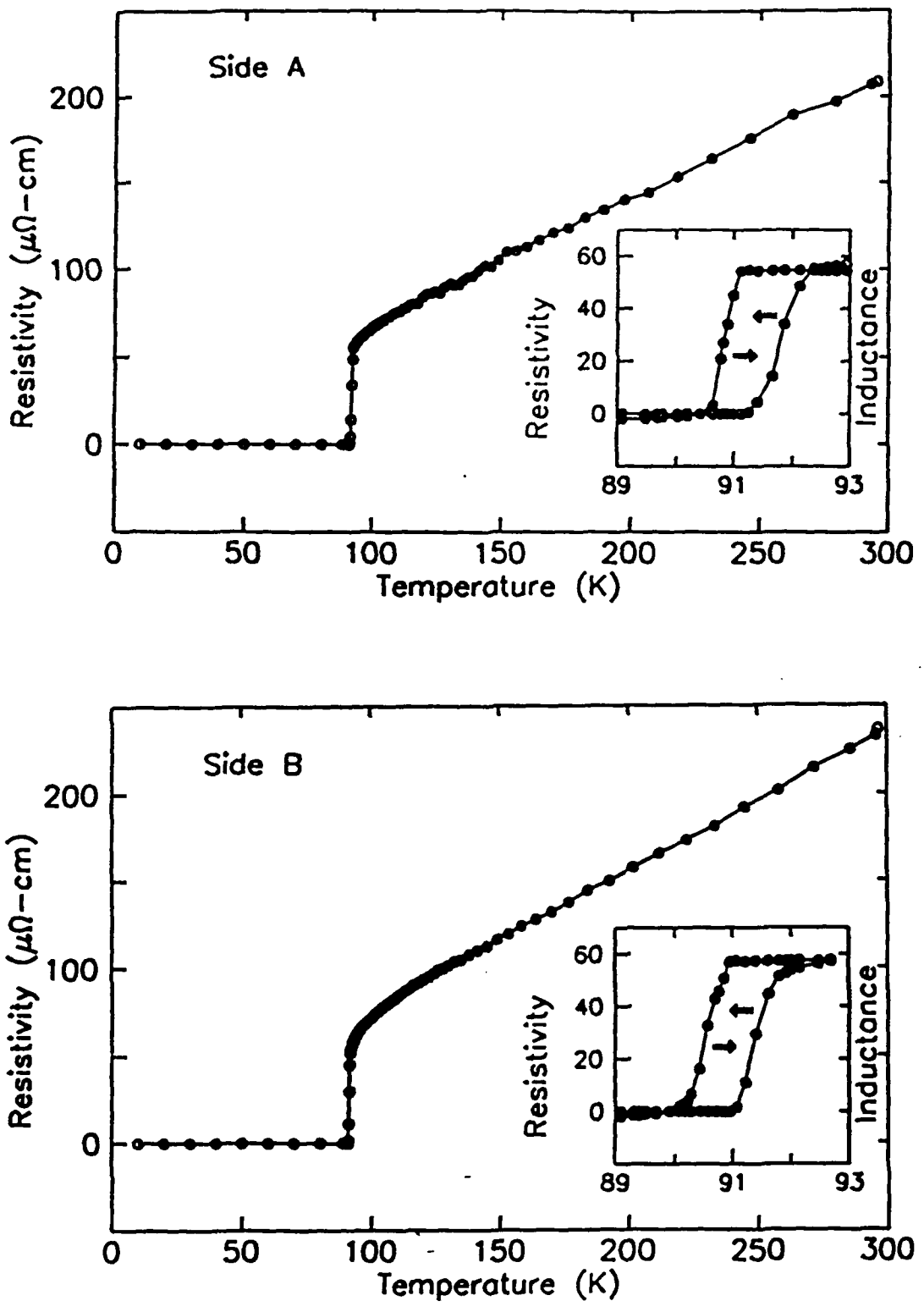


Fig. 3. Resistivity versus temperature for double-sided YBCO film deposited on a) side A and b) side B of a 2-in. dia. $LaAlO_3$ wafer. The inset figure compares the resistive and inductive transitions.

very closely the resistive transition. Resistive $T_c(R=0)$ values >90 K are obtained for both sides of this wafer. A series of $T_c$ measurements were made spanning the diameter of a 2-in. wafer and the results are presented in Figure 4. As can be seen the uniformity of $T_c$ is excellent – varying between 89 K and 91 K over the wafer diameter.

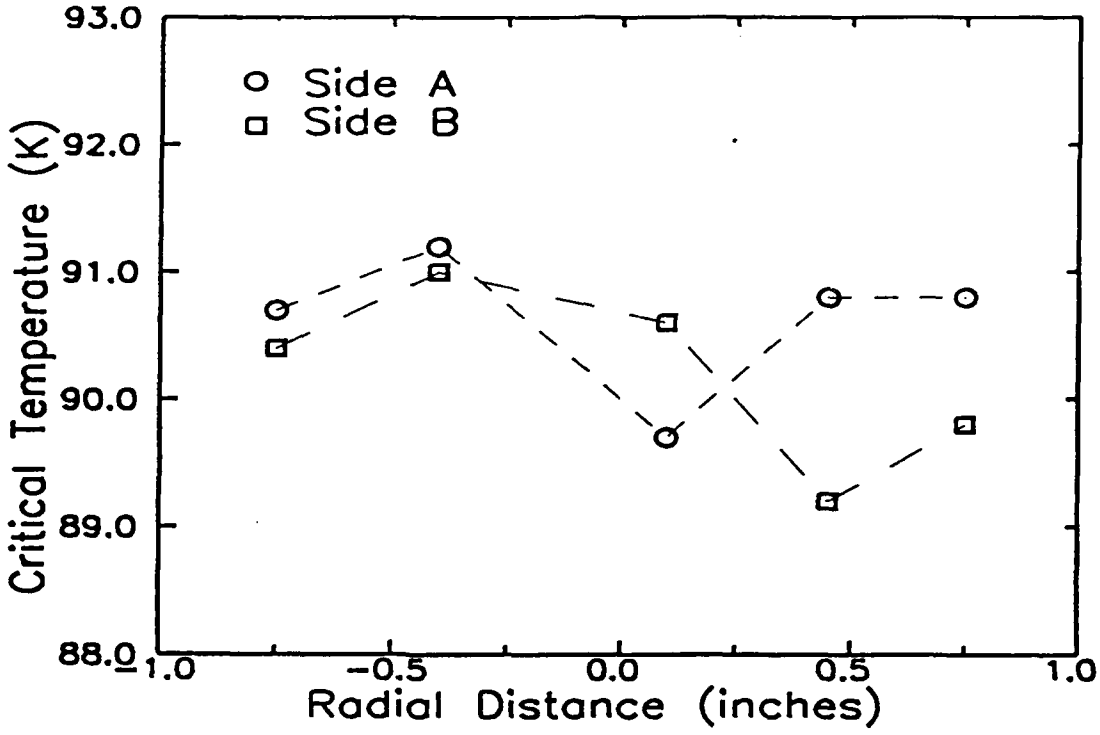


Fig. 4. Critical temperature (R = 0) for both sides of a double-sided film showing ±1 K uniformity over a 2-in. dia. substrate.

Of particular importance for the passive microwave components which are being fabricated from these wafers is the surface resistance at microwave frequencies. $R_s$ values, at 77 K and normalized to 10 GHz, have been measured on 1/4x1/2 in. test chips which surround microwave device patterns in the center of the 2-in. diameter wafer. The location of test chips for two types of devices are shown in Figures 5a and 5b. The $R_s$ test chips for the 'filter' wafer (Figure 5b) were measured after the filter was completely processed and the wafer was diced. As one side of the wafer was coated with gold (for electrical contact to the YBCO superconducting ground plane), $R_s$ could only be measured on one side, in this case side B, of the double-sided film. The two sets of test chips measured (chips 9 and 10, and 12 and 13 as noted in Figure 5b) showed $R_s$ values of 0.30 and 0.40 mΩ, respectively. On the 'antenna' wafer (Figure 5a) $R_s$ values averaged 0.65 mΩ for side A and 0.70 mΩ for side B were measured. The specific pairs of chips measured and the results obtained for $R_s$ are listed in Table 1. The $R_s$ data are shown in Figure 6 superimposed on a curve summarizing $R_s$ measurements from a number of laboratories as collected by Piel and Mueller.[6] As is evident from this figure, the $R_s$ values for these double-sided films fall within the scatter of the data summarized. These results also are very comparable to that of our earlier, smaller-area films which typically have $R_s$ values of 0.6 mΩ where our best value measured to date is 0.2 mΩ.

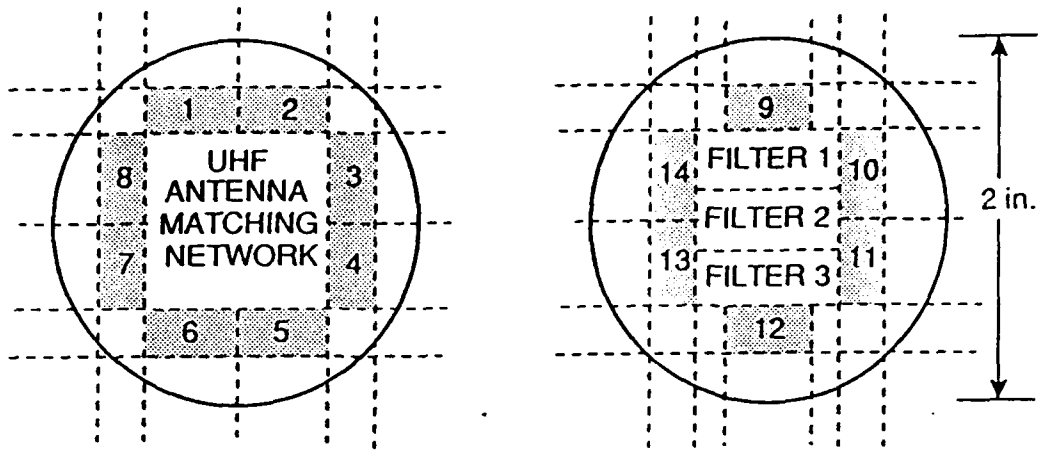


Fig. 5. Location of test chips used to determine surface resistance for a) 'antenna' wafer and b) 'filter' wafer.

## SUMMARY AND CONCLUSIONS

The deposition of YBCO thin films by in-situ off-axis sputtering on both sides of 2-in. dia. $LaAlO_3$ substrates has been demonstrated. $T_c > 90$ K is obtained for both sides of these films. Surface resistances of 0.65 and 0.70 mΩ at 77 K and normalized to 10 GHz have been measured for the first (side A) and second (side B) sides deposited, respectively. Moreover, $R_s$ as low as 0.30 mΩ has been measured on side B of a double-sided wafer which had undergone a complete microwave device processing cycle. The above results compare very favorably with our previous work with smaller area single-sided films.

Several enhancements to our deposition process can be readily envisioned. One would be to incorporate the necessary fixturing to turn over the sample after the first side is deposited which would eliminate the present requirement of opening the chamber to turn the sample over. Another would be the addition of a sample rotation capability to improve uniformity.

This initial work with double-sided depositions of high quality YBCO films on 2-in. diameter substrates has demonstrated a major milestone in the producibility of microwave components – allowing larger area devices or multiple devices per wafer to be fabricated which incorporate a superconducting ground plane on the back side of the wafer.

Table 1. Summary of surface resistance measurements made on test chips taken from 2-in. wafers. See Fig. 5 for location of test chips on wafers.

| Sample Numbers | $R_s$ (mΩ) 77K, 10 GHz SIDE A | $R_s$ (mΩ) 77K, 10 GHz SIDE B |
|---|---|---|
| 1/2 | 0.68 | 0.76 |
| 3/4 | 0.63 | 0.69 |
| 5/6 | 0.63 | 0.68 |
| 9/10 | – | 0.30 |
| 12/13 | – | 0.40 |

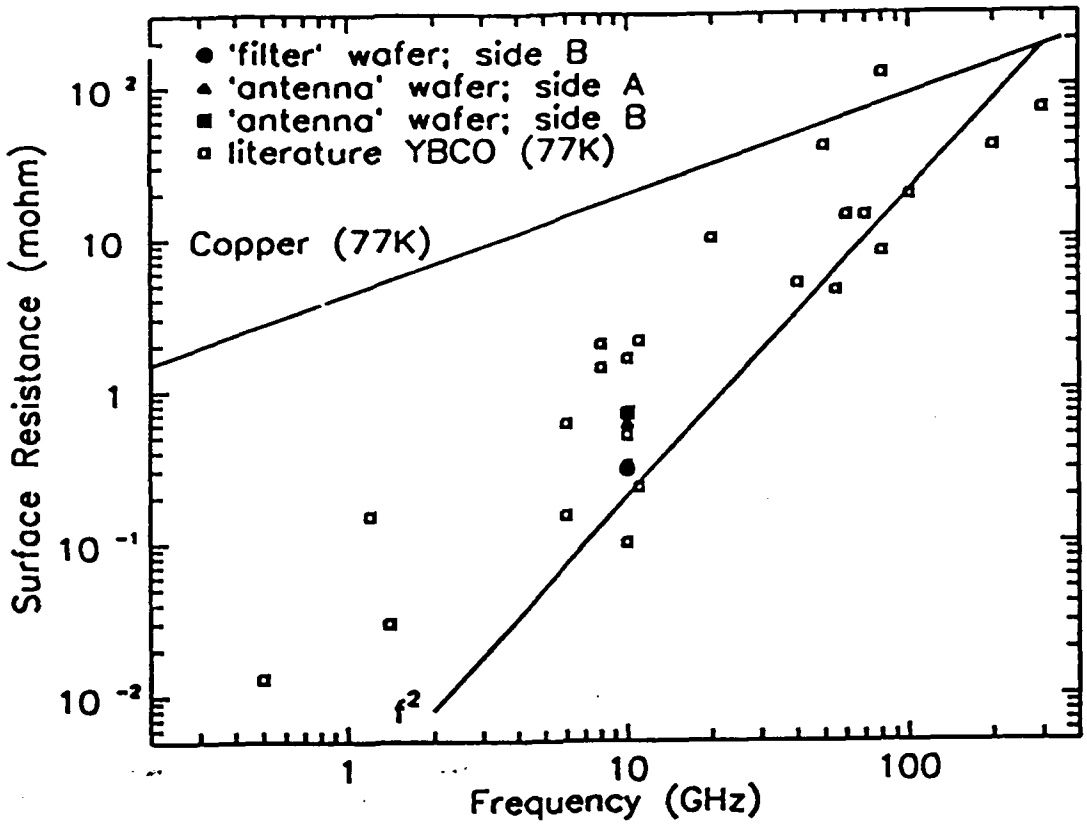


Fig. 6. Comparison of surface resistance measurements of double-sided films with literature values taken from Ref. 6. The surface resistance of copper is shown for comparison.

ACKNOWLEDGEMENTS

The technical assistance of J. H. Uphoff for $T_c$ measurements, A. M. Stewart for x-ray diffraction and G. B. Draper for $R_s$ characterization is gratefully acknowledged. The assistance of Dr. S. H. Talisa in establishing the $R_s$ measurement techniques is most appreciated.

REFERENCES

1. J. Talvacchio and G. R. Wagner, "High-$T_c$ Film Development for Electronic Applications," in Superconductivity Applications for Infrared and Microwave Devices, Proc. Vol. 1292, K. B. Bhasin and V. O. Heinen, eds., SPIE, Bellingham, Washington (1990), pp. 2-12.
2. J. Talvacchio, M. G. Forrester, J. R. Gavaler, and T. T. Braggins, "Large-Area YBCO Films for Microwave Applications," IEEE Trans. Magn. 27(2):978 (1991).
3. J. H. Takemoto, C. M. Jackson, H. M. Manasevit, D. C. St. John, J. F. Burch, K. P. Daly, and R. W. Simon, "Microstrip Resonators Using Two-sided Metalorganic Chemical Vapor Deposited Er-Ba-Cu-O Thin Films," Appl. Phys. Lett. 58(10):1109 (1991).
4. J. R. Gavaler, J. Talvacchio, T. T. Braggins, M. G. Forrester, and J. Greggi, "Critical Parameters in the Single-Target Sputtering of YBCO," submitted to J. Appl. Phys. (1991).
5. R. C. Taber, "A Parallel Plate Resonator Technique for Microwave Loss Measurements on Superconductors," Rev. Sci. Instrum. 61(8):2200 (1990).
6. H. Piel and G. Muller, "The Microwave Surface Impedance of High-$T_c$ Superconductors," IEEE Trans. Magn. 27(2):854 (1991).

MICROWAVE JOURNAL REVIEWED EDITORIAL BOARD

# High $T_c$ Film Development for Electronic Applications

**J. Talvacchio, G.R. Wagner and S.H. Talisa**
*Westinghouse Science and Technology Center*
*Pittsburgh, PA*

*The requirements and status of high $T_c$ superconductor (HTS) films for the development of electronic applications are described with an emphasis on passive microwave devices. One of the most general requirements, a low RF surface resistance relative to Cu, has been achieved in films of several different HTS compounds. However, the best films, made of $YBa_2Cu_3O_7$ (YBCO) by any one of several techniques, have in common a residual surface resistance that is much greater than predicted by conventional superconductivity theory. Improvement in films also is limited by the current size and selection of single crystal substrate materials. Other issues that must be resolved to develop a full integrated circuit technology for HTS are substrate heating during film deposition, deposited epitaxial insulators and determination of which interfaces in a multilevel circuit must be formed in situ.*

## Introduction

The emphasis of this paper is on the materials requirements for HTS passive microwave devices for three reasons. The development of HTS Josephson junctions is sufficiently difficult that a wide range of fabrication alternatives are being explored. To describe all of them would require a separate paper. Passive microwave devices are expected to be the first practical application of HTS. Many of the HTS materials issues considered here have broader implications. The general requirements of high speed and/or low noise operation in circuits with some level of integration apply to all of superconducting electronics. Only films on single crystal epitaxial substrates are considered here.

## Requirements for Specific Microwave Devices

Figures of merit for several passive devices are listed in Table 1. The most important requirement is an RF surface resistance $R_s$, which is low compared to normal metals (Cu, Au). For operation at $\leq 80°K$, the three of the highest $T_c$ superconductor families, YBCO, Bi-Sr-Ca-Cu-O (BSCCO), and Tl-Ba-Ca-Cu-O (TBCCO), can be considered. However, a search of the literature,[1] indicates that only three measurements of $R_s$ of BSCCO films have been published,[2-4] and no results were obtained in the frequency range of 2 to 19 GHz that were better than the $R_s$ of Cu. BSCCO films are considered to have largely unknown RF properties. Only three laboratories, including Westinghouse, have explored the properties of TBCCO

**TABLE I**
**MATERIAL ISSUED IN THE FABRICATION OF HTS MICROWAVE DEVICES**

| Device | Figures of Merit | Implication for Fabrication |
|---|---|---|
| Bandpass filter | insertion loss, bandwidth<br>volume | low $R_s$ — c-axis films<br>integration of a filter bank on a single wafer |
| Resonator (oscillator) | Q<br>phase noise | low loss dielectric, preferably sapphire<br>single crystal film |
| Delay line | delay length<br>volume | large film area<br>thin dielectric |
| Antenna array | efficiency<br>gain | very large areas (UHF)<br>very low $R_s$ (mm-wave) |
| Additional requirements for many devices | operation at $\leq 80°K$<br>mechanical, packaging<br>crossovers<br>interface with normal metal | YBCO, BSCCO & TBCCO are all feasible<br>films on both sides of substrate<br>deposited, epitaxial dielectrics<br>low resistance contacts |

films at microwave frequencies. The only information on $R_s$ of TBCCO has been published recently.[5,6]

In contrast, more than 100 papers have been published on the surface resistance of YBCO films. The lowest $R_s$ is obtained for films grown epitaxially on single crystal insulating substrates with the film's C-axis parallel to the growth direction. All of the components in Table 1 require such films. For high-Q resonators, the requirement of low phase noise also may demand that essentially single crystal films are used. Since YBCO is the most highly developed materials system, the fabrication issues listed in Table 1 are evaluated in this paper with reference to YBCO.

### Substrates for HTS Films

Several of the requirements in Table 1 relate to substrate properties. Table 2 contains a list of the important single crystal substrates for HTS films and their dielectric properties. Epitaxial C-axis YBCO films can be grown on the (100) face of any of these substrates. The best DC YBCO film properties generally are obtained in films grown on substrates with a perovskite or perovskite-related structure. The values of the loss tangent tan δ, shown in Figure 1, are too high for $SrTiO_3$ or yttria-stabilized zirconia (YSZ) to be used in RF applications. MgO, $LaAlO_3$, and $LaGaO_3$ have a tan δ for $T \leq 77°K$ that is acceptable for all but the highest-Q applications. For those applications, only sapphire has acceptably low dielectric losses.

The real part of the dielectric constant also can limit application. In microstrip configurations where two YBCO films are separated by the substrate thickness, the width of conducting lines and spacing between them are determined by the range of substrate thickness that can be used conveniently, ~ 0.3 to 0.6 mm. For UHF circuits, substrate area can be reduced by using a substrate with $\varepsilon_r$ = 20 to 25. For mm-wave circuits, fabrication tolerances become extremely small unless a low dielectric constant substrate is used.

Due to its combination of favor-

**TABLE II**
**DIELECTRIC PROPERTIES OF SUBSTRATES FOR HIGH $T_c$ FILMS**

| Substrate | $\varepsilon_r$ | f (GHz) | tan δ | Temperature (°K) | Reference Number |
|---|---|---|---|---|---|
| $SrTiO_3$ | 230 | 9.5 | $3 \times 10^{-2}$ | 300 | 7, 8 |
| | 215 | 10 kHz | $1.4 \times 10^{-1}$ | 300 | 9 |
| | 310 | 10 to 1000 | $3 \times 10^{-2}$ | 300 | 10 |
| | 1900 | 10 to 1000 | $6 \times 10^{-2}$ | 80 | 10 |
| | strongly T-dependent | 22 | 1 to $2 \times 10^{-3}$ | 77 to 500 | 11 |
| | strongly T-dependent | 22 | 2 to $24 \times 10^{-3}$ | 37 to 600 | 12 |
| $ZrO_2$(YSZ) | 38 | 33 | $4 \times 10^{-3}$ | 300 | 13 |
| | 27 | 1 MHz | $5.4 \times 10^{-3}$ | 300 | 14 |
| | 28 | 10 | $4 \times 10^{-3}$ | 300 | 15 |
| | 26 | 10 to 1000 | $1.6 \times 10^{-2}$ | 300 | 10 |
| | 25.4 | 10 to 1000 | $7.5 \times 10^{-3}$ | 80 | 10 |
| | 25 | 2 to 20 | 2 to $6 \times 10^{-4}$ | 4.2 | 16 |
| MgO | 9.8 | | $3 \times 10^{-4}$ | 300 | 7,17 |
| | 9.6 | 9.1 kHz | $2 \times 10^{-3}$ | 300 | 18 |
| | | 1 MHz | $9.1 \times 10^{-3}$ | 300 | 14 |
| | 9.87 | 10 to 1000 | $9 \times 10^{-4}$ | 300 | 10 |
| | 9.6 | 10 to 1000 | $4 \times 10^{-5}$ | 80 | 10 |
| | | 0.5 | $1 \times 10^{-6}$ | 4.2 | 19 |
| $Al_2O_3$ | 8.6 to 10.5 | | $1 \times 10^{-3}$ | 300 | 7 |
| | 9.5 to 11.5 | | $2 \times 10^{-4}$ | 300 | 8 |
| | 8.5 to 10.5 | 0.1 | $< 0.1$ | 750 | 7 |
| | | 9 | $1.5 \times 10^{-8}$ | 77 | 20 |
| | | 72 | $4.3 \times 10^{-7}$ | 77 | 20 |
| | | 3 | $2 \times 10^{-9}$ | 4.2 | 21 |
| | 10.65 | 10 | $6 \times 10^{-6}$ | | 17 |
| $LaGaO_3$ | 25 | 1 MHz | $1.8 \times 10^{-3}$ | 300 | 14 |
| | 25 | 0.5 to 15 | $1.5 \times 10^{-6}$ | 4.2 | 22 |
| $LaAlO_3$ | 23 | 9 | | 300 | 23 |
| | 16 | 10 | $5.8 \times 10^{-4}$ | 300 | 24 |
| | 16 | 10 | $8.3 \times 10^{-6}$ | 77 | 24 |
| | 16 | 10 | $1.5 \times 10^{-6}$ | 4.2 | 24 |
| | 20 | 500 | $< 5 \times 10^{-4}$ | 4.2 to 90 | 25 |
| | 24.5 | 0.5 to 15 | $2 \times 10^{-6}$ | 4.2 | 22 |
| $KTaO_3$ | 4000 | | | 300 | 26 |

able RF properties, mechanical properties and availability, sapphire appears a priori to be the preferred substrate. Epitaxial growth of C-axis YBCO occurs on the (1102) surface, which has a two-dimensional rectangular lattice. However, sapphire reacts more readily with YBCO than the other substrates of Table 1 and has a poor lattice match. From X-ray diffraction studies, it has been found that the YBCO (100) direction in the plane of the film lies parallel to the diagonal of the rectangular surface grid of sapphire, which is in agreement with previously published work.[27] Figure 2 shows how the lattice mismatch between various substrates and YBCO correlates with the X-ray rocking-curve width, full width at half maximum, for the (005) peak. For both sapphire and YSZ, the length of a diagonal in the two-dimensional surface grid is the appropriate lattice spacing. For all others, a $<100>$ direction in the film is parallel to a $<100>$ direction in the substrate. The rocking curve widths also correlate with DC critical current density[28] and $R_s$, with the best results obtained for films grown on $LaAlO_3$ and $SrTiO_3$.

Another advantage of the perovskite-structure substrates is a close thermal expansion match to YBCO. One disadvantage is the occurrence of a structural transformation at a temperature between the deposition and operating temperatures. After cycling through the transformation, strain in the crystal is relieved by twinning and through surface roughness. For $LaGAO_3$ a cubic-to-tetragonal transformation at 150°C results in a rough surface with, at times, discontinuities in the YBCO film. In the case of $LaAlO_3$ a cubic-to-rhombohedra 90.1° transformation at ~450°C does not disrupt the film although surface roughness is on the order of 50 nm, by profilometer measurement, with a period of 50 μm. Both perovskites can be produced by Czochralski growth and are available in sizes up to 2" in diameter. Substantially larger sizes would be useful for UHF antenna arrays. It is expected that $NdGaO_3$ will have all the advantages of $LaAlO_3$ without rough surfaces. Its structural transformation at 1350°C is at a temperature much greater than growth temperatures. Data on the dielectric properties of $NdGaO_3$ are not yet available.

In summary, $LaAlO_3$ is the preferred substrate at present for its lattice match to YBCO, chemical stability in contact with YBCO, availability in sizes up to 2" in diameter, reasonably low tan δ, and manageable dielectric constant. Nevertheless, there is a substantial effort underway to make use of sapphire by growing YBCO on a buffer layer of epitaxial MgO (100),[30,31] $LaAlO_3$ (100) or $SrTiO_3$ (100)[32] on sapphire.

### $R_s$ and YBCO Film Growth

The best YBCO films grown by sputtering, co-evaporation and laser ablation have comparable critical temperatures, transition widths, crit-

ical current densities and dependence on thickness for ultra-thin films (≤ 10 nm thick). The films have in common a deposition temperature of 650 to 750°C, growth in the presence of molecular or activated oxygen, and a cooldown from the deposition temperature in > 10 torr $O_2$ to transform to the orthorhombic YBCO structure.

Measurements of $R_s$ were made with X-band resonators in either a stripline, microstrip or parallel-plate configuration. In the stripline configuration, shown in Figure 3, an Nb film was patterned in a half-wavelength long line on one side of a 0.7" × 0.25" × 0.02" substrate and a Nb ground plane was deposited on the other side. An HTS film was used as the second ground plane,[33] and $R_s$ was calculated from the Q measured in transmission. The substrate of the HTS film was inside the resonator so current flowed in the film layer adjacent to the substrate. Measurements of $R_s$ were made only at 4.2° K. In the microstrip configuration, two nominally identical HTS films were mounted with both of their substrates in the cavity. One film was patterned in a half-wavelength line and the other was used as a ground plane. Again, $R_s$ was calculated[34] from Q measured in transmission.

For the third type of resonator, a parallel-plate design,[40] two unpatterned and nominally identical films on 0.25" × 0.5" substrates were placed face to face with a 12 μm thick teflon sheet separating them. The small separation between films resulted in a lower Q than for microstrip or stripline resonators. The low Q ensured that losses from the superconductor dominated over dielectric or radiation losses, even for the lowest $R_s$ films.[40] This configuration was not suitable for films with $R_s$ comparable to that of Cu at 10 GHz, that is, the parallel-plate resonator needed to have a thicker dielectric to obtain a measurable Q for high $R_s$ films. In all cases, including stripline, microstrip or parallel-plate resonators, the resonators were weakly coupled to the rest of the circuit so the unloaded Q could be assumed to be equal to the loaded Q.

Figure 4 shows the result of parallel-plate measurements at 10 GHz as a function of temperture for a pair of YBCO films deposited on $LaAlO_3$. Measurements were made in a cryorefrigerator. The range of $R_s$ values for chips cut from a single 2" diameter $LaAlO_3$ wafer were obtained from measurements made in liquid nitrogen. The YBCO films were deposited by off-axis sputtering from a stoichiometric $YBa_2Cu_3O_7$ target at a substrate temperature of 670°C by DC magnetron sputtering. The sputtering gas consisted of 20 mtorr $O_2$ and 130 mtorr Ar. Additional deposition details were published previously.[35] Figure 4 shows two general features of $R_s$ measurements made on state-of-the-art YBCO films; including a value of $R_s$ at X band that is signif-

[Continued on page 110]

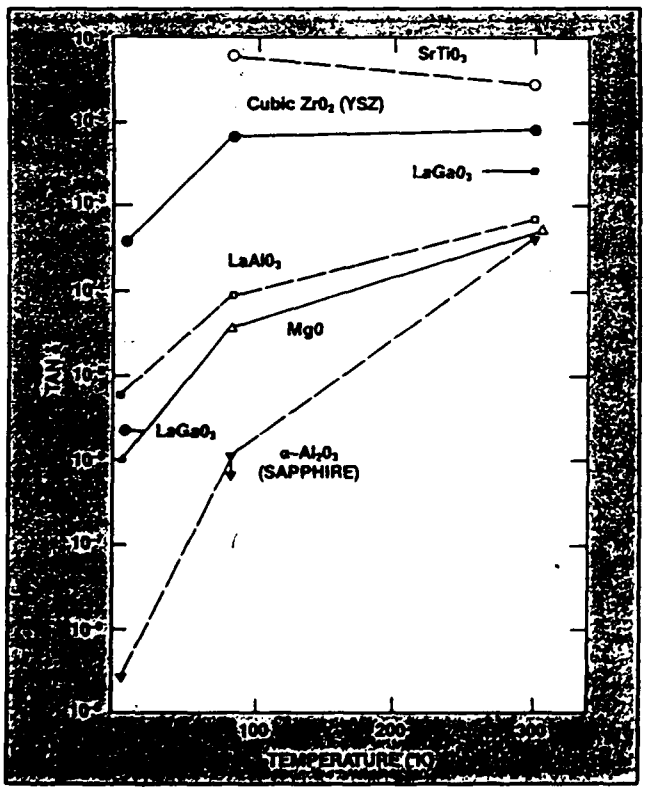


Fig. 1 A graph of the dielectric loss tangent (tan δ) as a function of temperature for single-crystal substrates. The data points represent a synthesis of the data in Table 1. The lines drawn between data points are included to distinguish data on different substrates.

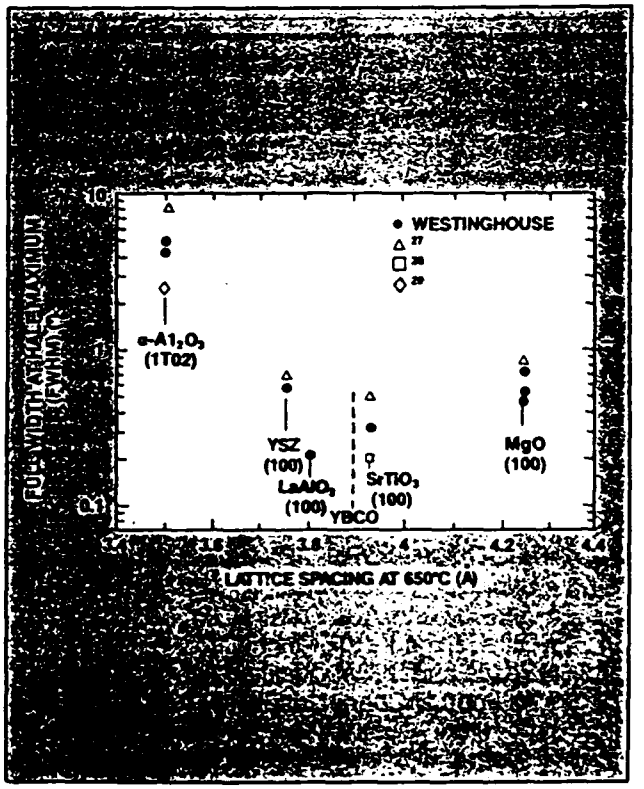


Fig. 2 X-ray rocking curve widths (FWHM) for the (005) peak of epitaxial YBCO films grown on various substrates. The data correlate with the difference between the lattice constant of YBCO and the substrate at the deposition temperature of ~ 650°C. For sapphire and YSZ, the lattice spacing is the length of a diagonal in the two-dimensional surface lattice that lies parallel to a < 100 > direction in the YBCO film.

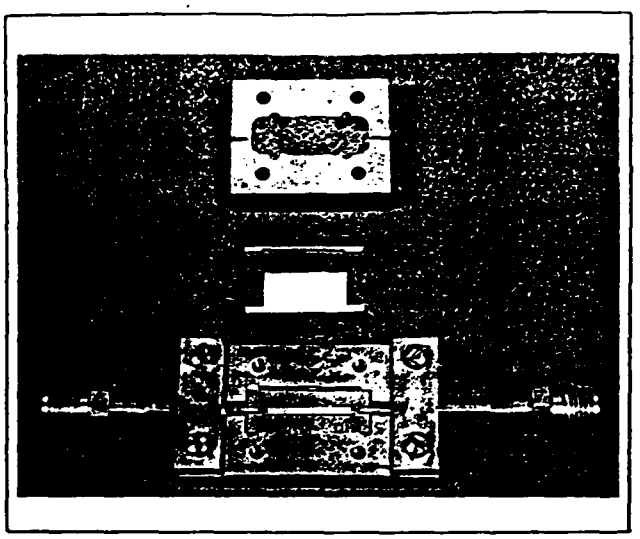

Fig. 3 *Nb and YBCO end-coupled stripline resonator.* The patterned conductor and bottom ground plane are epitaxial Nb films grown on sapphire. The top ground plane is a YBCO film to be evaluated. Capacitive coupling to the resonator is accomplished by adjustable pins.

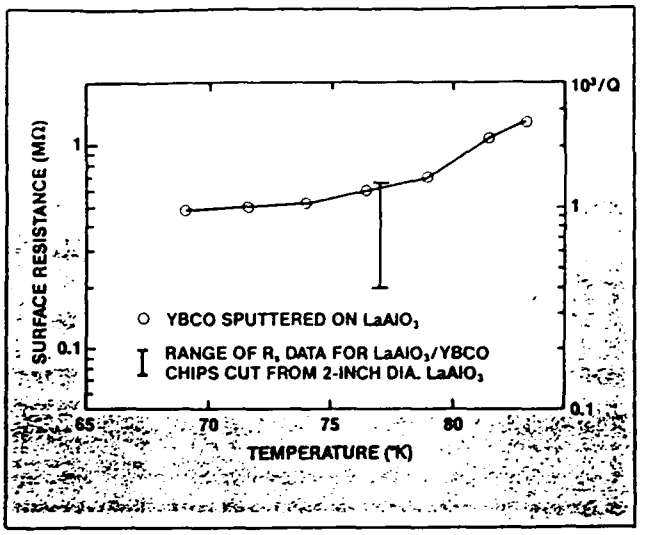


Fig. 4 $R_s$ and 1/Q as a function of temperature from parallel-plate resonator measurements at 10 GHz.

icantly lower than that of normal metals, for example, at 77°K and 10 GHz, copper has a surface resistance of 12 mΩ; and a slowly-varying temperature dependence of $R_s$ in the vicinity of 77°K. A priori concerns that 77°K is too close to the $T_c$ of YBCO for stable device operation appear to be resolved.

Conventional models for the electronic structure of superconductors predict that $R_s$ should decrease by several orders of magnitude as the temperature is reduced from 77°K to 4.2°K. It has been indicated that the behavior of $R_s$ of YBCO films at 77°K is similar to conventional superconductors, such as Nb ($T_c$ = 9.2°K), and that further improvements in $R_s$ at 77°K should be incremental.[45] However, at lower temperatures there is a substantial, temperature-independent, residual loss from an unidentified mechanism.

Table 3 shows a comparison between representative values of the surface resistance of YBCO films and superconducting niobium measured at 4.2°K. To permit a comparison of measurements at different frequencies to be made, it was assumed that $R_s$ scales with frequency as $f^2$. A straightforward interpretation of the data in Table 3 is that the best YBCO films made by different techniques and at different

**TABLE III**
**COMPARISON OF THE LOWEST $R_s$ MEASURED FOR YBCO AND Nb AT 4.2°K NORMALIZED TO 10 GHz by ASSUMING $R_s \propto f^2$**

| Reference | Side of Film Measured | Film Patterned | $R_s$ (Nb) | $R_s$ (YBCO) | $R_s$ (YBCO) / $R_s$ (Nb) | Deposition Technique* |
|---|---|---|---|---|---|---|
| Westinghouse | substrate | Y | 0.3 mΩ | 0.6 mΩ | 2 | L, S |
| Belohoubek, DSRC | substrate | Y | 0.15[29] | 0.3[37] | 2 | L, L** |
| Hammond, STI | both | N | | 0.6[37] | | L, S |
| Padamsee, Cornell | both | N | | 0.6[37] | | L, S |
| Drabeck UCLA | surface | Y | | 0.05[38] to 0.6[37] | | L, S |
| Piel, Wuppertal | surface | N | ~0.16[39] | 0.1[39] | <2 | L, S, E |
| Hewlett-Packard | surface | N | 0.02[40] | 0.02 to 0.04[40] | 1 to 2 | S, S |
| Cooke, LANL | surface | N | | 0.04[41] | | L, E |
| Oates, Lincoln Lab | both | Y | 0.05[42] to 0.2[39] | ≥0.4[39] | ≥2 | S, E |

*L — laser-ablated, S — sputtered, E — co-evaporated
**laser-ablated films obtained from two different sources
†NbR$_s$ (4.2°K, 87 GHz) ~10 to 25 mΩ; scaled to 10 GHz using Mattis-Bardeen theory instead of $f^2$

laboratories have a value of $R_s$ at 4.2°K within a factor of two of $R_s$ for Nb at 4.2°K. In this interpretation, the variation in the magnitude of $R_s$ from one laboratory to another must be due to differences in calibration of the measurement techniques. A second interpretation of Table 3 is that the measurement techniques used in most laboratories lack the sensitivity necessary to measure the low $R_s$ of either Nb or YBCO at 4.2°K. The correct interpretation could be determined if, for every technique used to measure $R_s$, a verification of sensitivity was made by cooling Nb below 4.2°K and observing a higher Q than obtained at 4.2°K.

Figure 4 and Table 3 lead to several important conclusions. Either the mechanism responsible for the residual resistance of YBCO is common to films made by all techniques and is independent of which film surface is being measured (free surface or interface with the substrate), or sputtered films with uniquely low residual losses[40] have a distinct advantage over laser ablated or evaporated films. The magnitude of the surface resistance at 10 GHz and $T << T_c$ is at least an order of magnitude lower than that of Cu. Since $R_s$ for a normal metal increases with frequency as the square root of f and for a superconductor as $f^2$, the state of the art represents a tremendous improvement over Cu for $f << 10$ GHz and little improvement for $f >> 10$ GHz. Whether or not the current YBCO film technology is sufficient to satisfy the requirements of a particular application depends not only on how high Q must be, but also on the operating frequency of a particular application. In regard to the previous discussion of substrates, all of the results in Table 3 were obtained for films grown on perovskite substrates with a close lattice match to YBCO.

**Remaining Materials Issues**

Since several film deposition techniques give comparable DC and RF YBCO film properties, an additional set of material requirements can be used to determine a preferred technique. The requirements include surface smoothness, integration with other deposited layers and scaling to large areas. These issues have been addressed partially for the techniques of sputtering, co-evaporation and laser ablation. Surface smoothness has the greatest impact on laser ablation since YBCO particles can be ejected from the target and deposited on the substrate. Sputtering has produced uniform YBCO films over substrate areas as large as 2" in diameter.[35,42] More recently, laser ablation has been used to deposit films on a comparable area by rastering the laser beam position on the substrate.

Integration of HTS films with epitaxial deposited dielectrics is important for crossovers and compact microstrip transmission and delay lines. The same insulators that have been used successfully as substrates and buffer layers on sapphire are the best candidates for dielectrics deposited between YBCO film layers. Epitaxial trilayers consisting of YBCO films separated by deposited $SrTiO_3$,[43] MgO,[31] and $LaAlO_3$[44] have been demonstrated, although $SrTiO_3$ is useful only for low frequency applications.

[Continued on page 113]

Another material requirement listed in Table 1 that has been addressed recently is growth of as-deposited crystalline films on both sides of a substrate. In the case of YBCO growth on sapphire, the optimum growth temperature falls in a range of 15°C. Temperature profiles that are uniform to this extent have to be obtained on a thermally-floating substrate that is maintained at 650 to 700°C by radiation rather than conduction. An unresolved issue is whether epitaxial multilayers must be formed in situ. Although epitaxial dielectric films will grow on YBCO underlayers that have been patterned, it is unknown whether the RF properties of either the superconductor or the insulating film are degraded compared to in-situ fabrication.

## Conclusion

Many of the requirements for RF applications using HTS films are attained by state-of-the-art YBCO films. At all frequencies up to mm-waves, and temperatures extending to within a few degrees of $T_c$, the surface resistance is much lower than that of normal metals. $LaAlO_3$ is a suitable substrate for all but the highest-Q applications and those requiring wafer areas greater than 2" in diameter.

## Acknowledgment

We would like to acknowledge the assistance of B.R. McAvoy, D.H. Watt and G.B. Draper with the measurements of surface resistance; T.T. Braggins, M.G. Forrester and J.R. Gavaler with YBCO film development; N.J. Doyle and A.M Stewart with X-ray measurements, and colleagues outside of Westinghouse who made their data available to us prior to publication through preprints and presentations. This paper was supported in part by AFOSR contract no. F49620-88-C-0039 and WRDC contract no. F33615-88-C-1841. This paper was presented at the 1990 SPIE Conference, SPIE Proc. Vol. 1292 (1990). ■

## References

1. "Bibliography of High $T_c$ Superconductivity," *J. Superconductivity*, Vol. 2, No. 1, 1989, pp. 1-210, Vol. 3, No. 1, 1990, pp. 1-153 and Vol. 4, No. 2, 1991, pp. 75-169.
2. C.L. Bohn, J.R. Delayen, U. Balachandran and M.T. Lanagan, "Radio Frequency Surface Resistance of Large-Area Bi-Sr-Ca-Cu-O Thick Films on Ag Plates," *Apl. Phys. Lett.*, Vol. 55, No. 3, 1989, pp. 304-306.
3. C.L. Lichtenberg, J. Wosik, M. Davis and J.C. Wolfe, "Microwave Microstrip Resonator Measurements of $YBa_2Cu_3O_{7-x}$ and $Bi_2Ca_1Cu_2O_{8-y}$ Thin Films," submitted to *Appl. Phys. Lett.*, 1989.
4. J.H. Takemoto, F.K. Oshita, H.R. Fetterman, P. Kobrin and E. Sovero, "Microstrip Ring Resonator Technique for Measuring Microwave Attenuation in High $T_c$ Superconducting Thin Films," IEEE Trans. Microwave Theory and Techniques, Vol. 37, No. 10, 1989, pp. 1650-1652.
5. R.B. Hammond, G.V. Negrete, M.S. Schmidt, M.J. Moskowitz, M.M. Eddy, D.D. Strother and D.L. Skoglund, "Superconducting Tl-Ca-Ba-Cu-O Thin Films Microstrip Resonator and its Power Handling Performance at 77°K," IEEE Microwave Symp., 1990.
6. D.W. Cooke, et al., "Microwave Characterization of High-Temperature Superconductors," submitted to SPIE's Symp. Microelectronic Integrated Processing: Growth, Monitoring & Control, Santa Clara, CA., 1989.
7. *Landolt-Bornstein Numerical Data and Functional Relationships*, Vol. II, Chapt. 6, Springer-Verlag, Heidelberg, 1959, pp. 462-558.
8. A.F. Harvey, *Microwave Engineering*, Academic Press, New York, 1963, pp. 253-254.
9. K. Araki, I. Iwasa, Y. Kobayshi, S. Nagata and M. Morisue, "Ultra Broad Band Measurements on High-$T_c$ Ceramic Superconducting Transmission Lines," IEEE Trans. Magn., Vol. 25, 1989, pp. 980-983.
10. B.P. Gorshunov, G.V. Kozlov, S.I. Krasnosvobodstev, E.V. Pechen, A.M. Prokhorov, A.S. Prokhorov, Q.I. Syrotynsky and A.A. Volkov, "Submillimetre Properties of High-$T_c$ Superconductors," *Physica C*, Vol. 153-155, 1988, pp. 667-670.
11. G. Rupprecht and R.O. Bell, "Microwave Losses in Cubic Strontium Titanate above the Phase Transition," *Phys. Rev.*, Vol. 123, No. 1, 1961, pp. 97-98.
12. G. Rupprecht, R.O. Bell and B.D. Silverman, "Nonlinearity and Microwave Losses in Cubic Strontium Titanate," *Phys. Rev.*, Vol. 125, No. 6, 1962, pp. 1915-1920.
13. J.S. Thorp and H.P. Buckley, "The Dielectric Constants of Current-Blackened Single Crystal Yttria-Stabilized Zirconia," *J. Mater. Sci.*, Vol. 8, 1973, pp. 1401-1408.
14. R.L. Sandstrom, E.A. Giess, W.J. Gallagher, A. Segmuller, E.I. Cooper, M.F. Chisholm, A. Gupta, S. Shinde and R.B. Laibowitz, "Lanthanum Gallate Substrates for Epitaxial High-$T_c$ Superconducting Thin Films," *Appl. Phys. Lett.*, Vol. 53, No. 19, 1988, pp. 1874-1876.
15. M.T. Lanagan, J.K. Yamamoto, A. Bhalla and S.G. Sankar, "The Dielectric Properties of Yttria-Stabilized Zirconia," *Mater. Lett.*, Vol. 7, 1989, p. 437.
16. A.C. Anderson, B.Y. Tsaur, J.W. Steinbeck and M.S. Dilorio, "RF Surface Resistance of $YBa_2Cu_3O_{7-x}$ Thin Films," MIT Lincoln Laboratory Quarterly Tech. Rep., March 11, 1988.
17. J. Musil and F. Zacek, "Microwave Measurements of Complex Permittivity by Free Space Methods and Their Applications," in *Studies in Electrical and Electronic Engineering*, Vol. 22, Elsevier, New York, 1986, pp. 254-262.
18. J.S. Thorp and N. Enayati-Rad, "The Dielectric Behavior of Single-Crystal MgO, Fe/MgO and Cr/MgO," *J. Mater. Sci.*, Vol. 16, 1981, pp. 255-260.
19. D. Oates, Lincoln Laboratory, unpublished.
20. V.B. Braginsky, V.S. Ilchenko and Kh.S. Bagdassarov, "Experimental Observation of Fundamental Microwave Absorption in High-Quality Dielectric Crystals," *Phys. Lett. A.*, Vol. 120, 1987, and references therein, pp. 300-303.
21. V.B. Braginsky and V.I. Panov, "Superconducting Resonators on Sapphire," IEEE Trans. Magn., MAG-15, No. 1, 1979, pp. 3-33.
22. W.G. Lyons, "Low Loss Substrates for High-Temperature Superconductors," MIT Lincoln Laboratory Quarterly Tech. Rep., October 1989.
23. J.D. Adam, Westinghouse, unpublished.
24. R.W. Simon, C.E. Platt, K.P. Daly, A.E. Lee and M.K. Wagner, "Improvement of Average Film Quality in $RBa_2Cu_3O_{7-x}$ Sputtered Films," IEEE Trans. Magn., MAG-25, 1989, pp. 2433-2436 and *Appl. Phys. Lett.*, Vol. 53, 1988, pp. 2677-2679.
25. M.C. Nuss, P.M. Mankiewich, R.E. Howard, B.L. Straughn, T.E. Harvey, C.D. Brandle, G.W. Berkstrasser, K.W. Goossen and P.R. Smith, "Propagation of Terahertz Bandwidth Electrical Pulses on $YBa_2Cu_3O_7$ Transmission Lines on $LaAlO_3$ Substrates," *Appl. Phys. Lett.*, Vol. 54, 1989, pp. 2265-2267.
26. R.W. Simon, A.E. Lee, C.E. Platt, K.P. Daly, J.A. Luine, C.B. Eom, P.A. Rosenthal, X.D. Wu and T. Venkatesan, "Growth of High-Temperature Superconductor Thin Films on Lanthanum Aluminate Substrates," in *Science and Technology of Thin-Film Superconductors*, R. McConnell and S.A. Wolf (eds.), Plenum, New York, 1989, pp. 337-346.
27. J. Geerk, G. Linker and O.Meyer, "Epitaxial Growth and Properties of YBaCuO Thin Films," *Mater. Sci Reports*, Vol. 4, 1989, pp. 192-260.
28. A. Inam, M.S. Hegde, X.D. Wu, T. Venkatesan, P. England, P.F. Miceli, E.W. Chase, C.C. Chang, J.M. Tarascon and J.B. Wachtman, "As-Deposited High $T_c$ and J. Superconducting Thin Films Made at Low Temperatures," *Appl. Phys. Lett.*, Vol. 53, No. 10, 1988, pp. 908-910.
29. K. Char, D.K. Fork, T.H. Geballe, S.S. Laderman, R.C. Taber, R.D. Jacowitz, F. Bridges, G.A.N. Connell and J.B. Boyce, "Properties of Epitaxial $YBa_2Cu_3O_7$ Thin Films on $Al_2O_3$ No. 1012, *Appl. Phys. Lett.*, Vol. 56, No. 8, 1990, pp. 183-185.
30. J. Talvacchio, G.R. Wagner and H.C. Pohl, "$YBa_2Cu_3O_7$ Films Grown on Epitaxial MgO Buffer Layers on Sapphire," *Physica C*, Vol. 162-164, 1989, pp. 659-660.

31. A.B. Berezin, C.W. Yuan and A.L. de Lozanne, "$Y_1Ba_2Cu_3O_{7-x}$ Thin Films Grown on Sapphire with Epitaxial MgO Buffer Layers," *Appl. Phys. Lett.*, Vol. 57, 1990, pp. 90–92.
32. K. Char, N. Newman, S.M. Garrison, R.W. Barton, R.C. Taber, S.S. Laderman and R.D. Jacowitz, "Microwave Surface Resistance of YBCO Thin Films on Sapphire," *Appl. Phys. Lett.*, Vol. 57, 1990, pp. 409–411.
33. A.C. Anderson, B.-Y. Tsaur, J.W. Steinbeck and M.S. Dilorio, "RF Surface Resistance of $YBa_2Cu_3O_{7-x}$ Thin Films," MIT Lincoln Laboratory Quarterly Tech. Rep., March 11, 1988.
34. M.V. Schneider, "Microstrip Lines for Microwave Integrated Circuits," *Bell System Technical Journal*, May-June 1969, pp. 1421–1444.
35. J. Talvacchio, J.R. Gavaler, M.G. Forrester and T.T. Braggins to appear in *Science and Technology of Thin Film Superconductors II*, R.D. McConnell and S.A. Wolf (eds.), Plenum, New York, 1990.
36. R. Brown, V. Pendrick and D. Kalokitis, "A Low Loss Substrate for Microwave Application of High Temperature Superconductor Films," *Appl. Phys. Lett.*, Vol. 57, 1990, pp. 1351–1353.
37. A. Inam, L. Nazar, M.S. Hedge, C.T. Rogers, T. Venkatesan, R.W. Simon, K. Daly, H. Padamsee, J. Kirchgessner, D. Moffat, D. Rubin, Q.S. Shu, D. Kalokitis, A. Fathy, V. Pendrick, R. Brown, B. Brycki, E. Belohoubek, L. Drabeck, G. Gurner, R. Hammond, F. Gamble, B.M. Lairson and J.C. Bravman, "Microwave Properties of Highly Oriented $Y_1Ba_2Cu_3O_{7-x}$ Thin Films," *Appl. Phys. Lett.*, Vol. 56, No. 12, 1990, pp. 1178–1180. Based on the temperature dependence of $R_3$ for the best Westinghouse films and the data presented by Inam in the range, 50° K to 90° K, a ratio, $R_3$ 77 K/$R_3$ 4.2 K = 2.5 was assumed.
38. Data presented at the Symposium on High Temperature Superconductors in High Frequency Fields, Williamsburg, VA, March 1990.
39. N. Klein, G. Muller, H. Piel, B. Roas, L. Schultz, U. Klein and M. Peiniger, "Millimeter Wave Surface Resistance of Epitaxially Grown $YBa_2Cu_3O_{7-x}$ Thin Films," *Appl. Phys. Lett.*, Vol. 54, No. 8, 1989, pp. 757–759.
40. R.C. Taber, "A Parallel Plate Resonator Technique for Microwave Loss Measurements on Superconductors," *Rev. Sci. Inst.*, Vol. 61, 1990, pp. 2200–2206.
41. D.W. Cooke, E.R. Gray, R.J. Houlton, B. Rusnak, E.A. Meyer, J.G. Beery, D.R. Brown, F.H. Garzon, I.D. Raistrick, A.D. Rollet and R. Bolmaro, "Surface Resistance of $YBa_2Cu_3O_7$ Films on $SrTiO_3$ and $LaGaO_3$ Substrates," *Appl. Phys. Lett.*, Vol. 55, No. 9, 1989, pp. 914–916.
42. N. Newman, K. Char, S.M. Garrison, R.W. Barton, R.C. Taber, C.B. Eom, T.H. Geballe and B. Wilkens, "YBCO Superconducting Films for Insulating Crossovers," *Appl. Phys. Lett.*, Vol. 56, No. 2, 1990, pp. 189–191.
43. J.J. Kingston, F.C. Wellstood, P. Lerch, A.H. Miklich and J. Clarke, "Multilayer $YBa_2Cu_3O_X$-$SrTiO_3$-$YBa_2Cu_3O_x$ Films for Insulating Crossovers, " *Appl. Phys. Lett.*, Vol. 56, No. 2, 1990, pp. 189–191.
44. R.W. Simon, J.F. Burch, K.P. Daly, W.D. Dozier, R. Hu, A.E. Lee, J.A. Luine, H.M. Manasevit, C.E. Platt, S.M. Schwarzbek, D. St. John, M.S. Wire and M.J. Zani, "Progress toward a YBCO Circuit Process," to appear in *Science and Technology of Thin Film Superconductors II*, R.D. McConnell and S.A. Wolf (eds.), Plenum, New York, 1990.
45. H. Piel and G. Müller, "The Microwave Surface Impedance of High $T_c$ Superconductors," IEEE Trans. Magn., Vol. 27, No. 2, 1991, pp. 854–862.


**John Talvacchio** *received his BS degree in physics from Case Western Reserve University, Cleveland, OH, in 1977 and his PhD in applied physics from Stanford University, Stanford, CA, in 1982. Since 1982, he has worked at the Westinghouse Science and Technology Center, in the area of materials for superconducting electronics. Talvacchio is a member of the American Physical Society and the Materials Research Society.*

**George R. Wagner** *received his BS in engineering physics from the University of Illinois in 1960, and his MS and PhD in physics from Carnegie Mellon University in 1962 and 1965, respectively. Since 1960, he has been at Westinghouse Science and Technology Center, where currently he is program manager of Superconductor Materials and Electronics. He has been active in several areas of research involving the magnetic and optical properties of solids, and superconductivity. Wagner is a member of Tau Beta Pi and the American Physical Society.*

**Salvador H. Talisa** *received his telecommunications degree from the Polytechnic University in Catalonia, Barcelona, Spain, in 1976. He received his MSc and PhD degrees in electrical engineering from Brown University in 1978 and 1982, respectively. Talisa's work has dealt with the theoretical analysis of ferrite-loaded planar structures, modeling microstrip and stripline nonreciprocal devices, such as isolators and phase shifters, for use at microwave frequencies. He also has been engaged in feasibility studies for nonreciprocal devices based on surface magnetoplasmons in GaAs-dielectric interfaces for operation at submm-wavelengths. Since 1982, Talisa has been with Westinghouse, where he has been involved in microwave device applications of magnetic and magneto-optic materials and the characterization of magnetic thin films for microwave aplications. Currently, he is working on high temperature superconducting thin-film microwave devices.*

# Effects of microstructure on flux pinning in epitaxial $YBa_2Cu_3O_x$ films

D. H. Kim, D. J. Miller, J. C. Smith, and R. A. Holoboff
*Materials Science Division, Argonne National Laboratory, Argonne, Illinois 60439*

**APPENDIX 10**

J. H. Kang and J. Talvacchio
*Westinghouse Science and Technology Center, Pittsburgh, Pennsylvania 15235*

(Received 6 May 1991)

The role of microstructure on flux pinning in *c*-axis-oriented epitaxial $YBa_2Cu_3O_x$ films grown on $LaAlO_3$ and $SrTiO_3$ has been studied. For a magnetic field parallel to the Cu-O planes, the resistivity and critical current density $J_c$ have been measured as a function of the angle $\theta$ between the applied field and the direction of the transport current. In addition to a Lorentz-force-independent resistivity, the Lorentz-force-dependent component showed several broad deviations from $\sin^2\theta$ when a field was aligned parallel to certain microstructural features which vary with the film thickness and substrate material. These features were identified by transmission-electron-microscopy analysis. For films of 5000 Å thickness on $LaAlO_3$, resistivity dips were observed for a field applied parallel to the *substrate* twin boundaries or along misoriented *a*-axis grains. In thinner films of 900 Å thickness also on $LaAlO_3$ in which *a*-axis grains were negligible, we observed dips corresponding to the orientation of *substrate* twin boundaries only. For thin films on $SrTiO_3$ in which substrate twins are absent, resistivity dips corresponding to the direction of twin boundaries in the *film* and, perhaps, interfacial dislocations were observed. Overall, such dips decreased with increasing transport current density and became negligible in $J_c$ measurements.

## I. INTRODUCTION

High-temperature superconductors (HTS's) exhibit unusually large magnetic-field-induced broadening of their resistive transitions, which generally increase with the anisotropy.[1-3] With the applied field H *parallel* to the superconducting Cu-O layers ($H\|a$), the broadening is not as large due to the anticipated intrinsic pinning of the insulating (or normal) region between layers.[4,5] In highly anisotropic HTS's, such as $Bi_2Sr_2CaCu_2O_x$ (Ref. 6) and $Tl_2Ba_2CaCu_2O_x$ (Refs. 2,7), Lorentz-force-independent resistive transitions were observed and an explanation other than flux motion has been proposed.[7] However, for less anisotropic $YBa_2Cu_3O_x$, intrinsic pinning is smaller due to the shorter interlayer spacing and the conducting Cu-O chains between superconducting Cu-O double layers. In this material, a Lorentz-force-induced flux flow resistivity which varies as $\sin^2\theta$ has been observed in high-quality single crystals,[8] where $\theta$ is the angle between the direction of the transport current and magnetic field. Moreover, when a magnetic field is aligned parallel to the twin boundaries, a sharp drop in resistivity was found at the foot of the transition, indicating substantial flux pinning by twin boundaries.[8] Magnetization measurements also show a similar effect of flux pinning by twin boundaries.[9,10] A larger magnetization-hysteresis loop was observed for fields parallel to twin boundaries than perpendicular to the boundaries.[9] In thin films, flux pinning is more complex mainly due to the presence of the substrates. Iye *et al.*[11,12] measured the angular-dependent resistivity in epitaxial $YBa_2Cu_3O_x$ films and observed four broad dips which were attributed to the Lorentz-force effect and the *ab*-plane anisotropy averaged over twin domains.

In this paper, angular-dependent transport studies of high-quality epitaxial $YBa_2Cu_3O_x$ films are reported. Resistivity and critical-current density for $H\|a$ as a function of angle $\theta$ were measured. Several dips are observed in the angular-dependent flux flow resistivity. In order to clarify the origins of the deviation from flux flow resistivity, transmission electron microscopy (TEM) was performed on samples prepared from the same batch. The relative orientations of the microstrip as well as various microstructural features with respect to the substrate were determined by TEM and electron diffraction to correlate with the angle $\theta$ between current and field at which the dips in resistivity were observed. Several dips were observed similar to the previous works of Iye *et al.*,[11,12] but we interpret the origin of dips as a pinning effect due to the microstructure in the films based on TEM rather than due to the *ab*-plane anisotropy. For films of 5000 Å thickness on $LaAlO_3$, four resistivity dips were observed in one period for a field applied parallel to substrate twin boundaries or along misoriented *a*-axis grains. In thinner films of 900 Å thickness also on $LaAlO_3$ in which *a*-axis grains were negligible, we observed only two dips, corresponding to the orientation of substrate twin boundaries. For thin films on $SrTiO_3$ in which substrate twins are absent, resistivity dips corresponding to the direction of twin boundaries in the film and, perhaps, interfacial dislocations were observed. Such pinning effects became weaker as the temperature or transport current was increased.

 ©1991 The American Physical Society

## II. EXPERIMENT

Films on $YBa_2Cu_3O_x$ were grown *in situ* by dc magnetron sputtering from a stoichiometric target onto $LaAlO_3$ (100) and $SrTiO_3$ (100) substrates. TEM showed that films are epitaxial and *c*-axis oriented. All of the films studied here exhibit vanishing zero-field resistance around $T_c = 88-89$ K. The samples were patterned to form a 6–25 $\mu$m wide strip with conventional photolithography and ion milling. Gold was sputtered on the current and voltage pads to reduce the contact resistance. The typical distance between the voltage probes was 0.1 cm, thus we are measuring an averaged effect of the microstructures. Samples are placed in the rotating holder so that we can vary the angle $\theta$ with 1° resolution in the *ab* plane. At every $\theta$ position, samples are tilted back and forth slightly in the *ac* plane to find the minimum resistance. In this manner, the angular resolution achieved for the *ac* plane is much better than the full width at half maximum of the rocking curve (0.4°–0.5°).

Conventional techniques were used to prepare planar and cross-section samples for TEM. After grinding and dimpling, the samples were ion milled using 4 kV Ar with a low beam current while maintaining at liquid nitrogen temperatures to minimize damage to the films. The samples were imaged in a Philips CM-30 operating at either 100 or 300 kV. Among five samples of $YBa_2Cu_3O_x$ films studied, the characteristics of three representative films are listed in Table I. The other two showed almost identical behavior to samples 2 and 3.

## III. RESULTS AND DISCUSSION

Figure 1 shows the resistive transition of a 5000 Å $YBa_2Cu_3O_x$ film on $LaAlO_3$ in zero field and 4 T for fields parallel to the current (H||I) and for fields perpendicular to the current (H⊥I). The inset shows the same transition plotted on a semilogarithmic scale. A slight double transition in zero field was usually observed in all samples grown on $LaAlO_3$ substrates but vanishes in finite fields (> 1 T). The Lorentz-force-dependent component is clearly observed in the 4 T field with a large Lorentz-force-independent background. This background broadening could be due to a mechanism other than flux-flow-induced dissipation[7,13] and is subject to future study. In this work, only the Lorentz-force-dependent part will be considered.

The angular-dependent resistivity at 90.5 K and 4 T

TABLE I. The characteristics of the three representative $YBa_2Cu_3O_x$ films are listed. $J_c$ was determined using a 2 $\mu$V/cm criterion. Samples 2 and 3 were grown from the same batch.

| Sample | Substrate | Thickness (Å) | Width of strip ($\mu$m) | $T_c$ (K) | $J_c$ at 77 K and 0 T (A/cm$^2$) |
|---|---|---|---|---|---|
| 1 | $LaAlO_3$(100) | 5000 | 25 | 89.2 | $1.0\times10^6$ |
| 2 | $LaAlO_3$(100) | 900 | 13 | 87.8 | $2.3\times10^6$ |
| 3 | $SrTiO_3$(100) | 900 | 6 | 89.4 | $4.1\times10^6$ |

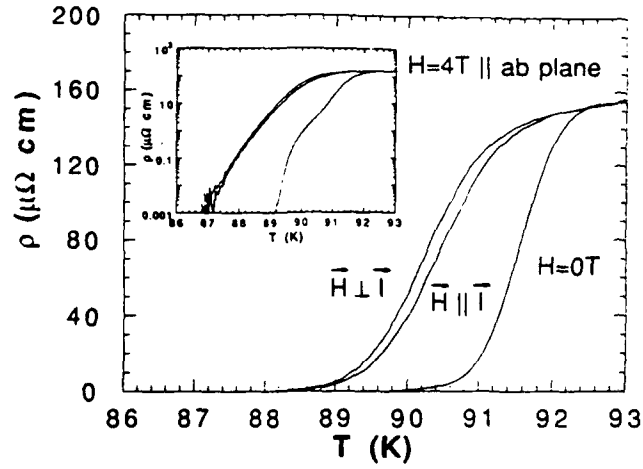


FIG. 1. Resistive transitions of sample 1 in 0 and 4 T fields are shown for H⊥I and H||I. A small Lorentz-force-dependent component with a large background broadening can be seen. Inset shows the same transition on a semilogarithmic scale.

with a measuring current density of 80 A/cm$^2$ is shown as circles in Fig. 2(a). A simple flux flow model predicts a $\sin^2\theta$ dependence with a maximum resistivity at H⊥I, shown as a solid line in Fig. 2(a), but data show additional four dips separated by 45° in one period. Deviation from an ideal flux flow resistivity, $\Delta\rho_{ff}$, is also plotted in Fig. 2(a) (diamonds) and four dips are seen more clearly. At a lower temperature, 87.9 K, the magnitudes of the dips increases [Fig. 2(b)] but a large transport current density of 8000 A/cm$^2$ significantly reduces the magnitude as shown in Fig. 2(c). This temperature- and current-dependent behavior suggests that the resistivity drop is due to the flux pinning effect. Such dips are no longer observable in $J_c$ measurements [Fig. 2(d)], but a slight asymmetry is observed which is reminiscent of the dips. It is worthwhile to note that a similar $J_c$ measurement in the low-$T_c$ material[14] showed an in-plane anisotropy of greater than 20 with a $\sin^{-1}\theta$ dependence except near $\theta = 0°$, consistent with the Lorentz-force-induced dissipation. In this work, $J_c$ anisotropy was found to be about 3 or less, considerably smaller than that in Ref. 14, and it decreased slightly at low temperatures and fields. In addition, a $\sin^{-1}\theta$ dependence was observed only near $\theta \approx 90°$. This behavior suggests that a mechanism other than flux-flow-induced dissipation limits $J_c$ over a substantial region around $\theta \approx 0°$.

A typical TEM micrograph of a planar section of sample 1 is shown in Fig. 3(a). Needle-shaped crystallites marked A are *a*-axis-oriented grains, while larger particles marked *B* are CuO, as identified by EDS and electron diffraction. Figure 3(b) shows a higher magnification image of a misoriented grain in which *c*-axis fringes can be clearly seen. Electron diffraction showed that these particles are oriented along either *a* or *b* axis of the *c*-axis-oriented background, so that these grains are aligned with the principal axes of the substrate. Epitaxial formation at the substrate and film boundaries can be seen in Fig. 4(a) in the cross-sectional TEM micrograph. The *a*-

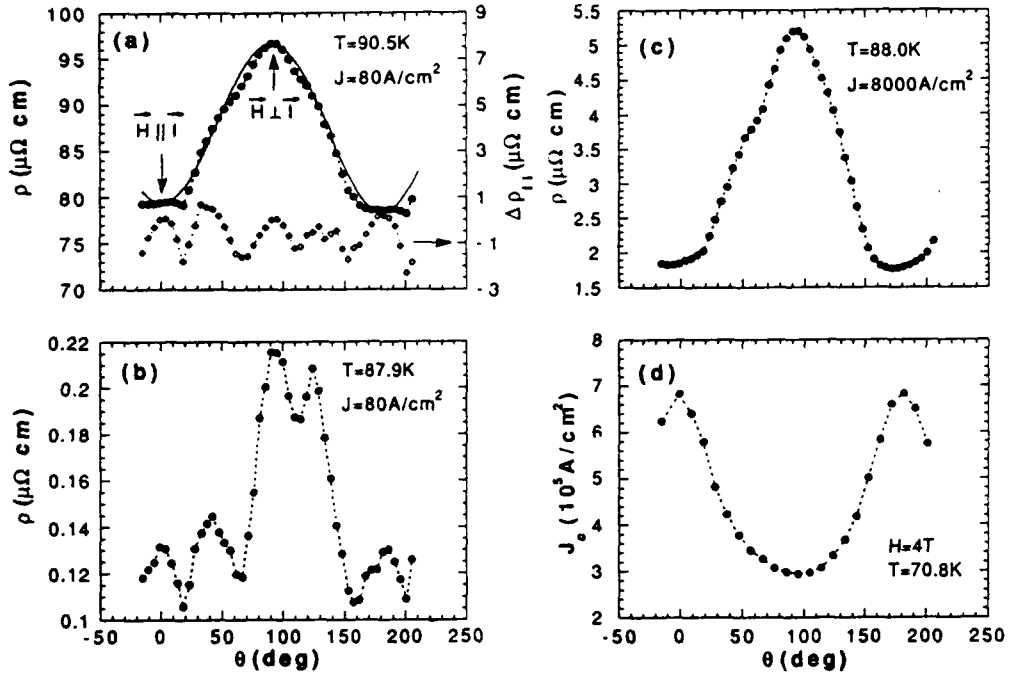


FIG. 2. (a) Angular-dependent resistivity of sample 1 at 90.5 K and 4 T with a measuring current density of 80 A/cm$^2$ is shown as circles. Solid lines are a $\sin^2\theta$ fit and dotted lines are a guide to the eye. Deviation from ideal flux flow resistivity, $\Delta\rho_{ff}$, is also plotted as diamonds and four dips separated by 45° are clearly seen. (b) Resistivity dips develop sharply at 87.9 K. Field and measuring current density are the same as (a). (c) At the same condition as (b), but a large transport current density of 8000 A/cm$^2$ reduces the magnitude of the dips. (d) The $J_c$ measurement at 70.8 K shows hardly any dip.

axis grains nucleate only beyond a certain film thickness of the order of a few hundred angstroms, not directly from the substrate as shown in Fig. 4(b).

$LaAlO_3$ substrates become heavily twinned during the cool-down process after the *in situ* growth of films and these twin boundaries are oriented 45° from the principal axis, thus any twin boundaries in $YBa_2Cu_3O_x$ films would be parallel to the substrate twin boundaries. However, it was not clear whether this film is twinned or not. In some plane-section images, evidence of twinning is observed, but selected area diffraction patterns do not show the typical spot splitting associated with twins in $YBa_2Cu_3O_x$. Additionally, the structure resembling twins is observed only when the underlying substrate is also present. In regions that have been thinned so that no substrate remains, this twin structure is absent. One might argue that the absence of twins in the free-standing part of the film is due to untwinning during sample preparation such as ion milling, but the samples were kept at 77 K during ion milling so that the resulting local heating is not sufficient enough to untwin the film. Similarly prepared specimen of the single crystals and films on $SrTiO_3$ showed no such untwinning effect. Thus, it is considered that this film is free of twins, but that the presence of substrate twins induces a change in the direction of strain associated with the slight misfit between $YBa_2Cu_3O_x$ and $LaAlO_3$.

There is a correlation between the orientation of each of the microstructural features with resistivity drops. The relatively broader dips at 65° and 155° in Fig. 2 correspond to the substrate twin boundary orientations. The resistivity drop for a field parallel to the substrate twin boundaries may be due to flux pinning by undetermined microstructural features in the sample induced by strain associated with the substrate twins. The other dips at 20° and 110° correspond to the directions along the needle shape of the *a*-axis-oriented particles. There are two possibilities for these two dips: flux pinning at the boundaries between the misoriented crystal and the background material or the resistivity anisotropy between $H\|c$ and $H\|a$ of the *a*-axis grains. In the latter case, the resistivity contribution from the *a*-axis grain is minimum when the field is aligned parallel to the Cu-O planes of the *a*-axis grains. Then the magnitude of the dip should be roughly the product of the volume occupied by *a*-axis grains and the resistivity difference between $H\|c$ and $H\|a$. The volume of *a*-axis grains was estimated from TEM micrographs and the resistivity difference at the corresponding temperatures was measured. It was found that about 30% of the resistivity drop can be accounted for on this basis. This suggests that other mechanism of pinning, perhaps due to a *a*-axis grain boundaries or some other features, are dominant.

Iye *et al.*[11,12] explained the dips for the field along the *a* or *b* axis (in this case, along the *a*-axis grains) as a result of the *ab*-plane anisotropy averaged over twin domains. However, the measurements on the twinned single crystals[8] did not show any dips associated with the *ab*-plane anisotropy, and recent magnetic measurements on the *untwinned* single crystals showed no significant *ab*-plane anisotropy in the lower[15] and upper critical fields.[16] The *ab*-plane resistivity anisotropy of the untwinned single crystals for magnetic fields parallel to the Cu-O planes has not been reported to our knowledge.

Since the *a*-axis-oriented grains start to grow only beyond a certain film thickness [Fig. 4(b)], the effect of the misoriented grains can be reduced by growing thinner films. The resistive transitions for a 900-Å-thick film on $LaAlO_3$ (sample 2) in 0 and 4 T fields for H||I and H⊥I are shown in Fig. 5 on a linear and logarithmic scale. Measurements of resistivity as a function of angle $\theta$ at 88.0 K display an ideal flux flow resistivity as shown in Fig. 6(a) for a measuring current density of 160 A/cm$^2$. This temperature is approximately equivalent to 90.5 K in the thicker film of sample 1 where resistivity dips due to microstructural features were observed. It implies that defect structures, such as *a*-axis-oriented grains, grow with film thickness and so does the pinning effect. At a lower temperature, 86.7 K, only *two* dips at 53° and 143° corresponding to the orientation of the substrate twin boundaries are evident as shown in Fig. 6(b). The dips resulting from the misoriented particles are negligible as expected. This result is consistent with the absence of *a*-axis grains as confirmed by TEM of a film cross section. Similar measurements on a 1500-Å-thick film on $LaAlO_3$ also showed only two dips corresponding to *a*-axis grains. At higher transport current densities, reduction of the dips has been observed similar to the case of sample 1, and the critical-current density at 77 K showed no dips at all. This behavior suggests that these microscopic structures are not effective pinning centers for high current applications, and more uniformly distributed pinning centers, such as oxygen vacancies and dislocations, could be more effective at low temperatures.

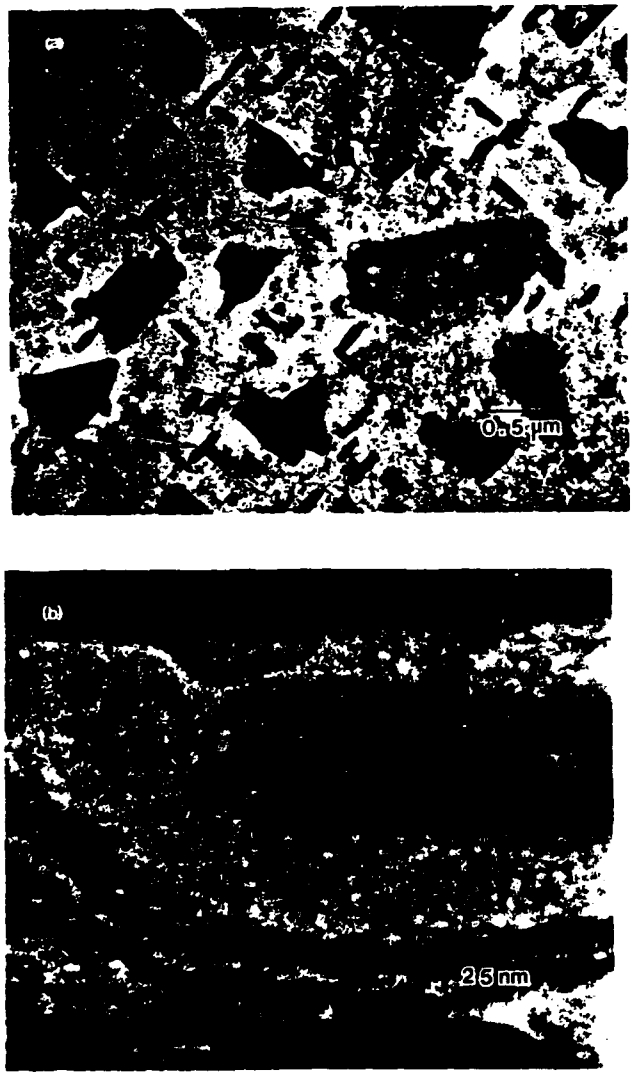


FIG. 3. (a) Bright-field electron micrograph of a planar section of $YBa_2Cu_3O_x$ on $LaAlO_3$. The needle-shaped crystallites marked A are *a*-axis-oriented grains, and the larger particles marked B are CuO. (b) Higher magnification image of the same plane section showing an *a*-axis-oriented particle. Electron diffraction pattern shows the *c* axis of this particle to be parallel to the *a* or *b* axis of the matrix grain.

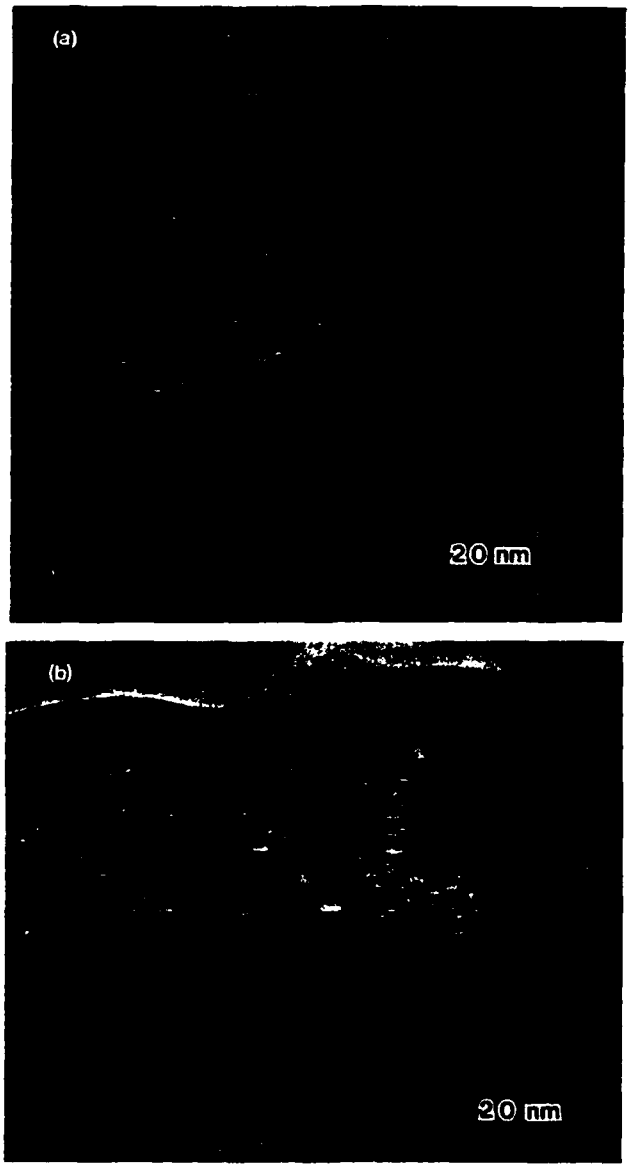


FIG. 4. (a) Bright-field electron micrograph of a cross section of the film showing epitaxial growth of a film near the substrate. (b) Low magnification image of the cross section showing *a*-axis grains which nucleate only when the film has reached a minimum thickness.

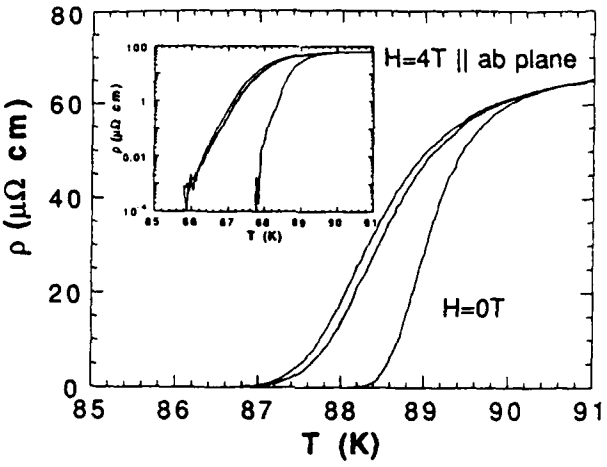


FIG. 5. Resistive transitions of sample 2 in 0 and 4 T fields are shown for H⊥I and H∥I.

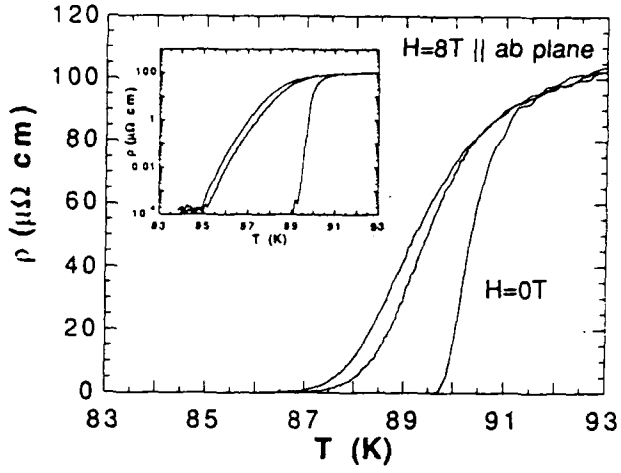


FIG. 7. Resistive transitions of sample 3 in 0 and 8 T fields are shown for H⊥I and H∥I.

So far, the discussion has been limited to samples grown on $LaAlO_3$ where *substrate* twin boundaries play an important role in flux pinning for small transport currents (typically $J < 10^4$ A/cm$^2$). On the other hand, $SrTiO_3$ does not form any twin structure, thus it is interesting to study films grown on this substrate for comparison. We have measured two samples on $SrTiO_3$ from the same batch as sample 2, and they exhibit almost identical behavior. Figure 7 shows resistive transitions in 0 and 8 T fields for sample 3 of 900 Å thickness.

The angular dependence of the resistivity at 88.3 K for 8 T with a measuring current density of 270 A/cm$^2$ is shown in Fig. 8(a), and an ideal flux flow resistivity is observed. At 86.3 K, three dips develop in one period as shown in Fig. 8(b). At higher transport current densities, reduction of the dips has been observed, similar to the case of samples 1 and 2. The critical-current density at low temperatures showed no structure at all. The TEM plane section (Fig. 9) shows twin boundaries in the sample, and electron diffraction indicates that the twin boun-

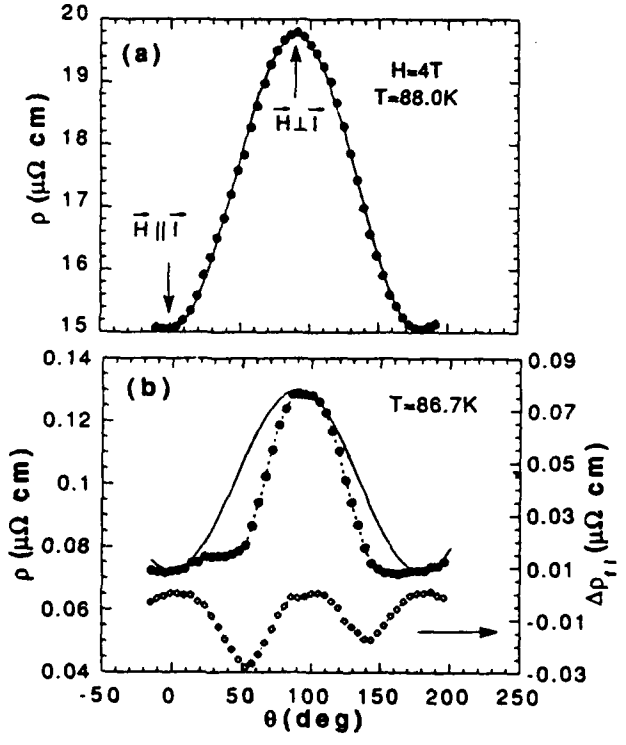


FIG. 6. Angular-dependent resistivities of sample 2 at (a) 88.0 K and (b) 86.7 K for a 4 T field with a measuring current density of 160 A/cm$^2$ are shown as circles. Ideal flux flow resistivity was observed at 88.0 K. At 86.7 K, two dips separated by 90° were observed. $\Delta\rho_{\parallel}$ are plotted as diamonds in (b).

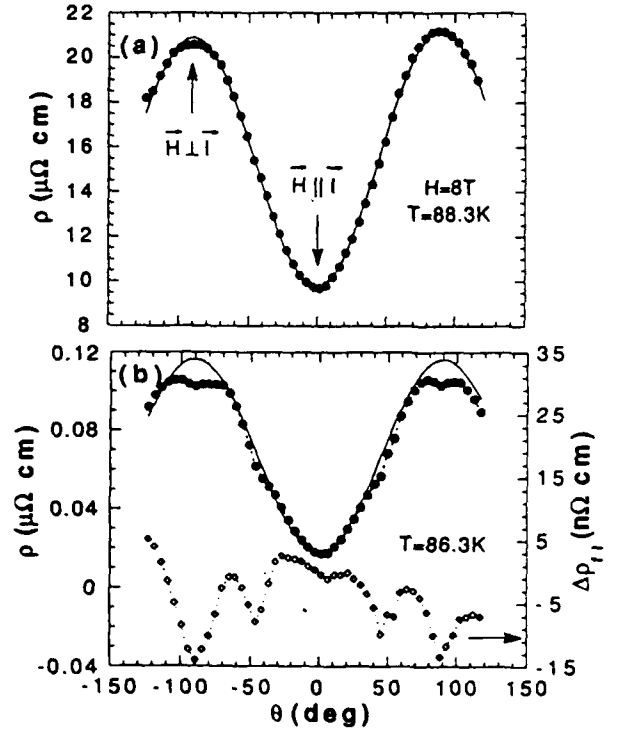


FIG. 8. Angular-dependent resistivities of sample 3 at (a) 88.3 K and (b) 86.3 K for an 8 T field with a measuring current density of 270 A/cm$^2$ are shown as circles. Ideal flux flow resistivity was observed at 88.3 K. At 86.7 K, three dips were observed in one period. $\Delta\rho_{\parallel}$ are plotted as diamonds in (b).

daries are along the [110] direction of the $SrTiO_3$, which is expected to be due to the epitaxial relationship between $YBa_2Cu_3O_x$ and $SrTiO_3$. Since the microstrip is patterned along the [100] direction of the substrates, the dips at $\pm 45°$ correspond to the twin boundary direction of the film. The resistivity drop may be due to the twin boundary pinning effect. The relatively broad dips compared to those of the single-crystal work[8] suggest that the orientations of the twin boundaries throughout the sample have a certain angular distribution ($\sim \pm 10°$), but strain associated with the slight misfit between $YBa_2Cu_3O_x$ and $SrTiO_3$ could be responsible for the broader dips.

It is interesting to note that the relative resistivity drops due to the twin boundaries in the films are noticeably smaller and narrower than the corresponding drops at the same angular positions in sample 2 on $LaAlO_3$ grown from the same batch. This suggests that the effects of certain microstructural features induced by the substrate twins are dominant over the pinning effect of the intrinsic twin boundaries in $YBa_2Cu_3O_x$ thin films.

The dips at $\pm 90°$ could be due to *a*-axis-oriented grains. Although no evidence of *a*-axis grains was observed in TEM cross sections, plane-section TEM revealed very small *a*-axis grains, and some of these are indicated by arrows in Fig. 9. Since these grains are quite small ($\approx 100$ Å), the overall effective volumes or surfaces are negligible. Furthermore, the effect of these grains was negligible in transport measurements of sample 2 from the same batch. Another possible origin of these dips could be the flux pinning along dislocations. A high density of interfacial dislocations typically oriented along the [100] and [010] directions of $SrTiO_3$ was observed. The dislocations were observed to be unique to films grown on $SrTiO_3$. However, we do not have further evidence to directly correlate the dips at $\pm 90°$ to the flux pinning at the dislocations. Both of these mechanisms predict a dip at every 90°, so a dip is expected at 0°. However, because the macroscopic Lorentz force vanishes for $\mathbf{H} \| \mathbf{I}$, no such dips are observable except a small glitch at 0°.

Finally, the double transition observed in films on $LaAlO_3$ in small fields ($< 1$ T) indicates a $T_c$ variation in the sample, and it is very likely that a part of the film along the substrate twin boundaries may have a different $T_c$ from the rest of the film due to the induced microstructural features. The absence of the double transition in films on $SrTiO_3$ is consistent with this speculation. A detailed study of the influence of the substrate twin boundaries of $LaAlO_3$ on the microstructures is under way.

## IV. SUMMARY

We have measured resistivity and critical-current density as a function of angle between the applied field and the direction of transport current for fields parallel to the Cu-O layers in high-quality epitaxial $YBa_2Cu_3O_x$ films. Several dips were observed in the angular-dependent flux

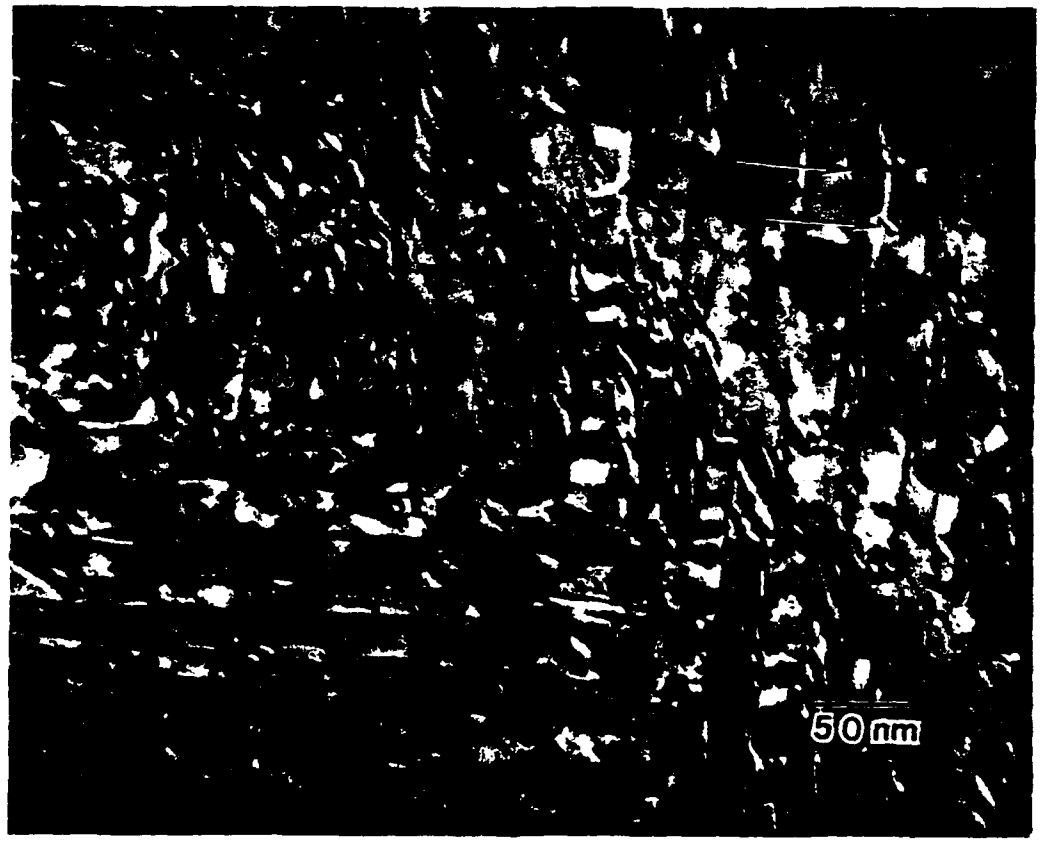


FIG. 9. Bright-field electron micrograph of a planar section of $YBa_2Cu_3O_x$ on $SrTiO_3$ showing a twinned structure. Some *a*-axis grains are indicated by arrows.

flow resistivity. TEM samples were prepared to investigate the origins of the deviation from flux flow resistivity. For thick films (5000 Å) on $LaAlO_3$, resistivity dips are observed when a field is aligned parallel to *substrate* twin boundaries or along the *a*-axis grains. In thinner films (900 Å) in which *a*-axis grains were negligible, only two dips were observed, corresponding to the orientation of substrate twin boundaries. The resistivity drop for a field parallel to the substrate twin boundary may be due to flux pinning by undetermined microstructural features in the sample induced by strain associated with the substrate twins. For fields along the *a*-axis grains, flux pinning at the grain boundaries and/or resistivity anisotropy between $\mathbf{H}\|c$ and $\mathbf{H}\|a$ can be responsible for resistivity dips.

Meanwhile, for films grown on $SrTiO_3$, twin structures in the film were observed in TEM, and the pinning effect due to the twin boundaries was also observed in the angular-dependent flux flow resistivity. In addition, a pinning effect due to the other microstructural features, perhaps interfacial dislocations, was observed in films grown on $SrTiO_3$. Overall, such pinning effects weaken as the transport current increases and become at most a perturbation in high-current applications.

## ACKNOWLEDGMENTS

The authors thank J. Hettinger for valuable discussions and K. E. Gray for a critical reading of the manuscript. This work is partially supported by the U.S. Department of Energy, Division of Basic Energy Sciences-Materials Sciences (W-31-109-ENG-38), the National Science Foundation (DMR 88-09854) through the Science and Technology Center for Superconductivity, and the AFOSR (F49620-88-C-0043). JCS and RAH acknowledge support from the Argonne Division of Educational Programs.

[1]T. T. M. Palstra, B. Batlogg, L. F. Schneemeyer, and J. V. Waszczak, Phys. Rev. Lett. **61**, 1662 (1988); T. T. M. Palstra, B. Batlogg, R. B. van Dover, L. F. Schneemeyer, and J. V. Waszczak, Appl. Phys. Lett. **54**, 763 (1989).

[2]K. C. Woo, K. E. Gray, R. T. Kampwirth, J. H. Kang, S. J. Stein, R. East, and D. M. McKay, Phys. Rev. Lett. **63**, 1877 (1989).

[3]D. H. Kim, K. E. Gray, R. T. Kampwirth, J. C. Smith, D. S. Richeson, T. J. Marks, J. H. Kang, J. Talvacchio, and M. Eddy, Physica C **177**, 431 (1991).

[4]M. Tachiki and S. Takahashi, Solid State Commun. **70**, 291 (1989).

[5]D. Feinberg and C. Villard, Phys. Rev. Lett. **65**, 919 (1990).

[6]Y. Iye, S. Nakamura, and T. Tamegai, Physica C **159**, 433 (1989).

[7]D. H. Kim, K. E. Gray, R. T. Kampwirth, and D. M. McKay, Phys. Rev. B **42**, 6249 (1990).

[8]W. K. Kwok, U. Welp, G. W. Crabtree, K. G. Vandervoort, R. Hulscher, and J. Z. Liu, Phys. Rev. Lett. **64**, 966 (1990).

[9]J. Z. Liu, Y. X. Jia, R. N. Shelton, and M. J. Fluss, Phys. Rev. Lett. **66**, 1354 (1991).

[10]L. J. Swartzendruber, A. Roitrurd, D. L. Kaiser, F. W. Gayle, and L. H. Bennett, Phys. Rev. Lett. **64**, 483 (1990).

[11]Y. Iye, S. Nakamura, T. Tamegai, T. Terashima, K. Yamamoto, and Y. Bando, Physica C **166**, 62 (1990).

[12]Y. Iye, A. Watanabe, S. Nakamura, T. Tamegai, T. Terashima, K. Yamamoto, and Y. Bando, Physica C **167**, 278 (1990); Y. Iye, S. Nakamura, A. Watanabe, and T. Tamegai (unpublished).

[13]T. Tsuneto, J. Phys. Soc. Jpn. **57**, 3499 (1989).

[14]G. D. Cody and G. W. Cullen, RCA Rev. **25**, 466 (1964); J. W. Heaton and A. C. Rose-Innes, Cryogenics **4**, 85 (1964); V. R. Karasik and V. G. Veresshchagin, Zh. Eksp. Teor. Fiz. **59**, 36 (1970) [Sov. Phys. JETP **32**, 20 (1971)].

[15]A. Umezawa, G. W. Crabtree, U. Welp, W. K. Kwok, K. G. Vandervoort, and J. Z. Liu, Phys. Rev. B **42**, 8744 (1990).

[16]U. Welp, M. Grimsditch, H. You, W. K. Kwok, M. M. Fang, G. W. Crabtree, and J. Z. Liu, Physica C **161**, 1 (1989).

# Effect of stress along the *ab* plane on the $J_c$ and $T_c$ of $YBa_2Cu_3O_7$ thin films

G. L. Belenky,* S. M. Green, A. Roytburd,† C. J. Lobb, S. J. Hagen, and R. L. Greene‡
*Center for Superconductivity Research, Department of Physics and Astronomy, University of Maryland, College Park, Maryland 20742-4111*

**APPENDIX 11**

M. G. Forrester and J. Talvacchio
*Westinghouse Science and Technology Center, 1310 Beulah Road, Pittsburgh, Pennsylvania 15235*

(Received 24 May 1991)

We studied the influence of elastic stress along the *ab* plane ($\sigma_{ab}$) on the critical current density ($J_c$) and transition temperature ($T_c$) of epitaxial *c*-axis-oriented $YBa_2Cu_3O_7$ thin films. We observed reversible and reproducible increases (with compression) and decreases (with extension) of $J_c$ and $T_c$ from their equilibrium values. By comparing $dT_c/d\sigma_{ab}=0.045-0.050$ K/kbar with the results of hydrostatic-pressure and thermodynamic experiments reported in the literature, we conclude that pressure-induced changes in the *ab* plane completely account for the changes in $T_c$ (within our experimental uncertainty). We also show that the mismatch strain between film and substrate does not substantially affect the change in $T_c$ caused by the external stress.

## INTRODUCTION

Continued study of the effect of pressure ($P$) on the transition temperature ($T_c$) of high-temperature superconductors (HTSC) is important to our understanding of the nature of superconductivity in these materials. In addition, external strain ($\varepsilon$) can affect another crucial characteristic of superconductors—the critical current density ($J_c$). Thus, deformation effects in HTSC is an important area of superconductivity research. The basic measured parameter is, as a rule, the pressure derivative $dT_c/dP$. Most data were obtained by studying the effect of hydrostatic compression ($P_h$) on HTSC ceramics and crystals. The results vary, but most fall within the range $dT_c/dP_h=0.05-0.12$ K/kbar.[1-4] Less data is available pertaining to *c*-axis uniaxial compression ($P_c$), and even the sign of $dT_c/dP_c$ is not consistent.[5,6]

In this paper, we present and discuss observed changes in $T_c$ and $J_c$ with compression and extension along the *ab* plane (parallel to the Cu-O planes) in the absence of external stress in the *c* direction. These conditions are realized by bending substrates on which sputtered epitaxial thin films have been deposited and patterned. Our preliminary results were presented previously.[7] The effect of stress along the substrate plane was reported earlier by Park *et al.*[8] for polycrystalline $YBa_2Cu_3O_7$ films on $Al_2O_3$ substrates. They attributed the interesting and complex behavior of their films to the effects of granularity and inhomogeneity. The consistency of our results, among several films on different substrates, strongly suggests that our observations are intrinsic to $YBa_2Cu_3O_7$.

## EXPERIMENT

Epitaxial *c*-axis-oriented thin films of $YBa_2Cu_3O_7$ were deposited by dc magnetron sputtering from a stoichiometric target onto rotating (100) $LaAlO_3$ and MgO substrates. A layer of Au sputtered onto the films *in situ* provided low-resistance contacts. The films had midpoint $T_c$'s of 87–89 K, and resistivities at $T=100$ K, $\rho(100\text{ K})$, of 150–200 or 250–300 $\mu\Omega$ cm for $LaAlO_3$ or MgO substrates, respectively. $\rho(T)$ curves and *I-V* characteristics (at $T=77$ K) were measured on 50-$\mu$m-wide patterned strips. $J_c$ was determined based on a threshold criterion of 2 $\mu$V/mm. Conventional four-terminal configurations were used for both the *I-V* and $\rho(T)$ measurements.

Strain along the *ab* plane was created by bending the substrate in a cantilevered arrangement (Fig. 1). When a force ($F$) is applied to the end of the substrate, the resulting strain$[\varepsilon_{xx}(x)]$ is given by[9]

$$\varepsilon_{xx}(x)=F\frac{6(l-x)}{E^s bh^2}\ . \tag{1}$$

Here, $l$ is the length of the substrate between the clamp and the point of force application, $x$ is the distance between the clamp and the film, $b$ is the width of the substrate, and $E^s$ is the flexural modulus (or corresponding combination of the elastic constants) of the substrate.

For an epitaxial film, the film's atoms have strong bonds with the substrate, so that substrate and film strains are identical. In a cantilevered experiment, the stress tensor component in the *z* direction, $\sigma_{zz}$, vanishes. In our experiment, $l-x\cong l$ allows a simplification of Eq. (1), and also implies $\varepsilon_{yy}\cong 0$. The stress along the *ab* plane, $\sigma_{ab}\equiv\sigma_{xx}+\sigma_{yy}$, is then given by

$$\sigma_{ab}=F\frac{6l}{E^s bh^2}\frac{(c_{11}+c_{12})c_{33}-2c_{13}^2}{c_{33}}\ . \tag{2}$$

Equation (2) is obtained from Hooke's law ($\sigma_{ik}=C_{iklm}\varepsilon_{lm}$ using the compact notation $xx\rightarrow 1$, $yy\rightarrow 2$, $zz\rightarrow 3$ for components of the elasticity tensor) and Eq. (1). The components of the elasticity tensor ($C_{iklm}$) of an

 ©1991 The American Physical Society

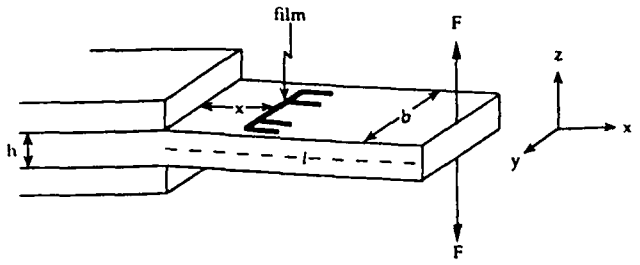


FIG. 1. The arrangement of the film on the substrate in the bending experiment. $l$, $b$, and $h$ are the length, width, and thickness of the substrate, respectively.

$YBa_2Cu_3O_7$ crystal as determined by neutron scattering are[10] $c_{11}=274$ GPa, $c_{12}=36.7$ GPa, $c_{33}=183$ GPa, and $c_{13}=61.3$ GPa. We measured the values of $E^s$ which control the flexural modes of the single crystal substrates directly using a flexural resonance technique.[11,12] For $LaAlO_3$ and MgO, $E^s=250$ and 300 GPa, respectively. The typical dimensions for our substrates were $(l,b,h)=(10\ mm, 6\ mm, 0.5\ mm)$. The strain $\varepsilon_{xx}$ did not exceed $6\times10^{-4}$.

Figure 2 shows the shift of $\rho(T)$ with extension and compression. The values of the derivative as determined from $\Delta T_C^{\text{midpoint}}/\sigma_{ab}$ for different samples are

$$\frac{dT_c}{d\sigma_{ab}}=0.045\text{–}0.050\ \text{K/kbar}\ .$$

The error of the derivative is dominated by the uncertainties in the components of the elasticity tensor (15–20%),[10] and is estimated to be 30%.

Figures 3 and 4 show the change in $J_c$ with extension and compression for films on $LaAlO_3$ and MgO, respectively. The insets to Figs. 3 and 4 present the stress dependence of $J_c$. The critical current density increases with compression along the *ab* plane, and decreases with extension. The shifts in both $T_c$ and $J_c$ are reversible and reproducible.

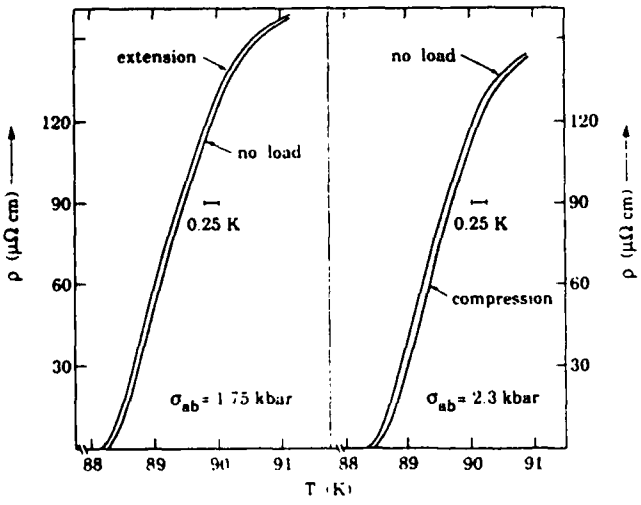


FIG. 2. Resistivity vs temperature of $YBa_2Cu_3O_7$ film on $LaAlO_3$ substrate, shown with extension and with compression. Film thickness = 1000 Å.

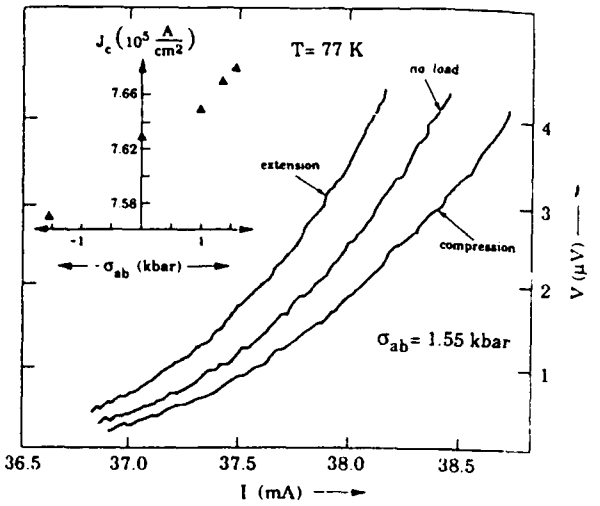


FIG. 3. The effect of stress along the *ab* plane on the *I-V* characteristics of $YBa_2Cu_3O_7$ film on $LaAlO_3$. Film thickness = 1000 Å; $\rho(100\ K)=200\ \mu\Omega$ cm. Inset: the dependence of $J_c$ on stress ($\sigma_{ab}>0$ is compression; $\sigma_{ab}<0$ is extension).

## DISCUSSION

The experimental results described above show that compression along the *ab* plane leads to an increase in $T_c$, while extension along this plane decreases $T_c$ in $YBa_2Cu_3O_7$ films. The results clearly indicate a direct correlation between changes in $T_c$ and changes in interatomic spacing in the *ab* plane. A correlation has been noted, in previous work,[13] between the *c* parameter and $T_c$. This correlation could be taken to suggest that

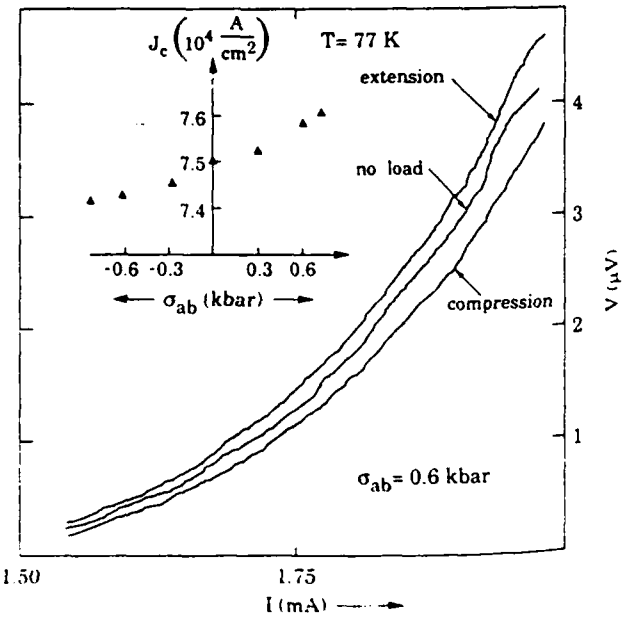


FIG. 4. The effect of stress along the *ab* plane on the *I-V* characteristics of $YBa_2Cu_3O_7$ film on MgO. Film thickness = 500 Å; $\rho(100\ K)=380\ \mu\Omega$ cm. Inset: the dependence of $J_c$ on stress ($\sigma_{ab}>0$ is compression; $\sigma_{ab}<0$ is extension).

changes in *c* parameter *cause* changes in $T_c$. Analysis of our data, combined with thermodynamic data from the literature, indicates that this is not the case, as discussed below.

Another result is the increase of $J_c$ under compression and the decrease of $J_c$ with extension (the increase of $J_c$ in thin $YBa_2Cu_3O_7$ films under hydrostatic pressure was reported in Ref. 14). The value $\Delta J_c/J_c^0$ ($J_c^0$ is the critical current density without deformation) did not exceed several percent. The behavior of $J_c(\sigma_{ab})$ turned out to be similar in experiments with several films on both $LaAlO_3$ and MgO. These films had different normal-state resistivities, and critical current densities which differed by two orders of magnitude (see, for example, Figs. 3 and 4). The similarity in their behavior cannot be readily explained within the framework of "weak link" models. It is our point of view that a direct connection between the changes in $T_c$ and $J_c$ cannot be neglected since compression along the *ab* plane causes both to increase just as extension leads to their decrease. It is also necessary to consider that external stress tends to concentrate near defects which may influence the pinning force. Thus, the nature of the reversible change in $J_c$ remains unclear.

We can compare our value of $dT_c/d\sigma_{ab}$ with the results of hydrostatic pressure experiments using the fact that the derivative $dT_c/dP_h$ is obtained by summing two contributions:

$$\frac{dT_c}{dP_h}=2\frac{dT_c}{d\sigma_{ab}}+\frac{dT_c}{d\sigma_c}\ ,$$

where $\sigma_c$ is stress (or pressure) along the *c* axis. The value calculated from our experiments, $2dT_c/d\sigma_{ab}$ $\approx$0.09–0.10 K/kbar, falls well within the range reported from hydrostatic experiments in the literature. This fact supports the conclusion that pressure-induced changes in interplanar spacing along the *c* axis do not contribute significantly to the change in $T_c$ for $YBa_2Cu_3O_7$.

Confirmation of this statement follows by considering both our results and the experimental results of thermodynamic investigations.[15,16] From the generalization of Ehrenfest's relation for second-order phase transitions, it is possible to write the following equation:

$$\frac{\Delta\alpha_{xx}\sigma_{xx}+\Delta\alpha_{yy}\sigma_{yy}+\Delta\alpha_{zz}\sigma_{zz}}{\Delta C_p/T_c}=\Delta T_c\ . \qquad (3)$$

Here, $\Delta\alpha_{ij}$ are the thermal expansion jumps of the lattice at $T_c$, $\Delta C_p$ is the jump in heat capacity at $T_c$, $\sigma_{ij}$ are the stress tensor components, and $\Delta T_c$ is the stress-induced change in $T_c$. For $YBa_2Cu_3O_7$ single crystals and oriented grained samples, $\Delta\alpha_{xx}+\Delta\alpha_{yy}$ is equal to $2.3\times10^{-7}$ $K^{-1}$ and $1.5\times10^{-7}$ $K^{-1}$, and $\Delta C_p/T_c$ is 27 mJ/mol $K^2$ and 43 mj/mol $K^2$, respectively.[15] Assuming that $\sigma_{ab}=\sigma_{xx}+\sigma_{yy}$ and $\sigma_{zz}=0$, we can calculate $dT_c/d\sigma_{ab}=0.089$ K/kbar for the single crystal and 0.038 K/kbar for the oriented grained sample. Taking into account that the value 0.089 K/kbar is too large due to the presence of Al doping impurities,[16] we believe that our experimental result of 0.045–0.050 K/kbar is in good agreement with Eq. (3).

Our deduction that pressure-induced changes in interplanar spacing do not contribute significantly to the change of $T_c$ is strongly supported by the fact that the jump in the component of thermal expansion along the *c* axis at $T_c$ is very small: $\Delta\alpha_{ab}/\Delta\alpha_{zz}>20$.[15] Our deduction agrees with the theoretical conclusion that a large change in Cu-O interplanar distance affects $T_c$ only slightly,[17] as well as data that establish a correlation between the $T_c$ and the in-plane Cu-O bond length in cuprate superconductors.[18]

Finally, we discuss the role of thermal contraction mismatch between the film and substrate. [A discussion of this internal strain ($\hat{\varepsilon}_m$) is presented in the literature.[19]] It is possible to describe the free energy of a film strained due to interaction with its substrate (strain tensor $\hat{\varepsilon}_m$) and an external stress $\hat{\sigma}$ (corresponding strain $\hat{\varepsilon}_\sigma$) by the following equation (using for simplicity the notation $\hat{\varepsilon}$ and $\tilde{C}$ instead of $\varepsilon_{ik}$ and $C_{iklm}$):

$$F(\varphi,\varepsilon)=F_0(T)+\tfrac{1}{2}a(T-T_c^0)\varphi^2+\tfrac{1}{4}B\varphi^4 +\tfrac{1}{2}[\hat{\varepsilon}-\hat{\varepsilon}_0(\varphi)]\tilde{C}[\hat{\varepsilon}-\hat{\varepsilon}_0(\varphi)]\ . \qquad (4)$$

The first three terms characterize the free energy of the unstrained state. Here $\varphi$ is the order parameter, $T_c^0$ is the critical temperature in the unstrained state, and $a/(2B)=\Delta C_p/T_c$.[20] The last term in (4) corresponds to the elastic energy of the superconductor at a given $\varphi$.[21] The elastic modulus $\tilde{C}=\tilde{C}_0+\Delta\tilde{C}\varphi^2$ near the transition point, $\tilde{C}_0$, corresponds to the normal state and $\Delta C$ characterizes the superconducting state, $\varepsilon$ is the total strain tensor $\hat{\varepsilon}=\hat{\varepsilon}_m+\hat{\varepsilon}_\sigma$, and $\hat{\varepsilon}_0(\varphi)=\hat{\varepsilon}_0(T)+\hat{\omega}\varphi^2$ is the self-strain directly connected with $\hat{\alpha}$ for equilibrium $\varphi$: $d\hat{\varepsilon}/dT=\hat{\alpha}$, $\Delta\hat{\alpha}=\hat{\omega}a/B$. It is possible to estimate the critical temperature $T_c$ of a film with internal (mismatch) strain [$T_c\neq T_c^0$ in (4)] as well as the shift of this temperature under external stress $\Delta T_c$, by equating to zero the sum of all terms containing $\varphi^2$ in (4). Taking into account that only terms containing $\hat{\varepsilon}_\sigma$ need to be kept, and neglecting the quadratic term $\hat{\varepsilon}_\sigma\Delta\tilde{C}\hat{\varepsilon}_\sigma$, we can write the following equation for $\Delta T_c$, which was measured in our experiment:

$$\Delta T_c=\frac{\Delta\hat{\alpha}\hat{\sigma}-(a/B)\hat{\varepsilon}_m\Delta\tilde{C}\hat{\varepsilon}_\sigma}{\Delta C_p/T_c}\ . \qquad (5)$$

The first term of Eq. (5) corresponds to the generalization of Ehrenfest's relation, Eq. (3), which has been shown to describe the results of our experiments satisfactorily. For all practical purposes, then, substrate mismatch does not contribute significantly to the change in $T_c$ caused by external stress. The consistency in our experimental results for films on different substrates strongly supports the conclusion that the $J_c$ and $T_c$ changes observed are intrinsic to $YBa_2Cu_3O_7$ and are not mismatch induced.

## CONCLUSION

We observed reversible and reproducible changes in $J_c$(77 K) and $T_c$ of *c*-axis-oriented epitaxial $YBa_2Cu_3O_7$ thin films due to compression and extension along the *ab*

plane. Compression increases and extension decreases both $J_c$ and $T_c$ from their unstressed values. We have determined that $dT_c/d\sigma_{ab} = 0.045-0.050$ K/kbar. Furthermore, it was shown that pressure-induced changes within the *ab* plane dominate the changes in $T_c$. Comparison of our result with thermodynamic considerations shows that mismatch strain between the film and substrate does not affect the change in $T_c$ caused by external stress.


## ACKNOWLEDGMENTS

We are grateful for helpful discussions with E. Suhir, T. Venkatesan, and M. Wuttig. The authors also appreciate the assistance provided by M. Wuttig and Harsh Deep Chopra during the measurements of the substrates' flexural moduli. Partial support for this work was provided by the Electric Power Research Institute.


---


*Present address: AT&T Bell Laboratories, Murray Hill, NJ 07974.

†Also at Department of Material and Nuclear Engineering.

‡Also at IBM Research Division, Yorktown Heights, NY 10538.



[1]C. W. Chu, Z. J. Huang, R. L. Meng, L. Gao, and P. H. Hor, Phys. Rev. B 37, 9730 (1988).

[2]R. Wingaarden and R. Griessen, in *Studies of High Temperature Superconductors*, edited by A. Narlikar (NOVA Science, New York, 1989).

[3]R. Wingaarden, E. N. van Eenige, J. I. Scholtz, and R. Griessen (unpublished).

[4]S. Klotz, W. Reith, and J. C. Shilling, Physica C **172**, 423 (1991); J. E. Schirber, B. Morosin, and D. S. Ginley, *ibid.* **157**, 237 (1989).

[5]U. Koch, J. Wittig, and B. Gegenheimer, Physica C **162-164**, 739 (1989).

[6]M. F. Crommie, A. Y. Liu, A Zettl, M. L. Cohen, P. Parillo, M. F. Hundley, W. N. Creager, S. Hoen, and M. S. Sherwin, Phys. Rev. B **39**, 4231 (1989).

[7]G. L. Belenky, S. M. Green, S. J. Hagen, A. Roytburd, R. L. Greene, M. G. Forrester, and J. Talvacchio (unpublished); G. L. Belenky, S. M. Green, S. J. Hagen, R. L. Greene, M. G. Forrester, and J. Talvacchio (unpublished).

[8]S. I. Park, M. R. Schenermann, C. C. Chi, and C. C. Tsuei, in *High Temperature Superconductors, Boston, 1987*, edited by M. B. Brodsky, R. C. Dynes, K. Kitazawa, and H. Tuller, MRS Symposia Proceedings No. 99 (Materials Research Society, Pittsburgh, 1988), p. 685.

[9]R. P. Feynman, R. Leighton, and M. Sands, *The Feynman Lectures on Physics* (Addison-Wesley, Reading, MA, 1964), Vol. 2, p. 38.

[10]S. K. Chan, B. W. Veal, and C. K. Loonge (private communication).

[11]A. S. Nowic and B. S. Berry, in *Anelastic Relaxation in Crystalline Solids* (Academic, New York, 1972), p. 360.

[12]M. Wuttig and C. H. Lin, Acta Metall. **31**, 1117 (1983).

[13]See, for example, C. B. Eom, J. Z. Sun, B. M. Lairson, S. K. Streiffer, A. F. Marshall, K. Yamamoto, S. M. Anlage, J. C. Bravman, T. H. Geballe, S. S. Laderman, R. C. Taber, and R. D. Jacowitz, Physica C **171**, 354 (1990).

[14]Q. Xiong, M. F. Davis, S. Dechmuch, Y. Q. Wang, Y. Y. Xue, J. C. Wolfe, D. Economou, P. H. Hor, and C. W. Chu (unpublished).

[15]C. Meingast, B. Blank, H. Bürkle, B. Obst, T. Wolf, and H. Wüne, Phys. Rev. B **41**, 11 299 (1990).

[16]C. Meingast, R. Ahrens, B. Blank, H. Bürkle, B. Rudolf, and H. Wüne, Physica C **173**, 309 (1991).

[17]D. Yoshioka, J. Phys. Soc. Jpn. **59**, 2627 (1990).

[18]M. H. Whangbo, D. B. Kang, and C. C. Torardi, Physica C **158**, 371 (1989).

[19]E. Suhir, J. Electron. Packag. **111**, 281 (1989); E. Suhir, in Proceedings of the International Society for Optical Engineering [SPIE J. **1187**, 227 (1989)].

[20]*Landau and Lifshitz Course on Theoretical Physics* (Pergamon, Elmsford, NY, 1980), Vol. 9, pt. 1.

[21]A. Roytburd, Fiz. Tverd. Tela (Leningrad) **26**, 2025 (1984) [Sov. Phys. Solid State **26**, 1229 (1984)].

FORTY-FIFTH ANNUAL SYMPOSIUM ON FREQUENCY CONTROL

# COOLED, ULTRA-HIGH Q, SAPPHIRE DIELECTRIC RESONATORS FOR LOW NOISE, MICROWAVE SIGNAL GENERATION*

M. M. Driscoll, J. T. Haynes, S. S. Horwitz, R. A. Jelen
Westinghouse Electronic Systems Group
Baltimore, MD 21203

**APPENDIX 12**

R. W. Weinert, J. R. Gavaler, J. Talvacchio, G. R. Wagner
Westinghouse Science & Technology Center
Pittsburgh, PA 15235

K. A. Zaki, Xiao-Peng Liang
University of Maryland
College Park, MD

## ABSTRACT

Ultra-high Q, X-band resonators, used in a frequency discriminator for stabilization of a low noise signal generator, can provide a means of obtaining significant reduction in phase noise levels. Resonator unloaded Qs on the order of 500K can be obtained in a sapphire dielectric resonator (DR) operating on a low order (i.e., $TE_{01}$) mode at 77K and employing high temperature superconducting (HTS) films installed in the DR enclosure covers.

Rigorous analysis for the determination of resonator frequency, modes, and unloaded Q have been carried out using mode matching techniques. Tradeoff studies have been performed to select resonator dimensions for the optimum mode yielding highest unloaded Q and widest spurious mode separation. Field distributions within the resonator have been computed to enable practical excitation of the required mode.

The results of both analysis and prototype device evaluation experiments are compared for resonators fabricated using enclosures consisting of conventional, metal sidewalls and covers employing high temperature superconducting films as a function of cover (i.e., HTS film) conductivity.

## INTRODUCTION

In a low noise, microwave signal generator, output signal phase noise characteristics are largely determined by generator reference oscillator resonator characteristics including loaded Q, insertion loss, operating frequency, drive level, short-term and long-term frequency stability, and frequency sensitivity to environmental stress [1,2].

Figure 1 depicts the X-band microwave signal phase-noise performance attainable using: (1) a VHF quartz crystal oscillator followed by a frequency multiplier and (2) a dielectric resonator oscillator (DRO) operating directly at the microwave frequency. As implied by the figure, a tradeoff exists with regard to near-carrier vs. noise floor spectral performance. The higher, relative noise floor level exhibited by the crystal oscillator-multiplier is an unavoidable consequence of the phase noise sideband level increase cause by the signal frequency multiplication process. On the other hand, the higher, relative near-carrier noise level exhibited by the DRO is primarily a consequence of the dielectric resonator loaded Q value (typically several thousand at X-band) that is much lower than that of the VHF quartz crystal resonator (100,000 at 80 MHz, for example). In order to simultaneously achieve the excellent noise floor performance provided by the DRO and near-carrier noise levels that are significantly superior to that currently attainable using quartz acoustic resonators, it is necessary to utilize resonators operating directly at microwave frequencies that exhibit: (1) loaded Q values in excess of several hundred thousand and (2) acceptably low values of self-noise and environmental stress sensitivities. The predicted phase-noise performance attainable through the use of ultra-high Q microwave resonators is shown in curves 3 and 4 in Figure 1.

The use of cooled, sapphire dielectric, microwave resonators as stable, ultra-high Q, frequency control elements has been reported in the literature. Resonator operation of high order modes has resulted in attainment of unloaded Qs in the range $10^7$ to $10^9$ at

*This work was partially supported by DARPA, Contract No. 972-88-C-0050.



CH2965-2/91/0000-700 $1.00 © 1991 IEEE

X-band in the liquid nitrogen to liquid helium temperature range [3,4]. The presence of closely frequency-spaced multiple resonant modes can constitute a disadvantage associated with device operation on a high order mode.

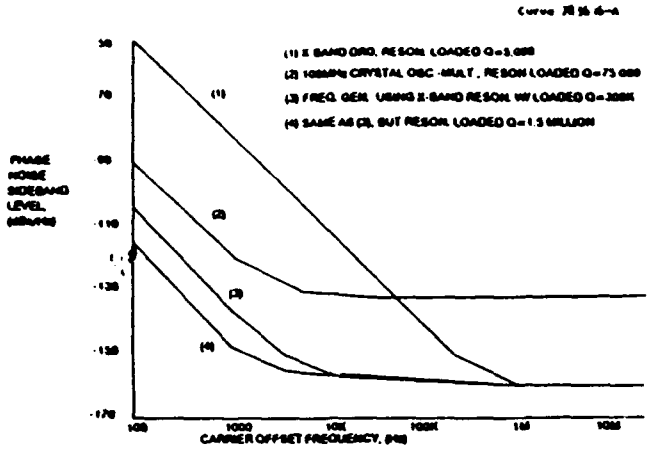


Figure 1. X-Band Signal Spectral Performance as a Function of Resonator Technology.

In a low noise, microwave signal generation application, lower resonator Qs (on the order of 500K) can provide improved signal spectral performance, compared to that currently available using conventional, non-cooled resonator technologies. In the case of resonator utilization in an AFC stabilization feedback loop, the lower (but significant) Q may be preferable from the standpoint of obtaining large loop correction bandwidth. The only resonator technology capable of providing high values, small size, and good mode separation is a cooled sapphire dielectric resonator operating on a low order mode. The loss tangent of sapphire decreases significantly with temperature [5], from $\sim 10^{-5}$ at room temperature to $\sim 10^{-7}$ at 77K. Attainable resonator unloaded Q values, for low order modes, at 77 ° K are limited not by sapphire losses but primarily by the surface losses of the metal enclosure in which the cylindrical, sapphire "puck" is mounted.

For a conventional, metal wall enclosure, resonators designed to operate on a low order mode exhibit unloaded Q values at X-band of several hundred thousand. When high temperature superconducting films are used in the resonator enclosure covers, the resultant decrease in surface resistance results in of unloaded Q values on the order of 1 million. Q values on the order of 0.5 million to 1 million are adequate for significant additional improvement in near-carrier phase noise level. The combined use of high temperature superconducting films and cooled sapphire dielectric technologies is the key to obtaining the requisite resonator performance.

## HTS RESONATOR UTILIZATION

The proposed circuit mechanization for utilizing the HTS sapphire dielectric resonator, as shown in Figure 2, employs the resonator in a microwave discriminator. Ultra-high resonator Q results in achievement of high discriminator sensitivity, allowing the detection of FM/PM noise levels in a microwave signal derived from a conventional, low noise acoustic wave oscillator multiplier. As indicated in the figure, the discriminator may be configured to utilize either the resonator transmission or reflection response, or both [5,6]. The reflection and/or transmission plus reflection schemes have the advantage of providing higher values of effective detector gain. An automatic frequency control (AFC) feedback loop is employed for reduction of oscillator-multiplier signal phase noise.

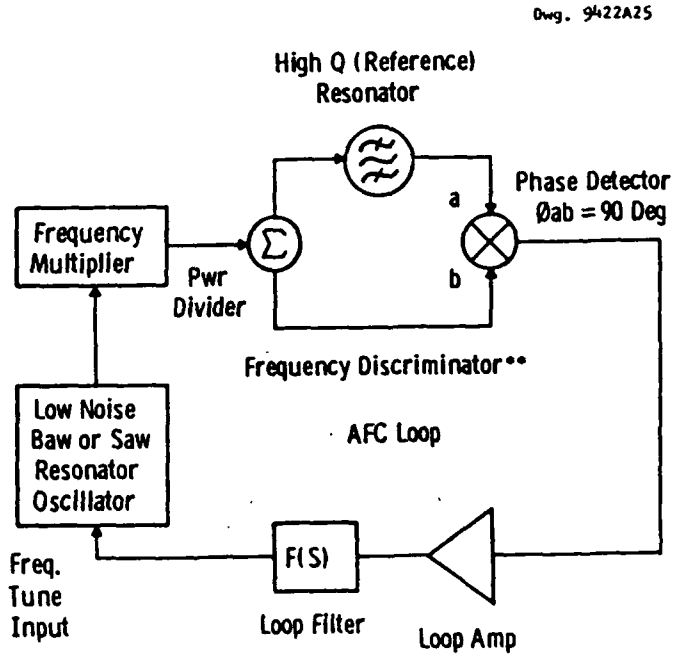


**Resonator May be Operated in Reflection Mode as Well as Transmission Mode, or Both

Figure 2. HTS Resonator Utilization in a Frequency Discriminator for AFC Stabilization of an External Oscillator-Multiplier.

There are several important advantages provided by the AFC feedback loop approach, compared to resonator use directly in a microwave oscillator. With the HTS-sapphire dielectric resonator employed in an X-band oscillator, the oscillator sustaining stage would require a GaAs amplifier. GaAs amplifier flicker-of-phase noise levels (converted to flicker-of-frequency noise in the oscillator) are 20 to 30 dB higher than those exhibited by the Schottky diode phase detector

employed in the discriminator approach. In addition, the discriminator does not dissipate DC power (as an oscillator would), so that integration of the non-resonator discriminator components are part of the cooled resonator assembly is possible, and cryocooler heat removal requirements are minimized. An integrated discriminator assembly is desirable from the standpoint of eliminating the need for critical length RF cables to traverse the cooled/uncooled interface. Finally, the AFC loop results in achievement of signal phase-noise reduction not only in the final microwave frequency output signal, but also in the oscillator and multiple interstage signals.

## HTS RESONATOR DESIGN

The structure of the resonator is shown in Figure 3. It consists of a cylindrical dielectric resonator of relative dielectric constant $e_{r1}$, diameter d, and length t, placed symmetrically inside a cylindrical conducting enclosure of diameter D and length L. The resonator is supported on its ends by two low loss foam discs of relative dielectric constant $e_{r2}$, diameter D and length G each.

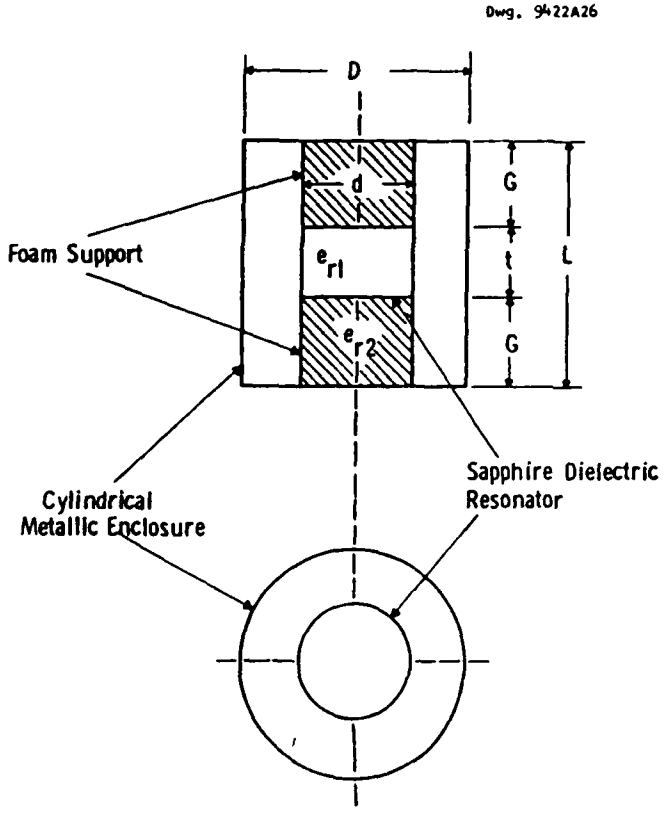


Figure 3. Structure of the Resonator.

Rigorous methods for the analysis of this type of structure have been recently developed [7-11]. These methods are based on the mode matching technique and involve significant amounts of numerical computations. The method divides the region within the conducting enclosure into subregions whose eigenmode fields can be determined analytically. In each of the sub-regions, the electromagnetic fields are expanded as a linear combination of the sub-region eigenmodes that satisfy Maxwell's equations and the boundary conditions on the conducting surfaces. The boundary conditions at the interfaces among the sub-regions are then introduced. By applying a weighted integrated criterion to the equations expressing the boundary conditions, an infinite set of linear homogeneous equations in the unknown coefficients of the eigenmodes is obtained. The characteristic equation for the resonant frequencies of the structure is obtained by equating the determinant of a truncated subsystem of N equations from the infinite set, to zero. Once the resonant frequencies are determined (by numerical solution of the characteristic equation), they are substituted back into the homogeneous system of equations, which is then solved numerically for all the eigenmode coefficients in terms of one single coefficient. The knowledge of the resonant frequencies and the corresponding eigenmode coefficients provide complete characterization of the electromagnetic fields in the structure. Determination of the unloaded Qs involves the calculation of the energy (U) stored in the structure, and the power ($W_L$) lost in the metallic walls, the dielectric resonator and the surrounding supporting media. The unloaded Q is then calculated from:

$$Q_u = \frac{\omega_o U}{W_L}$$

where $\omega_0$ is the resonant frequency.

Contribution to $W_L$ can be separated for each of the enclosure surfaces (i.e., the top and bottom planes of enclosure, and the cylindrical walls), for the resonator loss and for the supporting foam. This helps to understand the loss mechanism and in optimizing the structure parameters to obtain the highest Q, when HTS films are installed in the enclosure end planes (covers).

The resonant electromagnetic field configurations that can exist on the resonant structure shown in Figure 3 are:

(1) Transverse electric modes ($TE_{on}$ modes) which have no axial electric field and its fields have no angular variation.

(2) Transverse magnetic modes ($TM_{om}$ modes) which have no axial magnetic fields and its fields have no angular variation.

(3) Hybrid electromagnetic modes ($HE_{mn}$) modes which have both electric and magnetic fields in the axial direction, and its fields have angular variations of sin ($n\phi$) and cos ($n\phi$).

Since the objective of this work is to achieve high unloaded Qs in the 10 GHz frequency range, the $TE_{on}$ modes which generally have the highest Q values were considered. In particular the small volume $TE_{01}$ mode DR is considered in detail. Figure 4 shows the computed results of the variation of the resonant frequency at 77K of the $TE_{01}$ with the end wall spacing G of the enclosure, where measured values are indicated in the figure. The total unloaded Q and the contributions of the various parts of the structure to the unloaded Q are shown in Figures 5 and 6 for room temperature and 77K, respectively. In these figures the total unloaded Q is related to the individual contributions by:

$$\frac{1}{Q_T} = \frac{2}{Q_{EW}} + \frac{1}{Q_{SW}} + \frac{1}{Q_{DR}} + \frac{1}{Q_{foam}}$$

where: $1/Q_{EW}$ is the contribution due to one end wall, $1/Q_{SW}$ is the contribution due to the side wall, $1/Q_{DR}$ is the contribution due to the sapphire resonator, and $1/Q_{foam}$ is the contribution due to the foam support.

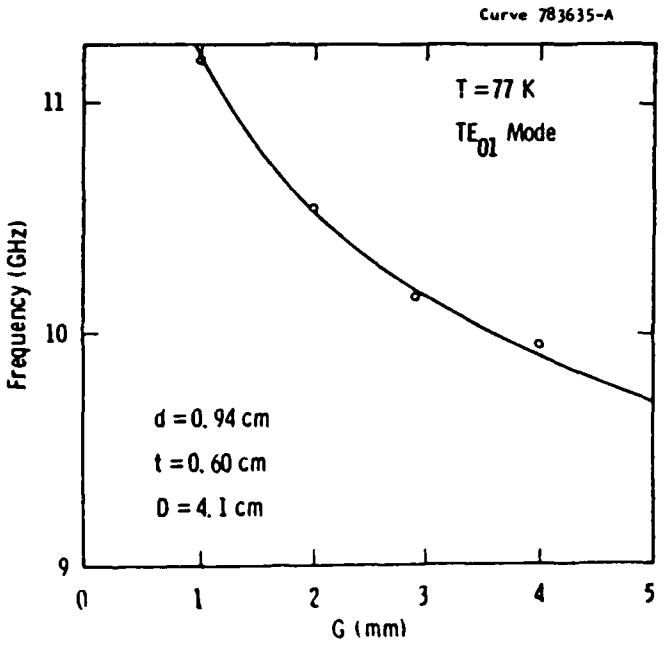


Figure 4. Resonator ($TE_{01}$ mode). Resonant Frequency vs. End Wall Spacing.

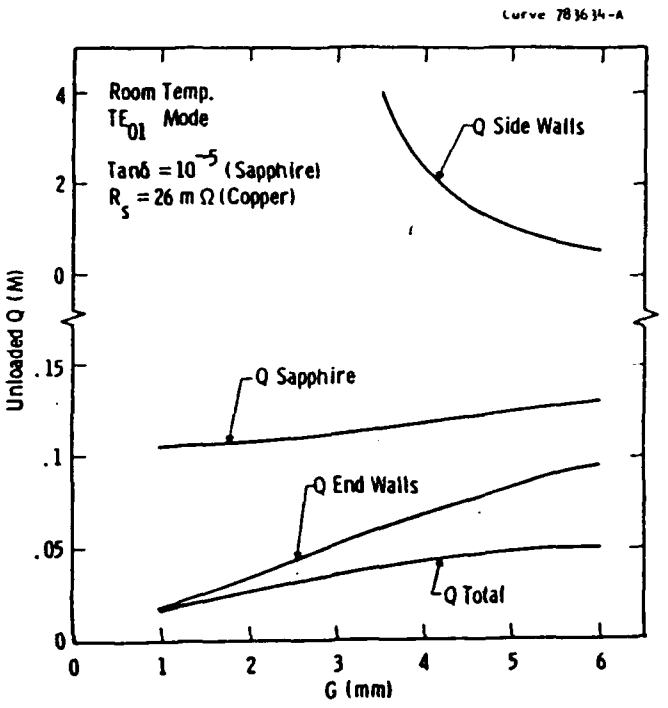


Figure 5. Contributors to Resonator Q-Factor at Room Temperature.

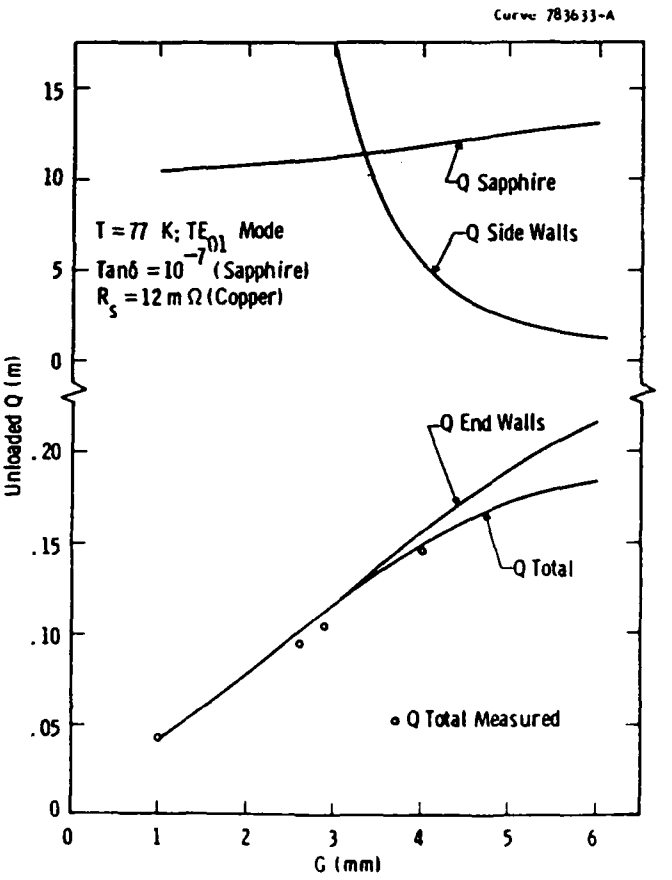


Figure 6. Contributors to Resonator Q-Factor at 77K.

At room temperature the total unloaded Q is controlled by the dielectric loss of the sapphire puck and the ohmic loss of the end walls (covers). At 77K, the dielectric loss in sapphire becomes small, and the total Q is controlled primarily by the ohmic loss in the end walls and loss in the solid foam sapphire puck supports is not considered. The foam supports actually used to obtain the measured Q values (Figure 6) were not a solid, but a "ring" structure, and the measured Q values obtained are close to the calculated "no foam" values. The difference between calculated and measured Q values is taken as a measure of the loss of the foam ring mounting structure.

Examination of the Figure 6 data indicates that, for resonator-to-end plane distances less than 0.5 cm, the primary limitation in attainable Q is due to enclosure end walls losses. Reduction of end plane losses via utilization of HTS films installed in the enclosure covers provides a means of obtaining higher overall resonator Q, with additional Q increase obtainable using a lower loss (compared to foam) DR support structure. Figure 7 shows attainable ($TE_{01}$ mode) resonator Q values for different ratios of HTS film conductivity (compared to copper) values.

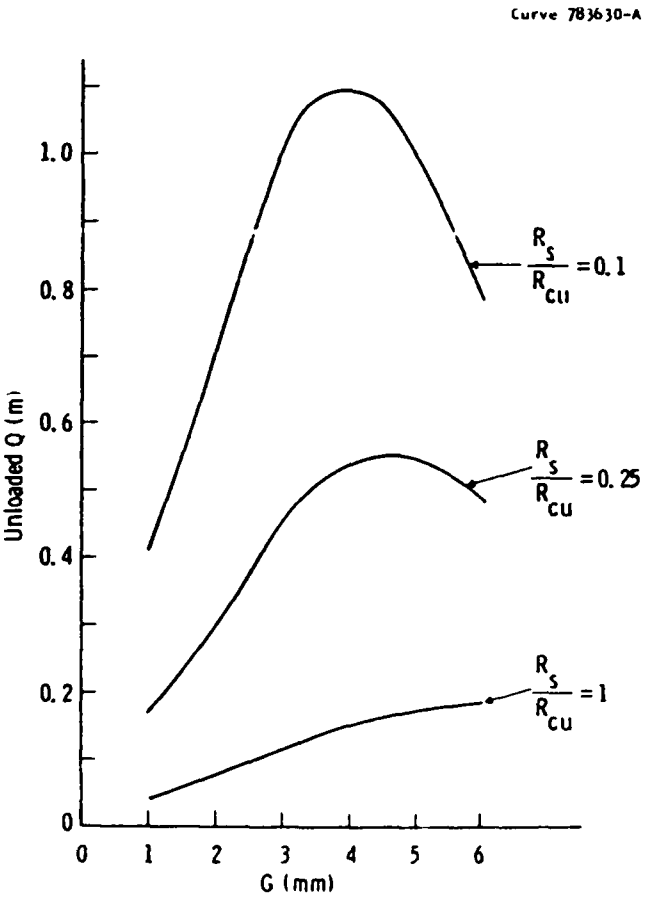


Figure 7. Resonator Unloaded Q as a Function of End Plate Surface Resistance and DR-to-End Plate Dimension.

## HTS FILM FABRICATION

The YBCO films utilized were made by a single target sputtering techniques which has been previously described [12]. The substrates were positioned on a quartz holder located 90° off-axis below the sputter gun. There was no bonding or clamping of the substrate to the holder. The substrates were 1.4 inch diameter, 20 mil thick $LaAlO_3$, and the YBCO films were approximately 300 nm thick.

The particular films used in this work were too large for characterization. Films made under nominally identical conditions on large-area substrates were diced for measurement of structural and superconducting properties. The films had a c-axis growth orientation with an x-ray rocking curve width of 0.2 degrees. They grew epitaxially with their c-axis normal to the substrate and with the a and b axes of YBCO parallel to <100> directions in the $LaAlO_3$ substrate. Typical superconducting transition temperatures were 89-91K for resistive transitions (R = 0) and 88-90K for transitions measured by ac susceptibility. The rf surface resistance, $R_S$ was measured on small chips, 1/4 × 1/2 inch, by a parallel-plate resonator technique [13]. At 77K and 10 GHz, $R_S$ varied from wafer to wafer from 0.3 to 1.0 mΩ with variation across a single wafer of ±10% [14].

## HTS RESONATOR FABRICATION AND TEST

The $TE_{01}$ DR configuration is shown in Figure 8a. The styrofoam ring mounts are compressed between the enclosure covers and hold the sapphire puck firmly in place. The 1.4 inch diameter YBCO/$LaAlO_3$ disks, placed between the foam supports and covers, are held in place with the compressed foam. Loop couplers are used to excite and detect the device resonant response, and the degree of coupling was adjusted by changing the orientation of the loop and/or the loop penetration into the cavity.

Liquid nitrogen (LN) was used as the coolant, and all measurements were made with the unsealed DR assembly in contact with, but not submerged in, the LN near the bottom of a dewar enclosure. The styrofoam plate of Figure 8b was used as a "Dewar" for the photograph and allows showing the complete assembly.

The magnitude of S21, S11, S22, QL, and frequency were measured using an automatic network analyzer (ANA) and synthesized sweep generator combination. Coupling coefficients and unloaded Q

values were calculated from the ANA loaded Q and reflection loss measurements. Most of our measurements were made at 10.16 GHz (G = 2.9 mm).

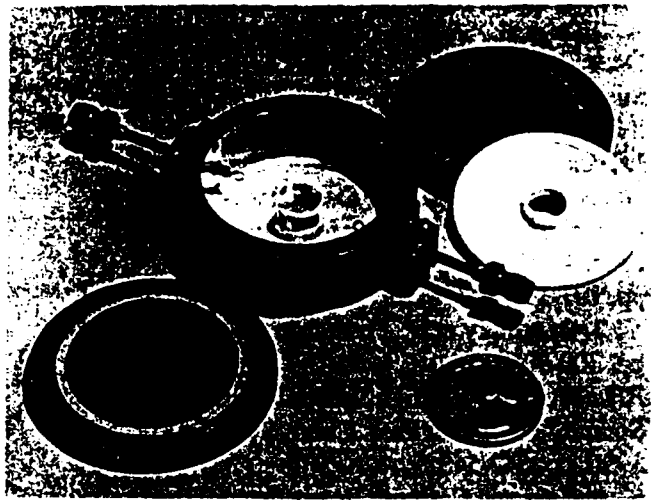

(a)

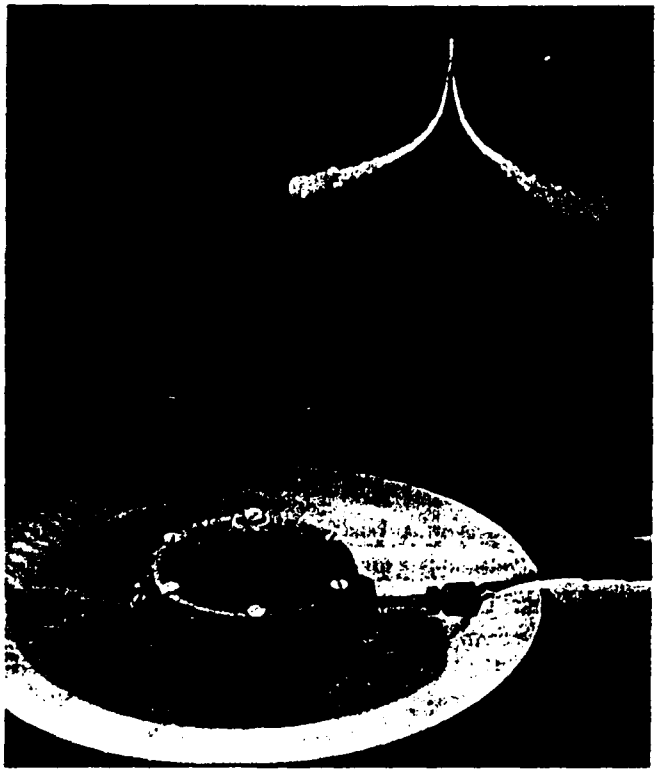

(b)

Figure 8. (a) HTS-Sapphire Dielectric Resonator.
(b) Assembled and Operating at T ~ 77K.

Results of initial measurements are listed in Table 1 for copper and for (two different conductivity values) YBCO end walls. Resistance ratios, $R_{s,Cu}$:$R_{s,YBCO}$ (10 GHz, 77K), are calculated from the measured $Q_u$ and foam support ring mount loss. The highest resistane ratio was 4.0. Resistance ratios of greater than 10 are typically obtained at 77K for small area films cut from large wafers.

| $\frac{R_s\ (Cu)}{R_s\ (YBCO)}$ | $Q_u$ (k) |
|---|---|
| 1.0 | 102 |
| 2.5 | 200 |
| 4.0 | 320 |

## RESONATOR SHORT TERM FREQUENCY STABILITY

In an effort to verify that the HTS portion of the resonators did not contribute to excess resonator self-noise, prototype resonators were tested at Ft. Monmouth, NJ using an HBAR (higher overtone, bulk acoustic resonator)-based, X-band signal generator designed and built by Westinghouse for the U.S. Army Electronic Device and Technology Laboratory [15]. The HBAR-based source exhibits state-of-the-art phase noise performance that is only 10-15 dB poorer than that predicted for the HTS-sapphire-based source (Figure 1). The results of these measurements are shown in Figure 9 and indicate that, within the resolution of the test equipment, the HTS-sapphire resonator self-noise level is immeasurable. The primary contributor to instrumentation noise level is associated with low test set phase detector drive and resulting sensitivity (70 mv/radian) rather than the HBAR-based source spectral characteristics. This result is significant and encouraging, especially, in light of the relatively high (16 dBm) level of resonator drive employed.

In addition to resonator self-noise measurements, the phase noise performance of low 1/f noise, X-band, Schottky diode phase detectors (double balanced mixers) operated at 77K was also measured. These tests were performed in order to demonstrate the feasibility of cooling both the resonator and detector in an integrated, frequency discriminator assembly in order to avoid the need for critical length, RF coaxial cables traversing the cooled/uncooled interface. The results, shown in Figure 10, are also encouraging and show no increase in detector 1/f noise at 77K.

## CONCLUSIONS

We have shown that with high quality, large area, YBCO films and simple, styrofoam mounts, unloaded, X-band Q values of over 250 thousand are

attainable for $TE_{0n}$ mode operation of a sapphire dielectric resonator, operated at 77K. With improvement in the yield of HTS films with good uniformity over areas of 10 $cm^2$, unloaded Q values greater than 500 thousand will be attainable from small volume, $TE_{01}$ shielded, sapphire dielectric resonators.

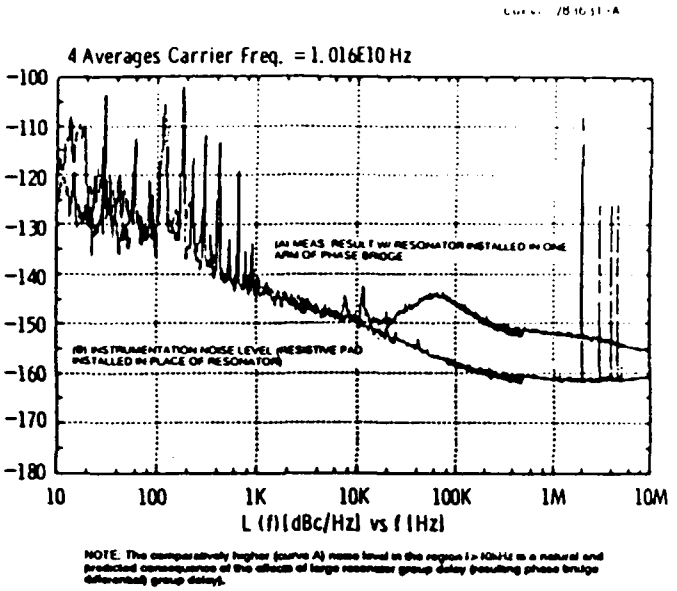


Figure 9. HTS-Sapphire Dielectric Resonator Noise Measurement Results.

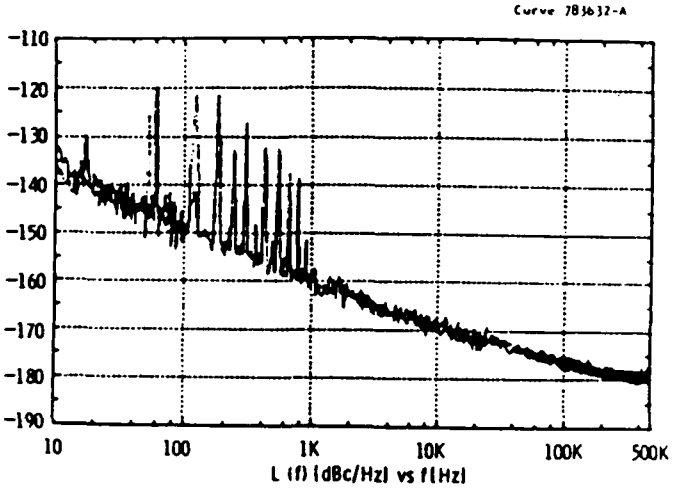


Figure 10. Measured 1/f Noise for WJ M76HC Mixer (Phase Detector) at Room Temperature and 77K.

## REFERENCES


1. M. M. Driscoll, "Low Noise Signal Microwave Signal Generation Using Bulk and Surface Acoustic Wave Resonators," IEEE Trans. Ultrason. Ferroel., and Freq. Contr., Vol. 35, No. 3, May 1988, pp. 426-434.
2. M. M. Driscoll, "Advances in Resonator Technology Support Improved Microwave Signal Spectral Performance," Microwave Journal, Vol. 33, No. 6, June 1990, pp. 153-163.
3. A. Giles et al., "A High Stability Microwave Oscillator Based on a Sapphire Loaded Superconducting Cavity," Proc. 43rd Freq. Contr. Symp., May 1989, pp. 89-93.
4. J. Dick and J. Saunders, "Measurement and Analysis of a Microwave Oscillator Stabilized by a Sapphire Ring Resonator for Ultra-Low Noise," Proc. 43rd Freq. Contr. Symp., May 1989, pp. 107-114.
5. V. B. Braginsky et al., Phys. Lett. A, 120, 1987, pp. 300-305.
6. F. L. Walls et al., "High Spectral Purity X-band Source," Proc. 44th Freq. Contr. Symp., May 1990, pp. 542-548.
7. K. A. Zaki and C. Chen, "Intensity and Field Distribution of Hybrid Modes in Dielectric Loaded Waveguides," IEEE Transactions on Microwave Theory and Techniques, Vol. MTT-33, pp. 1442-1447, December 1985.
8. K. A. Zaki and C. Chen, "Loss Mechanism Dielectric Loaded Resonators," IEEE Transactions on Microwave Theory and Techniques, Vol. MTT-33, pp. 1448-1452, December 1985.
9. K. A. Zaki and C. Chen, "New Results in Dielectric Loaded Resonators," IEEE Transactions on Microwave Theory and Techniques, Vol. MTT-34, pp. 815-826, December 1985.
10. X. P. Liang, H. C. Chang, and K. A. Zaki, "Hybrid Mode Dielectric Resonators on Suspended Substrate," Proceedings of the 19th European Microwave Conference, pp. 1141-1146, September 1989.
11. H. C. Chang and K. A. Zaki, "Unloaded Q's of Axially Asymmetric Modes of Dielectric Resonators," IEEE MTT-S International Microwave Symposium, Digest, pp. 1231-1234, June 1989.
12. J. R. Gavaler and J. Talvacchio, Physics B, 1513, 1990, pp. 165-166.
13. R. C. Taber, "A Parallel Plate Resonator Technique for Microwave Loss Measurements on Superconductors," Rev. Sci. Instrum. 61(8), 2200 (1990).
14. T. T. Braggins, J. R. Gavaler, and J. Talvacchio, accepted for Proc. ICMC, Advances in Cryogenic Engineering (Materials), (Plenum, New York, 1991).
15. M. M. Driscoll et al., "Extremely Low Phase Noise UHF Oscillators Utilizing High Overtone, Bulk Acoustic Resonators," Proc. 1990 IEEE Ultrason. Symp., December 1990.

PHYSICAL REVIEW B VOLUME 45, NUMBER 13 1 APRIL 1992-I

# Josephson tunneling for magnetic fields perpendicular to discrete Nb junctions: Implications for the irreversibility crossover in high-temperature superconductors

D. H. Kim and K. E. Gray
*Materials Sciences Division, Argonne National Laboratory, Argonne, Illinois 60439*

**APPENDIX 13**

J. H. Kang
*Westinghouse Science and Technology Center, Pittsburgh, Pennsylvania 15235*

(Received 14 November 1991)

It was recently suggested that coupling between the superconducting Cu-O bilayer or trilayer units in the *highly anisotropic*, high-temperature superconductors (HAHTS) can be described by *incoherent* Josephson tunneling. This paper confirms the assumed inverse dependence of the coupling energy on field, $H$, through measurements of the zero-bias resistance of discrete, high-quality, thin-film Nb Josephson junctions. This $1/H$ dependence was used to explain the flux-motion-induced broadening of resistive transitions in HAHTS for equivalent geometry with $H$ parallel to the $c$ axis. The Nb junction results also unambiguously confirm another recent suggestion: that field-induced dissipation can occur in Josephson junctions without the motion of vortices from an externally applied field, which in this case are pinned in the Nb electrodes.

Recently,[1] the effects of anisotropy and fluctuations on the field-induced broadening of resistivity transitions, $\rho(T,H)$, and the critical current densities, $J_c(T,H)$, have been studied in high-temperature superconductors (HTS). For *highly anisotropic* HTS in an applied field, $H$, oriented parallel to the $c$ axis ($H\|c$) one explanation considers fluctuations which affect the Josephson coupling across the interlayer junctions.[2] Fluctuations of the relative phase across these junctions occur if $kT$ exceeds $E_{cj}(T,H)$, the Josephson coupling energy[3,4] between adjacent Cu-O bilayer or trilayer units (multilayers). For $H$ perpendicular to the interlayer Josephson junctions, this results in a crossover from three-dimensional (3D) vortex lines to 2D pancake vortices in the isolated Cu-O multilayers, and the experimental fits to this model[2] indicated that the effective junction area in $E_{cj}$ is $\Phi_0/H$.

Josephson fluctuations have also been used recently to explain the broadened $\rho(T,H)$ in *granular* NbN films[5] and $J_c(T,H)$ in *granular* multilayers[6] of NbN with AlN. It was suggested that motion of the external flux could be suppressed by the relatively strong pinning, e.g., in the insulating AlN layers where a distinct crossover in the field dependence of $J_c(H)$ was observed between depinning of the *external* flux and dephasing of intergranular Josephson junctions.[6]

The results presented in this paper confirm both of these ideas by direct measurements on discrete, high-quality Josephson junctions made with Nb films. For fields perpendicular to the film plane (up to 0.03 T), broadened resistive transitions which are very similar to those found in HTS materials are observed in these junctions. For $H \geq 0.005$ T, the experimental activation energy *quantitatively* equaled the theoretical[3] $E_{cj}(T,H)$ with an effective junction area of $\Phi_0/H$. These measurements used a current density of 0.1 A/cm$^2$, for which the resistive transitions of the Nb electrodes were very sharp, indicating that the external flux was completely pinned in the electrodes. Thus the field-induced dissipation was not caused by motion of the external flux, but by self-field, Josephson vortex cores which are independent of, and perpendicular to, the applied field.

The Nb films were sputter deposited in the system equipped with load-lock chamber. The substrate was a 2-in. silicon wafer, onto which a 200-nm layer of $SiO_2$ was formed by a thermal process. The background pressure of the system was maintained at $\sim 10^{-9}$ torr. During film deposition, the substrates were kept in contact with a water-cooled copper plate. The residual resistivity ratios of such Nb films were normally 8–9, with $T_c = 9.2$ K. The Nb junctions used in this paper were fabricated[7] on such films using an $AlO_x$ barrier, which was formed by exposing a 7.5-nm-thick Al layer to 150 mtorr of pure oxygen gas for 30 min, which resulted in $J_c \sim 1500$ A/cm$^2$. Junction areas were defined by the selective niobium etching process (SNEP), which uses reactive ion etching and anodization of Nb. The figure of merit of these junctions, $V_m$, was normally about 50 mV, measured at $V = 2$ mV and $T = 4.2$ K. The magnetic-field penetration depth of the Nb films, $\lambda_{Nb}$, was 62 nm, as measured from diffraction patterns of Josephson critical current, while the Josephson penetration depth, $\lambda_J$, defined by

$$\lambda_J = \left( \frac{\hbar}{2e\mu_0 J_c (2\lambda_{Nb} + d_i)} \right)^{1/2}, \quad (1)$$

was about 12 $\mu$m using the above parameter values and a reasonable insulator thickness, $d_i$.

Resistances were obtained using a standard four-terminal, ac lock-in technique. All measurements were taken in a gas-flow cryostat after cooling the sample from above $T_c$ in the applied field perpendicular to the thin-film electrodes. The measurements described below show that $H_{c2}(T)$ is much larger than that of pure Nb: Consequently, $H_{c1}(T)$ will be much lower. From this, $H_{c1}$ *at zero temperature* can be estimated from the dirty limit formula to be $\sim 0.023$ T. This fact plus the favorable width-to-

© 1992 The American Physical Society

thickness ratio ($>50$) of the films, explains why small fields can remain in the samples after field cooling. In order to achieve transitions to a Josephson supercurrent at low temperatures, it was necessary to cool the samples quickly (and even faster as the field increased). Possibly this was necessary to keep the flux cores frozen in their initial aligned positions in each electrode, thereby preventing any parallel component in the barrier due to misalignment. Note that in a parallel field, the junction resistance periodically returned towards the quasiparticle resistance of the junction (which is greater than the normal-state value) when an integral number of flux quanta filled the junction. This manifestation of the usual Fraunhofer pattern measured in $I_c(H)$ is seen here as a function of temperature, because of the temperature dependence of $\lambda_{Nb}(T)$. For each perpendicular-field value, the resistive transitions were measured repeatedly: For analysis, we used those with the steepest slope which were reproducible and showed no evidence of vortex cores from the external field being parallel to the junction in the temperature dependence.

The resistive transitions of one junction and its electrode are shown in Fig. 1 for a field of 0.03 T. These measurements use a current density of 0.1 A/cm$^2$, and the extremely sharp resistive transition in the electrode indicates that *the external flux is completely pinned at all temperatures*, $T<0.98T_c$. The initial drop in apparent junction resistance corresponds to the incomplete four-terminal cancellation of both electrode resistances when they are not superconducting. Figure 2 shows the complete field dependence of this junction's resistance. Note that $H_{c2}(T)$ can be extracted from the initial drop at $T_c(H)$, and is given by 0.27 T/K near $T_c$.

In the theory[4] of Josephson junctions for zero field, a finite junction resistance appears even below $T_c$ due to thermal fluctuations and it is given [for $E_{cj}(T,H)\gg k_BT$] by $R\propto\exp[-E_{cj}(T,H)/k_BT]$ where $k_B$ is the Boltzman constant. The Josephson coupling energy, $E_{cj}$ is proportional to $I_c$, the critical current in the absence of thermal fluctuations, which is proportional to the product of the superconducting order parameters on each side of the junction, $\psi_a$ and $\psi_b$, divided by the normal-state resistance, $R_N$. Near $T_c$, $\psi_a\psi_b\propto(1-t)$, where $t=T/T_c$, so for convenience we define $U_0(H)=E_{cj}(T,H)/(1-t)k_B$ to obtain $R\propto\exp(-U_0(1-t)/T)$. This expression is used to fit the resistance data of Fig. 2 and determine $U_0$, which is plotted in Fig. 3 together with the data for two other junctions. For $H\geq 0.005$ T, $U_0$ agrees *quantitatively* with theory[3] if an effective junction area of $\Phi_0/H$ is used for the $R_N$ going into $E_{cj}$.

In zero field, the low-temperature $I_c$, in the absence of

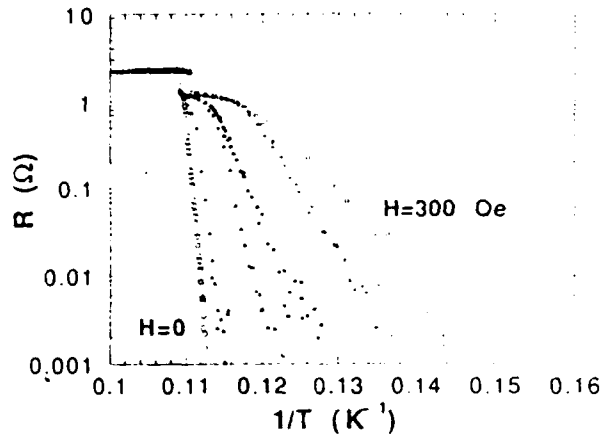


FIG. 2. The field dependence of the resistive broadening of Nb/Nb thin-film Josephson tunnel junctions looks very similar to high-temperature superconducters. Magnetic fields: 300 Oe (squares); 200 Oe (pluses); 100 Oe (diamonds); 50 Oe (open triangles); 20 Oe (solid triangles); zero applied field (circles).

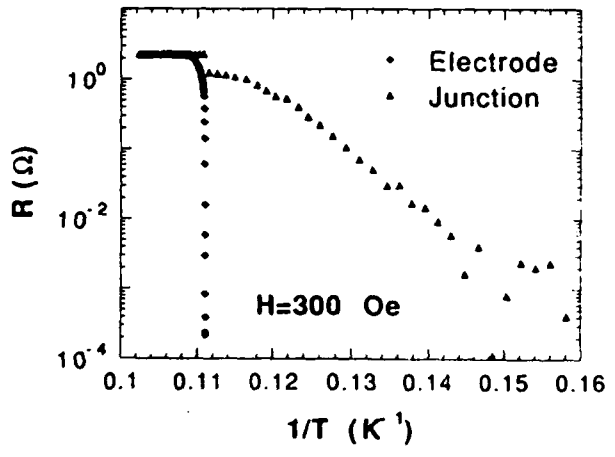


FIG. 1. The resistance of a Nb/Nb thin-film Josephson tunnel junction in a field of 300 Oe which is perpendicular to the film plane (triangles). For comparison, the resistance of one of the electrodes (diamonds) is plotted in scaled units under the same conditions. Clearly vortices from the external field are well pinned in the electrodes at temperatures just below $T_c$, whereas the junction dissipation extends to much lower temper-

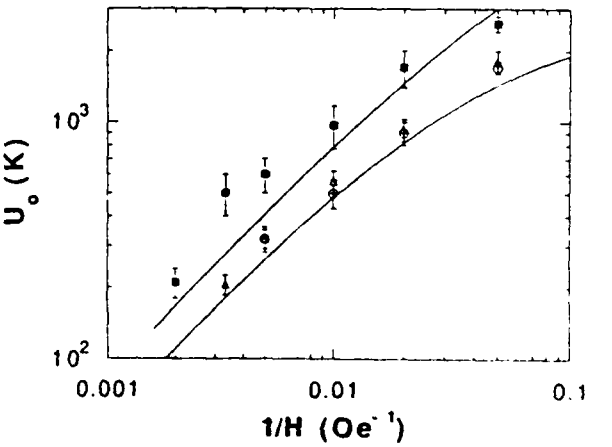


FIG. 3. The activation energy obtained from fitting data of Fig. 2 (triangles), for a Nb/Nb junction of area $8\times12$ $\mu$m$^2$, and those of two other Nb/Nb junctions, of the same area (circles) and of area $16\times16$ $\mu$m$^2$ (squares). The lines are calculated from the model described in the text: At high fields they represent an effective junction area of $\Phi_0/H$ with no adjustable pa-

thermal fluctuations, was measured to be $\sim 1.4$ mA, which is about 70% of that predicted by using the measured junction resistance (e.g., from Fig. 2) in $E_{cj}$. However, a fit to the broadened resistive transition in zero field requires a much larger resistance in $E_{cj}$. This can be understood if the junction is sectioned into phase-coherent areas which are significant smaller ($A_0 \sim 1\ \mu m^2$) than the geometrical area ($\sim 96\ \mu m^2$), and may be caused by disorder in the films, which were deposited at low temperatures. Then each section, and the junction as a whole, will have the same broader transition. However, the low-temperature critical current *density* is expected to be little changed by such sectioning, so $I_c$, which sums the (super) conductivity of all the phase-coherent sections in parallel, should be affected very little, and the above measurements confirm this. The solid line in Fig. 3 interpolates between the low-field limit of area ($A_0$) and the high-field limit ($\Phi_0/H$), using an effective area, $A = (A_0^{-1} + H/\Phi_0)^{-1}$.

A potential picture to understand the effective area being $\Phi_0/H$ has been proposed[8] to explain the $c$-axis resistivity in $Bi_2Sr_2CaCu_2O_x$ crystals. It borrows the concept of a coherence radius used for superconducting fluctuations in a magnetic field,[9] either above $T_c$ or in resistive states below $T_c$. However, the Nb electrodes are in a zero-resistance state with the vortices pinned, and the above interpretation would miss the long-range coherence of the phase of $\psi$ in these electrodes. A more conventional[10] approach begins with thermally activated Josephson vortex cores, which are parallel to the films in the insulating region of the junction. For finite dissipation, these must cross the entire junction area, $A_0$, and thus, e.g., in zero field, $E_{cj} \propto 1/R_N \propto A_0$. However, we may suggest that in a finite field, the minimum-sized Josephson core excitation is a loop of area $\sim \Phi_0/H$, since then it is possible to *connect* the Josephson cores to those of the external field which are pinned in the Nb electrodes on a lattice of that unit-cell size. It is necessary to make the unproven presumption that this reconnection makes the thermally activated loop more stable against collapse. In such a case, $E_{cj}$ would correspond to an effective junction area, $\Phi_0/H$. Note that the energy barrier for flux-line cutting associated with this reconnection is small: The field of the Josephson cores is weakly localized ($\sim 2\lambda_J = 24\ \mu m$) compared to the flux-line spacing ($\sim 0.4\ \mu m$ at 100 G) and the magnitude of $\psi$ in the insulating regions is small (its value is $\sim 0.007$ of that in the Nb electrodes, i.e., the square root of the ratio of the critical current densities of the Josephson junction to that for depairing in Nb).

Dissipation eventually occurs when these loops further expand in size and/or merge with others to cross the entire junction area. The junction current favors both the formation and expansion of one sense of the circulation in the loops, as it does in zero field. This may be viewed as the result of a Lorentz-like force between the Josephson cores and the tunnel current. However, the tunnel current is *parallel* to the applied field, so there is no *macroscopic* Lorentz force, except in the electrodes where pinning prevents any flux motion. Further theoretical analysis is highly desirable, and it can be noted here that the pinned flux cores in the Nb may be analogous to the role of dislocations in dislocation-mediated shearing (melting) of crystals.[11]

In summary, we report the field dependence of the zero-bias resistance of discreet, high-quality, thin-film Nb Josephson junctions and find a $1/H$ dependence for the thermally activated Josephson coupling energy for $H$ perpendicular to the film plane. This confirms the use of such a field dependence to explain[2] the flux-motion-induced broadening of resistive transitions for the HTS with $H$ parallel to the $c$ axis. The Nb junction results have also unambiguously confirmed another recent suggestion,[6] that field-induced dissipation can occur in Josephson junctions without the motion of vortices from an externally applied field.

One of us (J.H.K.) acknowledges John Talvacchio for useful discussions of junction properties. One of us (K.E.G.) thanks Seb Doniach for insights into the picture of Josephson core loops and Valerii Vinokur for discussions including the analogy to shearing of crystal lattices. The authors also thank Richard S. Nye for technical assistance in junction fabrication and Mark Trochet for other technical assistance. This work is supported by the U.S. Department of Energy, Basic Energy Sciences-Materials Sciences under Contract No. W-31-109-Eng-38.

[1] D. H. Kim, K. E. Gray, R. T. Kampwirth, and D. M. McKay, Phys. Rev. B 42, 6249 (1990).

[2] D. H. Kim, K. E. Gray, R. T. Kampwirth, J. C. Smith, D. S. Richeson, T. J. Marks, J. H. Kang, J. Talvacchio, and M. Eddy, Physica (Amsterdam) 177C, 431 (1991).

[3] P. W. Anderson (unpublished); V. Ambegaokar and A. Baratoff, Phys. Rev. Lett. 10, 486 (1963).

[4] V. Ambegaokar and B. I. Halperin, Phys. Rev. Lett. 22, 1364 (1969).

[5] D. H. Kim, K. E. Gray, R. T. Kampwirth, K. C. Woo, D. M. McKay, and S. J. Stein, Phys. Rev. B 41, 11642 (1990).

[6] K. E. Gray, R. T. Kampwirth, D. J. Miller, J. M. Murduck, D. Hampshire, R. Herzog, and H. W. Weber, Physica (Amsterdam) 174C, 340 (1991).

[7] J. H. Kang, D. L. Miller, J. X. Przybysz, and M. A. Janocko, IEEE Trans. Magn. MAG-27, 3117 (1991).

[8] G. Briceno, M. F. Crommie, and A. Zettl, Phys. Rev. Lett. 66, 2164 (1991).

[9] R. Ikeda, T. Ohmi, and T. Tsuneto, J. Phys. Soc. Jpn. 58, 1377 (1989); S. Ullah and A. T. Dorsey, Phys. Rev. B 44, 262 (1991); M. Tinkham, *Introduction to Superconductivity* (McGraw-Hill, New York, 1975), p. 240.

[10] This approach was suggested by S. Doniach (private communication).

[11] This analogy was pointed out by V. M. Vinokur (private communication).

# Field-Dependent Crossover in the Vortex Response at Microwave Frequencies in $YBa_2Cu_3O_{7-\delta}$ Films

J. Owliaei and S. Sridhar

*Department of Physics, Northeastern University, Boston, Massachusetts 02130*

J. Talvacchio

*Westinghouse R&D Center, Pittsburgh, Pennsylvania 15201*

**APPENDIX 14**

(Received 26 May 1992)

We observe anomalous magnetic field dependence of the microwave vortex response of epitaxial $YBa_2Cu_3O_{7-\delta}$ films, which we identify as a crossover from flux pinning to flux flow, occurring near a characteristic field $H^*(T)$. We show that the presence of the crossover depends only on adequate softening of the pinning potential $U(T,H)$ (i.e., it is independent of the nature of the vortex transition). However, the data are in good agreement with a thermal activation model in which $U(T,H)=A(T)/H$. A separate analysis of the high-field, high-frequency superconducting transition yields a measure of the upper critical field $H_{c2}$.

PACS numbers: 74.30.Gn, 74.60.Ec, 74.60.Ge, 74.75.+t

Probing vortex dynamics in superconductors at high frequencies is well known to provide important information regarding the mixed state. In the low-$T_c$ superconductors, it was shown by Gittleman and Rosenblum [1] that, at fixed magnetic field, a crossover occurs from pinned vortices to free flux flow, as the probe frequency crosses a characteristic frequency ($\sim$100 MHz typically). An understanding of these results was developed in terms of the viscoelastic response of individual vortices, in which the frequency scale is the viscoelastic relaxation frequency, and the only field scale which enters is the upper critical field $H_{c2}$.

In this paper we present experimental evidence, based on measurements of the 10-GHz microwave surface resistance $R_s(T,H)$, that this description is inadequate at high fields in $YBa_2Cu_3O_{7-\delta}$ films. We observe, for the first time, *a crossover as a function of field at fixed frequency*, from a pinning dominated regime to a flow dominated regime. This occurs near a characteristic field which we call $H^*(T)$, which is comparable to the so-called "irreversibility" line [2]. We show that the experimental results are well described by a theory [3] by Coffey and Clem which includes a field-dependent pinning potential and the influence of thermal fluctuations on the surface impedance, and we connect the observed crossover field with the pinning potential $U(T,H)$. However, we also show that this crossover is model independent, and requires only an adequate softening of the pinning potential or force constant caused by the magnetic field. The analysis of the data yields experimental results for the flux viscosity $\eta(T)$, the flux pinning force constant $\alpha_p(T)$, and the pinning potential $U(T,H)$. The $T$ dependence of $\eta(T)$ suggests a rapid decrease of the quasiparticle scattering rate below $T_c$. Our work demonstrates significantly new phenomenology of vortex electrodynamics in $YBa_2Cu_3O_{7-\delta}$, which were not recognized or are absent in low-$T_c$ superconductors.

Near the (high frequency, high field) superconducting transition, the dominant field scale is the upper critical field $H_{c2}$. We analyze the transition in terms of the temperature derivative $(\partial R_s/\partial T)_H$, from which we obtain a measure of $H_{c2}$.

Epitaxial ($\hat{c}$-axis oriented) $YBa_2Cu_3O_{7-\delta}$ films (0.5 $\mu$m thick) were deposited onto $LaAlO_3$ substrates (nominally 0.5 in. square) using standard off-axis sputtering techniques. Extensive characterization [4] of these films has shown them to have high-quality properties, with sharp transitions and $J_c > 10^6$ A/cm$^2$ at 77 K. Using a Nb superconducting cavity, high sensitivity measurements of the *absolute* zero-field $R_s(H=0,T)$ were also carried out. The $R_s(H=0,t)$ measurements are consistent (see inset to Fig. 1) with BCS calculations with $\lambda(0)\sim 1400$ Å and $2\Delta(0)/kT_c=4.2$, and are in good agreement with measurements on single crystals [5] and laser ablated films.

The high-field measurements were carried out using sapphire-loaded Cu cavities with the sample as an end plate. Magnetic fields up to 7 T were applied parallel to the $\hat{c}$ axis using a NbTi superconducting magnet. The surface resistance $R_s(T,H)$ was obtained from the measured cavity $Q$'s, using $R_s(T,H)=\Gamma[Q^{-1}(T,H)-Q_b^{-1}(T,H)]$, where $Q_b$ refers to the background $Q$ and was obtained separately, and $\Gamma$ is a known geometric fac-

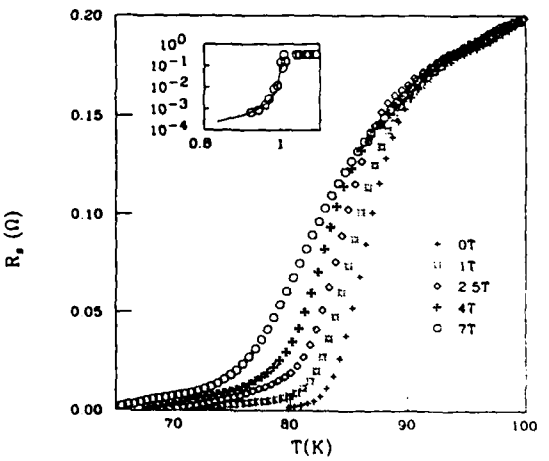


FIG. 1. $R_s$ vs $T$ at several fields from 0 to 7 T. Inset: $R_s$ vs $T/T_c$ at $H=0$ measured using a superconducting cavity. The solid line represents a BCS calculation.

© 1992 The American Physical Society

tor. Experiments were carried out under both field-cooled (FC), and zero-field-cooled conditions with subsequent application of the magnetic field, and were consistent with each other. Results for $R_s$ vs $T$ at various cooling fields up to 7 T are shown in Fig. 1. (Similar curves taken at several other fields in the same range are not shown to avoid crowding.) Note that the experiments yield absolute values for the $T$- and $H$-dependent $R_s$, which is crucial for obtaining material parameters, as the subsequent discussion shows.

Vortex dynamics in the mixed state ($H_{c1} \ll H \ll H_{c2}$) is best examined by considering the field dependence of $R_s$. From curves such as in Fig. 1, we have constructed the field dependence $[R_s(H) - R_s(H=0)]$ at fixed $T$, as shown in Fig. 2(a) for a representative temperature $T = 81.2$ K. We now turn to understanding the field dependence as shown in Fig. 2.

The simplest model of the response of vortices to ac driving fields is obtained from the equation of motion: $\eta\dot{x} + \alpha_p x = J_\omega \Phi_0$. One can show that this leads to a constitutive equation $J_\omega = [(\alpha_p + i\omega\eta)/(i\omega\Phi_0 B)]E_\omega$ from which both the absorption represented by $R_s(\omega,T,H)$ and the reactive response represented by the penetration depth $\lambda(\omega,T,H)$ can be calculated. The above model yields $R_s(\omega,T,H) = f(\omega,T)\sqrt{H}$, i.e., *a single $\sqrt{H}$ behavior for both $R_s$ and $\lambda$ at all $H$ ($\gg H_{c1}$) for fixed frequency experiments* such as the one discussed here.

The data in Fig. 2(a) are clearly not described by a single $\sqrt{H}$ dependence (two examples are shown to which we return later). We examine this further by replotting as $[R_s(H) - R_s(0)]^2$ vs $H$ in Fig. 2(b), now including data for other temperatures. It is now obvious that a single straight line is inadequate in Fig. 2(b). Instead there is a clear crossover from a low- to a high-field behavior. This feature of the data is not described by the simple model discussed above, according to which a crossover only occurs as a function of $\omega$, not $H$. This is because the field dependence of the pinning parameters is not included. As discussed below, the entire behavior is well described by considering a field-dependent pinning potential.

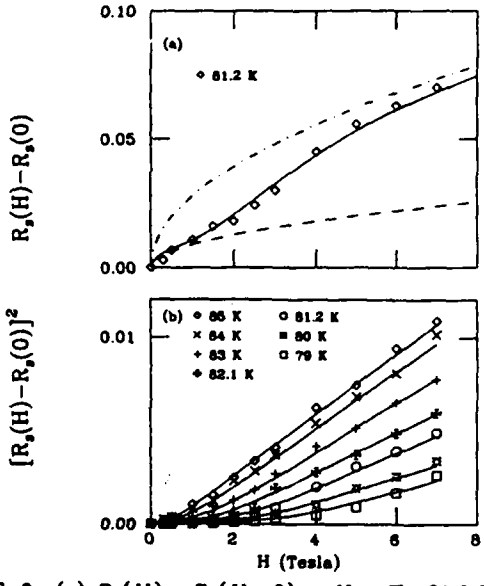


FIG. 2. (a) $R_s(H) - R_s(H=0)$ vs $H$ at $T = 81.2$ K, and (b) $[R_s(H) - R_s(0)]^2$ vs $H$, at several temperatures. The solid lines represent theoretical calculations. Note that the data and theory indicate a crossover from a low-field $\sqrt{H}$ dependence to a high-field $\sqrt{H}$ dependence [these limiting behaviors are shown as dashed (pinning) and dot-dashed (flow) lines in (a)].

We consider this in terms of a more general equation of motion: $\eta\dot{x} + \alpha_p L/2\pi \sin(2\pi x/L) = J_\omega\Phi_0 + \tilde{F}(t)$, where the last term represents a stochastic driving force due to thermal fluctuations. Coffey and Clem [3] have analyzed the high-frequency response of vortices in terms of this equation, based upon the analogy of the equation of motion to that of a Brownian particle in a periodic potential $U_0 = U[1 - \cos(2\pi x/L)]$ driven by an alternating field. They obtain a result for the frequency-dependent mobility of a vortex: $\bar{\mu}(\omega,T,H) = \eta^{-1}(1 + \{i\omega\tau_0/\alpha + 1/[I_0^2(\nu) - 1]\}^{-1})^{-1}$, from which a corresponding resistivity $\bar{\rho}_r = \Phi_0 B\bar{\mu}$ can be defined. This leads to a $J$-$E$ relation: $J_\omega = \bar{\rho}_r^{-1}E_\omega$, yielding a complex penetration depth $\bar{\lambda}_r^2(\omega,H,T) = \bar{\rho}_r(\omega,H,T)/-i\omega\mu_0$. Here $\alpha = I_1(\nu)/I_0(\nu)$, $\nu = U/2k_bT$, $I$'s are modified Bessel functions, and the bare viscoelastic relaxation time $\tau_0 = \eta/\alpha_p$.

In order to make contact to experimental data, we introduce [6] a field scale $H^*(T)$ which is obtained from a separable potential of the form $U(H,T) = A(T)/H$, where $H^*(T) = A(T)/2k_bT$, and a length scale $\delta^*(T) \equiv [\Phi_0 H^*(T)/\mu_0\omega\eta(T)]^{1/2}$. This enables $R_s$ to be written as

$$R_s = -\omega\mu_0 \mathrm{Im}[\bar{\lambda}_r] = -\omega\mu_0\delta^*(T)\mathrm{Im}[ixg(\omega\tau_0,x)]^{1/2}, \quad (1)$$

where $g$ is defined by $\bar{\rho}_r = \rho_f g(\omega\tau_0,x)$, and $\rho_f$ is the flux flow resistivity. The field dependence of the vortex contribution to the surface resistance is then defined in terms of the scaled variable $x = 1/\nu = H/H^*(T)$.

An examination of the high- and low-field limits of Eq. (1) shows that the characteristic field $H^*(T)$ demarcates the regions of flux-pinning-dominated and flux-flow-dominated response, at fixed frequency. The limits are

$$H \ll H^*(T), \text{ pinning limit: } R_s \to (\Phi_0\mu_0\omega^4\eta^2/4\alpha_p^3)^{1/2}\sqrt{H}, \quad (2a)$$

$$H \gg H^*(T), \text{ flux flow limit: } R_s \to (\Phi_0\mu_0\omega/2\eta)^{1/2}\sqrt{H}. \quad (2b)$$

The principal feature of the model described above is that the field dependence of $R_s \propto \sqrt{H}$ in the high- and low-field limits, with a crossover near $H^*(T)$. (The exact location of the crossover in the $H$-$T$ plane is determined also by the measurement frequency in terms of $\omega\tau_0$.) This is very like the experimental results presented in Fig. 2.

The results of numerical calculations using the above model are shown in Figs. 2(a) and 2(b) as the solid lines. It is clear that the theory *quantitatively* describes the ex-

perimental results, in particular the crossover as a function of $H$, which is not obtained from the simple model. Comparisons as in Fig. 2 yield the vortex parameters $\eta(T)$, $\alpha_p(T)$, and $H^*(T)$ using the following procedure. From the *limiting* low- (pinning) and high-field (flow) $\sqrt{H}$ behavior shown in Fig. 2(a) as the dashed lines, the parameters $\eta(T)$ and $\alpha_p(T)$ are obtained using Eq. (2). This defines two of the inputs to the calculations. The remaining parameter $H^*(T)$ is then obtained from fits as in Fig. 2(b).

The vortex field scale $H^*(T)$ vs $T$ is shown in Fig. 3. Also shown in Fig. 3 are the "irreversibility" line $T_{irr}(H)$ of Malozemoff and Worthington *et al.* [7], and the $T_{cg}(H)$ data of Gammel, Schneemeyer, and Bishop [8], which has been described in terms of a vortex glass transition, both scaled to $T_c(0)=90.0$ K. It is noteworthy that $H^*(T)$ is in very good agreement with these other data arrived at by entirely different measurement methods and analysis, which probe vortex dynamics on much longer time scales. In the framework of the model discussed in this paper, this field is related to the barrier height and thus the present experiments provide a measure of the barrier height in these films. An approximate fit to the data (Fig. 3) is $H^*(T)=100(1-t)^{3/2}/t$ (tesla), from which we obtain $U\sim 1.8\times 10^4(1-t)^{3/2}/H$ (tesla kelvin), which is in reasonable agreement (as regards magnitude) with other measurements [9]. We note that $H^*(T)$ may be more closely identified with the so-called "depinning" line [10,11].

Although we have used a specific model which incorporates thermal fluctuations in order to analyze our data quantitatively, it should be stressed that the crossover observed in our results is really a generic feature of the dynamic response of the flux lattice, and requires only that the pinning parameters (potential or force constant) decrease adequately with magnetic field, viz., (1) as $H\to 0$, $\alpha_p(T)\equiv[\partial^2 U(x,H,T)/\partial x^2]_{x\to 0}$ is finite, and (2) as $H\to$ "$\infty$," $\alpha_p(H)\ll\omega\eta$. In these two limits one recovers the results of Eqs. (2a) and (2b) for the pinning and flow regimes, and hence these requirements guarantee that a crossover (as a function of $H$ at fixed $\omega$) exists. It should also be noted that the softening of the pinning parameters can be related to a $J_c(H)$ which decreases with increasing field, as is commonly observed.

The generic nature of the crossover implies that it should be present regardless of the nature of the vortex transition. The detailed behavior of $R_s(H)$ will of course depend on the form used for $U(T,H)$ or $\alpha_p(T,H)$. It should be possible to incorporate [12] appropriate forms relevant to flux lattice melting [13], and also disorder, which is relevant to the vortex glass [14] description. In general, for a first-order transition in which the potential vanishes, one expects a sharp feature in $R_s(H)$ in a narrow region of the $H$-$T$ plane. Our work suggests that an exploration [15] of the response in the $H$-$T$ plane near the vortex transition could address this issue—here we have focused on the broad features.

The flux viscosity $\eta(T)$ obtained from the analysis is shown in Fig. 4. We also obtain a measure of the "quasiparticle resistivity" using $\rho_n(T)=\Phi_0 H_{c2}(T)/\eta(T)$, where $H_{c2}(T)=115(1-t)$ (tesla) (see below). This is also shown in Fig. 4. The data imply that the quasiparticle scattering rate is decreasing rapidly with $T$, as has also been observed in other measurements [16]. This is a feature peculiar to the high-$T_c$ superconductors. Note that the magnitude of $\rho_n$ (an extrapolation yields 45 $\mu\Omega$ cm at 90 K) is approximately consistent with dc resistivity values. $\alpha_p(T)$ increases from $1.3\times 10^3$ to $1.7\times 10^4$ N/m$^2$ with decreasing $T$, comparable with Ref. [17] for single crystals over the same $T$ range. From $\eta$ and $\alpha_p$, we can obtain $f_c=\alpha_p/2\pi\eta$ which increases from 3 to 15 GHz. (The analysis of these parameters is limited to $T<85$ K because of the limited dynamic range of the

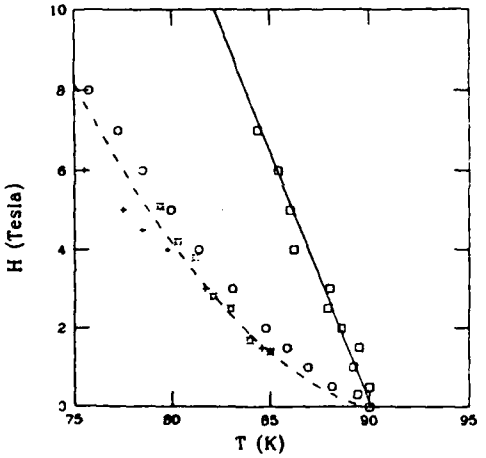


FIG. 3. $H$-$T$ phase diagram obtained from the analysis of the $R_s(T,H)$. $H_{c2}$ (squares), vortex field $H^*$ (stars). Also shown are scaled data (circles) for $T_{irr}(H)$ from Ref. [7], and $T_{cg}(H)$ (plusses) from Ref. [8]. The lines represent: dashed, $H^*(T)=100(1-t)^{3/2}/t$ (tesla); solid, $H_{c2}(T)=115(1-t)$ (tesla).

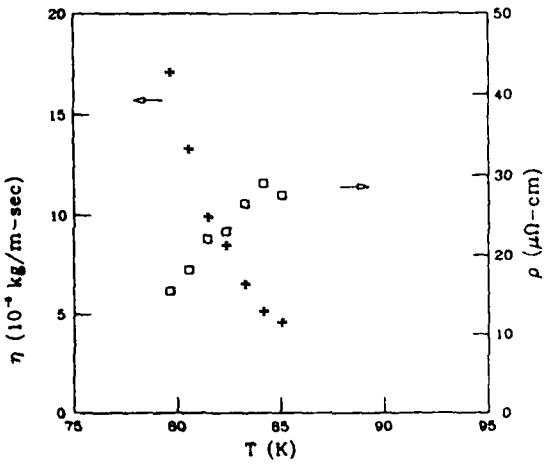


FIG. 4. Flux viscosity $\eta(T)$ vs $T$. Also shown is the quasiparticle resistivity given by $\rho_n(T)=H_{c2}(T)/\Phi_0\eta(T)$, showing the freezing out of the scattering in the superconducting state.

data at higher $T$.)

Although Fig. 1 appears to be similar to dc resistivity measurements, the broadening of the high-frequency transition is distinctly different from the dc transition. This is because the behavior of $R_s$ near $T_c$ is dominated by the penetration depth, and hence is closer in character to magnetization data, even though we are examining a dissipative process. Indeed it is possible to quantitatively analyze the data and obtain $T_c(H)$ and hence $H_{c2}$, as discussed below.

It is more informative to analyze the high-frequency transition in terms of the derivative $(\partial R_s/\partial T)_H$, which is shown in Fig. 5, rather than $R_s(T,H)$. The overall shape of the curves in Fig. 5, viz., the presence of the peak, can be understood in terms of conventional models for the condensate, such as BCS or two-fluid (which we use for simplicity). Detailed numerical calculations were carried out for $(\partial R_s/\partial T)_H$ using a unified expression [3] for the impedance:

$$\tilde{\lambda}^2(H,T)=\frac{\lambda_L^2(H,T)+\tilde{\lambda}_n^2(\omega,H,T)}{1+i2\lambda_L^2(H,T)/\delta_{nf}^2(H,T,\omega)}$$

and $R_s=-\omega\mu_0\,\mathrm{Im}(\tilde{\lambda})$. For the condensate contribution, we use two-fluid approximations for simplicity:

$$\lambda_L^2(H,T)=\lambda_{L0}^2/\{1-[T/T_c(H)]^4\}[1-H/H_{c2}(T)]$$

and

$$\delta_{nf}^2(H,T)\propto(1-\{1-[T/T_c(H)]^4\}[1-H/H_{c2}(T)])^{-1}.$$

Guided by these calculations, we obtain a measure of $T_c(H)$ by the following procedure. We obtain the shift $T_c(H)-T_c(0)$ at the peak point, and using $T_c(0)=90$ K, we obtain $T_c(H)$ at various fields. Although an apparent onset is observed as high as 93 K, we use the value of 90 K based upon consistency with these and other transport measurements. The resulting $T_c(H)$ is displayed in Fig. 3, and it is noteworthy that the data has a clearly linear behavior. This may be contrasted with attempts to obtain $H_{c2}$ from the dc resistivity, which are known [18] to yield anomalous results. The data are well described by $H_{c2}(T)=115(1-t)$ (tesla). This implies

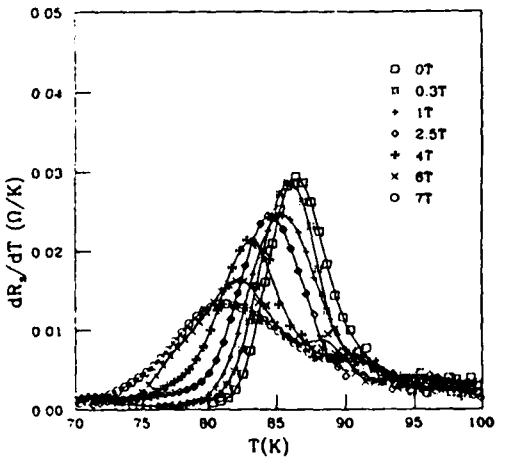


FIG. 5. Temperature derivative $(\partial R_s/\partial T)_H$ of the data in Fig. 1, used to obtain $H_{c2}$.

that $-(dH_{c2}/dT)_{T_c}=1.28$ (T/K), somewhat small than the value of 1.9 (T/K) obtained by Welp *et al.* [18]

The model used above as a guide predicts a discontinuity in $(\partial R_s/\partial T)_H$ at $T_c(H)$, which is not present the data due to the rounding of the transition, likely du to fluctuations. A more complete understanding of th transition is clearly worthwhile, and further work incorporating fluctuations is underway.

We note that the present high-frequency measuremen which have yielded $H_{c2}$ and a vortex field scale $H^*$, whe combined with earlier results [5,17] [6 MHz $\lambda(T,H$ which measure $H_{c1}$, have yielded the complete $H$-phase diagram for $YBa_2Cu_3O_y$. Thus the electrodynam measurements have a wide range of sensitivity, fro sub-Oe to tesla fields. These measurements yield info mation regarding the gap parameter $\Delta(T,H)$ in th Meissner state, and the pinning potential $U(T,H)$ in th mixed state. While the various field scales $H_{c1}$, $H^*$, an $H_{c2}$ are common to other measurements, the electr dynamic phenomenology in different regions of the pha diagram are governed by the short time scales and hig frequencies that are relevant.

We thank R. S. Markiewicz, C. A. Shiffman, B. A Willemsen, and D. H. Wu for useful discussions. Wor at Northeastern was supported by the AFOSR throug Rome Labs, Hanscom and at Westinghouse by AFOSF F-494620-91-C-0034.

[1] J. I. Gittleman and B. Rosenblum, Phys. Rev. Lett. 1 734 (1966).
[2] K. A. Muller, M. Takashige, and J. G. Bednorz, Ph Rev. Lett. 58, 1143 (1987).
[3] M. W. Coffey and J. R. Clem, Phys. Rev. Lett. 67, 3 (1991).
[4] J. Talvacchio *et al.*, IEEE Trans. Magn. 24, 978 (1991)
[5] S. Sridhar, W. Kennedy, and Dong-Ho Wu, Phys. R Lett. 63, 1873 (1989).
[6] S. Sridhar *et al.*, Phys. Rev. Lett. 68, 2220 (1992).
[7] A. P. Malozemoff, MRS Bull. 15, 50 (1990); T. Worthington *et al.*, Cryogenics 30, 417 (1990).
[8] P. L. Gammel, L. F. Schneemeyer, and D. J. Bish Phys. Rev. Lett. 66, 953 (1991).
[9] A. P. Malozemoff *et al.*, in *Strong Correlations and S perconductivity*, edited by H. Fukuyama, S. Maekaw and A. P. Malozemoff (Springer-Verlag, Heidelbe 1989).
[10] Y. Kopelevich *et al.*, Physica (Amsterdam) 183C, 3 (1991); A. Hebard *et al.*, Phys. Rev. B 40, 5243 (1989)
[11] J. van den Beek and P. Kes, Phys. Rev. B 43, 130 (1991).
[12] N. C. Yeh, Phys. Rev. B 43, 523 (1991); A. Koshelev a V. M. Vinokur, Physica (Amsterdam) 173C, 465 (199 E. H. Brandt, Phys. Rev. Lett. 67, 2219 (1991).
[13] D. Nelson, Phys. Rev. Lett. 60, 1973 (1988).
[14] M. P. A. Fisher, Phys. Rev. Lett. 62, 1415 (1989).
[15] H. Olsson *et al.*, Phys. Rev. Lett. 66, 2661 (1991).
[16] D. A. Bonn *et al.*, Phys. Rev. Lett. 68, 2390 (1992).
[17] Dong-Ho Wu and S. Sridhar, Phys. Rev. Lett. 65, 20 (1990).
[18] U. Welp *et al.*, Phys. Rev. Lett. 62, 1908 (1989).

# Infrared properties of epitaxial $La_{2-x}Sr_xCuO_4$ thin films in the normal and superconducting states

F. Gao, D. B. Romero,* and D. B. Tanner
*Department of Physics, University of Florida, Gainesville, Florida 32611*

**APPENDIX 15**

J. Talvacchio and M. G. Forrester
*Westinghouse Science and Technology Center, Pittsburgh, Pennsylvania 15235*

(Received 23 July 1992; revised manuscript received 14 September 1992)

The $CuO_2$-plane optical reflectance of superconducting $La_{2-x}Sr_xCuO_4$ thin films ($T_c \simeq 31$ K) has been measured over a wide frequency and temperature range. The optical conductivity in the normal state is well described by a temperature-dependent weak-coupling ($\lambda \approx 0.25$) free-carrier term plus an overdamped, weakly temperature-dependent, midinfrared component. The free-carrier plasma frequency is nearly constant, $\omega_{pD} = 6300\ cm^{-1}$, whereas the relaxation rate varies linearly with temperature above $T_c$. In the superconducting state, according to our two-component approach, most of the Drude oscillator strength condenses to a $\delta(\omega)$ function. A two-fluid analysis gives a rapid drop in the quasiparticle damping rate below $T_c$. A reasonable estimate ($\sim 2750$ Å) for the *ab*-plane London penetration depth is obtained from the superfluid density. We observe that the midinfrared strength increases below $T_c$, suggesting that some ($\sim 15\%$) of the free carriers do not condense into superconducting pairs and may have a strong interaction with pair-breaking excitations. Two absorption edges around 80 $cm^{-1}$ (3.7 $k_BT_c$) and 400 $cm^{-1}$ (18 $k_BT_c$) are seen but neither is assigned to the superconducting gap. Comparisons with a one-component picture described by a frequency-dependent scattering rate and effective mass are made and discussed. The far-infrared *ab*-plane phonons show systematic changes with temperature, which are associated with the structural transition near 250 K.

## I. INTRODUCTION

Since the discovery of high-temperature superconductors (HTSC),[1,2] tremendous efforts have occurred in the studies of these cuprate oxides. Most optical studies have concentrated on the 90-K transition temperature $YBa_2Cu_3O_{7-\delta}$ (YBCO) system, which contains both $CuO_2$ planes and CuO chains. (For reviews, see Refs. 3–6). It has been observed, however, that the quasi-one-dimensional CuO chains in YBCO have a substantial contribution to the optical conductivity,[7,8] which has complicated the analysis of this material. In contrast, the $La_{2-x}Sr_xCuO_4$ (LSCO) system, which contains only single $CuO_2$ layers, has been studied in most cases in sintered polycrystalline samples.[9–15] Because the LSCO materials are strongly anisotropic, it is difficult to determine the intrinsic nature of the $CuO_2$ layers from measurements of polycrystalline samples. A few optical measurements, mostly restricted to room temperature, on LSCO single crystals or thin films have been made,[16–21] but we are not aware of a systematic temperature-dependent optical study on the oriented samples of this material.

It is widely believed that the electron-phonon interaction plays a minor role in the superconductivity for YBCO materials. However, a significant isotope shift ($\alpha \simeq 0.2$) due to partial substitute of $^{18}O$ for $^{16}O$ in $La_{1.85}Sr_{0.15}CuO_4$ has been observed and interpreted as evidence for strong electron-phonon coupling.[22,23] This implies that phonons may still play an important role, if not a key role, in the pairing mechanism. On the other hand, the observed linear behavior of the dc resistivity for LSCO up to 1100 K implies a weak electron-phonon coupling for the free carriers.[24]

A lot of effort has been made in recent years to study the non-Drude response in the midinfrared (MIR) region and to discover the superconducting energy gap. It has been observed that the MIR absorption is absent in the undoped parent compounds such as $La_2CuO_4$ and $YBa_2Cu_3O_6$. For $La_{2-x}Sr_xCuO_4$, Uchida *et al.*[21] have reported that the MIR absorption band develops with increasing dopant concentration and then exhibits a saturation in the higher compositional range $0.1 \le x \le 0.25$. Similar effects are observed in doping of *n*-type $Pr_{2-x}Ce_xCuO_4$ by Cooper *et al.*[25] As a consequence of the redistribution of the O $2p$ and Cu $3d$ orbitals upon doping, spectral weight is rapidly transferred from the in-plane O $2p \rightarrow$ Cu $3d$ charge-transfer (CT) excitations above 2 eV to the free-carrier absorption (Drude band) and the low-energy excitations (MIR band) below 1.5 eV. Therefore, both the Drude and MIR absorptions in HTSC appear to be related to the introduction of holes on the $CuO_2$ layers (or CuO chains) by doping. For LSCO, the CT gap becomes weaker or fills in and the phonons are obscured as holes are added upon substituting $Sr^{2+}$ for $La^{3+}$. In contrast to these changes, the plasma minimum in the reflectance is pinned at 0.9 eV and insensitive to the dopant concentration.[14,15,26,27]

Although there is fairly good agreement among various groups for the optical conductivity of the high-$T_c$ copper oxides, the interpretation of these results still remains controversial. In no case can the normal-state infrared

 ©1993 The American Physical Society

conductivity be described by a simple Drude model. In many studies,[3-5,28-33] this non-Drude conductivity has been described by a two-component approach: a narrow, strongly temperature-dependent Drude absorption centered at the origin and a broad, nearly temperature-independent midinfrared band. The Drude absorption is due to the free carriers which are responsible for the dc transport and which condense into a superfluid below $T_c$ whereas the MIR absorption is due to the bound carriers which have a semiconductorlike gap. An alternative is a single-component approach: all of the infrared absorption is due to one type of carrier, with a strong frequency dependence in the scattering rate and effective mass. This approach also leads to a broad range of optically inactive excitations in the midinfrared region, and has been described in the framework of the "marginal Fermi liquid"[34] (MFL) and "nested Fermi liquid" (NFL).[35]

In this paper, we present the in-plane spectra of reflectance $\mathcal{R}(\omega,T)$ and conductivity $\sigma(\omega,T)$ of a high-quality $La_{2-x}Sr_xCuO_4$ film over a wide frequency range of 30–40 000 $cm^{-1}$ (4 meV–5 eV) and for temperatures between 5 and 350 K. We make an extensive optical study on the infrared dynamics of the film. In Sec. II, the sample preparation and the characteristic transport properties are discussed. We also describe in detail the optical measurement technique and discuss the uncertainties in the Kramers-Kronig (KK) analysis. Section III presents the spectra of reflectance and other optical functions derived from the KK analysis. Details of the infrared phonons and optical conductivity $\sigma(\omega)$ in the normal and superconducting states are discussed. Comparisons of the normal-state data to both two- and one-compound descriptions of the optical dielectric function are also made in Sec. III. Finally, the conclusions are summarized in Sec. IV.

## II. EXPERIMENT

### A. Sample characteristics

$La_{2-x}Sr_xCuO_4$ films were prepared by off-axis dc magnetron sputtering. Details of sample preparation and dc transport properties have been described previously.[36] Films were grown on $SrTiO_3$ or $LaAlO_3$ substrates. Both kinds of substrates have a perovskite structure which enables a good lattice match with the films. Parameters of the samples are summarized in Table I. Thinner films (270 nm thickness) were transparent enough that some features of the substrate could be seen in the reflectance spectra. Consequently, the work described here will focus on an especially thick film with thickness greater than the electromagnetic penetration depth ($d > \delta$) to avoid the substrate complications. This film, grown on the (100) face of a $SrTiO_3$ substrate, has dimensions of 10 mm×10 mm×820 nm. Figure 1 shows an x-ray-diffraction pattern for a film grown at the same time as the film used for infrared measurements, showing that it is highly *ab*-plane oriented. In addition to its *c*-axis texture, the film is epitaxial. That is, the [100] and [010] directions, which lie in the plane of the film, are parallel to the [100] and [010] directions in the substrate. The *ab*-plane dc resistivity, shown in Fig. 2, displays a sharp

TABLE I. $La_{2-x}Sr_xCuO_4$ thin-film characteristics.

| Sample no. | Thickness (nm) | Area ($mm^2$) | $x$ | $T_c$ (K) | $\Delta T_c$ (K) | Substrate |
|---|---|---|---|---|---|---|
| 1,2 | 270 | 6.3×6.3 | 0.15 | 27 | 1.5 | $LaAlO_3$ |
| 3 | 820 | 10×10 | 0.17 | 31 | 1.5 | $SrTiO_3$ |

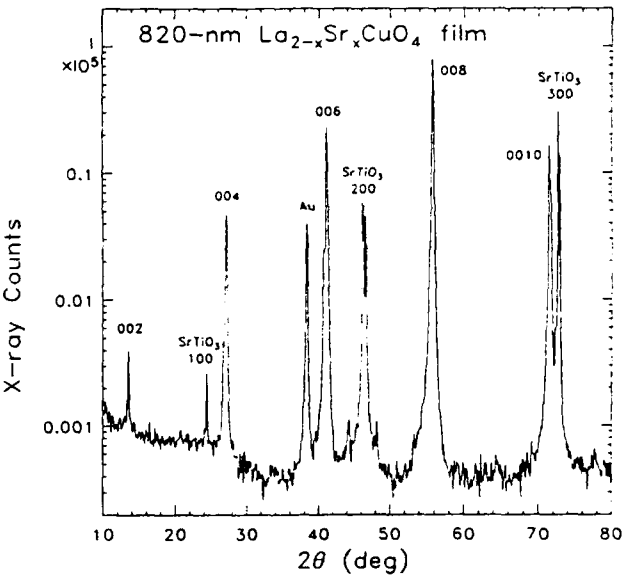


FIG. 1. X-ray-diffraction pattern for a $La_{2-x}Sr_xCuO_4$ thin film grown at the same time as the one used this work. The film was grown on a $SrTiO_3$ substrate, and the growth orientation can be seen in this figure.

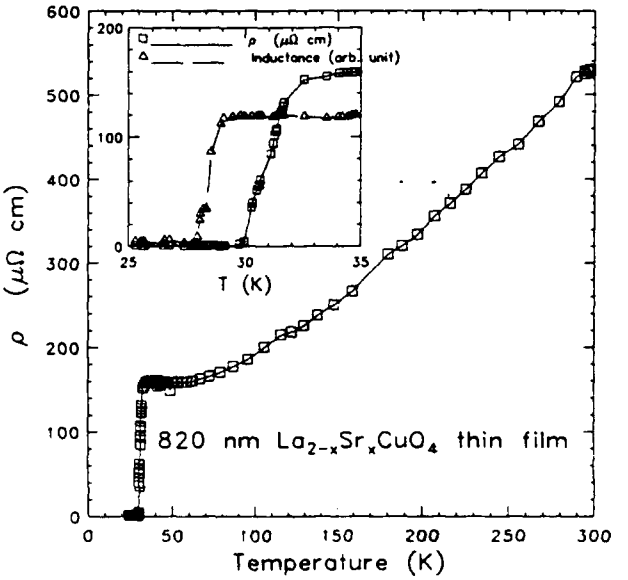


FIG. 2. Resistivity in the *ab* plane, as a function of temperature, for the same $La_{2-x}Sr_xCuO_4$ film ($x \sim 0.17$) as shown in Fig. 1. The inset shows an expanded view of the region near $T_c$ for the same sample and compares the resistive transition to the inductive transition. The lines connecting points are guides to the eye.

superconducting transition near $T_c = 31$ K with a transition width $\Delta T_c \simeq 1.5$ K. The normal-state resistivity is roughly linear in temperature with a nearly zero intercept, i.e., of the form of $\rho(T) = \rho_0 + \alpha T$ ($\alpha \sim 1.2$ $\mu\Omega$ cm/K). Deviations from this behavior are evident in the plateau below $\sim 100$ K. The inset in Fig. 2 shows that the inductive transition, as measured by the change of inductance of a coil placed against the film, is at approximately 2-K lower temperature than the resistive transition and has about the same transition width. The composition of the film is at an optimum value ($x \sim 0.17$) for the superconductivity. The resistivity is consistent with the published reports of good quality LSCO crystals.[20,21]

### B. Infrared measurements and uncertainties

The reflectance measurements were performed using two spectrometers with a variety of light sources, beamsplitters, and detectors for different overlapping frequency ranges. The angle of incidence of the incident light was about 11° from the surface normal, so that the electric field of the infrared radiation was dominantly parallel to the *ab* plane. Reflectance spectra in the far- and midinfrared range 30–4000 $cm^{-1}$ (4–500 meV) were measured using a Bruker 113 v fast scanning Fourier transform interferometer with a 4.2-K bolometer detector (30–600 $cm^{-1}$) and a B-doped Si photoconductor (450–4000 $cm^{-1}$). At higher frequencies of 1000–40 000 $cm^{-1}$ (0.125–5 eV), the reflectance was measured with a Perkin Elmer 16U grating monochromator. The reflectance was calibrated with a reference mirror of 2000-Å-thick aluminum evaporated on an optically polished glass substrate. The sample and Al mirror reference were mounted on a helium-cooled cold tip, along with a silicon thermometer and a resistance heater, to allow the temperature to be varied from 5 to 350 K. The sample and reference could be exchanged by rotating the cryostat.

As the overall scale of the reflectance is very crucial to the analysis of HTSC, we carefully tested the stability and measured the absolute reflectance at each temperature. Thermal contraction of the sample holder and position variation between the sample and reference were also compensated for. In order to study the temperature dependence of the midinfrared band and the plasma edge, we measured the reflectance at each temperature up to 4000 $cm^{-1}$ (0.5 eV), and at selected temperatures up to 40 000 $cm^{-1}$ (5 eV). The coincidence of spectra in each of the overlap frequency range was usually within 0.5%. As the film thickness (820 nm) was much greater than the penetration-skin depth ($\sim 250$ nm), features attributable to the $SrTiO_3$ substrate effect were not detected. Because the sample surface was extremely smooth and shiny, specular reflection was assumed and there was no need to coat the sample with a metal film to correct for diffuse scattering losses. Also, the large sample area ($1 \times 1$ $cm^2$) enabled us to obtain a high signal-to-noise ratio, making it unnecessary to smooth the data for analysis.

The experimental uncertainty in our reflectance measurements is estimated to be $\pm 0.5\%$. This error arises mainly from the difficulty in establishing precise optical alignment as the reference and the sample are interchanged, and partly from the slight temperature dependence of the Al reflectance at low frequencies. This small uncertainty in $\mathcal{R}(\omega)$, however, will cause a larger propagated error at low frequencies in the optical conductivity $\sigma(\omega)$ generated by the Kramers-Kronig transformation.

### C. Kramers-Kronig analysis

After obtaining satisfactory results for a wide range of reflectance spectra $\mathcal{R}(\omega)$, we have confidence in using the Kramers-Kronig transform to determine the real part of the optical conductivity $\sigma_1(\omega)$, a more fundamental quantity than $\mathcal{R}(\omega)$ for describing particle-hole excitations of a material by the absorption of photons of energy $\hbar\omega$. In principle, the KK integral requires a knowledge of $\mathcal{R}(\omega)$ at all frequencies.[37] Thus, reasonable and careful extrapolations of the reflectance beyond the measured range must be made.

#### *1. High-frequency extrapolation*

The high-frequency extrapolation usually has significant influence on the results, primarily on the sum rule derived from the optical conductivity. This effect has been reduced by merging our data to the reflectance spectra of Tajima *et al.*,[19] which extend up to 37 eV (300 000 $cm^{-1}$). We find their spectra are in excellent agreement (within $\pm 0.8\%$ in absolute reflectance) with our high-frequency data at room temperature.

After careful measurements, however, we observe a significant decrease in the overall level of $\mathcal{R}(\omega)$ at frequencies above the plasma edge ($\sim 7000$ $cm^{-1}$) as the temperature is lowered below 250 K. This decrease persists up to 40 000 $cm^{-1}$, the upper limit of our experimental data, the reflectance at 250 K being about 80% of that at room temperature in this frequency region. However, as the temperature is further decreased below 250 K, aside from the steepening of the plasma edge, there is very little temperature dependence down to 5 K in this high-frequency region as shown in Fig. 3. We have carefully repeated the measurements several times and found this behavior reproducible in both the cooling and warming process. At the same time, we have observed no change at all temperatures in the signal level reflected from the Al reference which has been mounted near the sample. In addition, the reflectance remains unchanged as the sample is heated up from 300 to 350 K. These tests have convinced us that the extraneous influence such as thermal expansion-contraction of the sample holder or condensation of water on the sample can be ruled out. We therefore have readjusted the high-frequency room-temperature reflectivity given by Tajima *et al.*[19] with a factor of 5% increase in the range 5–8 eV, but no change above this range, before appending it to our data for temperatures below 250 K. After doing so, we have assumed $\mathcal{R}(\omega) \sim \omega^{-4}$, a free-electron asymptotic behavior, above 37 eV. These changes preserve the sum rule at 20 eV.

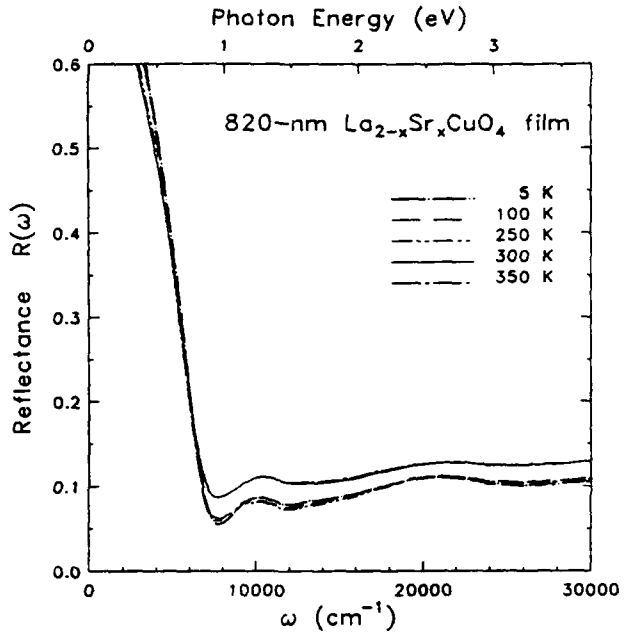


FIG. 3. Temperature dependence of the reflectance in the interband region. There is a remarkable change in $\mathcal{R}(\omega)$ between 300 and 250 K but no appreciable change above or below this temperature range.

### 2. *Low-frequency extrapolation*

The low-frequency extrapolation is equally important. We find that using the Hagen-Rubens relation, $\mathcal{R}(\omega)=1-A\sqrt{\omega}$, for the normal state leads to a slightly depressed conductivity near the low-frequency end followed by a sharp rise towards zero frequency. This distortion may affect the estimate of the dc conductivity and also of the sum rule, from which we want to find the superconducting condensate by calculating the missing area below $T_c$. Since the Hagen-Rubens relation, a good approximation for ordinary metals, seems not appropriate for the HTSC because of the presence of phonons and of low-frequency (midinfrared) absorption processes, we make a least-squares fit to the optical conductivity, $\sigma_1(\omega)$, derived from the initial KK transform of $\mathcal{R}(\omega)$ using a two-component dielectric function (Drude plus midinfrared and phonon oscillations):

$$\epsilon(\omega)=-\frac{\omega_{pD}^2}{\omega^2+i\omega/\tau}+\sum_{j=1}^{N}\frac{\omega_{pj}^2}{\omega_j^2-\omega^2-i\omega\gamma_j}+\epsilon_\infty, \quad (1)$$

where the first term is a Drude oscillator described by a plasma frequency $\omega_{pD}$ and a relaxation time $\tau$ of the free carriers; the second term is a sum of oscillators for midinfrared and phonon absorptions with $\omega_j$, $\omega_{pj}$, and $\gamma_j$ being the resonant frequency, strength, and width of the $j$th Lorentz oscillator; and the last term $\epsilon_\infty$ is the high-frequency limit of $\epsilon(\omega)$. This last parameter is found from a fit to $\mathcal{R}(\omega)$.

Using the fit parameters, we recalculate the low-frequency reflectance for the normal state. Then, after extending the experimental $\mathcal{R}(\omega)$ with this calculated reflectance, a second KK transform is made. The results of this "second" $\sigma_1(\omega)$ give a more reasonable low-frequency behavior. In the superconducting state, we have used the formula $\mathcal{R}=1-B\omega^4$, as the way that $\mathcal{R}$ goes to unity. For temperatures well below $T_c$, the low-frequency reflectance is nearly constant, with some noise fluctuations around unity. We have set $\mathcal{R}\equiv 1$ in this region for the KK transformation. As mentioned earlier, the experimental uncertainty in $\mathcal{R}(\omega)$ is about $\Delta\mathcal{R}=\pm 0.5\%$. As $\mathcal{R}(\omega)\rightarrow 1$ at low $\omega$ and low $T$, the KK transform will give propagated error in $\sigma_1(\omega)$—primarily coming from the propagated error in the real index of refraction $n(\omega)$—roughly equal to $\Delta\sigma_1/\sigma_1=[1/(1-\mathcal{R})](\Delta\mathcal{R}/\mathcal{R})$, i.e., the percentage uncertainty in $\sigma_1$ is about $1/(1-\mathcal{R})$ times higher than that in $\mathcal{R}$. We will address this issue later.

## III. RESULTS AND DISCUSSION

### A. Infrared phonons

Figure 3 shows the measured *ab*-plane reflectance $\mathcal{R}(\omega,T)$ of a $La_{2-x}Sr_xCuO_4$ thin film on a linear scale. The low-frequency behavior is shown in Fig. 4 at several temperatures. The inset, which is plotted on a logarithmic frequency scale for the entire measured frequency range at three typical temperatures, illustrates the strongly damped plasma edge around 0.8 eV (6000 $cm^{-1}$) and the interband features around the visible region. As we can see from Fig. 4, $\mathcal{R}(\omega,T)$ increases over a broad frequency range with decreasing temperature, as expected. A few infrared-active phonons in the *ab*-plane are visible. These phonons are more obvious in the spectrum than in the case of YBCO.[3-5,31-33] This indicates that the LSCO crystal has a lower free-carrier concentration and

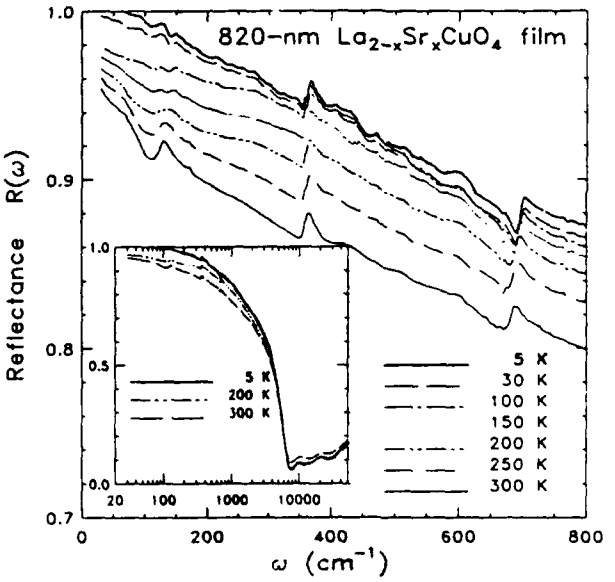


FIG. 4. Measured reflectance $\mathcal{R}(\omega)$ at selected temperatures between 5 and 300 K. The inset shows the same data over the entire measured frequency range (note the logarithmic frequency scale).

a higher vibrational oscillator strength. The phonon parameters can also be extracted from $\sigma_1(\omega)$, the real part of the optical conductivity, shown in Fig. 5. Of the seven IR-active phonon modes ($3A_{2u}+4E_u$) expected at the $\Gamma$ point for the body-centered tetragonal $D_{4h}^{17}$-$I4/mmm$ symmetry, three distinct $ab$-plane $E_u$ modes are observed at 126, 359, and 681 $cm^{-1}$ for $T=300$ K. These eigenenergies are close to those previously reported by Collins *et al.*,[18] 132, 358, and 667 $cm^{-1}$, from a room-temperature reflectance study of a LSCO single crystal. These three phonons have been assigned as external, bending, and stretching modes, respectively.[38,39] More details regarding the phonon mode assignment have been reported in Ref. 40.

### 1. Structural phase transition

We note that the lowest phonon mode at $\omega=126$ $cm^{-1}$, corresponding to an in-plane translational vibration of the La atoms against the $CuO_6$ octahedron unit, broadens and splits into two distinct modes as $T$ decreases below 250 K. The splitting begins at the tetragonal-to-orthorhombic structural transition which involves a staggered rotation of $CuO_6$ octahedron. At 200 K, the degeneracy of the two modes is lifted but their energies are so close that they can barely be resolved. The splitting develops upon further cooling as depicted in Fig. 6. Similar results in neutron-scattering measurements have been reported and associated with a soft phonon mode.[41] For comparison, the inset in Fig. 6 shows the results of Keane *et al.*[42] for the in-plane lattice constants of a $La_{1.85}Sr_{0.15}CuO_4$ sample as a function of temperature. The structural distortion is evident in their data at $T \lesssim 200$ K.

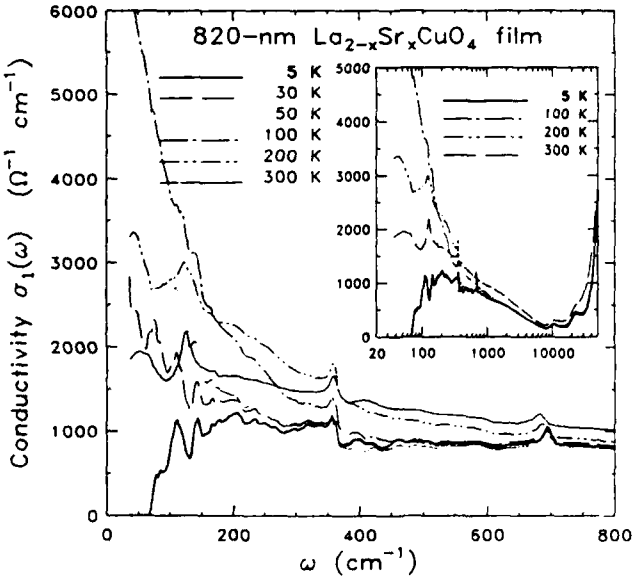


FIG. 5. The real part of the $ab$-plane conductivity $\sigma_1(\omega)$ derived from the Kramers-Kronig transformation of the reflectance data in Fig. 4. The inset shows the entire measured frequency range.

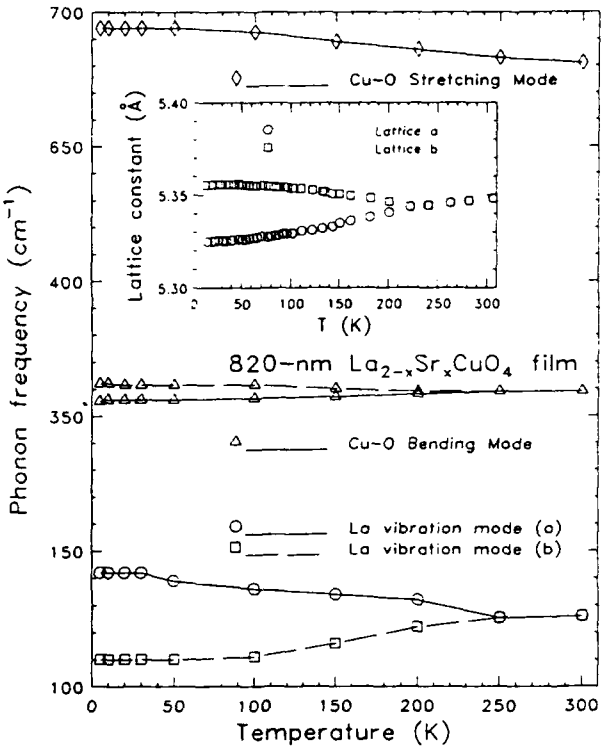


FIG. 6. The in-plane phonon frequency as a function of temperature (the lines are guides to the eye). For comparison, the inset shows the results of Keane *et al.* for the $T$-dependent $ab$-plane lattice constants of $La_{1.85}Sr_{0.15}CuO_4$ (Ref. 42).

### 2. Frequency shift and lifetime

We also observe that the Cu-O stretching mode at 681 $cm^{-1}$ hardens by 13 $cm^{-1}$ as the sample cools from 300 to 100 K, as expected for thermal contraction. It stops shifting, however, upon further cooling. In contrast, the frequency of the Cu-O bending mode at 359 $cm^{-1}$ remains constant at all temperatures yet exhibits a discernible splitting at low $T$. We thus conclude that the stretching mode is much more sensitive to the Cu-O bond length than the bending mode. Tajima *et al.*[38] have recently found a similar result when they measured the room-temperature phonon frequencies of different cuprates with different lattice constants $a$ but almost the same reduced mass by substituting the La atom by other rare-earth elements. A similar effect has also been observed in the $T'$-$RE_2CuO_4$ system by Herr *et al.*[43] In our case the absence of further hardening at lower temperatures is probably due to the fact that the real part of the phonon self-energy $\Sigma_{ph}=\Delta+i\Gamma$ has three contributions:

$$\Delta(T)=\Delta^{(0)}(T)+\Delta^{(1)}(T)+\Delta^{(2)}(T)\ , \tag{2}$$

where $\Delta^{(0)}$ accounts for thermal expansion, $\Delta^{(1)}$ and $\Delta^{(2)}$ for the cubic and quartic anharmonic terms in the lattice potential, respectively. These contributions are generally of the same order of magnitude but may have different signs. Thus, $\Delta^{(0)}$ may be compensated by the sum of $\Delta^{(1)}+\Delta^{(2)}$ at low temperatures. Another possibility is the saturation of the $T$ dependence of all three contributions

below 100 K. Such an effect has been found in silver and thallium halides.[44] Indeed, Tranquada, Heald, and Moodeneabaugh[45] and Keane *et al.*[42] have observed that the interatomic distances of $La_{2-x}Sr_xCuO_4$ saturate below 100 K.

It has been reported[46,47] that the two lower-lying IR-active phonons at 149 and 190 $cm^{-1}$ for $YBa_2Cu_3O_7$ ceramic samples narrow dramatically but have no softening upon entering into superconducting state. In contrast, the phonons above 275 $cm^{-1}$ exhibit the opposite behavior (i.e., little change in width but apparent softening below $T_c$). The anomalous, dramatic narrowing in phonon widths for $YBa_2Cu_3O_{7-\delta}$ has been attributed to the disappearance of interaction between electrons and phonons with energies less than the superconducting gap when the electrons condense into Cooper pairs below $T_c$.[3] The phonon lifetime will increase as a result of decreased probability of colliding with quasiparticles, because the number of quasiparticle excitations decreases rapidly below $T_c$. The frequency shift has been explained within the framework of conventional strong-coupling theory.[48] It is interesting that such a narrowing effect observed in YBCO ceramic samples has not been seen in single crystals.[49,50] Note in both cases the observed phonons are the *c*-axis modes, because the *ab*-plane phonon modes are screened by the strong plasmon background. The difference between these two cases may be attributed to the fact that $YBa_2Cu_3O_7$ is insulating along the *c* direction hence the *c*-axis modes in the oriented samples do not sense the change when the free carriers condense into the superfluid, whereas the same *c*-axis phonons in the randomly oriented samples may be affected by the *ab*-plane carriers due to intergrain hopping. In any event, we do not see a dramatic $T$ dependence in the observed *ab*-plane phonons for $La_{2-x}Sr_xCuO_4$, perhaps because the lowest phonon mode at 126 $cm^{-1}$ is far above the BCS gap energy, which would be $\sim 80$ $cm^{-1}$ for a $T_c = 31$-K sample.

### B. Two-component approach

Returning to the conductivity spectra shown in Fig. 5, we note that the normal state $\sigma_1(\omega,T)$ at the low-frequency limit is nearly equal to the dc conductivity and exhibits a Drude response. A definite loss of spectral weight can be seen at 30 K for $\omega < 150$ $cm^{-1}$, implying a shift of weight to the origin accompanying the superconducting condensation. At $T \ll T_c$, the inductive current, governed by the imaginary part of the complex conductivity $\sigma_2$, is dominant for $\omega < 150$ $cm^{-1}$. It diverges as $\omega \to 0$, showing an $A/\omega$ dependence as demonstrated in Fig. 7. The constant $A$ is associated with the strength of the superconducting condensate and the London penetration depth. However, when $\omega > 150$ $cm^{-1}$, $\sigma_2$ falls off slowly, deviating significantly from a $1/\omega$ dependence. Above $T_c$, $\sigma_2$ changes slope at low frequencies and extrapolates to the origin; the maximum moves to higher frequency and decreases with increasing temperature, as expected.

In contrast to the simple free-carrier response, at $\omega > 300$ $cm^{-1}$, the normal-state $\sigma_1(\omega)$ in Fig. 5 decays much more slowly than the $\omega^{-2}$ dependence that one expects in a Drude model. Additionally, $\sigma_1(\omega)$ has much weaker temperature dependence at high frequencies than at low frequencies. This "non-Drude" behavior, which is universal for all copper oxide superconductors,[3-6,28-33,51-53] can be described in a two-component picture, in which a narrow (with a width of order $k_BT$) and strongly $T$-dependent free carrier (Drude) absorption peaked at $\omega = 0$ combines with a broad bound-carrier (MIR) absorption centered at higher frequencies. According to this picture, the cuprates are viewed as consisting of two types of carriers: free carriers which track the dc conductivity above $T_c$ and which condense to superconducting pairs below $T_c$, and bound carriers which are responsible for the broad MIR excitation. The dielectric function is made up of four parts:

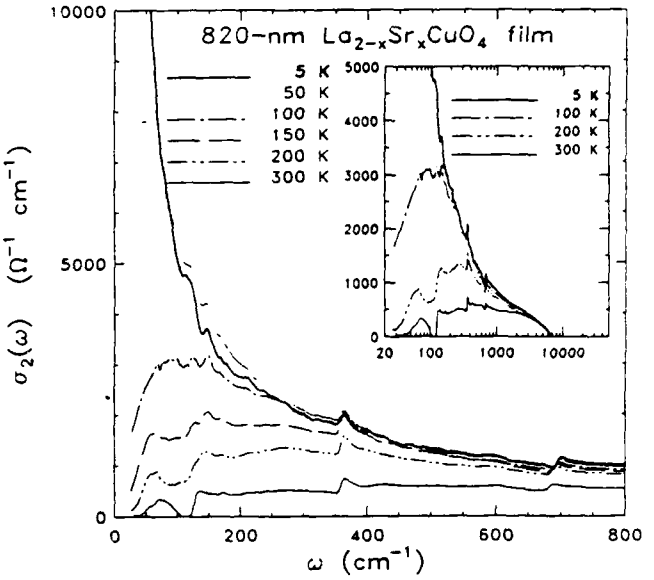


FIG. 7. The imaginary part of the conductivity, $\sigma_2(\omega)$, showing the inductive response. The inset plots the same data in the entire measured frequency range.

$$\epsilon(\omega) = \epsilon_D + \epsilon_{\text{MIR}} + \epsilon_{\text{phonon}} + \epsilon_\infty , \tag{3}$$

where $\epsilon_D$ is the free carrier or normal Drude interband contribution; $\epsilon_{\text{MIR}}$ is the bound-carrier contribution; $\epsilon_{\text{phonon}}$ is the phonon contributions, a sum of harmonic oscillators; and $\epsilon_\infty$ is the high-frequency contribution.

To decompose the total conductivity into two components, we can assume that the conductivity at 5 K, $\sigma_1(\omega, 5\text{ K})$, is a good first approximation of $\sigma_{1\text{MIR}}$, namely, $\sigma^{(1)}_{1\text{MIR}} = \sigma_1(\omega, 5\text{ K})$, for the Drude part is presumed to have collapsed to a $\delta(\omega)$ function. Thus, the Drude conductivity at higher temperatures can be initially estimated by subtracting $\sigma_1(\omega, 5\text{ K})$ from the experimental $\sigma_1(\omega,T)$, namely, $\sigma^{(1)}_{1D} = \sigma_1 - \sigma^{(1)}_{1\text{MIR}}$. Here the superscripts denote the number of iterations. Since

$$\sigma_{1D} = \frac{1}{4\pi} \frac{\omega_{pD}^2 \tau}{1 + \omega^2 \tau^2} , \tag{4}$$

we can determine $\omega_{pD}$ and $1/\tau$ from a linear fit to $1/\sigma^{(1)}_{1D}$

vs $\omega^2$. Once $\omega_{pD}$ and $1/\tau$ are determined from the slope and the intercept of this straight line, we can again estimate the midinfrared conductivity from the difference between a calculated Drude conductivity and the measured conductivity, namely, $\sigma_{1\text{MIR}}^{(2)}=\sigma_1-\sigma_{1D}$, where $\sigma_{1D}$ is *calculated* according to Eq. (4). By averaging $\sigma_{1\text{MIR}}^{(2)}$ at temperatures above $T_c$, we find the average $\langle\sigma_{1\text{MIR}}^{(2)}\rangle\approx\sigma_{1\text{MIR}}^{(1)}$ [or $\sigma_1(\omega, 5\text{ K})$], but there are noticeable differences. Therefore, we repeat the above procedure with $\sigma_{1\text{MIR}}^{(2)}$ replacing $\sigma_{1\text{MIR}}^{(1)}$, and find convergence after a few iterations.

### 1. *The free-carrier component: $\omega_{pD}$ and $\tau$*

Figure 8 illustrates the comparison between the free-carrier contribution, $\sigma_1-\langle\sigma_{1\text{MIR}}\rangle$, and the calculated Drude conductivity. This figure shows that the conductivity is in good agreement with the ordinary Drude behavior after the MIR component is subtracted. The Drude plasma frequency, $\omega_{pD}=6300\pm100$ cm$^{-1}$, obtained from the above analysis, is essentially $T$ independent, whereas $1/\tau$ is linear in $T$. Writing $\hbar/\tau=2\pi\lambda k_B T$, we obtain a weak-coupling value for the coupling constant, $\lambda=0.25$. This small value of $\lambda$ is consistent with the observed absence of saturation up to 1100 K for the dc resistivity.[24] Taking the Fermi velocity in the basal plane to be $v_F=2.2\times10^7$ cm/s, as calculated by Allen, Pickett, and Krakauer[54] for $La_{1.85}Sr_{0.15}CuO_4$, and using our relaxation rate we can estimate the mean free path to be

$$l=v_F\tau\approx(110\text{ Å})\frac{100\text{ K}}{T}\ . \tag{5}$$

At $T=1000$ K, $l\sim11$ Å, which is still longer than the interatomic spacing $a$ (here taken to be 3.8 Å, the in-plane lattice constant). The resistivity is expected to saturate if $l\lesssim a$, because the mean free path can no longer be properly defined in this region.[55] On the other hand, at a temperature close to $T_c$, the mean free path $l$ [e.g., $l_{50\text{ K}}\sim220$ Å according to Eq. (5)] is much longer than the coherence length $\xi$ ($\sim10$ Å). It is this case that places the HTSC in the "clean limit," which, in turn, gives a significant impact on the observability of the superconducting gap.

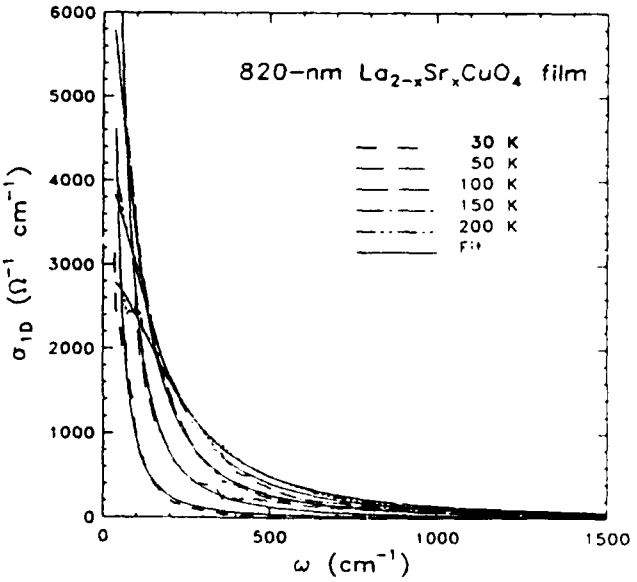


FIG. 8. The Drude conductivity, obtained by subtracting the averaged midinfrared contribution from the total conductivity. The solid curves are Drude fits to the data.

Figure 9 depicts the temperature dependence of $1/\tau$ in comparison with $(1/\tau)_{dc}$ calculated from the measured four-probe dc resistivity $\rho_{dc}$ and the value of $\omega_{pD}$ found above,

$$(1/\tau)_{dc}=\frac{\omega_{pD}^2}{4\pi}\rho_{dc}. \tag{6}$$

As seen in Fig. 9, $(1/\tau)_{dc}$ or $\rho_{dc}$ decreases quasilinearly from room temperature followed by a plateau and then a sudden drop as the temperature approaches $T_c$ whereas the far-infrared scattering rate shows a quasilinear $T$ variation followed by a faster-than-linear drop ($1/\tau\sim T^2$) below $T_c$. This is evident when the same data are plotted on a log-log scale, as shown in the inset of Fig. 9. The excellent agreement in both the slopes and overall levels between the dc transport and infrared measurements strengthens our confidence in the determination of the normal-state plasma frequency $\omega_{pD}$ and scattering rate $1/\tau$. The sudden drop in $1/\tau$ just below $T_c$ is interesting and has received considerable attention recently. Such observations on quasiparticle damping have been reported previously for laser-ablated $YBa_2Cu_3O_{7-\delta}$ films[56,33] and a free-standing $Bi_2Sr_2CaCu_2O_8$ crystal.[57,58] Similar

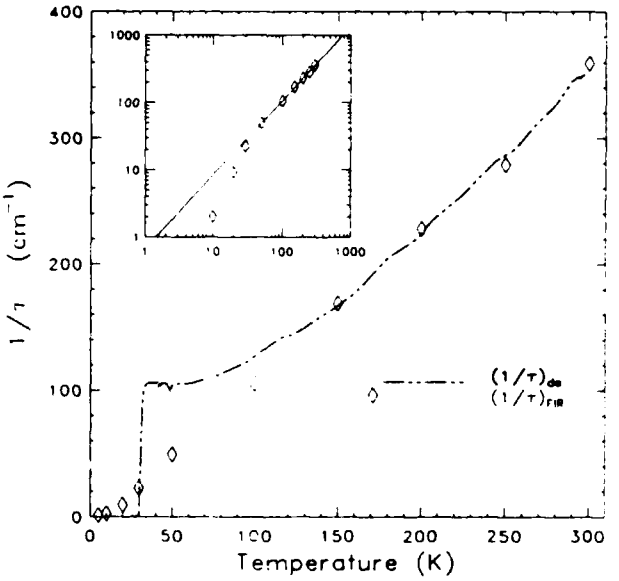


FIG. 9. Drude scattering rate, $1/\tau$, as a function of temperature. For comparison are shown the values obtained from fits to the infrared conductivity (diamond symbols) and the ones estimated from the measured dc resistivity (dashed lines). Note both of these two cases exhibit a small negative intercept due to a slight deviation from $T$ linear dependence. This is illustrated in the inset plotted on a log-log scale. The slope of the solid straight line gives a power of 1.1 instead of 1 to temperature $T$. Below $T_c$, the quasiparticle damping rate has a sudden drop and goes roughly as $1/\tau\sim T^2$.

behavior has also been found for YBCO and BSCCO in femtosecond optical transient absorption experiments.[59] This result may suggest that the excitation that scatters the free carriers is also strongly suppressed below $T_c$, or forms its own gap, as the free carriers condense. Another interpretation is that the number of unoccupied states available near the Fermi levels decreases rapidly as a result of the depression of the density of quasiparticle states near $E_F$ as the gap opens, causing a dramatic decrease in the probability of quasiparticle elastic scattering. Nicol and Carbotte[60] have recently calculated the quasiparticle scattering rate and found such a fast drop within the phenomenological marginal Fermi-liquid model. However, due to the large error bars at low frequencies (below 100 $cm^{-1}$) and the limited number of temperatures below $T_c$ (31 K) in our data, we are unable to observe a "coherence" peak in $\sigma_1(T)$, as has been calculated by Nicol and Carbotte[60] and found in YBCO by Nuss *et al.*,[61] and in BSCCO by Romero *et al.*[58]

### 2. *The midinfrared absorption*

Figure 10 presents the MIR conductivity in the normal and superconducting states. This quantity is obtained by subtracting the calculated free-carrier contribution (shown in Fig. 8 as solid lines) from the total conductivity. Some features that are common at all temperatures include an onset near 80 $cm^{-1}$, a maximum around 250 $cm^{-1}$, a notchlike structure at 400 $cm^{-1}$, and a broad peak around 800 $cm^{-1}$. As we can see, the MIR conductivity $\sigma_{1MIR}(\omega,T)$ has a relatively weak temperature dependence. There do appear to be three distinct temperature regimes: $>250$ K, $T_c-200$ K, and below $T_c$. In each, there is a noticeable conductivity increase in the region of 150–1500 $cm^{-1}$ compared to the higher-temperature regime. The enhancement is more obvious for $T<T_c$ and will be discussed below.

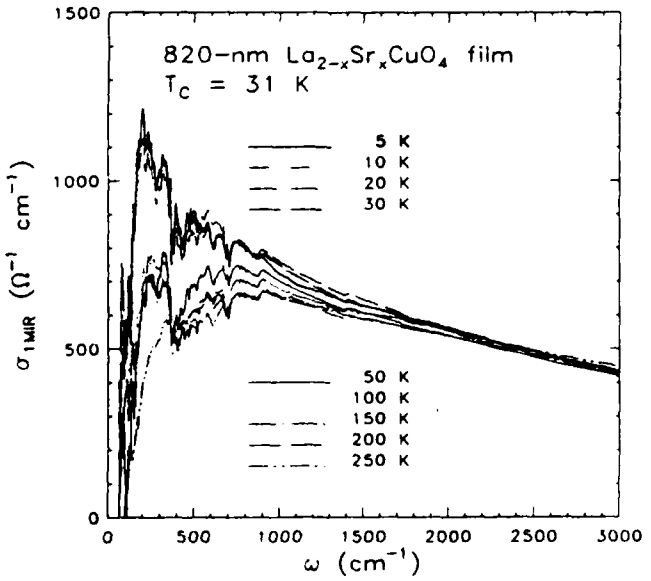


FIG. 10. $\sigma_{1MIR}$, the frequency-dependent conductivity with Drude contribution subtracted. The data fall into three groups, $5-T_c$, $T_c-200$, and $\geq 250$ K.

According to the data in Fig. 10, the "two-feature" structure of an onset near 80 $cm^{-1}$ ($3.7k_BT_c$) and a notch around 400 $cm^{-1}$ ($18k_BT_c$) is present both below and above $T_c$. This structure is shown more clearly in Fig. 11, where we plot the average of the curves above and below $T_c$. Thus, we cannot associate either feature with the superconducting gap, since that presumably would not appear above $T_c$. Furthermore, there is no shift in any feature in the superconducting state as would be expected for a Holstein sideband associated with the condensate. Such features have also been observed[32,57,62] in $YBa_2Cu_3O_{7-\delta}$ and $Bi_2Sr_2CaCu_2O_8$ films. The structure at 400 $cm^{-1}$ (50 meV), which appears common to the cuprate superconductors, has been explained as due to strong bound-carrier–phonon coupling.[63] It cannot be accepted as a superconducting gap for $La_{2-x}Sr_xCuO_4$ simply because its magnitude is too large. The value of the lower-energy onset usually varies for different samples. The presence of this structure above $T_c$ and the lack of evidence of an energy shift with varying temperature below $T_c$ make it difficult to associate it with the BCS gap.

### 3. *Holstein effect*

Lee, Rainer, and Zimmermann[64] have calculated the dynamic conductivity in the framework of strong-coupling theory, including the Holstein mechanism.[65,66] They obtain a two-gap structure in the superconducting state. The first onset is presumed to be the superconducting gap, while the "second gap" is interpreted as the consequence of inelastic scattering with phonons due to the Holstein effect.

To estimate this effect, we have calculated the conductivity according to the Holstein theory for our film and

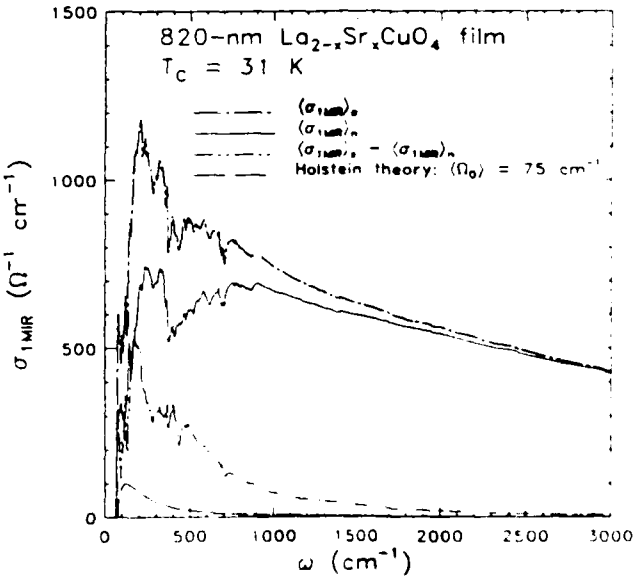


FIG. 11. Averaged midinfrared conductivity in the normal and superconducting states. Also shown is the difference between them. The dash-dotted curve is a calculation within the framework of Holstein theory.

find that the enhancement of the MIR strength below $T_c$ may not be accounted for by the inelastic-scattering contribution. In the Holstein model, the scattering rate at low temperature can be obtained by[66]

$$1/\tau(\omega)=\frac{2\pi}{\omega}\int_0^{\omega}\alpha^2F(\Omega)(\omega-\Omega)d\Omega\ , \tag{7}$$

where $\alpha^2F(\Omega)$ is the Eliashberg function or electron-phonon spectral density. The parameters used in our calculation were $\omega_p=6300\ \mathrm{cm}^{-1}$ (from the two-component model fit outlined above), $\lambda(\omega=0)=0.25$, and the average boson frequency $\Omega_0=75\ \mathrm{cm}^{-1}$. In general, the coupling parameter is given by[66]

$$\lambda(\omega)=-\frac{2}{\omega}\int_0^{\infty}\alpha^2F(\Omega)\left[\ln\left|\frac{\omega-\Omega}{\omega+\Omega}\right|-\frac{\Omega}{\omega}\ln\left|\frac{\omega^2-\Omega^2}{\Omega^2}\right|\right]d\Omega \tag{8}$$

with a zero-frequency limiting value

$$\lambda(\omega\rightarrow 0)=2\int_0^{\infty}\frac{\alpha^2F(\Omega)}{\Omega}d\Omega\ . \tag{9}$$

For simplicity, we have assumed the Eliashberg function has the form (in an Einstein model) $\alpha^2F(\Omega)=A\delta(\Omega-\Omega_0)$, where $A=\frac{1}{2}\lambda\Omega_0$ according to Eq. (9). The calculated result is illustrated as the dash-dotted curve in Fig. 11. The size of the Holstein sideband could be enlarged to match the measured MIR spectral weight by increasing $\lambda$ and $\omega_p$, but this would be in disagreement with the values determined experimentally.

#### 4. *Superconducting-to-normal ratios*

Another unconventional behavior is seen in the superconducting to normal-state conductivity ratio shown in Fig. 12. Ratios of conductivity have been used frequently in the past to suggest superconducting gap structure.[49,52] In Fig. 12, we compare $\sigma_{1s}$ and "$\sigma_{1n}$" at the *same* temperature (we note that if $\sigma_{1s}$ and $\sigma_{1n}$ are compared at *different* temperatures, the result is totally different as shown in the inset, resembling the BCS-like behavior). To estimate $\sigma_{1n}(\omega,T)$ below $T_c$, we presume that the "normal state" $\omega_{pD}$ and $1/\tau$ below $T_c$ follow the "normal" behavior, i.e., $\omega_{pD}$ remains a constant ($6300\ \mathrm{cm}^{-1}$) and $1/\tau$ follows the linear extrapolation of the relaxation rate above $T_c$. Then $\sigma_{1n}$ below $T_c$ can be calculated as the sum of the calculated Drude component and the averaged MIR conductivity $\langle\sigma_{1\mathrm{MIR}}\rangle_n$, namely,

$$\sigma_{1n}=\begin{cases}\text{measured }\sigma_1, & T>T_c\ ,\\ \dfrac{1}{4\pi}\dfrac{\omega_{pD}^2\tau}{1+\omega^2\tau^2}+\langle\sigma_{1\mathrm{MIR}}\rangle_n, & T<T_c\ .\end{cases} \tag{10}$$

As we can see in Fig. 12, the ratio $\sigma_{1s}/\sigma_{1n}$ exhibits a sharp edge near $100\ \mathrm{cm}^{-1}$ and has a peak around $180\ \mathrm{cm}^{-1}$. The peak is suppressed but does not shift as $T$ approaches $T_c$ from below. $\sigma_{1s}$ "overshoots" $\sigma_{1n}$ up to $1000\ \mathrm{cm}^{-1}$ and then gradually joins the normal-state conductivity at higher frequencies. This surprising result can be attributed first to the observed enhancement of the midinfrared conductivity in the superconducting state, and second to the observed faster-than-linear decrease in the quasiparticle scattering rate as demonstrated in Fig. 9.

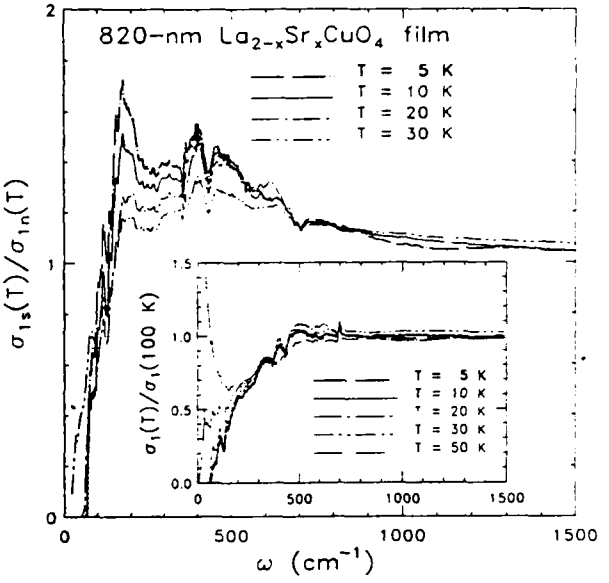


FIG. 12. The ratio of the real part of the conductivity in the superconducting state to an estimated normal-state conductivity at the *same* temperature. For comparison, the inset demonstrates the ratio of the conductivity at a temperature $T$ to that at a *fixed* temperature of 100 K.

#### 5. *Extra spectral weight below $T_c$*

We turn to the differences between the MIR conductivity above and below $T_c$. An enhancement is evident in the raw data of Fig. 5, in which we can see the conductivity at 5 K is higher than that at 50 K, above $T_c$, for $\omega\gtrsim 360\ \mathrm{cm}^{-1}$. By calculating the difference between the averaged midinfrared conductivity in the superconducting state, $\langle\sigma_{1\mathrm{MIR}}\rangle_s$, and the one in the normal state, $\langle\sigma_{1\mathrm{MIR}}\rangle_n$, we find an extra spectral weight below $T_c$ in the MIR region which accounts for roughly 15% of the Drude oscillator strength. This difference is shown in Fig. 11. (Note that the actual fraction may be smaller for the reason of large error bars in $\sigma_1$ at low $\omega$ below $T_c$, as will be discussed below; thus the difference, $\langle\sigma_{1\mathrm{MIR}}\rangle^{bs}-\langle\sigma_{1\mathrm{MIR}}\rangle_n$, may be exaggerated at low frequencies.) This anomalous behavior suggests the existence of another type of excitation visible in the superconducting state, with the normal Drude carriers not completely condensing into the superfluid below $T_c$. However, this argument cannot be taken as rigorous, since our approach of extracting the Drude component has neglected the $\omega$ dependence of the electronic scattering rate, though it may be weak as suggested by the small value of coupling constant $\lambda\sim 0.25$.

To confirm our observation of the extra spectral weight below $T_c$ in the MIR conductivity obtained by the two-component analysis, we use two other independent

methods to estimate the oscillator strength of the superconductor condensate: the dielectric function and the $f$-sum rule. According to the clean-limit picture, when $2\Delta \gg 1/\tau$ the Drude oscillator strength will condense into a $\omega=0$ $\delta$ function for $T \ll T_c$. Thus, the real part of the dielectric function at low frequencies is

$$\epsilon_1(\omega)=\epsilon_{1b}-\frac{\omega_{ps}^2}{\omega^2}\ , \tag{11}$$

where $\omega_{ps}$ is the superconducting plasma frequency defined as $\omega_{ps}=4\pi n_s e^2/m_b$ with $n_s$ being the density of superfluid carriers of mass $m_b$; and $\epsilon_{1b}$ is the bound-carrier contribution to $\epsilon_1(\omega)$, i.e., the low-frequency sum of all finite frequency absorption. In principle, $\epsilon_{1b}$ is $\omega$ dependent. It is constant only at frequencies well below the lowest bound-carrier resonant frequency.

Figure 13 shows the plot of $\epsilon_1(\omega)$ [obtained from KK transform of $\mathcal{R}(\omega)$] against $\omega^{-2}$. The data fall on a straight line, as predicted by Eq. (11), in the low-frequency range. The slope obtained from a linear regression fit at $T=5$ K gives $\omega_{ps}\approx 5800\pm 100$ cm$^{-1}$, from which the London penetration depth can be estimated to be $\lambda_L=1/2\pi\omega_{ps}=275\pm 5$ nm. This value, which is much less than the film thickness (820 nm), is comparable to the 250 nm in-plane $\lambda_L$ found by muon-spin-relaxation ($\mu$SR) measurements[67] for $La_{1.85}Sr_{0.15}CuO_4$ at $T=6$ K. We note that only a fraction $f_s=\omega_{ps}^2/\omega_{pD}\approx 85\%$ of the free carriers condense into the superfluid, in agreement with the observation that $\sim 15\%$ of the Drude spectral weight has shifted to the MIR region below $T_c$ as outlined above. Further evidence that supports this argument is obtained from the $f$-sum rule that will be discussed next.

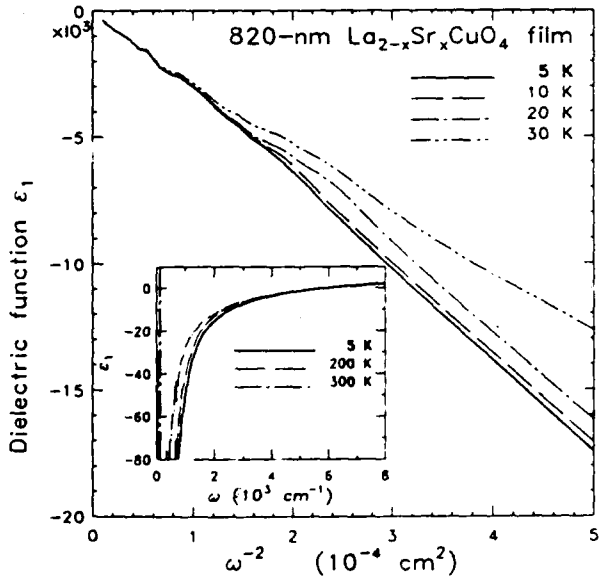


FIG. 13. Real part of the dielectric function $\epsilon_1$ against $\omega^{-2}$ below $T_c$. The frequency range shown is 45–300 cm$^{-1}$. Inset: $\epsilon_1$ vs $\omega$ at 5, 200, and 300 K, illustrating the $\omega$-dependent metallic response and the zero-crossing near the plasma edge ($\sim 6000$ cm$^{-1}$).

### C. Sum rule: Superconducting condensate

Figure 14 illustrates the spectral weight, $N_{\rm eff}(\omega)m/m_b$, as defined according to

$$N_{\rm eff}(\omega)\frac{m}{m_b}=\frac{2mV_{\rm cell}}{\pi e^2}\int_0^{\omega}\sigma(\omega')d\omega'\ , \tag{12}$$

where $e$ and $m$ are the free-electron charge and mass, respectively. $m_b$ is the averaged high-frequency optical or band mass, and $V_{\rm cell}$ is the volume (95 Å$^3$) of one formula unit. In this expression, $N_{\rm eff}(\omega)$ equals to the effective number of carriers per formula unit participating in optical transition at frequencies below $\omega$.[37] The normal-state $N_{\rm eff}(\omega)$ curves at 10000 cm$^{-1}$ give, if $m_b=m$, roughly 0.18 hole per $CuO_2$ layer, which is a value close to the dopant concentration of our film ($x\sim 0.17$) assuming each Sr atom donates one hole to the $CuO_2$ layer.

In the normal state, the curves exhibit a sharp rise in the far infrared followed by a broad plateau before another rise beginning near 10000 cm$^{-1}$ due to the charge-transfer transition. As the temperature is lowered, spectral weight transfers to lower frequency in response to a decreasing relaxation rate. Below $T_c$, the spectral weight is reduced as expected due to superconducting condensation. From the difference between $N_{\rm eff}(\omega)m/m_b$ for the normal and the superconducting states, the plasma frequency of the superfluid charge carriers [or the missing area in the curve of $\sigma_1(\omega)$] can be estimated. This difference gives $\Delta(N_{\rm eff}m/m_b)=\omega_{ps}^2 mV_{\rm cell}/4\pi e^2$, from

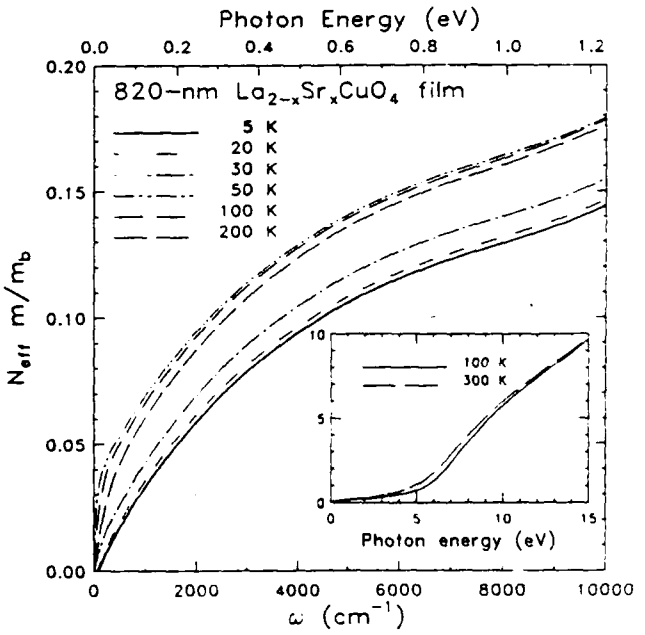


FIG. 14. Effective carrier density per Cu atom, $N_{\rm eff}m/m_b$, as a function of frequency for various temperatures. The data are obtained from the area under the curves of $\sigma_1(\omega)$. The spectral weight of the superfluid condensate can be estimated from the difference of $N_{\rm eff}m/m_b$ in the normal and superconducting states. The inset illustrates the behavior at higher energy for $T=100$ and 300 K where the high-frequency reflectivity data of Tajima *et al.* (Ref. 19) have been utilized.

which we find $\omega_{ps}=5800\ \mathrm{cm}^{-1}$ at 5 K, in excellent agreement with the value determined from the real dielectric function as discussed earlier.

One surprising result of our measurements is that the $N_{\mathrm{eff}}(\omega)m/m_b$ in the charge-transfer region is larger at $T\geq 300$ K than at other temperatures below 250 K, as shown in the inset of Fig. 14. The mechanism that causes this difference is not clear at this moment. One speculation is that the structural transition at around 250 K may change the band structure due to the doubling of the unit cell. The transformation introduces new Brillouin zone planes at which the semiconductorlike gaps are opened, transferring oscillator strength to higher-frequency regions. The band mass may also charge accordingly. Our choice of extrapolation makes this difference disappear above 15 eV, where the $N_{\mathrm{eff}}(\omega)m/m_b$ curves come together. 15 eV is the end point of the interband excitations from the O $2p$ valence bands to the La $5d/4f$ conduction bands above the Fermi level and the starting point of excitations from the Cu $3d$ bands to the La $5d/4f$ bands.

Figure 15 shows the temperature dependence of the Drude ($\omega_{pD}$) and superconducting ($\omega_{ps}$) plasma frequencies. Here $\omega_{pD}$ is determined from the fit to $\sigma_1(\omega)$ as described earlier and is consistent with a picture of constant carrier concentration in the normal state. This magnitude of $\omega_{pD}$ ($\sim$0.8 eV) is smaller in comparison with the values ($\sim$1.2 eV) obtained in YBCO or BiSrCaCuO crystals, presumably indicating lower carrier concentration on the $CuO_2$ planes. Below $T_c$, $\omega_{ps}$ is estimated from the sum rule, the linear fit to $\epsilon_1(\omega)$ vs $\omega^{-2}$, and the least-squares fit to the reflectance data using a two-fluid model. These three approaches give very close results in $\omega_{ps}$ and we take the average value. Shown in the inset is the superfluid electronic density fraction $f_s(T)$. This superconducting condensate is calculated according to

$$f_s(T)=n_s(T)/n=\omega_{ps}^2(T)/\omega_{pD}^2$$

with $\omega_{pD}=6300\ \mathrm{cm}^{-1}$, the normal-state value. This quantity $f_s(T)$ is essentially a measure of the strength of the $\delta$ function in $\sigma_1(\omega,T)$, and is related to the $T$ dependence of the penetration depth $\lambda_L(T)$. The solid curves in Fig. 15 and its inset show the phenomenological behavior predicted by BCS theory according to

$$\frac{f_s(T)}{f_s(0)}=\left[\frac{\Delta(T)}{\Delta(0)}\right]^2, \tag{13}$$

where $\Delta(T)$ is the $T$-dependent BCS order parameter. It gives a nearly constant $\Delta(T)$ at $T\ll T_c$. Near $T_c$, $\Delta(T)$ drops to zero with a $(1-T/T_c)^{1/2}$ dependence. The behavior of $f_s(T)$ in our data agrees with this expression and it demonstrates that the normal carriers condense rapidly into the superfluid below $T_c$, as expected.

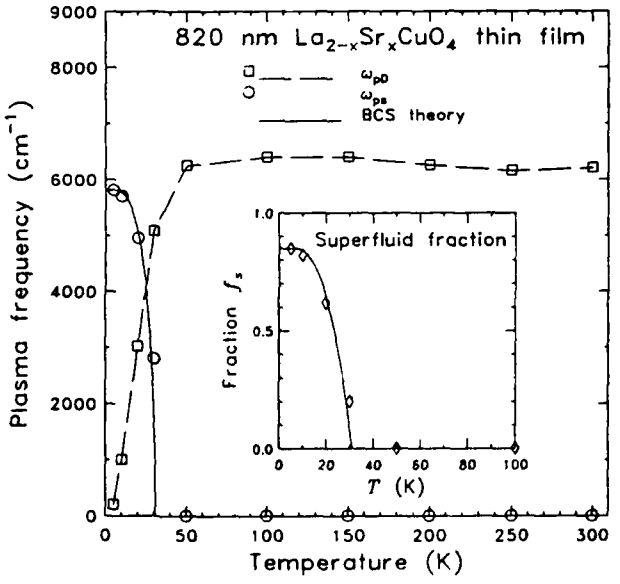


FIG. 15. Temperature dependence of the Drude plasma frequency $\omega_{pD}(T)$, the superconducting plasma frequency $\omega_{ps}(T)$, and the superfluid density $f_s(T)=n_s(T)/n$. The solid lines are calculated in the framework of BCS theory, taking $f_s(0)=0.85$ and $T_c=31$ K.

### D. One-component approach

An alternative approach to analysis of the optical conductivity is the one-component model with a frequency-dependent mass and scattering rate.[53,68–70] In this approach, the infrared absorption is entirely due to free carriers, in which are divided into "coherent" and "incoherent" parts caused by the interaction of the free carriers with some sort of optically inactive excitations (charge or spin fluctuations).[62] This approach has been proposed by Anderson[71] and applied to heavy-fermion superconductors.[72] The normal Drude component is regarded as the coherent part centered at $\omega=0$. The incoherent part occurs at frequencies characteristic of the excitations and shifts away from $\omega=0$ due to interactions with the excitations. In this model, the complex dielectric function is described by a generalized Drude formula:

$$\epsilon(\omega)=\epsilon_h-\frac{\omega_p^2}{\omega[\omega-\Sigma(\omega)]}, \tag{14}$$

where $\epsilon_h$ is the "background" dielectric associated with the high-frequency contributions, $\omega_p$—defined by $4\pi Ne^2/m_b$—is the bare plasma frequency of the free carriers, and $\Sigma(\omega)=\Sigma_1(\omega)+i\Sigma_2(\omega)$ is the self-energy of the carriers.

Because $\epsilon(\omega)$ is causal, $\Sigma_1(\omega)$ and $\Sigma_2(\omega)$ are related by the Kramers-Kronig equations. It is important to stress that the interband contributions, which can be lumped into $\epsilon_h$, are excluded from $\omega_p$ and $\Sigma(\omega)$. To find $\Sigma(\omega)$, knowledge of $\omega_p$ and $\epsilon_h$ is required. In order to identify the interband components, we fit the experimental $\sigma_1(\omega)$ at frequencies higher than 800 $\mathrm{cm}^{-1}$ with Lorentz oscillators to parametrize the interband absorption. By subtracting the contribution due to these interband oscillators from the total conductivity and calculating the area under $\sigma_1(\omega)$, we obtain $\omega_p=13\,000\ \mathrm{cm}^{-1}$, corresponding to a carrier density of $n=1.8\times10^{21}\ \mathrm{cm}^{-3}(m_b/m)$ or 0.17 holes per $CuO_2$ unit if $m_b=m$. As we have found $\omega_{pD}=6300\pm100\ \mathrm{cm}^{-1}$ in the two-component analysis, we

can also estimate the strength of MIR absorption or the "incoherent" component as

$$\omega_{pm}=(\omega_p^2-\omega_{pD}^2)^{1/2}\approx 11\,370\ \text{cm}^{-1}\ .$$

$\epsilon_h$ can be estimated from the interband oscillators. This gives $\epsilon_h\sim 4$ in the far-infrared region; at higher frequencies $\epsilon_h$ becomes complex and $\omega$ dependent.

### 1. *Mass enhancement $m^*/m_b$ and self-energy $\Sigma(\omega)$*

Once $\omega_p$ and $\epsilon_h$ are determined, the self-energy $\Sigma(\omega)$ can be calculated at each frequency from the experimental $\epsilon(\omega)$ according to Eq. (14). If we rewrite Eq. (14) as

$$\epsilon(\omega)=\epsilon_h-\frac{\omega_p^{*2}}{\omega[\omega+i/\tau^*(\omega)]} \tag{15}$$

and compare Eq. (15) with Eq. (14), we can extract the renormalized scattering rate $1/\tau^*(\omega)=-\Sigma_2(\omega)m_b/m^*$, and the effective plasma frequency $\omega_p^*=\omega_p(m_b/m^*)^{1/2}$, where the effective mass enhancement is given by

$$m^*/m_b=1-\Sigma_1/\omega\ . \tag{16}$$

Note both the real and imaginary parts of $\Sigma(\omega)$ are negative definite. The resulting curves of $m^*(\omega)/m_b$ and $\Sigma_2(\omega)$ are shown in Fig. 16. The effective mass $m^*$ is greatly enhanced at low $\omega$ and $m^*\approx m_b$ at high $\omega$, as expected for the MFL and NFL theories.[34,35]

The behavior of $m^*(\omega)/m_b$ and $\Sigma_2(\omega)$ as shown can be viewed as arising from a local Coulomb interaction of carriers with a broad spectrum of other excitations. At low frequencies, the carriers drag a low-energy excitation cloud along with them, causing a mass enhancement. As frequency increases, the scattering rate $1/\tau^*$ increases when the low-lying states are excited; hence, a new *inelastic* scattering occurs. The carrier mass decreases to approach the band mass as $\omega$ increases, for the low-lying excitations cannot follow the rapid carrier motion. We can estimate the characteristic energy range of the low-lying excitations from the frequencies at which $m^*(\omega)$ and $\Sigma_2(\omega)$ change from their low- to high-frequency behaviors. This range appears to be between 300 and 1000 $\text{cm}^{-1}$ (0.04–1.2 eV). We note that a pronounced peak near 0.1 eV reported by Uchida *et al.*[21] is not observed in our spectra of $m^*/m_b$ and $\Sigma_2$. The present values of $\Sigma_2$ are comparable with their result for the unnormalized scattering rate. The mass enhancement here is, however, a factor of 0.15 smaller than their result. The high value of $m^*$ in their data would imply an even stronger coupling between the free carriers and the low-lying excitations, which is difficult to understand. Note that the value of $m^*/m_b$ at low $\omega$ and low $T$ can also be predicted from the conductivity sum rule from Fig. 14 or simply from $\omega_p^2/\omega_{pD}^2\sim 4.2$, which agrees well with the result in Fig. 16. Writing $m^*/m_b=1+\lambda$, we find the low-frequency limit value of coupling constant $\lambda\approx 3$ at low temperatures, suggesting strong interaction of carriers with a spectrum of other excitations. One major difficulty with this model is that this large $\lambda$ would give a high $T_c$, inconsistent with the actually measured $T_c$ value.

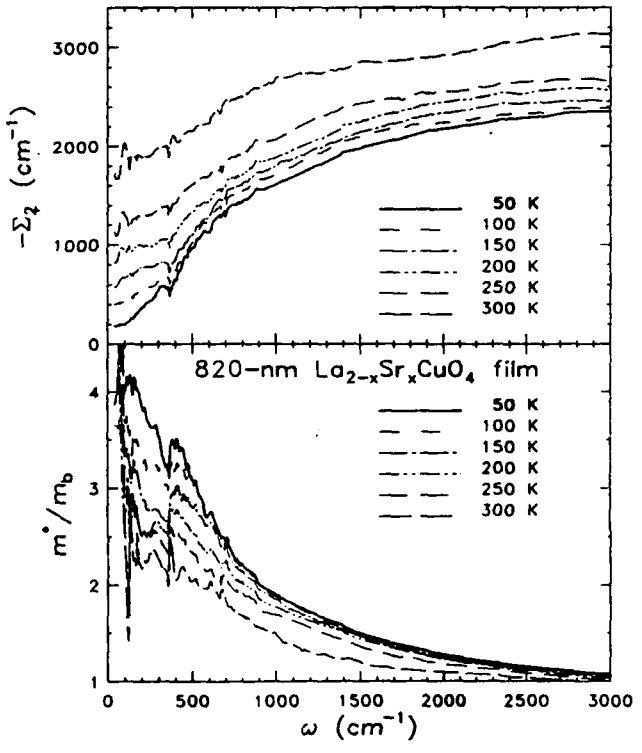


FIG. 16. Frequency-dependent mass enhancement (lower panel) and imaginary part of the self-energy (upper panel) derived from the experimental complex dielectric function with interband contributions subtracted.

### 2. *Effective scattering rate $1/\tau^*(\omega)$*

A linear $T$-dependent scattering rate at $\omega\sim 0$ implies it is also linear in $\omega$ at higher frequencies. The effective renormalized scattering rate can be obtained by $1/\tau^*=-(m_b/m^*)\Sigma_2$. This quantity is shown in Fig. 17. The extrapolated $\omega=0$ values of $1/\tau^*$ are compatible to those obtained above in the two-component fit by assuming a constant scattering rate. This is not surprising since both the one- and two-component approaches have described the dc transport behavior well. At higher frequencies, we observe $1/\tau^*$ is of order $\max(T,\omega)$ before it saturates. According to the MFL theory, however, it is not $1/\tau^*$ but the imaginary part of the quasiparticle self-energy $\Sigma_1$ that has the form $-\Sigma_1=\lambda\max(\pi T,\omega)$, as long as $\omega<\omega_c\simeq 1000\ \text{cm}^{-1}$. Thus, $\Sigma_2$ would change from constant to linear in $\omega$ at $\omega>\pi T$. At low $\omega$, our results agree with this prediction, and $\Sigma_2$ tends to saturate at frequencies above $\omega_c$. Since $\lambda$ is, in principle, $T$ independent, one expects the slope of $\Sigma_2(\omega)$ to be constant at all temperatures in MFL theory. However, our data indicate a gradual decrease of slope with increasing temperature.

It is difficult to interpret the frequency-dependent scattering rate as a consequence of inelastic scattering due to the Holstein effect,[65,66] in which a carrier can absorb a photon of energy $\hbar\omega$, emit an excitation (or a phonon) of energy $\varepsilon$ ($\varepsilon\sim 300\ \text{cm}^{-1}$ in this case), and scatter. First, the large value of $\lambda$ ($\sim 3$) implied by the analysis of

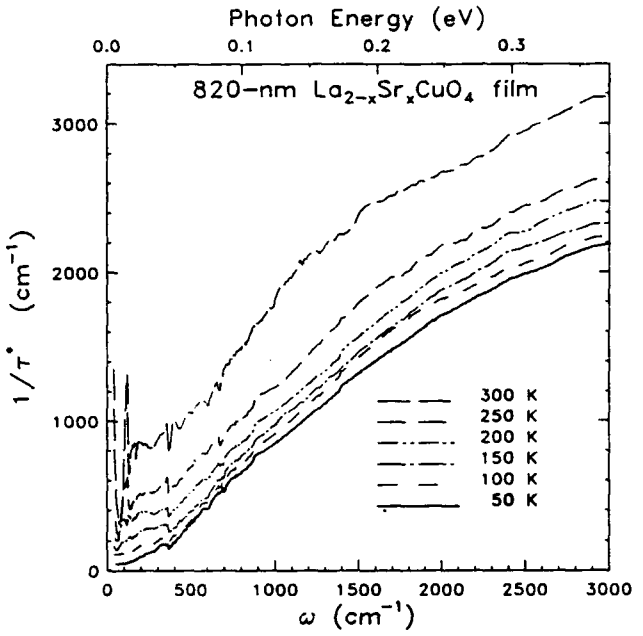


FIG. 17. Renormalized scattering rate given by $1/\tau^* = -(m_b/m^*)\Sigma_2$.

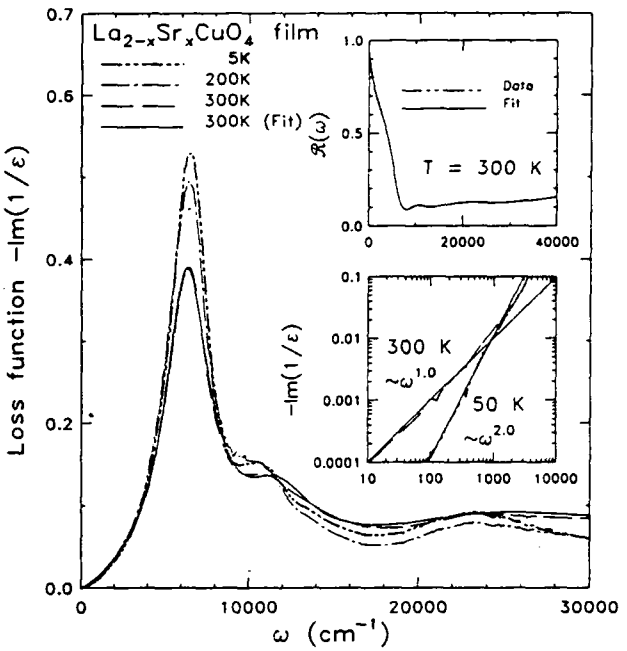


FIG. 18. Energy-loss function calculated from the Kramers-Kronig analysis of $\mathcal{R}(\omega)$ at selected temperatures. The solid line is a calculation using the oscillator parameters obtained from a two-component model fit to $\mathcal{R}(\omega)$ as shown in the upper inset. The lower inset illustrates the different low $\omega$-dependent behavior of the loss function at 50 and 300 K.

Fig. 16 suggests a strong coupling between the conduction carriers and the excitation. Therefore, at $T > \epsilon \sim 400$ K, the dc resistivity should significantly deviate from its linear $T$-dependent behavior. Such a large $\lambda$ would also imply that the mean free path is of the same order of the lattice constant at room temperature, thus the dc resistivity would be expected to saturate, inconsistent with the observed linear behavior which persists up to 1100 K for LSCO materials.[24] Second, the Holstein sideband would shift upwards by $2\Delta$, the threshold energy for exciting two quasiparticles, in the superconducting state. On the contrary, our spectra in Fig. 5 do not show such shift. However, this structure could have been smeared out as the size of the Holstein effect depends sensitively on the shape of the Eliashberg function $\alpha^2F(\Omega)$ and on impurity scattering.[64] The possibility of a Holstein effect therefore may not be completely ruled out.

### E. Loss function

In the temperature-dependent reflectance spectra of Figs. 3 and 4, we have observed that the reflectivity edge sharpens and slightly moves to higher frequency with decreasing temperature. This may be attributed mainly to the effect of volume contraction. The behavior can also be seen in the electronic loss function $-\mathrm{Im}(1/\epsilon)$ as demonstrated in Fig. 18. Upon cooling, the peak position at the screened plasma frequency $\tilde{\omega}_p \approx 6400$ cm$^{-1}$ ($\sim 0.8$ eV) shifts to slightly higher energies along with a slight narrowing of the broad peak. This can be understood in terms of the generalized Drude model, in which the maximum value in $-\mathrm{Im}(1/\epsilon)$ is given approximately by $\tilde{\omega}_p\tau^*/\epsilon_h$ at $\omega = \tilde{\omega}_p \approx \omega_p/\sqrt{\epsilon_h}$ with a width of $1/\tau^*(\tilde{\omega}_p)$. This broad width (0.4 eV) is caused by the anomalous midinfrared background absorption.

Bozovic[73] found that $-\mathrm{Im}(1/\epsilon) = \beta\omega^2$ for small $\omega$ in both Y-Ba-Cu-O and Bi-Sr-Ca-Cu-O, and conjectured that the quadratic law was universal for all layered cuprate superconductors. In addition, it has been suggested that the two-component oscillator model fails to reproduce accurately the experimental loss function.[73] After making careful analysis on our $La_{2-x}Sr_xCuO_4$ film, however, we find our results are in sharp contrast to these conclusions. By using the dielectric function with a two-component model in the form of Eq. (1) to fit the room-temperature reflectance, we obtain a set of oscillator parameters which can almost exactly reproduce the measured $\mathcal{R}(\omega)$ as shown in the upper inset to Fig. 18. The oscillator parameters are listed in Table II. When the same set of parameters is used to calculate the loss function, we can see an excellent agreement with the experimental $-\mathrm{Im}(1/\epsilon)$ curve throughout the entire measured range as illustrated in the main part of Fig. 18. We want to stress here that the peak in $-\mathrm{Im}(1/\epsilon)$ is determined not only by the free carriers, but also by the bound carriers participating the charge-transfer and interband transitions. The loss function can be well fit only after the interband oscillators are taken into account.

When looking into the small-$\omega$ behavior of the loss function, we note that for our film the low-frequency quadratic law $-\mathrm{Im}(1/\epsilon) \sim \omega^2$ suggested by Bozovic *et al.*[73,74] is valid only at low temperatures (or at higher frequencies). A linear $\omega$ dependence, instead, is more appropriate for high temperatures. The result is more evident when our data are plotted in log-log scale as shown in the lower inset of Fig. 18. This behavior can be understood quantitatively in the one-component approach.

TABLE II. Parameters of a two-component oscillator fit to the measured $\mathcal{R}(\omega)$ at room temperature. $\epsilon_\infty = 1.5$.

| Oscillator no. | $\omega_0$ ($cm^{-1}$) | $\omega_p$ ($cm^{-1}$) | $\gamma$ ($cm^{-1}$) |
|---|---|---|---|
| Drude | 0 | 6240 | 358 |
| Mid-IR no. 1 | 250 | 2320 | 210 |
| Mid-IR no. 2 | 950 | 10640 | 2850 |
| Mid-IR no. 3 | 3180 | 6580 | 4330 |
| Phonon no. 1 | 126 | 750 | 28 |
| Phonon no. 2 | 359 | 455 | 22 |
| Phonon no. 3 | 681 | 450 | 25 |
| CT band | 11260 | 6720 | 4820 |
| Interband no. 1 | 23650 | 16620 | 15630 |
| Interband no. 2 | 59370 | 94290 | 33410 |

Starting with Eq. (14), one can derive the approximation for $\omega \ll \omega_p$:

$$-\mathrm{Im}(1/\epsilon) \approx -\frac{\omega\Sigma_2}{\omega_p^2} \propto -\omega\Sigma_2 , \tag{17}$$

where $\omega_p = 13000\ cm^{-1}$ for our film. If $\Sigma_2$ has the form of $-\Sigma_2 = \lambda \max(\pi T, \omega)$, as suggested by Fig. 16, then $-\mathrm{Im}(1/\epsilon)$ will be quadratic in $\omega$ when $T < \omega/\pi$ but linear in $\omega$ when $T > \omega/\pi$. We can see the 300-K curve in the inset changes its slope at $\omega_c \simeq 700\ cm^{-1} \sim \pi T$, giving a $\sim\omega^2$ dependence above $\omega_c$ and an $\omega$ linear dependence below $\omega_c$. [In fact, the 50-K curve also becomes linear in $\omega$ at frequencies below $100\ cm^{-1} \sim \pi T$ (not shown).] This behavior can also be explained qualitatively in the two-component analysis. At small $\omega$, the dielectric function $\epsilon(\omega)$ is dominated by the Drude term, thus the loss function exhibits the ordinary $\omega$ linear dependence. At higher frequencies, the midinfrared tail becomes important, causing the loss function to deviate from this linear behavior.

### F. The superconducting gap

In the conventional Bardeen-Cooper-Schreiffer superconductors,[75] it has been demonstrated successfully that the superconducting-to-normal ratio in transmission[76–78] would give a maximum very near $2\Delta$, the superconducting gap energy. Other experiments[79,80] showed that the gap corresponded to a threshold in surface resistance or conductivity. Many attempts have been made to identify the superconducting gap of HTSC at the peak in the reflectance ratio $\mathcal{R}_s(T)/\mathcal{R}_n$ or at the onset of the conductivity $\sigma_{1s}(\omega)$. However, it is problematic to make such assignments. First, the reflectance data (see Fig. 4, for example) do not exhibit a clear edge. Second, the phonon structure and MIR absorption tail as well as the $T$ dependence of the scattering rate complicate this approach. Finally, the propagated errors in $\sigma_{1s}(\omega)$ at low frequencies are large due to the fact that $\mathcal{R}(\omega) \to 1$. The experimental accuracy in $\mathcal{R}(\omega)$ in the far infrared is not much better than $\pm 0.5\%$. We repeated the reflectance measurements on our sample five times, finding agreement within $\pm 0.5\%$ above $300\ cm^{-1}$ but variations from the average up to $\pm 1\%$ at $40\ cm^{-1}$. This is illustrated in Fig. 19 where we plot in the upper panel the average reflectance at 5 and 200 K as solid lines. The dashed curves represent upper and lower estimates of the uncertainty in $\mathcal{R}$: $\pm 0.5\%$ at 200 K and above $300\ cm^{-1}$ at 5 K; the highest and lowest measured reflectances below $200\ cm^{-1}$, with a smooth merge between 200 and $300\ cm^{-1}$. We can then estimate the uncertainty in $\sigma_1(\omega)$ by performing the KK transformation. The results are in the lower panel of Fig. 19. The propagated uncertainty goes roughly $\Delta\sigma_1/\sigma_1 = [1/(1-\mathcal{R})](\Delta\mathcal{R}/\mathcal{R})$, as mentioned in the end of Sec. II. As we can see, the absorption edge of $\sigma_{1s}(\omega)$, whose value ($\sim 3.7 k_B T_c$) appears to coincide with the prediction of BCS theory,[75] is largely dependent on the accuracy of $\mathcal{R}(\omega)$. This prevents any gap assignment based on the onset of $\sigma_{1s}$.

Kamarás *et al.*[32] have argued that a superconducting gap cannot be unambiguously identified in the infrared spectra if the material is in the clean limit, $1/\tau \ll 2\Delta$ or $l \gg \xi$, with $l$ the electronic mean free path and $\xi$ the coherence length. In our sample, the free-carrier relaxation rate is $1/\tau \sim 2.5 k_B T_c$ at 50 K ($\tau = 0.1$ ps), smaller than the expected BCS superconducting gap. One expects an even smaller value of $1/\tau$ well below $T_c$, thus the clean-limit condition will be met. This low free-carrier relaxation rate implies that most of the free-carrier oscillator strength would move to the zero-frequency $\delta$ function of the superconductor, leaving little strength—only a factor $1/(\pi\tau\Delta)$ of the Drude spectral weight— avail-

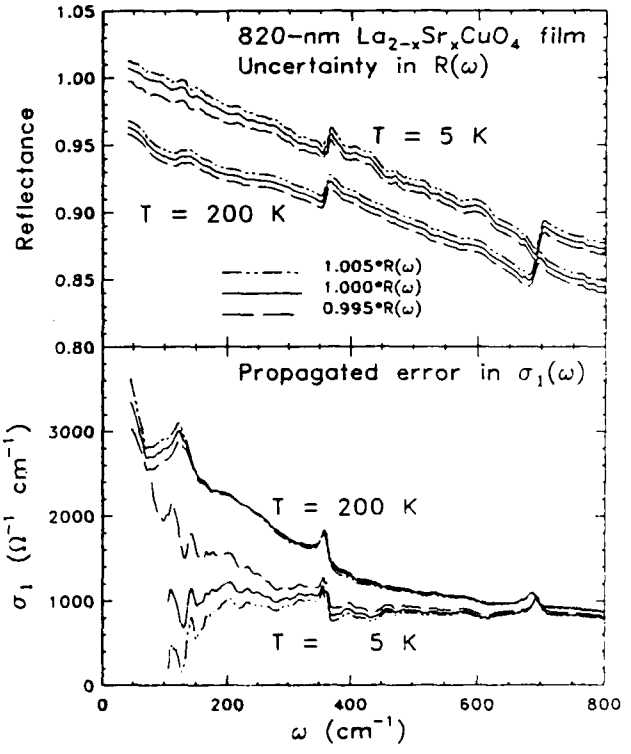


FIG. 19. The propagated uncertainty in values of the conductivity derived from the reflectance $\mathcal{R}$, in which $\mathcal{R}$ is close to unity and has the uncertainty shown.

able for the gap transition. As seen in Fig. 10, there is already considerable second-component (MIR) absorption in the low-frequency region, making it likely that any remaining gap structure is obscured by the intense midinfrared absorption.

## IV. CONCLUSIONS

In this paper, we presented a set of temperature- and frequency-dependent optical spectral functions from the far-infrared through the ultraviolet region. We made a systematic analysis for an epitaxial $La_{2-x}Sr_xCuO_4$ thin film with a transition temperature $T_c=31$ K. We emphasized the two-component analysis for both the normal and superconducting states. Then we discussed the alternative of a one-component approach.

Our results show that the temperature dependence of the *ab*-plane infrared phonons is sensitive to the tetragonal-to-orthorhombic phase transition near 250 K. One anomalous behavior which appears to be associated with the structural transition is that the reflectance in the charge-transfer region is significantly depressed below 250 K, implying a shift of spectral weight to the higher-energy region. The electronic behavior is similar to that observed in other cuprate superconductors like YBCO or BiSrCaCuO crystals. On the other hand, the LSCO crystal has a lower free-carrier concentration but a higher phonon oscillator strength on the $CuO_2$ layers. The normal-state infrared properties of LSCO materials exhibit an extremely unusual non-Drude response over most of the infrared range. This anomalous behavior can be interpreted either by absorptions due to free and bound carriers in the two-component approach, or by a strong frequency-dependent scattering rate and a mass enhancement in a single-component approach.

The two-component picture analysis shows a narrow (of order $k_BT$) Drude absorption and a broad, strong midinfrared band. The Drude plasma frequency is essentially temperature independent, whereas the scattering rate is roughly linear in $T$ in the normal state followed by a fast drop below $T_c$. A weak-coupling strength $\lambda\sim0.25$ is derived. The midinfrared absorption exhibits a weak temperature dependence in the normal state. In the superconducting state, the absorption is similar to the midinfrared band, but is enhanced in the 150–1500 $cm^{-1}$ range. The superconducting condensate carries most ($\sim85\%$) of the free-carrier oscillator strength. No superconducting gap is discernible as the film is near the clean limit. The absorption edge near 80 or 400 $cm^{-1}$ cannot be assigned as the superconducting gap and is attributed to the tail of low-energy excitations or to the strong bound-carrier–phonon coupling. The single-component picture analysis in the normal state shows a strongly frequency-dependent scattering rate of the order $k_BT+\hbar\omega$ at low frequencies and a large mass enhancement, which leads to a strong-coupling strength $\lambda\sim3$. This analysis has the features predicted by marginal Fermi liquid of nested Fermi liquid, but has a temperature dependent slope in the imaginary part of the quasiparticle self-energy.

## ACKNOWLEDGMENTS

Research at the University of Florida is supported by NSF Grant No. DMR-9101676. Westinghouse was supported in part by AFOSR through Contract No. F49620-91-C-0034.

*Present address: Department of Physics, Virginia Tech, Blacksburg, VA 24061.

[1]J. G. Bednorz and K. A. Müller, Z. Phys. B **64**, 189 (1986).

[2]M. K. Wu, J. R. Ashburn, C. J. Tong, P. H. Hor, R. L. Meng, L. Gao, Z. J. Huang, Y. Q. Wang, and C. W. Chu, Phys. Rev. Lett. **58**, 908 (1987).

[3]T. Timusk and D. B. Tanner, in *Physical Properties of High Temperature Superconductors I,* edited by D. M. Ginsberg (World Scientific, Singapore, 1989), p. 339.

[4]G. A. Thomas, in *Proceedings of the Thirty-Ninth Scottish Universities Summer School in Physics of High-Temperature Superconductivity,* edited by D. P. Tunstall and W. Barford (Hilger, Bristol, 1991), p. 169.

[5]D. B. Tanner and T. Timusk, in *Physical Properties of High Temperature Superconductors III,* edited by D. M. Ginsberg, (World Scientific, Singapore, 1992), p. 363.

[6]K. F. Renk, in *Studies of High Temperature Superconductors,* edited by A. V. Narlikar (Nova Science, New York, 1991), Vol. 10.

[7]B. Koch, H. P. Geserich, and T. Wolf, Solid State Commun. **71**, 495 (1989).

[8]Z. Schlesinger, R. T. Collins, F. Holtzberg, C. Feild, S. H. Blanton, U. Welp, G. W. Crabtree, Y. Fang, and J. Z. Liu, Phys. Rev. Lett. **65**, 801 (1990).

[9]D. A. Bonn, J. E. Greedan, C. V. Stager, T. Timusk, M. G. Doss, S. L. Herr, K. Kamarás, C. D. Porter, D. B. Tanner, J. M. Tarascon, W. R. McKinnon, and L. H. Greene, Phys. Rev. B **35**, 8843 (1987); S. L. Herr, K. Kamarás, C. D. Porter, M. G. Doss, D. B. Tanner, D. A. Bonn, J. E. Greedan, C. V. Stager, and T. Timusk, *ibid.* **36**, 733 (1987).

[10]J. Orenstein, G. A. Thomas, D. H. Rapkine, C. G. Bethea, B. F. Levine, R. J. Cava, E. A. Reitman, and D. W. Johnson, Jr., Phys. Rev. B **36**, 729 (1987); J. Orenstein, G. A. Thomas, D. H. Rapkine, C. G. Bethea, B. F. Levine, B. Batlogg, R. J. Cava, D. W. Johnson, Jr., and E. A. Reitman, *ibid.* **36**, 8892 (1987).

[11]Z. Schlesinger, R. T. Collins, M. W. Shafer, and E. M. Engler, Phys. Rev. B **36**, 5275 (1987); Z. Schlesinger, R. L. Greene, J. G. Bednorz, and K. A. Müller, *ibid.* **35**, 5334 (1987).

[12]G. A. Thomas, A. J. Millis, R. N. Bhatt, R. J. Cava, and E. A. Rietman, Phys. Rev. B **36**, 736 (1987).

[13]U. Walter, M. S. Sherwin, A. Stacy, P. L. Richards, and A. Zettl, Phys. Rev. B **35**, 5327 (1987).

[14]G. L. Doll, J. T. Nicholls, M. S. Dresselhaus, A. M. Rao, J. M. Zhang, G. W. Lehman, P. C. Eklund, G. Dresselhaus, and A. J. Strauss, Phys. Rev. B **38**, 8850 (1988).

[15]S. Etemad, D. E. Aspnes, M. K. Kelly, R. Thompson, J. M. Tarascon, and G. W. Hull, Phys. Rev. B **37**, 3396 (1988).

[16]J. Tanaka, M. Shimada, U. Mizutani, and M. Hasegawa, Physica C **153-155**, 651 (1988).

[17]S. Tajima, S. Uchida, H. Ishii, H. Takagi, S. Tanaka, U. Kawabe, H. Hasegawa, T. Aita, and T. Ihisba, Mod. Phys. Lett. B **1**, 353 (1988).

[18]R. T. Collins, Z. Schlesinger, G. V. Chadrashekhar, and M.

W. Shafer, Phys. Rev. B **39**, 2251 (1989).
[19]S. Tajima, H. Ishii, T. Nakahashi, T. Takagi, S. Uchida, M. Seki, S. Sugai, Y. Hidaka, M. Suzuki, T. Murakami, K. Oka, and H. Unoki, J. Opt. Soc. Am. B **6**, 475 (1989).
[20]M. Suzuki, Phys. Rev. B **39**, 2312 (1989).
[21]S. Uchida, T. Ido, H. Takagi, T. Arima, Y. Tokura, and S. Tajima, Phys. Rev. B **43**, 7942 (1991).
[22]B. Batlogg, G. Kourouklis, W. Weber, R. J. Cava, A. Jayaraman, A. E. White, K. T. Short, L. W. Rupp, and E. A. Rietman, Phys. Rev. Lett. **59**, 912 (1987).
[23]T. A. Faltens, W. K. Ham, S. W. Keller, K. J. Leary, J. N. Michaels, A. M. Stacy, H.-C. zur Loye, D. E. Morris, T. W. Barbee, III, L. C. Bourne, M. L. Cohen, S. Hoen, and A. Zettle, Phys. Rev. Lett. **59**, 915 (1987).
[24]M. Gurvitch and A. T. Fiory, Phys. Rev. Lett. **59**, 1337 (1987).
[25]S. L. Cooper, G. A. Thomas, J. Orenstein, D. H. Rapkine, A. J. Millis, S.-W. Cheong, A. S. Cooper, and Z. Fisk, Phys. Rev. B **41**, 11 605 (1990).
[26]S. Tajima, S. Uchida, S. Tanaka, S. Kanabe, K. Kitazawa, and K. Fueki, Jpn. J. Appl. Phys. **26**, L432 (1987).
[27]S. L. Herr *et al.*, in *High Temperature Superconducting Materials: Preparations, Properties and Processing*, edited by William Hatfield and J. J. Miller (Marcel Dekker, New York, 1988), p. 275.
[28]D. A. Bonn, A. H. O'Reilly, J. E. Greedan, C. V. Stager, T. Timusk, K. Kamarás, and D. B. Tanner, Phys. Rev. B **37**, 1574 (1988).
[29]C. M. Foster, K. F. Voss, T. W. Hagler, D. Mihailović, A. J. Heeger, M. M. Eddy, W. L. Olsen, and E. J. Smith, Solid State Commun. **76**, 651 (1990).
[30]T. Timusk, M. Reedyk, R. Hughes, D. A. Bonn, J. D. Garrett, J. E. Greedan, C. V. Stager, D. B. Tanner, F. Gao, S. L. Herr, K. Kamarás, G. A. Thomas, S. L. Cooper, J. Orenstein, L. F. Schneemeyer, and A. J. Millis, Physica C **162-164**, 841 (1989).
[31]S. L. Cooper, G. A. Thomas, J. Orenstein, D. H. Rapkine, M. Capizzi, T. Timusk, A. J. Millis, L. F. Schneemeyer, and J. V. Waszczak, Phys. Rev. B **40**, 11 358 (1989).
[32]K. Kamarás, S. L. Herr, C. D. Porter, N. Tache, D. B. Tanner, S. Etemad, T. Venkatesan, E. Chase, A. Inam, X. D. Wu, M. S. Hedge, and B. Dutta, Phys. Rev. Lett. **64**, 84 (1990).
[33]F. Gao, G. L. Carr, C. D. Porter, D. B. Tanner, E. S. Etemad, T. Venkatesan, A. Inam, B. Dutta, X. D. Wu, G. P. Williams, and C. J. Hirschmugl, Phys. Rev. B **43**, 10 383 (1991).
[34]C. M. Varma, P. R. Littlewood, S. Schmitt-Rink, E. Abrahams, and A. Ruckenstein, Phys. Rev. Lett. **63**, 1996 (1989); **64**, 497E (1990); C. M. Varma, Int. J. Mod. Phys. B **3**, 2083 (1989); P. B. Littlewood and C. M .Varma, J. Appl. Phys. **69** 4979 (1991).
[35]A. Virosztek and J. Ruvalds, Phys. Rev. B **42**, 4064 (1990); Physica B **165&166**, 1267 (1990).
[36]J. Talvacchio, M. G. Forrester, J. R. Gavaler, and T. T. Braggins, in *Science a d Technology of Thin Film Superconductors II*, edited by R. McConnel and S. A. Wolf (Plenum, New York, 1990).
[37]Frederick Wooten, *Optical Properties of Solids* (Academic, New York, 1972).
[38]S. Tajima, T. Ido, S. Ishibashi, T. Itoh, E. Eisaki, Y. Mizuo, T. Arima, H. Takagi, and S. Uchida, Phys. Rev. B **43**, 10 496 (1991).
[39]F. Gervais, P. Echegut, J. M. Bassat, and P. Odier, Phys. Rev. B **37**, 9364 (1988).
[40]R. Feile, Physica C **159**, 1 (1989).
[41]T. R. Thurson, Phys. Rev. B **39**, 4327 (1989).
[42]D. T. Keane, G. A. Held, J. L. Jordan-Sweet, M. W. Shafer, P. M. Horn, G. Guntherodt, J. Langen, M. Weit, A. Erle, S. Blumenroder, and E. Zirngiebl, Physica C **153-155**, 594 (1988).
[43]S. L. Here, K. Kamarás, D. B. Tanner, S.-W. Cheong, G. R. Stewart, and Z. Fisk, Phys. Rev. B **43**, 7847 (1991).
[44]R. P. Lowndes, Phys. Rev. B **6**, 1490 (1972).
[45]J. M. Tranquada, S. M. Heald, and A. R. Moodeneabaugh, Phys. Rev B **36**, 8401 (1987).
[46]D. A. Bonn, J. E. Greedan, C. V. Stager, T. Timusk, M. G. Doss, S. L. Herr, K. Kamarás, and D. B. Tanner, Phys. Rev. Lett. **58**, 2249 (1987).
[47]F. Gao, D. B. Tanner, D. A. Bonn, J. E. Greedan, C. V. Stager, and T. Timusk, Bull. Am. Phys. Soc. **34**, 1036 (1989).
[48]R. Zeyher and G. Zwicknagl, Z. Phys. B **78**, 175 (1990).
[49]R. T. Collins, Z. Schlesinger, F. Holtzberg, and C. Feild, Phys. Rev. Lett. **63**, 422 (1989).
[50]B. Koch, M. Dürrler, H. P. Geserich, Th. Wolf, G. Roth, and G. Zachmann, in *Electronic Properties of High-$T_c$ Superconductors and Related Compounds*, edited by H. Kuzmany, M. Mehrig, and J. Fink, Springer Series in Solid State Sciences, Vol. 99 (Springer-Verlag, Berlin, 1990), p. 290.
[51]K. Kamarás, C. D. Porter, M. G. Doss, S. L. Herr, D. B. Tanner, D. A. Bonn, J. E. Greedan, A. H. O'Reilly, C. V. Stager, and T. Timusk, Phys. Rev. Lett. **60**, 969 (1988).
[52]Z. Schlesinger, R. T. Collins, F. Holtzberg, C. Feild, G. Koren, and A. Gupta, Phys. Rev. B **41**, 11 237 (1990).
[53]G. A. Thomas, J. Orenstein, D. H. Rapkine, M. Capizzi, A. J. Millis, R. N. Bhatt, L. F. Schneemeyer, and J. V. Waszczak, Phys. Rev. Lett. **61**, 1313 (1988).
[54]P. B. Allen, W. E. Pickett, and H. Krakauer, Phys. Rev. B **36**, 3926 (1987).
[55]P. B. Allen, Z. Fisk, and A. Migliori, in *Physical Properties of High Temperature Superconductors I*, edited by D. M. Ginsberg (World Scientific, Singapore, 1989), p. 213.
[56]F. Gao, G. L. Carr, D. B. Tanner, S. Etemad, T. Venkatesan, B. Dutta, X. D. Wu, A. Inam, G. P. Williams, and C. J. Hirschmugl, Bull. Am. Phys. Soc. **35**, 814 (1990).
[57]D. B. Tanner, D. B. Romero, K. Kamarás, G. L. Carr, L. Forro, D. Mandrus, L. Mihály, and G. P. Williams, in *Electronic Structure and Mechanisms for High-Temperature Superconductivity*, edited by G. C. Vezolli *et al.* (Plenum, New York, 1991).
[58]D. B. Romero, C. D. Porter, D. B. Tanner, L. Forro, D. Mandrus, L. Mihaly, G. L. Carr, and G. P. Williams, Phys. Rev. Lett. **68**, 1590 (1992).
[59]J. M. Chwalek, C. Uher, J. F. Whitaker, G. A. Mourou, J. Agostinelli, and M. Lelental, Appl. Phys. Lett. **57**, 1696 (1990).
[60]E. J. Nicol and J. P. Carbotte, Phys. Rev. B **44**, 7741 (1991).
[61]M. C. Nuss, P. M. Mankiewich, M. L. O'Malley, E. H. Westerwick, and P. B. Littlewood, Phys. Rev. Lett. **66**, 3305 (1991).
[62]J. Orenstein, G. A. Thomas, A. J. Millis, S. L. Cooper, D. H. Rapkine, T. Timusk, L. F. Schneemeyer, and J. V. Waszczak, Phys. Rev. B **42**, 6342 (1990).
[63]T. Timusk and D. B. Tanner, Physica C **169**, 425 (1990).
[64]W. Lee, D. Rainer, and W. Zimmermann, Physica C **159**, 535 (1989).
[65]T. Holstein, Phys. Rev. **96**, 535 (1954); Ann. Phys. (N.Y.) **29**, 410 (1964).
[66]P. B. Allen, Phys. Rev. B **3**, 305 (1971).
[67]G. Aeppli, R. J. Cava, E. J. Ansaldo, J. H. Brewer, S. R. Kreitzman, G. M. Luke, D. R. Noakes, and R. F. Kiefl, Phys.

Rev. B 35, 7129 (1987).
[68]R. T. Collins, Z. Schlesinger, F. Holtzberg, P. Chaudhari, and C. Feild, Phys. Rev. B 39, 6571 (1989).
[69]L. D. Rotter, Z. Schlesinger, R. T. Collins, F. Holtzberg, C. Feild, U. Welp, G. W. Crabtree, J. Z. Liu, Y. Fang, G. Vandervoort, and S. Fleshler, Phys. Rev. Lett. 67, 2741 (1991).
[70]S. L. Cooper, A. L. Kotz, M. A. Karlow, M. V. Klein, W. C. Lee, J. Giapintzakis, and D. M. Ginsberg, Phys. Rev. B 45, 2549 (1992).
[71]P. W. Anderson, Mater. Res. Bull. 8, 153 (1973); P. W. Anderson, Science 235, 1196 (1987); P. W. Anderson, in *Frontiers and Borderlines in Many Particle Physics*, edited by J. R. Schrieffer and R. A. Broglia (North-Holland, Amsterdam, 1989); R. B. Laughlin, Science 242, 525 (1988); P. W. Anderson, Phys. Rev. Lett. 64, 1839 (1990).
[72]B. C. Webb, A. J. Sievers, and T. Mihalisin, Phys. Rev. Lett. 57, 1951 (1986).
[73]Ivan Bozovic, Phys. Rev. B 42, 1969 (1990).
[74]J. H. Kim, I. Bozovic, J. S. Harris, Jr., C. B. Eom, T. H. Geballe, W. Y. Lee, E. S. Hellman, and J. T. Cheung, Bull. Am. Phys. Soc. 37, 283 (1992).
[75]J. Bardeen, L. N. Cooper, and J. R. Schrieffer, Phys. Rev. 108, 1175 (1957).
[76]R. E. Glover and M. Tinkham, Phys. Rev. B 107, 844 (1956); 108, 243 (1957).
[77]D. M. Ginsberg and M. Tinkham, Phys. Rev. 118, 990 (1960).
[78]P. J. M. van Bentum and P. Wyder, Physica B 138, 23 (1986).
[79]H. D. Drew and A. J. Sievers, Phys. Rev. Lett. 19, 697 (1967).
[80]L. H. Palmer and M. Tinkham, Phys. Rev. 165, 588 (1968).

# YBCO-BASED MULTILAYER STRUCTURES ON LARGE-AREA SUBSTRATES*

APPENDIX 16

J. R. GAVALER AND J. TALVACCHIO
Westinghouse STC, 1310 Beulah Road, Pittsburgh, PA 15235

## ABSTRACT

We have deposited $YBa_2Cu_3O_7$ (YBCO) films on $LaAlO_3$ substrates up to two inches in diameter using 90° off-axis magnetron sputtering from a single stoichiometric target. With this same method, epitaxial bilayers and trilayers of insulating $SrTiO_3$, $LaAlO_3$, MgO, metallic $PrBa_2Cu_3O_7$ (PrBCO), or superconducting $La_{2-x}Sr_xCuO_4$ (LSCO) were deposited in combinations with YBCO. In the resulting structures with c-axis orientations, the YBCO had $T_c$'s of 90K or higher over the entire surface area. Maximum resistivity values of $6 \times 10^9$ Ω-cm in YBCO/insulator/YBCO structures were obtained in vertical transport measurements with $SrTiO_3$. An important cause for degraded electrical properties in the structures incorporating epitaxial insulators was the presence of copper oxide particles on the YBCO surface. Methods used to minimize the number of these particles are discussed.

## INTRODUCTION

Superconducting electronic circuits are patterned from a series of deposited film layers incorporating Josephson junctions, interconnects, ground planes, insulators, and resistors. The insulating layers are required for isolating the conductive layers in microstrip transmission lines, crossovers, flux transformers, and lumped-element capacitors. Normal conductors are needed in some Josephson junction configurations and for resistors. One of the differences between Nb and YBCO-based circuits is that YBCO circuits require epitaxial insulators and normal conductors for some of the circuit layers to provide a suitable substrate for a subsequent YBCO film deposition. Indeed, the best candidate materials for epitaxial insulators are the same materials used as single-crystal substrates.

Most of the multilayer circuits fabricated with YBCO films are deposited on small-area substrates, on the order of 1 cm × 1 cm.[1-6] As the emphasis of circuit development switches from proof of principle to reproducibility, whole-wafer processing is the most practical way to obtain working circuits while improving process yield.

The sputtering method used to deposit the films for this study is now generally recognized as one of preferred techniques for depositing YBCO films; details of this method have been reported by many workers. However, its use for depositing YBCO-based multilayer structures, particularly on substrates as large as two inches diameter, presents some unique problems which have thus far received much less attention. In this paper we focus primarily on these problems and report on our efforts toward their solution.

## EXPERIMENTAL PROCEDURE

We have previously reported in detail the experimental procedure employed by us for depositing YBCO films.[7,8] Briefly, the films are sputtered from a two inch diameter stoichiometric YBCO target, mounted in the 90° off-axis configuration, using approximately 100 watts of rf power. Typically the gas composition consisted of 100 mtorr of argon, 50 mtorr of oxygen, and 10 mtorr

* *Supported in part by AFOSR Contract No. F49620-91-C-0034.*

of water vapor. The deposition temperature was ~700°C for c-axis films and ~580°C for a-axis films. For depositing multilayer structures, a second sputtering gun was mounted into the system and used with the appropriate two inch diameter stoichiometric target to deposit $SrTiO_3$, $LaAlO_3$, MgO, PrBCO, or LSCO films. The distance and orientation of this gun with respect to the substrates were the same as those for the YBCO gun. For the depositions from this second gun, the experimental conditions were the same as those for the the YBCO layers.

In our early work, substrates were bonded to a metal (nickel) holder with silver paste to insure a uniform temperature across the entire area of a depositing film. The use of this method, however, with large-area substrates risked wafer breakage and therefore another method for holding substrates was developed. Presently, the large-area substrates are placed, without bonding, directly on a quartz holder and the heating is done primarily by radiation rather than by conduction through a bonding paste. The details of this method are described in Reference 8.

Critical temperatures of our films were measured resistively, using the van der Pauw technique, and inductively by noting the change of inductance for a copper coil driven at 100 kHz and positioned against the film. The resistive $T_c$ was defined as the temperature at which the resistance goes to zero and the inductive $T_c$ as the temperature at the midpoint of the change in inductance. Resistivities of nominally-insulating films incorporated in multilayer structure were determined by patterning 100 $\mu$m to 800 $\mu$m diameter circular mesas, contacting them with two probes and the base YBCO film with two probes in a wafer probe station with the sample immersed in liquid nitrogen at 77K. Approximately 10 different spots were measured for each chip. Structural analyses of the films were done by x-ray diffraction, electron diffraction, and by SEM.

## RESULTS AND DISCUSSION

We have found that all of the films that were deposited on $LaAlO_3$ substrates, whether singly or in combination with other films, grew epitaxially. In Figure 1 the x-ray diffraction pattern for a YBCO/LSCO bilayer structure (YBCO deposited first) is shown. The c-axis orientation of both film layers can be seen from the presence of YBCO(00n) and LSCO(00n) diffraction peaks. There was no evidence for unoriented grains as the largest diffraction peaks observed in powder patterns, YBCO(110) and (103) and LSCO(103), were not obtained. It is not possible to resolve the YBCO(200) peak from $LaAlO_3$(200) on the scale shown in Figure 1. Analysis of these peaks indicated that a minor fraction of a-axis growth was always present as shown for single YBCO film layers in Reference 8. The absence of YBCO(110), (103), and (200) diffraction peaks in x-ray patterns of YBCO/(MgO, $SrTiO_3$, $LaAlO_3$, PrBCO, or LSCO)/YBCO trilayers was taken as evidence that c-axis trilayers were grown with any one of the intermediate layers studied.

X-ray diffraction scans recorded while varying $2\theta$ provided information about the orientation of the film structures in the growth direction but did not show whether films grew epitaxially with alignment in the plane of the film. For evidence of epitaxy, low-energy and reflection high-energy electron diffraction patterns (LEED and RHEED) were obtained. Figure 2a shows a LEED pattern obtained from a $LaAlO_3$(100) single-crystal substrate prior to film growth. The indexing of crystal orientation used here treats $LaAlO_3$ as a pseudo-cubic structure. Figure 2b shows the LEED pattern obtained from the top surface of a YBCO/PrBCO/YBCO(001) trilayer. It indicates that in-plane orientation was maintained throughout the structure. Figure 2c shows a LEED pattern from the same type of structure deposited at lower deposition temperatures to obtain an a-axis growth orientation. The pattern in Figure 2c appears to have a 3x1 "surface reconstruction" characterized by additional diffraction spots at 1/3 of the spacing of Figure 2a or 2b. The additional spots are due to the two possible

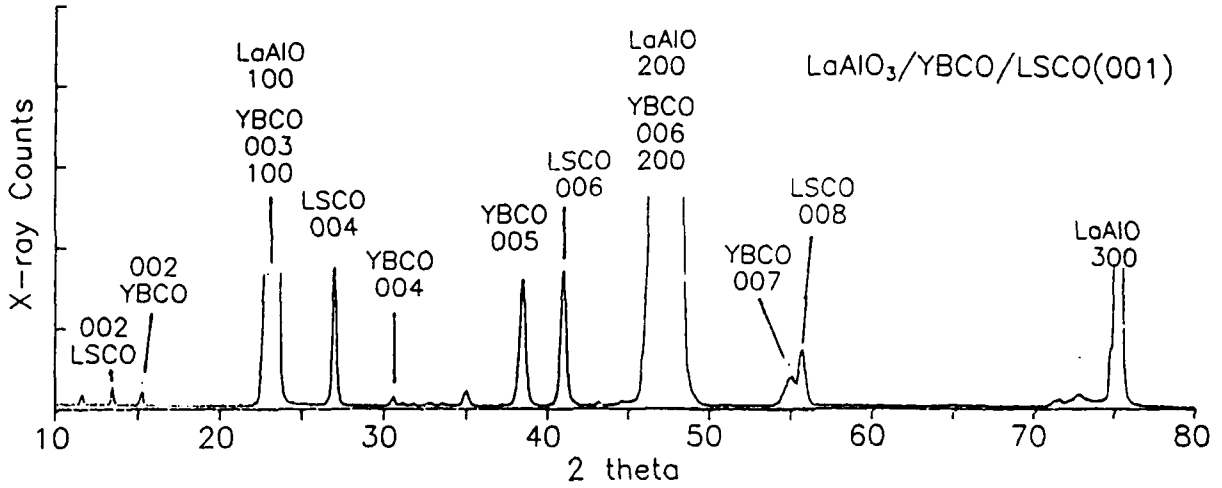


Figure 1. X-ray diffraction pattern of a multilayer structure consisting of a LSCO layer deposited on a YBCO layer deposited on a $LaAlO_3$ substrate.

in-plane directions for the c-axis which has a lattice constant, $c_o \simeq 3a_o$. Figure 2d is a RHEED pattern of the same a-axis sample shown in 2c in which the 1/3 spacing of diffraction streaks is particularly evident. Electron diffraction patterns equivalent to Figure 2b were observed for bilayers and trilayers formed with each type of intermediate film layer.

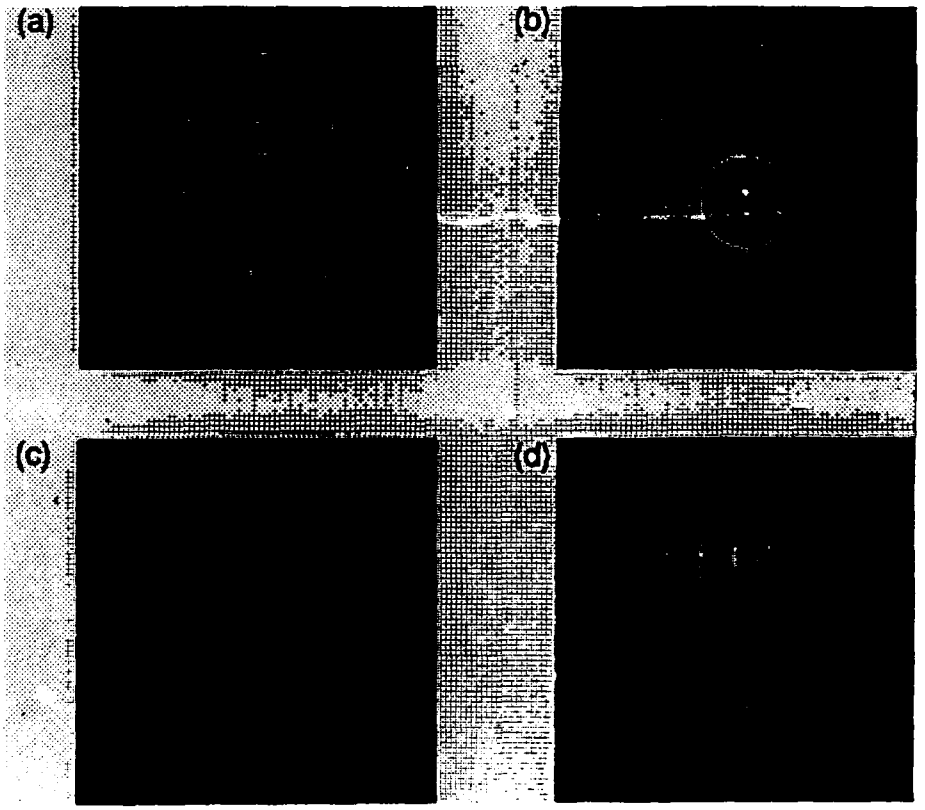


Figure 2. LEED and RHEED patterns showing the in-plane orientation of the top surface of epitaxial film structures: (a) $LaAlO_3$(100) single-crystal substrate, (b) YBCO/PrBCO/YBCO(001) trilayer, (c) YBCO/PrBCO/YBCO(100) trilayer, and (d) a RHEED pattern of the same a-axis structure used in (c).

Table I - Resistivities of Insulating Film Layers

| Insulating Layer | Thickness | Resistivity |
|---|---|---|
| $SrTiO_3$ | 100 - 300 nm | $1\times10^{8}$ - $6\times10^{9}$ Ω-cm |
| $LaAlO_3$ | 100 - 150 nm | $2\times10^{4}$ - $8\times10^{5}$ Ω-cm |
| MgO | 100 nm | $4\times10^{1}$ - $1\times10^{3}$ Ω-cm |

Although there were no significant differences in their diffraction patterns, large variations were found in the dc resistivity of epitaxial insulating layers. Table I lists the range of thicknesses and resistivities measured for the three insulators. Only in the case of $SrTiO_3$ was the resistivity close to the bulk value, indicating that the structural quality of only this film was approaching the ideal. The resistivity reported in Reference 1 for laser-ablated $SrTiO_3$ films deposited on a smaller area falls within the range shown in Table I. Figure 3 shows SEM micrographs of YBCO/insulator bilayers with each of the materials listed in Table I. Only the $SrTiO_3$ overlayers had smooth surfaces comparable to those of the YBCO base layers. Our speculation is that the cubic-to-rhombohedral structural transformation of $LaAlO_3$ and large lattice mismatch between YBCO and MgO led to the rough surfaces seen in Figures 3b and 3c, respectively.

Additional evidence of the quality of $SrTiO_3$ sputtered films is shown in Figure 4. In this figure are SEM photomicrographs of two YBCO films, one grown directly on a $LaAlO_3$ substrate and the other on a 200 nm $SrTiO_3$ film, previously sputtered on the $LaAlO_3$. Despite the presence of the $SrTiO_3$ layer, the two YBCO structures appear essentially identical indicating that the quality of the intermediate $SrTiO_3$ was sufficiently high that it had no deleterious effect on the epitaxial growth of the YBCO.

As also can be seen in this figure, the YBCO grains tended to be square in shape. This type of grain growth in YBCO films has previously been reported by Raistrick et al. from scanning tunneling microscopy studies.[9] In their STM micrographs there is sufficient definition so that the formation of the squarish grain can be observed via the spiral growth of YBCO apparently starting at a defect on the substrate surface.

In addition to the structural quality of the films themselves there is another significant factor which can limit the performance of the insulating film layers. We have found significant degradation in the electrical properties when

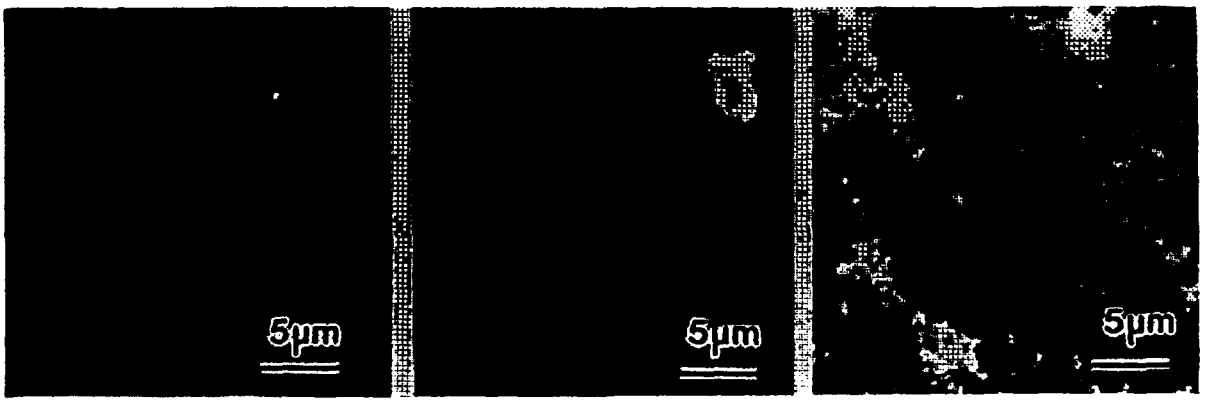


(a) (b) (c)

Figure 3. SEM micrographs of YBCO/epitaxial insulator bilayers with (100) orientation insulating films of (a) $SrTiO_3$, (b) $LaAlO_3$, and (c) MgO grown on c-axis-oriented YBCO.

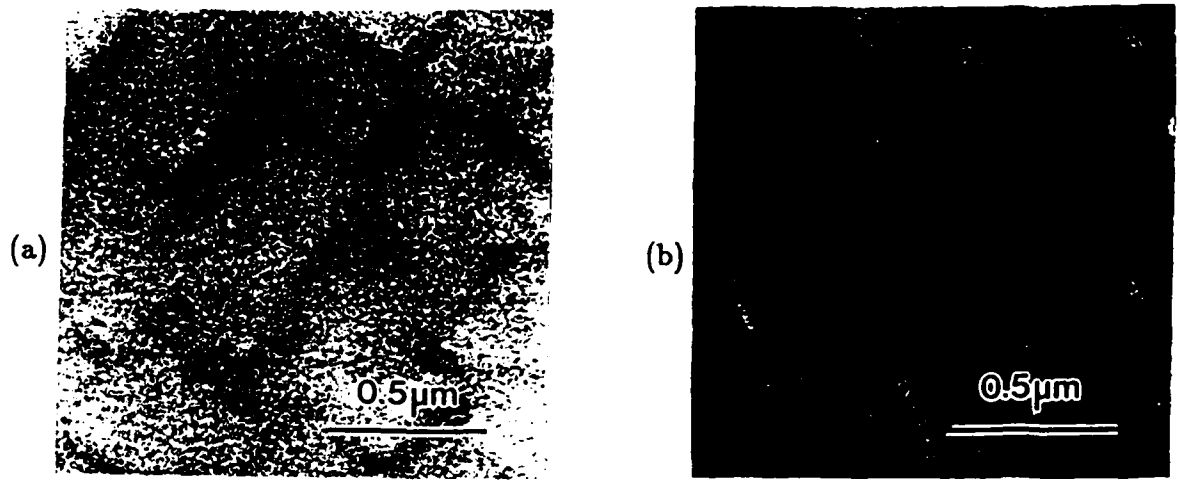


Figure 4. SEM photomicrographs of two sputtered YBCO films. Film (a) was deposited directly on a $LaAlO_3$ substrate and (b) on an intermediate $SrTiO_3$ layer.

second phase particles were present on the YBCO surface on which the insulator was deposited. Specifically, the data in Table I was obtained for overlayers grown on smooth single-phase YBCO films. However, $LaAlO_3$ films grown under the same conditions but on YBCO layers with approximately 5% of their surfaces covered with second phase particles, had a resistivity four orders of magnitude lower.

The problem of the formation of second phase particles during the deposition of YBCO films is not new. Depending on the growth process and conditions these particles can have a variety of sizes and compositions. Under the conditions used to deposit our films we have found that when particles are formed, they typically are irregularly shaped and about 500 nm across the longest dimension. Chemical analyses showed that they consisted of copper oxide.

We have previously reported data indicating that such particles can arise from a variety of sources including substrate surface contamination and the backsputtering of material onto the substrates from the adjacent area.[7] By taking steps to minimize these two sources we have been able to grow essentially particle-free films. However, during the sputtering of large-area YBCO films another source of Cu-O particles was identified. We found that under what was believed to be optimum conditions, YBCO sputtered on two inch diameter $LaAlO_3$ substrates often showed a large particle concentration. However when such a film was turned over and YBCO deposited on the second side, the particle count was invariably less and usually negligible.

We believe that the particles formed during the first deposition were due to a non-uniform heating of the substrate. Due to the uncoated $LaAlO_3$ being essentially transparent to radiation, some significant fraction of the substrate heating occurred by conduction. Because the wafer was not bonded to the heater this conduction heating was not uniform. We believe that since the YBCO deposited on the first side of the wafer absorbed radiation well its presence equilibrated the substrate temperature during the crucial nucleation period of the deposition on the second side. Despite the presence of particles on the first side, however, the >90K $T_c$'s of the two films were essentially the same. In addition, their rf surface resistances were found to be similar, i.e., 0.5 ± 0.1 mohm measured at 10GHz and 77K, and x-ray diffraction patterns of the two sides were also essentially indistinguishable.[8]

## CONCLUSIONS

We have demonstrated that YBCO-based multilayer structures incorporating either $SrTiO_3$, $LaAlO_3$, MgO, PrBCO, or LSCO can be grown epitaxially on $LaAlO_3$ substrates of up to at least two inches in diameter. The relatively poorer electrical properties of $LaAlO_3$ and MgO layers compared to $SrTiO_3$ are attributed to the inferior structural quality of these films when grown on YBCO. An important source of degradation in the dc resistivity was the presence of second phase Cu-O particles which sometimes formed during the growth of the YBCO layers. In their absence, resistivities were measured for $SrTiO_3$ which approached the ideal value.

We acknowledge the assistance of J. H. Uphoff, C. L. Jones, and B. A. Blankenship in film preparation and electrical measurements, and A. M. Stewart with x-ray measurements.

1. J. J. Kingston, F. C. Wellstood, P. Lerch, A. H. Miklich, and J. Clarke, "Multilayer $YBa_2Cu_3O_x$-$SrTiO_3$-$YBa_2Cu_3O_x$ Films for Insulating Crossovers," Appl. Phys. Lett. 56(2), 189-191 (1990).
2. M. Tonouchi, Y. Yoshizako, M. Iyori, and T. Kobayashi, "Double Heteroepitaxy of YBaCuO/MgO/YBaCuO System," Proc. Int. Supercond. Elec. Cont. (Tokyo, 1989) p. 433.
3. A. E. Lee, J. F. Burch, R. W. Simon, J. A. Luine, R. Hu, and S. M. Schwarzbek, "$LaAlO_3$-YBCO Multilayers," IEEE Trans. Magn. 27(2), 1365 (1991).
4. J. Talvacchio, M. G. Forrester, J. R. Gavaler, and T. T. Braggins, "YBCO and LSCO Films Grown by Off-Axis Sputtering," in Science and Technology of Thin Film Superconductors II, edited by R. McConnell and S. A. Wolf (Plenum, New York, 1990).
5. O. Eibl, H. E. Hoenig, J. M. Triscone, O. Fischer, L. Antognazza, and O. Brunner, "Microstructure of $YBa_2Cu_3O_7/PrBa_2Cu_3O_7$ Superlattices Deposited on (100) $SrTiO_3$ Single Crystals," Physica C 172, 365-372 (1990).
6. A. Inam, C. T. Rogers, R. Ramesh, K. Remschnig, L. Farrow, D. Hart, T. Venkatesan, and B. Wilkens, "A-Axis Oriented Epitaxial $YBa_2Cu_3O_{7-x}$-$PrBa_2Cu_3O_{7-y}$ Heterostructures," Appl. Phys. Lett. 57(23), 2484 (1990).
7. J. R. Gavaler, J. Talvacchio, T. T. Braggins, and M. G. Forrester, "Critical Parameters in the Single-Target Sputtering of YBCO," J. Appl. Phys. 70, 4383 (1991).
8. T. T. Braggins, J. R. Gavaler, and J. Talvacchio, "In-Situ Deposition of YBaCuO Films on Both Sides of Two-Inch-Diameter Wafers by Off-Axis Sputtering," accepted for publication in Proc. ICMC, Advances in Cryogenic Engineering (Materials), (Plenum, New York, 1992).
9. I. D. Raistrick, M. Hawley, J. G. Beery, F. H. Garzon, and R. J. Houlton, "Microstructure and Growth Mechanism of Thin Sputtered Films of $YBa_2Cu_3O_7$ on MgO Substrates," Appl. Phys. Lett. 59(24), 3177 (1991).

To be Published
IEEE Transactions on
Applied Superconductivity
(ASC '92)

# ARTIFICIAL BARRIERS FOR Ba-K-Bi-O TUNNEL JUNCTIONS

B.A. Baumert*
Department of Materials Science and Engineering
Carnegie Mellon University
Pittsburgh, PA 15213
and
J. Talvacchio†
Westinghouse Science and Technology Center
Pittsburgh, PA 15235

**APPENDIX 17**

*Abstract*—We have grown epitaxial bilayers and trilayers which utilize $Ba_{1-x}K_xBiO_3$ (BKBO) base electrodes, native or artificial (MgO or $SrTiO_3$) insulating barriers, and Ag or BKBO counter electrodes, respectively. The layers were deposited in-situ by rf magnetron sputtering and characterized in-situ with RHEED, LEED, and XPS. Electron diffraction showed the layers to be epitaxial with the symmetry of the desired structure maintained even in the first monolayer at the surface. XPS showed no evidence of a chemical reaction at the BKBO/barrier interfaces. Tunneling measurements through a native insulating layer grown by exposing BKBO surfaces to air showed a gap of ~2.5 mV to be present. In the range of thicknesses used for artificial barriers, 3-6 nm, the barriers apparently contained pinholes which caused the junctions to short. The BKBO films were K-rich with $x \approx 0.5$. Critical temperatures and lattice constants were consistent with reports for bulk superconductors with this composition. Normal-state resistivities of 70-100 μΩ-cm at 30 K were the lowest ever reported in this system and significantly lower than for the highest-$T_c$ composition of $x = 0.4$. Rocking curve widths of 0.7° both in the growth direction and in the plane of the film were observed by x-ray diffraction for BKBO films on MgO and $SrTiO_3$.

BKBO is a BCS-like superconductor with a transition temperature of 30 K.[1] All-BKBO Josephson junctions could potentially be operated at 20 K in reliable closed-cycle refrigerators. Since the structure of the $Ba_{1-x}K_xBiO_3$ composition with $0.4 \le x \le 0.5$ is cubic with a space group of $Pm\bar{3}m$,[1] it is the highest $T_c$ oxide superconductor which has isotropic properties. It has additional advantages over higher-$T_c$ superconductors for development of tunnel junctions. It possesses a relatively long coherence length of 5-7 nm. Tunneling measurements with SIN junctions[2-6] and SIS point-contact junctions[7] have demonstrated a superconducting energy gap with a low density of electronic states below the gap energy. The goal of this work is to fabricate epitaxial trilayer SIS junctions in competition with junctions fabricated with higher-$T_c$ superconductors capable of operating at 50-70 K. The disadvantage of 20 K operation can only be overcome if the unique properties of BKBO permit all-BKBO junctions to be made with significantly more-reproducible Josephson current densities than can be made with the higher-$T_c$ superconductors.

In this study, the two best substrate materials for BKBO film growth, MgO(100) and $SrTiO_3$(100), were selected for evaluation as tunnel barriers. The only previous attempts to make junctions with BKBO counter-electrodes used a $BaBi_2O_y$ barrier,[8] or a $SrTiO_3$ barrier grown on a YBCO base electrode.[9] The first part of this paper presents results on the structural and superconducting properties of BKBO films. The second part addresses the structural and chemical characteristics of the junction interfaces as well as electronic behavior.

Multilayer structures were deposited in-situ using rf magnetron sputtering in an off-axis configuration with a target of composition $Ba_{0.6}K_{0.6}BiO_3$. Pressures of 100 mTorr of $O_2$ and 200 mTorr of Ar were used in the growth of the BKBO. The substrates were heated to 375-400°C during deposition and to 400°C during a 15-minute post-anneal in one atmosphere of oxygen. This anneal was done only after all layers were deposited to ensure clean interfaces. However, the $O_2$ anneal was performed before a Au contact layer was sputter-deposited in-situ. Low-resistivity Au contacts could be made in this manner but could not be made when the BKBO films were exposed to air prior to Au deposition.

The multilayer structures were grown on MgO(100), $LaAlO_3$(100), $NdGaO_3$(110), $SrTiO_3$(100), and $SrTiO_3$(110) single-crystal substrates. These structures consisted of a BKBO base electrode, a barrier layer, and a counter electrode of silver or gold in the SIN junctions and BKBO capped with with gold for the trilayers. The barrier consisted of either the native insulating layer formed upon exposure to air, evaporated MgO, or sputtered $SrTiO_3$. The base electrode was ~150 nm thick, the barrier 3-6 nm, and the BKBO counter electrode ~20 nm, with 50 nm of gold. Silver paint was then applied to the gold contacts and used as a mask when the samples were subsequently Ar ion-milled at 150 V

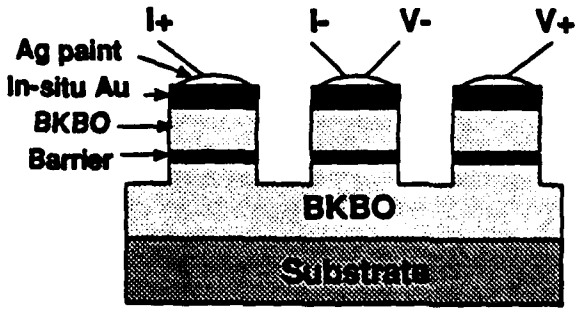


Fig. 1 Schematic of the tunnel junction configuration. The BKBO top electrode was not present for SIN measurements

*Supported by AFOSR Contract No. F49620-92-J-0415.
†Supported in part by AFOSR Contract No. F49620-92-C-0039
Manuscript received August 24, 1992.

to isolate areas of the samples for junction measurements. A schematic view of the configuration used for tunneling measurements is shown in Figure 1. Each junction was approximately 2 mm in diameter. Photolithography and Ar ion milling were used as well for patterning single BKBO films for $J_c$ measurements

Immediately following the deposition of each layer, in-situ studies were made of each film surface using LEED, RHEED, and XPS. Samples were evaluated upon removal from the chamber with EDX and x-ray diffraction. The latter included evaluations of orientation in the plane of the film as well as in the growth direction. Resistivity and ac susceptibility were measured as a function of temperature and, subsequent to patterning, I-V characteristics and $J_c$ were measured.

X-ray diffraction results on single-layer BKBO films are summarized in Figures 2 and 3. Figure 2 contains a typical $\phi$ scan measured for the BKBO{110} diffraction peaks. Four peaks spaced 90° apart were observed for BKBO films deposited on any of the (100)-orientation substrates. Comparisons between the BKBO{110} $\phi$ scans and similar scans obtained for the substrates showed that [001] directions in the substrates and the films were aligned. There was no evidence for a misalignment of BKBO(100) grains in the plane of the film. The lattice constant for films grown on any of these substrates was 0.4270 ± 0.0005 nm with no deviation from a cubic structure measured within this experimental uncertainty.

Figure 3(a) is a plot of BKBO (420) x-ray rocking-curve widths, $\Delta\omega$, as a function of the lattice mismatch between BKBO and various substrates. Generally, the narrowest $\Delta\omega$ values of 0.6-0.7° were found for BKBO films grown on the two substrate types with the smallest lattice mismatch, MgO and $SrTiO_3$. There was little difference in the results of two rocking-curve measurements which quantify distinctly different types of film texture. The first, $\Delta\omega_1$, is the standard

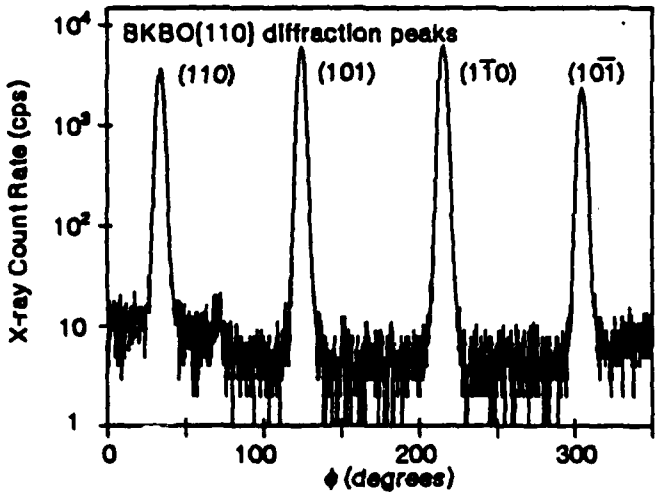


Fig. 2 The in-plane orientation of a BKBO(100) film grown on $NdGaO_3$(1110) shown with a $\phi$ scan of the BKBO{110} x-ray diffraction peaks. From a comparison of this scan with a similar scan from the substrate, it was confirmed that BKBO[001] was parallel to $NdGaO_3$[001]. There was no evidence for a fraction of the BKBO grains rotated out of alignment.

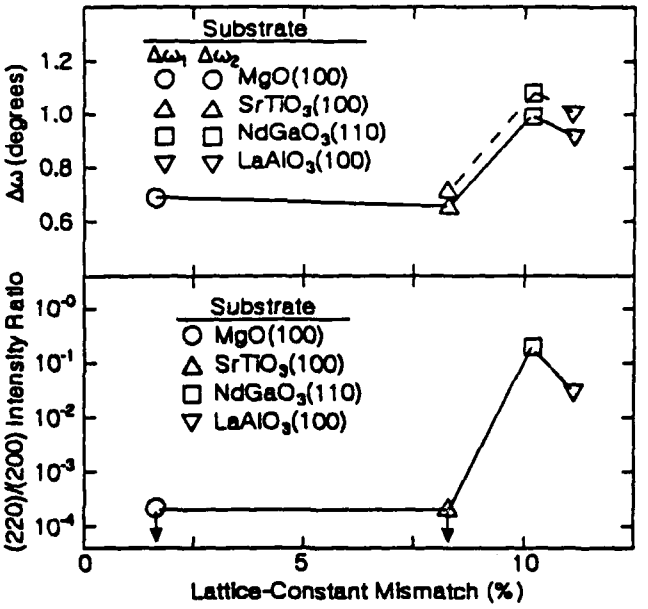


Fig. 3 Mosaic spread and fraction of misaligned grains for BKBO(100) films as a function of lattice mismatch. $\Delta\omega_1$ is the rocking curve width in the growth direction, and $\Delta\omega_2$ is that for {420} planes averaging growth-direction and in-plane reflections.

measurement of the mosaic spread in the growth direction. In principle, this value could be small in a film which was highly-textured in the growth direction even if there was no alignment whatsoever in the plane of the film. To obtain the second rocking curve width for the (420) planes, $\Delta\omega_2$, the film was rocked in a plane perpendicular to the one used in the measurement of $\Delta\omega_1$. This second value contains information about both the texture in the growth direction and texture in the plane of the film, thus quantifying the epitaxial relationship between the film and substrate observed in the $\phi$ scans.

Figure 3(b) shows that some grains with a BKBO(110) orientation were present in the films grown on substrates with the largest lattice mismatch, $LaAlO_3$ and $NdGaO_3$. There were no indications of BKBO(110) grains in the films on MgO or $SrTiO_3$. The most surprising of the results summarized in Figure 3 was that the structural properties of BKBO films grown on $SrTiO_3$(100) substrates with their 7% mismatch were as good as BKBO grown on MgO with just a 2% mismatch. The explanation most likely lies in the fact that BKBO and $SrTiO_3$ both have perovskite structures. The $SrTiO_3$(110) substrates were as effective as $SrTiO_3$(100) for obtaining a single growth orientation for BKBO and narrow rocking-curve widths of 0.7°.

Measurements of $T_c$ of BKBO films revealed very low resistivities of 70-100 μΩ-cm at temperatures just above the transition as well as fairly sharp transitions ($\Delta T_c$ = 1 K) which occurred consistently between 18 and 19 K. The films were metallic with a ratio of the resistivity at 300 K to that at 25 K of 1.6-1.7. Based on the x-ray diffraction data, it was not surprising that the lowest-resistivity films were those grown on $SrTiO_3$. However, as shown in Figure 4, even films grown on $LaAlO_3$ had low resistivities.

A comparison of $\rho$ vs. T curves from one set of samples on various substrates deposited as a single batch is shown in

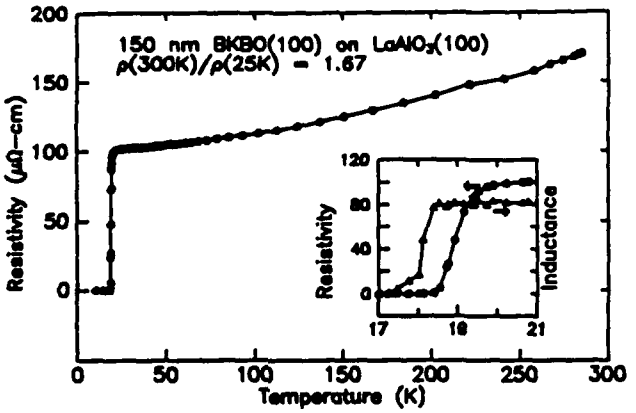


Fig. 4 Resistivity and ac susceptibility vs. temperature for a BKBO film. The ac susceptibility was an uncalibrated measurement of the change of inductance with temperature of a single copper coil placed against the film.

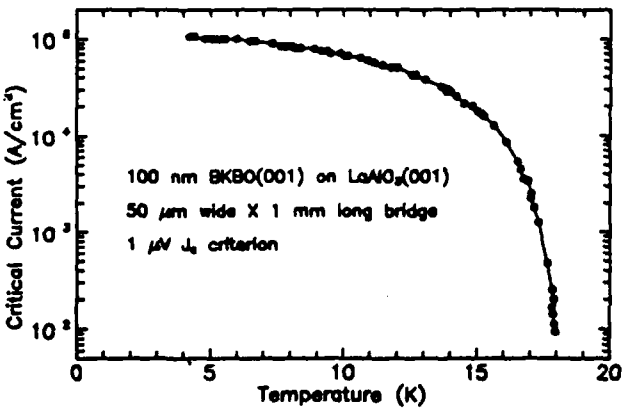


Fig. 6 Critical current density measurement of a BKBO film.

Figure 5. It can be seen that the $T_c$'s of films on $SrTiO_3$, $NdGaO_3$, and $LaAlO_3$ are higher and that the films have sharper transitions than that of a film on MgO. A film on $Al_2O_3$ was also measured but did not have a transition above 5 K..

The results of critical current density measurements made on a film grown on $LaAlO_3$ are shown in Figure 6. This film was found to have a $J_c \approx 10^4$ A/cm$^2$ just 2 K below the resistive transition and $10^5$ A/cm$^2$ at 4.2 K. Another important result of this experiment was the proof that these films were homogeneous and capable of being patterned without degradation.

EDX results showed the BKBO films to be potassium-rich. The lattice constant and $T_c$ measurements were consistent with those of bulk samples with composition, $x \approx 0.5$.[1] Raising the substrate temperature during film growth decreases the K content, which may be a necessary step in obtaining the highest-$T_c$ film composition.

For bilayer and trilayer structures, LEED and RHEED patterns indicated that each of the layers grew epitaxially. Figure 7 shows examples of LEED patterns obtained for an artificial barrier layer and BKBO top electrode. Figure 7(a) contains the LEED pattern for the BKBO counter-electrode of a trilayer grown on $NdGaO_3(110)$ with a $SrTiO_3$ barrier. Figure 7(b) shows an evaporated MgO barrier layer on BKBO grown on an MgO(100) substrate. It can be seen in both cases that a (100) orientation has been obtained. RHEED patterns for (100)-orientation films are shown in Figure 8. Figure 8(a) shows the pattern for a BKBO base electrode, Figures 8(b) and (c) show patterns for MgO and $SrTiO_3$ barrier layers, respectively, and Figure 8(d) has a RHEED pattern for a BKBO top electrode grown on a $SrTiO_3$ barrier. The streaked spots present indicate smoothness of the films, whereas the Kikuchi lines which are clearly visible in Figure 8(a) are typical of a well-ordered crystalline surface.

The LEED and RHEED data showed that the symmetry of the bulk of the BKBO films was evident even in the surface layer. LEED patterns are particularly surface-sensitive, indicating that the first monolayer on the surface had the desired structure. A comparison of XPS spectra recorded before and after the barrier layers were deposited showed that the Ba, K, and Bi photoelectron intensities were greatly attenuated by the presence of an overlayer, thus negating the possibility of the barrier layer having grown as islands around which the LEED and RHEED patterns in Figures 2(a), 3(b), and 3(c) might have been recording the symmetry of the underlying BKBO. Since RHEED patterns are determined by a surface layer approximately 2-5 nm thick, on the same order as the coherence length of BKBO, the RHEED pattern in Figure 3(a) was a measure of the structure of the surface layer which determines the gap voltage and temperature dependence of a tunnel junction.

X-ray photoelectron spectroscopy (XPS) probes a similar

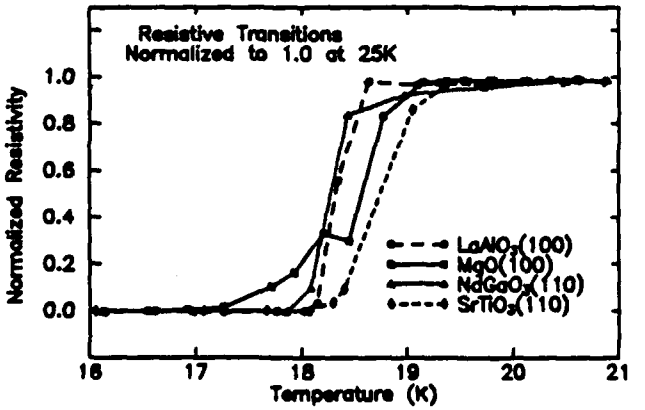


Fig. 5 A comparison of typical resistive transitions of BKBO on various substrates

Fig. 7 LEED patterns of (a) a BKBO counter-electrode and (b) an MgO barrier. The electron energies were 20.3 and 143.0 eV, respectively

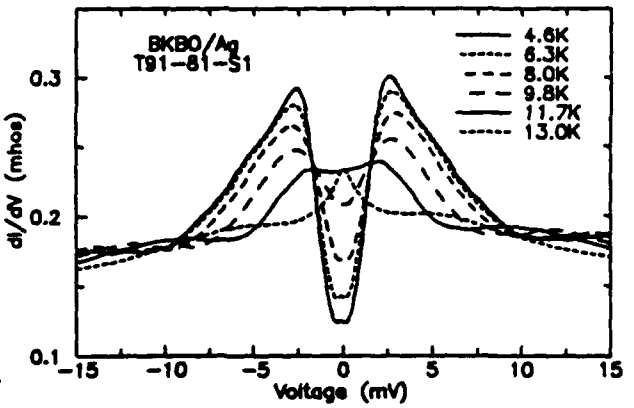


Fig. 10 SIN tunneling data for a BKBO/native barrier/Ag junction at various temperatures

Fig. 8 RHEED patterns for (a) a BKBO base electrode (b)MgO on BKBO (c)$SrTiO_3$ on BKBO (d) a BKBO counter-electrode grown on $SrTiO_3$.

distance into the surface of a film as RHEED, 0.2-0.5 nm. After artificial barrier layers were deposited on a BKBO base, the Ba, K, and Bi photoelectron spectra were recorded for comparison with the clean BKBO surface. No evidence was found for chemical shifts that would indicate reaction between the barrier materials and BKBO. However, upon exposure of the BKBO surface to air, a carbon peak was introduced in the XPS spectrum indicating that the native insulating layer formed on the BKBO was probably one of carbonates.

The current-voltage characteristics in Figures 9 and 10 from an SIN junction formed on a 15 K BKBO film using its native barrier, showed a gap of ~2.5 mV at 4.2 K which closed by 13 K. A value for $2\Delta/kT$ of 4.1 was obtained, indicating strong electron-phonon coupling. Tunneling measurements through artificial barriers resulted in shorting due to pinholes, presumably because the barriers were too thin.

In conclusion, we have grown well-aligned, very low-resistivity BKBO films with reproducible $T_c$'s and have demonstrated that these films can indeed be fabricated into epitaxial trilayers with a great potential for use in SIS junctions.

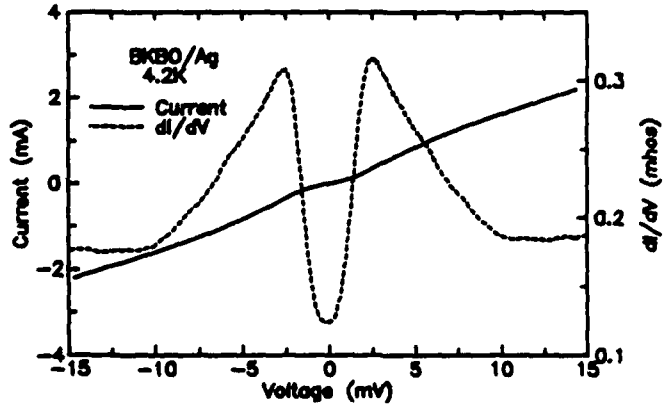


Fig. 9 SIN tunneling data for a BKBO/native barrier/Ag junction at 4.2 K

The authors would like to acknowledge B. A. Baumert's thesis advisor, M.E. McHenry, and are grateful to M.G. Forrester and J.D. McCambridge for a great deal of advice and assistance as well as to J.H. Uphoff, R.L. Grassel, C.L. Jones, A.M. Stewart, and G.M. Burcin for technical assistance.

*Note added in proof:* After the submission date of this paper, BKBO films were deposited at approximately 25°C higher substrate temperature. This was sufficient to reduce the potassium content of the films and raise $T_c$ to >26 K. There is no indication that the recent decrease in potassium or increase in $T_c$ in the BKBO electrodes have an effect on the structural or electrical properties of BKBO trilayer structures.

[1] S. Pei, J.D. Jorgensen, B. Dabrowski, D.G. Hinks, D.R. Richards, A.E. Mitchell, J. M. Newsam, S.K. Sinha, D. Vaknin, and A.J. Jacobson, "Structural phase diagram of the $Ba_{1-x}K_xBiO_3$ system," Phys. Rev. B, vol. 41, pp. 4126-4141, 1990.

[2] H. Sato, H. Takagi, and S. Uchida, "Gap observation by tunneling measurement on superconducting BKBO Thin Films: A Finite Energy Gap in BKBO," Physica C, vol. 169, pp.391-395, 1990.

[3] Q. Huang, J.F. Zasadzinski, K.E. Gray, D.R. Richards, and D.G. Hinks, "Ideal tunneling characteristics in BKBO point-contact junctions with Au and Nb tips," Appl. Phys. Lett., vol 57, p. 2356, 1990.

[4] F. Sharifi, A. Pargellis, R.C. Dynes, B. Miller, E.S. Hellman, J. Rosamilia, and E.H. Hartford, "Electron tunneling in the high-$T_c$ bismuthate superconductors," Phys. Rev. B, vol. 44, p. 12521, 1991.

[5] B.M. Moon, C.E. Platt, R.A. Schweinfurth, and D.J. Van Harlingen, "In-situ pulsed laser deposition of superconducting BKBO thin films," Appl. Phys. Lett., vol. 59, pp. 1905-07, 1991.

[6] C.J. Hou, R.L. Fink, C. Hillbert, and H. Kroger, "Low-leakage thin-film superconductor-insulator-normal metal tunnel junctions on co-evaporated BRBO and rf-sputtered BKBO," Appl. Phys. Lett., vol. 60, pp. 1262-1264, 1992.

[7] A.N. Pargellis, F. Sharifi, R.C. Dynes, B. Miller, E.S. Hellman, J. M. Rosamilia, and E.H. Hartford, "All high-$T_c$ Josephson tunnel junction: BKBO/BKBO junctions," Appl. Phys. Lett., vol. 58, pp. 95-97, 1991.

[8] E.S. Hellman, S. Martin, E.H. Hartford, D.J. Werder, G.M. Roesler, and P.M. Tedrow, "$Ba_{1-x}K_xBiO_3$ sandwich-type tunnel junctions grown by molecular beam epitaxy," to be published in Appl. Phys. Lett., 1992.

[9] R.L. Fink, M. Thompson, C. Hilbert, and H. Kroger, "Hysteretic Josephson junctions from YBCO/$SrTiO_3$/BKBO trilayer films," Appl. Phys. Lett., vol. 61, pp. 595-597, 1992.

# OPTICAL CONDUCTIVITY OF THE HIGH-$T_c$'s: SEARCH FOR THE ENERGY GAP

D.B. TANNER, F. GAO, and M. QUIJADA
Department of Physics, University of Florida, Gainesville, FL 32611
D.B. ROMERO
Department of Physics, Virginia Tech, Blacksburg, VA 24061
J.P. RICE, and D.M. GINSBERG
Department of Physics and Materials Research
Laboratory, University of Illinois, Urbana, IL 61801
J. TALVACCHIO and M.G. FORRESTER
Westinghouse Science and Technology Center, Pittsburgh, Pennsylvania 15235
L. FORRO, D. MANDRUS, and L. MIHALY
Department of Physics, SUNY, Stony Brook, NY 11794
G.L. CARR
Grumman Corporate Research Center, Bethpage, NY 11714
G. P. WILLIAMS
National Synchrotron Light Source, Brookhaven
National Laboratory, Upton, NY 11973

**ABSTRACT**—The infrared absorption of oxide superconductors will be discussed. In the normal state, $\sigma_1(\omega)$ consists of a strongly $T$-dependent part in the far infrared, above which is a weakly-$T$-dependent midinfrared absorption. In the superconducting state, there is absorption to very low frequencies, well below where the superconducting gap is expected to be. It is argued that this absorption is due to a second ("midinfrared") component which is only weakly affected by the onset of superconductivity. The free carrier component is in the clean limit and most of its oscillator strength goes into the superfluid condensate zero-frequency delta function response.

**Key words:** High-$T_c$, infrared

## INTRODUCTION

An ordinary superconductor has a gap $\Delta$ in its excitation spectrum. This gap causes the frequency-dependent conductivity $\sigma_{1s}(\omega)$ to be zero up to $\omega = 2\Delta$; above this frequency $\sigma_{1s}(\omega)$ rises to join the normal-state conductivity at several times $2\Delta$. The area removed from $\sigma_{1s}(\omega)$ appears under the zero-frequency delta function of the superconductor. The superconductor has zero absorption (100 % reflectivity) at frequencies below $2\Delta$ and reduced absorption up to several times $2\Delta$.

Far-infrared reflection and transmission measurements were important in establishing the existence of a gap in metallic superconductors and in determining its magnitude. (Glover 1956, Ginsberg 1960, Palmer 1968, Drew 1967) With the discovery of the high-$T_c$ compounds, there have been many attempts to do the same. (Timusk 1989, Tanner 1992) At the present time there is a lot of controversy—to say the least—about infrared determinations of the gap. This is a very complicated issue, and so we discuss it in some detail in the following paragraphs.

Very similar $ab$-plane reflectance spectra have been presented by a number of workers. (Timusk 1988, Thomas 1988, Schützmann 1989, Kamarás 1990, Renk 1990, Schlesinger 1990a, Cooper 1989, Orenstein 1990, Schlesinger 1987, Reedyk 1988, Collins 1989) In the superconducting state, the reflectance cannot be distinguished from 100% for $\omega \lesssim 140$ cm$^{-1}$ (17 meV). Above 140 cm$^{-1}$ there is a clear increase in absorption, and the reflectance drops to a plateau of about

98% which extends to a shoulder at $\approx 400$ cm$^{-1}$ (50 meV). At higher frequencies, the reflectance drops to join the normal-state data.

Both the 140 cm$^{-1}$ onset and the 400 cm$^{-1}$ shoulder have been assigned to the superconducting gap. Thomas *et al.*(1988) suggested that the apparent onset of absorption at $\approx$ 140 cm$^{-1}$ in $ab$-plane data for reduced $T_c$ samples might be the gap; this would give $2\Delta/k_BT_c = 3.2$. Schützmann *et al.*(1989) also put the gap at 140 cm$^{-1}$ in measurements of 91 K $T_c$ samples, which would make $2\Delta/k_BT_c = 2.1$

Schlesinger *et al.*(1987, 1990, Collins 1989) have interpreted the 400 cm$^{-1}$ shoulder as the gap. When the ratio of superconducting to normal state reflectance, $\mathcal{R}_s/\mathcal{R}_n$, is plotted, this shoulder appears as a maximum. A maximum in $\mathcal{R}_s/\mathcal{R}_n$ does occur at $2\Delta$ in ordinary superconductors because $\mathcal{R}_s$ is 100% out to $2\Delta$ and then decreases to join $\mathcal{R}_n$, which has been decreasing like $1 - A\sqrt{\omega}$. This similarity to ordinary superconductors was the motivation for the $8k_BT_c$ assignment. (Schlesinger 1987, Collins 1989, Schlesinger 1990a, Schützmann 1989)

Data on untwinned crystals of $YBa_2Cu_3O_{7-\delta}$ show for $T = 30$ K an apparent 99–100% reflectance out to 500 cm$^{-1}$ ($8k_BT_c$) for $\vec{E} \parallel a$ at which point there is a shoulder and decreasing reflectance. (Schlesinger 1990b, Rotter 1991) For $\vec{E} \parallel b$, the reflectance is smaller, with the shoulder less pronounced. Schlesinger *et al.*(1990) argue that the gap for $ab$-plane carriers must correspond to this onset and attribute the absorption below this frequency to carriers on the chains.

However, a more sensitive experiment than reflectance is direct bolometric absorption. Such experiments have been carried out by Pham *et al.*(1990, 1991) In untwinned crystals, they find a finite absorption down to their low frequency limit of 80 cm$^{-1}$ ($1.2k_BT_c$) at all frequencies for both $E \parallel a$ and $E \parallel b$. The absorption for $E \parallel a$ is ~0.3% at 150 cm$^{-1}$ and below. The direct absorption data are in agreement with reflectance data, but the better signal/noise ratio allows absorption to be seen at frequencies where the reflectance appears to reach 100%.

In this paper, we discuss the gap issue, using recent data on single-domain $YBa_2Cu_3O_{7-\delta}$ crystals, free-standing $Bi_2Sr_2CaCu_2O_8$ crystals, and $La_{2-x}Sr_xCuO_4$ thin films.

## EXPERIMENTAL DETAILS

The single-domain crystals were prepared at the University of Illinois. The growth technique has been described previously. (Friedmann 1990) The crystals studied were about 2×2 mm in size and had extremely high quality surfaces. $T_c$ was above 90 K. The reflectance was measured using Fourier and grating spectrometers and the optical constants determined using Kramers-Kronig analysis. (Quijada 1992) Estimated error in the far-infrared reflectance measurements, from reproducibility of different samples, is ±1–2%.

$La_{2-x}Sr_xCuO_4$ films were grown by off-axis magnetron sputtering on $SrTiO_3$ substrates at Westinghouse. Growth conditions and film properties have been described previously. (Talvacchio 1990) The film studied in detail was nearly 1 cm$^2$ in area, 8000 Å thick, and had good quality surfaces. X-ray analysis showed the film to be highly oriented with the $c$-axis normal to the surface. $T_c$ was 31 K and $x$ is $\approx 0.17$. The reflectance was measured using Fourier and grating spectrometers and the optical constants determined using Kramers-Kronig analysis. (Gao 1992) No features attributable to the substrate could be seen in the spectra. Estimated error in the far-infrared reflectance measurements, from reproducibility of different samples, is ±0.5%.

Free-standing films (or flakes) of $Bi_2Sr_2CaCu_2O_8$ were prepared and characterized at SUNY Stony Brook as described in an earlier report. (Forro 1990) The samples were approximately 0.3 mm$^2$ in area and 1300–2000 Å thick. $T_c$ was $\approx$ 82 K The transmittance was measured using Fourier and grating spectrometers and the optical constants determined using Kramers-Kronig analysis. (Romero 1991, Romero 1992a, Romero 1992b) Estimated relative error in the

far-infrared transmittance measurements, from reproducibility of different samples, is ±5%. We note that transmittance is potentially more accurate than reflectance because an accurate 100% level is not required and that a 5% error in transmittance gives smaller errors in $\sigma_1(\omega)$ than a 0.5% error in reflectance. This is because the "signal" in the reflectance measurement is essentially $1 - \mathcal{R}$, and when $\mathcal{R} \rightarrow 1$ the signal goes to zero.

## EXPERIMENTAL RESULTS

Fig. 1 shows the optical conductivity of a $YBa_2Cu_3O_{7-\delta}$ single crystal at three temperatures. The magnitude of the conductivity for $\vec{E} \parallel b$ is larger than for $\vec{E} \parallel a$ but otherwise the two spectra are similar and resemble the conductivity of twinned $YBa_2Cu_3O_{7-\delta}$ crystals (Orenstein 1990, Schlesinger 1990a) and films. (Schützmann 1989, Kamarás 1990) There is a strongly $T$ dependent peak at low frequencies above $T_c$; below $T_c$ a considerable amount of low-frequency oscillator strength is removed to the zero-frequency delta function conductivity of the superfluid. (That the oscillator strength moves to zero frequency and not, say, to some high energy can be proved by looking at the real part of the dielectric function. See Ref. Kamarás 1990 for an example.)

Below $T_c$ there is a finite value of $\sigma_1(\omega)$ maintained to the lowest frequency measured (180 $cm^{-1}$) for both polarizations, in agreement with the results of Pham *et al.*(1991) (However, we should note that the uncertainties in the determination of $\sigma_1(\omega)$ are relatively large and reach nearly 100% at the low frequency limit of 180 $cm^{-1}$) A notch-like minimum is observed for both polarizations at around 500 $cm^{-1}$—above and below $T_c$—but no "gap" occurs in the spectrum at this frequency.

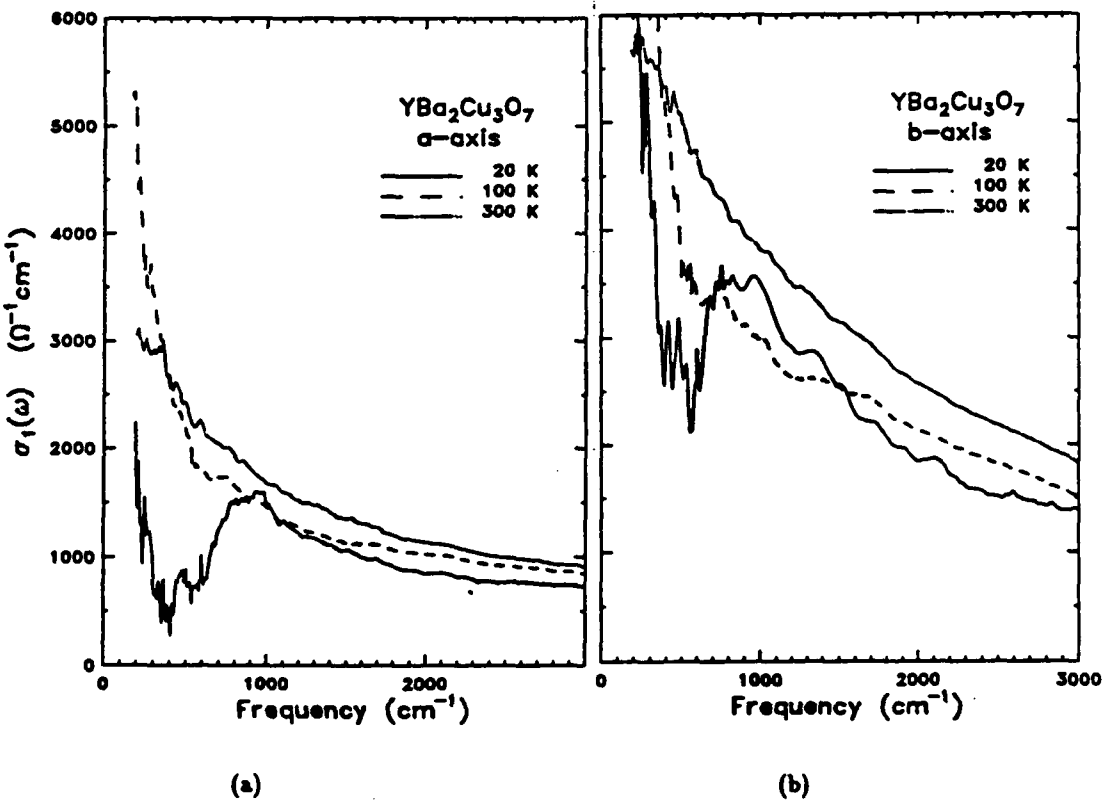


Fig. 1. Optical conductivity of $YBa_2Cu_3O_{7-\delta}$ at three temperatures. (a) $\vec{E} \parallel a$. (b) $\vec{E} \parallel b$.

Fig. 2 shows the optical conductivity of $La_{2-x}Sr_xCuO_4$ at several temperatures. The inset shows (on a logarithmic frequency scale) the data into the visible region. As in the case of

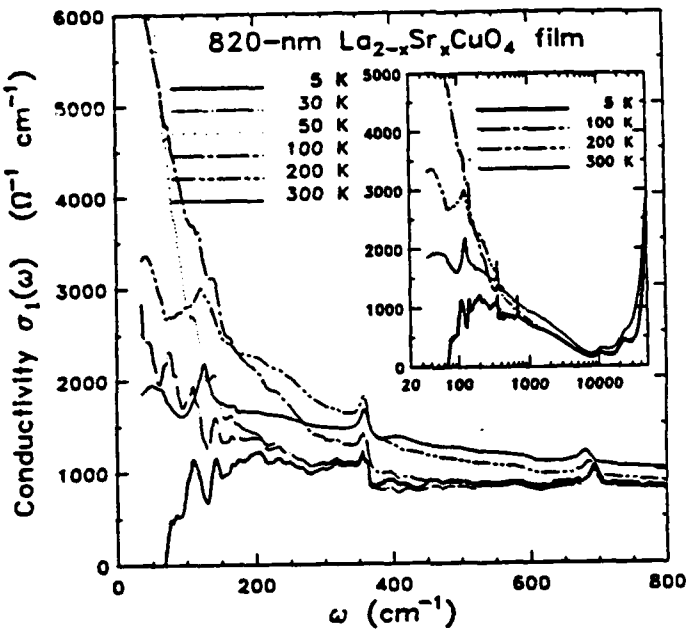


Fig. 2. Optical conductivity of $La_{2-x}Sr_xCuO_4$ at several temperatures. The inset shows the wide-frequency-range conductivity.

$YBa_2Cu_3O_{7-\delta}$, there is a strong $T$ dependent peak at low frequencies. Below $T_c$ a substantial amount of oscillator strength goes into the condensate.

The 5 K conductivity curve shows a threshold at 70 $cm^{-1}$ but this is a consequence of the extrapolation; the uncertainty at 70 $cm^{-1}$ is $\pm 600\ \Omega^{-1}cm^{-1}$. This uncertainty is illustrated in Fig. 3, which shows the effect of scaling the reflectance up or down by the estimated uncertainty of $\pm 0.5\%$. Propagated to $\sigma_1(\omega)$, this error becomes $\pm 100\%$ by $100cm^{-1}$. Another way of stating the same result is that our data is consistent with zero absorption below 100 $cm^{-1}$ but not above 100 $cm^{-1}$.

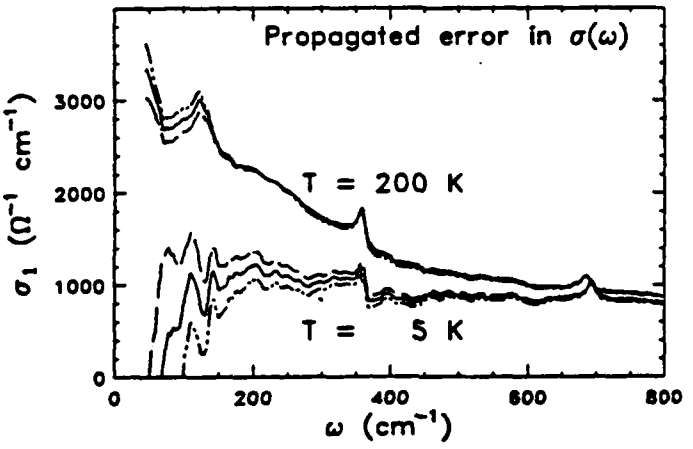


Fig. 3. Propagated uncertainty in $\sigma_1(\omega)$ from an uncertainty in reflectance of $\pm 0.5\%$.

Fig. 4 shows the optical conductivity of $Bi_2Sr_2CaCu_2O_8$ at several temperatures. As in the other materials, the normal-state conductivity shows a strongly $T$-dependent upturn at low frequencies but minimal temperature dependence at higher frequencies. Below $T_c$, lots of

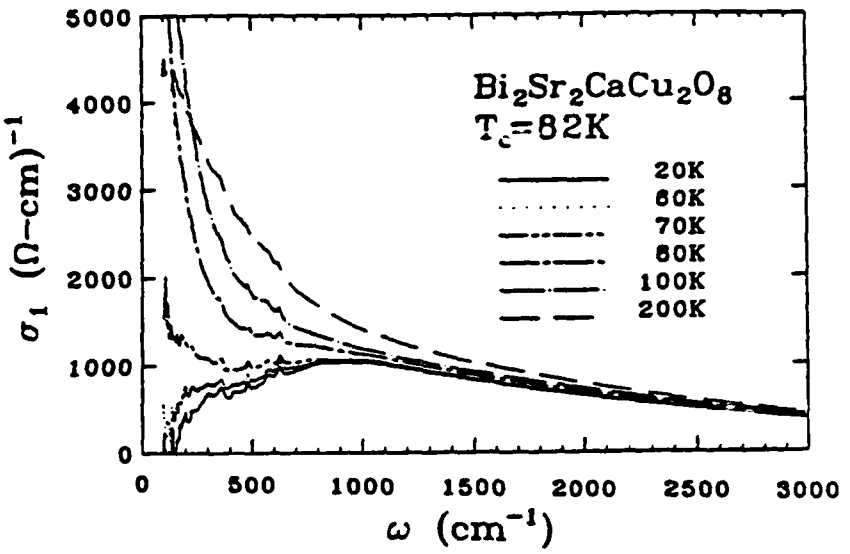


Fig. 4. Optical conductivity of $Bi_2Sr_2CaCu_2O_8$ at various temperatures above and below $T_c$.

oscillator strength moves into the condensate, but the conductivity is finite to 110 cm$^{-1}$. The error here is relatively small; there is definitely a positive value of $\sigma_1(\omega)$ at 140cm$^{-1}$ and above.

## DISCUSSION

We return now to the question of the superconducting gap. The results for thresholds in the optical conductivity are summarized in Table I. In all cases, the absorption threshold is well below $8k_BT_c$; only in $La_{2-x}Sr_xCuO_4$ would the data be consistent with a BCS gap value.

Table I. Energy scales in high $T_c$ superconductors.

| Material | Reference | $T_c$ | $3.5k_BT_c$ | $8k_BT_c$ | Absorption threshold |
|---|---|---|---|---|---|
| | | K | cm$^{-1}$ | cm$^{-1}$ | cm$^{-1}$ |
| $YBa_2Cu_3O_{7-\delta}$ $\vec{E} \parallel a$ | This work | 90 | 220 | 500 | < 200 |
| $YBa_2Cu_3O_{7-\delta}$ $\vec{E} \parallel a$ | Pham *et al.* (1990) | 90 | 220 | 500 | < 80 |
| $YBa_2Cu_3O_{7-\delta}$ twinned | Many. See Tanner and Timusk (1992). | 92 | 230 | 511 | < 140 |
| $Bi_2Sr_2CaCu_2O_8$ | This work | 82 | 200 | 450 | < 140 |
| $La_{2-x}Sr_xCuO_4$ | This work | 31 | 75 | 170 | < 100 |

This finite conductivity to low frequencies is difficult to interpret by analogy to conventional superconductors, where the picture of a superconducting gap works well. The difficulty is especially strong for $Bi_2Sr_2CaCu_2O_8$ where photoemission (Chang1989, Olson 1990) gives a rather convincing picture of a gap near $7k_BT_c$. As Fig. 4 shows, there is no particular anomaly in the spectrum at this frequency (400 cm$^{-1}$); indeed most of the fine structure in this region is also evident above $T_c$.

One resolution of this dilemma is to postulate that there are two contributions (or components) to the low-frequency optical conductivity: free carriers, which are responsible for the

dc conductivity and which condense to form the superfluid below $T_c$, and bound carriers, which are relatively inert and which are not much affected by the superconducting transition. A wide variety of data have been analyzed in this picture. (Timusk 1989, Tanner 1992, Kamarás 1988, Bonn 1988, Timusk 1988, Thomas 1988, Schützmann 1989, Kamarás 1990, Renk 1890, Cooper 1989)

The dielectric function is then a sum free carriers (*i.e.*, a Drude model) and the midinfrared bound carrier terms,

$$\epsilon(\omega) = \epsilon_{MIR} - \frac{\omega_{pD}^2}{\omega^2 + i\omega/\tau} + \epsilon_\infty \tag{1}$$

where $\omega_{pD}$ is the plasma frequency of the free carriers and $1/\tau$ is their (essentially $\omega$-independent) relaxation rate. The $T$-linear temperature dependence of the resistivity is assumed to come from the temperature dependence of $1/\tau$ since in the Drude model, $\rho = 4\pi/\omega_{pD}^2\tau$. The bound carriers are in a broad, nearly $T$-independent, band throughout the midinfrared.

The midinfrared contribution to the data of Fig. 4 is illustrated by Fig. 5. A Drude function has been subtracted from the total conductivity in order to obtain these curves. The Drude contribution has a plasma frequency of 10,300 $cm^{-1}$, a $T$-linear scattering rate, and agrees well with the dc conductivity. (Romero 1992) The mid-infrared contribution is almost independent of temperature above $T_c$, in agreement with hypothesis, but there are some systematic variations around 0.1 eV. Below $T_c$ the Drude contribution has condensed, revealing more clearly the midinfrared band.

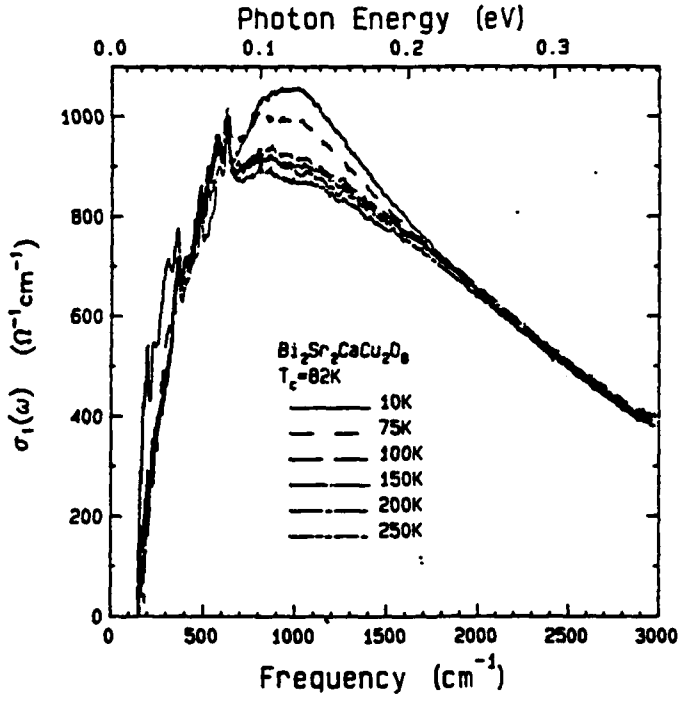


**Fig. 5. The midinfrared contribution to the conductivity of $Bi_2Sr_2CaCu_2O_8$ crystals, obtained by subtracting a Drude dielectric function from the data in Fig. 4.**

If the two-component picture of the midinfrared absorption is correct, then the presence of the second component can obscure any gap absorption and make its determination difficult. This effect occurred some time ago in early studies of $La_{2-x}Sr_xCuO_4$ ceramics, which showed a sharp reflectance drop in the 50 $cm^{-1}$ region. This initially was assigned to the gap, but it later was shown to be caused by a zero-crossing of $\epsilon_1(\omega)$, due to an interplay between the negative

contribution of the superfluid and a strong positive contribution from a phonon. (Bonn 1987, Sherwin 1988) Using a similar approach, Timusk *et al.*(Timusk 1988) argued that the maximum seen in $\mathcal{R}_s/\mathcal{R}_n$ in $YBa_2Cu_3O_{7-\delta}$ was affected by dispersion as well.

Kamarás *et al.*(1990) showed that various features in the superconducting-state conductivity spectrum of $YBa_2Cu_3O_{7-\delta}$ which have been assigned to the gap can also be seen in the normal-state conductivity. (This is also evident in the $Bi_2Sr_2CaCu_2O_8$ data of Fig. 5, where the total conductivity below $T_c$ resembles closely the midinfrared contribution above $T_c$.) Because the features persist above $T_c$, it was argued that they were from the non-Drude midinfrared absorption and not associated with the superconducting gap. Above $T_c$ this absorption is partially masked by the absorption of the free carriers; below $T_c$, when the free carriers condense into a delta function, the midinfrared absorption becomes fully revealed.

The question naturally arises: why should the gap not seen? Kamarás *et al.*(1990) suggested that this is because the high-$T_c$ materials are in the "clean limit," with $2\Delta \gg 1/\tau$. In this limit, all of the free-carrier oscillator strength exists at low frequencies and goes into the zero-frequency delta function conductivity of the superconductor. None is left for transitions across the gap. The presence of the midinfrared absorption is a key point in the clean limit argument. Given sufficient sensitivity, the gap can be seen even in the clean limit of ordinary metals with no other low energy excitations. However, in the presence of the midinfrared absorption, especially if there is some temperature dependence in it, picking out the gap becomes more difficult.

## ACKNOWLEDGEMENTS

This research has been supported by National Science Foundation grants DMR-9101676 (Florida), DMR-9017371 (Illinois), DMR-9016456 (Stony Brook), and AFOSR contract F49620-91-C-0034.

## REFERENCES

D.A. Bonn, J.E. Greedan, C.V. Stager, T. Timusk, M.G. Doss, S.L. Herr, K. Kamarás, C.D. Porter, D.B. Tanner, J.M. Tarascon, W.R. McKinnon, and L.H. Greene, *Phys. Rev. B* 35 (1987) 8843.

D.A. Bonn, A.H. O'Reilly, J.E. Greedan, C.V. Stager, T. Timusk, K. Kamarás, and D.B. Tanner, *Phys. Rev. B* 37 (1988) 1574.

Y. Chang, Ming Tang, R. Zanoni, M. Onellion, Robert Joynt, D.L. Huber, G. Margaritondo, P.A. Morris, W.A. Bonner, J.M. Tarascon, and N.G. Stoffel, *Phys. Rev. Lett.* 63 (1989) 101.

R.T. Collins, Z. Schlesinger, F. Holtzberg, and C. Feild, *Phys. Rev. Lett.* 63 (1989) 422.

S.L. Cooper, G.A. Thomas, J. Orenstein, D.H. Rapkine, M. Capizzi, T. Timusk, A.J. Millis, L.F. Schneemeyer, and J.V. Waszczak, *Phys. Rev. B* 40 (1989) 11358.

H.D. Drew and A.J. Sievers, *Phys. Rev. Lett.* 19 (1967) 697.

L. Forro, D. Mandrus, R. Reeder, B. Keszei, and L. Mihaly, *J. Appl. Phys.* 68 (1990) 4876.

T.A. Friedmann, W.M. Rabin, J. Giapintzakis, J.P. Rice, and D.M. Ginsberg, *Phys. Rev. B* 42 (1990) 6217.

Feng Gao, D.B. Romero, D.B. Tanner, J. Talvacchio, and M.G. Forrester, *Phys. Rev. B*, submitted.

D.M. Ginsberg and M. Tinkham, *Phys. Rev.* 118 (1960) 990.

R.E. Glover and M. Tinkham, *Phys. Rev. B* 107 (1956) 844; 108, 243, (1957).

K. Kamarás, C.D. Porter, M.G. Doss, S.L. Herr, D.B. Tanner, D.A. Bonn, J.E. Greedan, A.H. O'Reilly, C.V. Stager, and T. Timusk, *Phys. Rev. Lett.* 60 (1988) 969.

K. Kamarás, S.L. Herr, C.D. Porter, N. Tache, D.B. Tanner, S. Etemad, T. Venkatesan, E. Chase A. Inam, X.D. Wu, M.S. Hegde, and B. Dutta, *Phys. Rev. Lett.* **64** (1990) 84.

C.G. Olson, R. Liu, D.W. Lynch, R.S. List, A.J. Arko, B.W. Veal, Y.C. Chang, P.Z. Jiang and A.P. Paulikas, *Phys. Rev. B* **42** (1990) 381.

J. Qrenstein, G.A. Thomas, A.J. Millis, S.L. Cooper, D.H. Rapkine, T. Timusk, L.F. Schneemeyer, and J.V. Waszczak, *Phys. Rev. B* **42** (1990) 6342.

L.H. Palmer and M. Tinkham, *Phys. Rev.* **165** (1968) 588.

T. Pham, H.D. Drew, S.H. Moseley, and J.Z. Liu, *Phys. Rev. B* **41** (1990) 11,681.

T. Pham, H.D. Drew, S.H. Moseley, and J.Z. Liu, *Phys. Rev. B* **44** (1991) 5377.

M. Quijada, D.B. Tanner, J.P. Rice, and D.M. Ginsberg, unpublished.

M. Reedyk, D.A. Bonn, J.D. Garrett, J.E. Greedan, C.V. Stager, T. Timusk, K. Kamarás, and D.B. Tanner, *Phys. Rev. B* **38** (1988) 11981.

K.F. Renk, H. Eschrig, U. Hoffman, J. Keller, J. Schützmann, and W. Ose, *Physica C* **165** (1990) 1.

D.B. Romero, G.L. Carr, D.B. Tanner, L. Forro, D. Mandrus, L. Mihály, and G.P. Williams, *Phys. Rev. B* **44** (1991) 2818.

D.B. Romero, C.D. Porter, D.B. Tanner, L. Forro, D. Mandrus, L.Mihaly, G.L. Carr, G.P. Williams, *Phys. Rev. Lett.* **68** (1992) 1590.

D.B. Romero, C.D. Porter, D.B. Tanner, L. Forro, D. Mandrus, L. Mihaly, G.L. Carr, and G. P. Williams, *Solid State Comm.* **82** (1992) 183.

L.D. Rotter, Z. Schlesinger, R.T. Collins, F. Holtzberg, C. Field, U. Welp, G.W. Crabtree, J.Z. Liu, and Y. Fang G. Vandervoort, and S. Fleshler, *Phys. Rev. Lett.* **67** (1991) 2741.

Z. Schlesinger, R.T. Collins, D.L. Kaiser, and F. Holtzberg, *Phys. Rev. Lett.* **59** (1987) 1958.

Z. Schlesinger, R.T. Collins, F. Holtzberg, C. Feild, G. Koren, and A. Gupta, *Phys. Rev. B* **41** (1990) 11,237.

Z. Schlesinger, R.T. Collins, F. Holtzberg, C. Feild, S.H. Blanton, U. Welp, G.W. Crabtree, Y. Fang, and J.Z. Liu, *Phys. Rev. Lett.* **65** (1990) 801.

J. Schützmann, W. Ose, J. Keller, K.F. Renk, B. Roas, L. Schultz, and G. Saemann-Ischenko, *Europhys. Lett.* **8**, 679 (1989); U. Hoffmann *et al.*, *Solid State Comm.* **70** (1989) 325.

M.S. Sherwin, P.L. Richards, and A. Zettl, *Phys. Rev. B* **37** (1988) 1587.

J. Talvacchio, M.G. Forrester, J.R. Gavaler, and T.T. Braggins in *Science and Technology of Thin Film Superconductors II*, edited by R. McConnel and S.A. Wolf (Plenum, New York, 1990).

D.B. Tanner and T. Timusk in *Physical Properties of High Temperature Superconductors III*, D.M. Ginsberg, editor, (World Scientific, Singapore, 1992) p. 363.

G.A. Thomas, J. Orenstein, D.H. Rapkine, M. Capizzi, A.J. Millis, R.N. Bhatt, L.F. Schneemeyer, and J.V. Waszczak, *Phys. Rev. Lett.* **61** (1988) 1313.

T. Timusk, S.L. Herr, K. Kamarás, C.D. Porter, D.B. Tanner, D.A. Bonn, J.D. Garrett, C.V. Stager, J.E. Greedan, and M. Reedyk, *Phys. Rev. B* **38** (1988) 6683.

T. Timusk and D.B. Tanner in *Physical Properties of High Temperature Superconductors I*, D.M. Ginsberg, editor, (World Scientific, Singapore, 1989) p. 339.

MICROWAVE JOURNAL REVIEWED EDITORIAL BOARD

# In-Situ Deposition of YBCO Films on Wafers by Off-Axis Sputtering†

T.T. Braggins, J.R. Gavaler and J. Talvacchio
*Westinghouse Science and Technology Center*
*Pittsburgh, PA*

*YBCO thin films have been magnetron-sputtered in the off-axis geometry from stoichiometric targets on $LaAlO_3$ substrates resulting in in-situ superconducting films with resistive and inductive $T_c$s of 90°K. Double-sided sputter deposition on 2" diameter, radiantly-heated substrates performed sequentially on each side is reported. Low surface resistances in the range of 0.3 to 0.7 mΩ at 77°K and 10 GHz for double-sided films are attained.*

## Introduction

One of the first applications of high temperature superconductors (HTS) was the development of passive microwave components. Much of the work has focused on thin films of the HTS $YBa_2Cu_3O_7$ (YBCO) deposited on lattice-matched substrates. Except for the most demanding applications where very low loss sapphire substrates are required, $LaAlO_3$ is the preferred substrate owing to its close lattice match, moderately low loss and moderately high dielectric constant.[1] It has been shown that highly C-axis oriented YBCO films with high transition temperatures $T_c$ and low surface resistances $R_s$ at microwave frequencies can be deposited over large (2" diameter) areas using a technique in which silver paste is used to attach the wafer to the sample block.[2] Although this method provides good thermal contact and uniformity, it precludes using the back side of the wafer for a second YBCO layer and, because of the fragility of $LaAlO_3$, results in intolerable wafer breakage for large area samples.

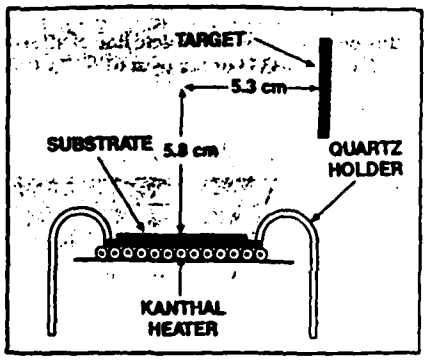


Fig. 1 Sputter-down configuration for off-axis sputtering.

For several types of microwave components, such as microstrip filters, the proximity of a superconducting ground plane is highly desirable. Therefore, it is necessary to develop techniques for the deposition of YBCO films on both sides of a substrate. Larger diameter (2" to 4") substrates will become increasingly important for components that must be critically matched. In addition, they provide an economic advantage because they can fabricate many dies per processing cycle. In this paper, the techniques for double-sided deposition of high quality YBCO films on 2" diameter substrates and the characterization of these films are described.

## Experimental Method

The experimental techniques that are used for the in-situ growth of YBCO films by off-axis sputtering have been reported previously.[2] For this paper, the geometry (relative position of source and sample) is unchanged except that a sputter-down rather than sputter-up configuration is used, as shown in Figure 1. This is so because the samples are rested on a quartz plate that covers 3" diameter kanthal heater. The sample is stationary during film deposition. In this configuration, 20 large area wafers have been processed. Sputtering is performed from a 2" diameter stoichiometric YBCO target using 110 W of RF power in a continuously pumped gaseous atmosphere consisting of 200 mtorr argon, 50 mtorr oxygen and 20 mtorr water vapor. Small variations of the gas composition are not critical.[3] However, it has been found that small additions of water vapor are beneficial, yielding consistently >90°K superconducting transition temperatures.[3] The sample temperature during deposition, determined by infrared pyrometry, is 670°C with an estimated accuracy of 20°C. Under these conditions, a deposition rate of 20 nm/hr is obtained. Following growth, the sample is cooled in 25 torr $O_2$ to 400°C, where it is held for 20 minutes prior to cooling to room temperature. For double-sided depositions, the chamber is opened, the sample is turned over and the process repeated.

The critical temperature was measured both resistively, using the standard Van der Pauw technique, and as a change of inductance for a copper coil placed against the film and driven at 100 kHz. Resistive $T_c$

†Supported in part by AFOSR Contract No. F-49620-91-C-0034.

[Continued on page 108]

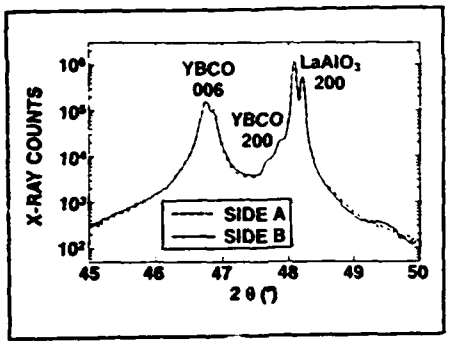


Fig. 2 X-ray diffraction pattern for side A and side B of a double-sided film showing very small a-axis (200) contribution.

**TABLE I**
**SURFACE RESISTANCE MEASUREMENTS MADE ON TEST CHIPS TAKEN FROM 2" WAFERS**

| Sample Numbers | $R_s$ (mΩ) 77°K, 10 GHz Side A | $R_s$ (mΩ) 77°K, 10 GHz Side B |
|---|---|---|
| 1/2 | 0.68 | 0.70 |
| 3/4 | 0.63 | 0.69 |
| 5/6 | 0.63 | 0.68 |
| 9/10 | — | 0.30 |
| 12/13 | — | 0.40 |

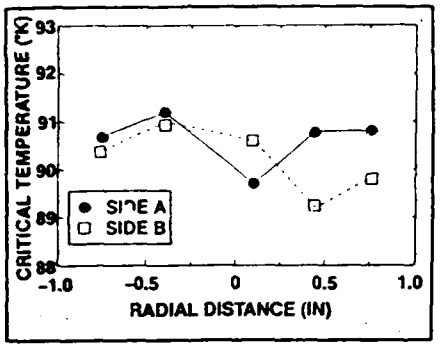


Fig. 4 The critical temperature (R = 0) for both sides of a double-sided film showing ±1°K uniformity over a 2" diameter substrate.

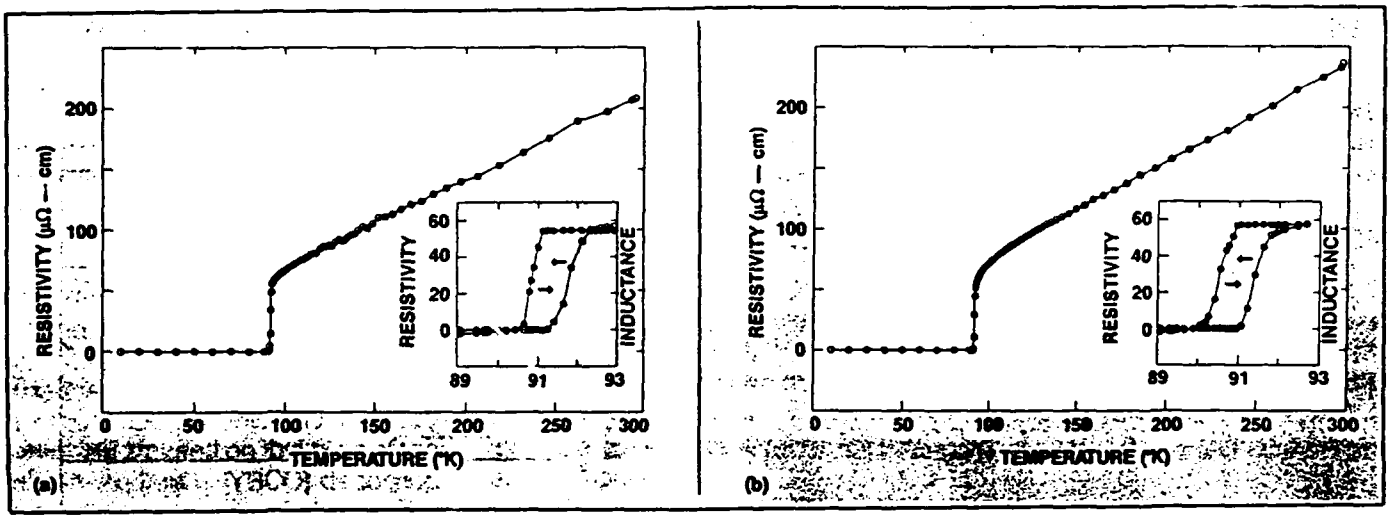


Fig. 3 Resistivity vs. temperature for a double-sided YBCO film deposited on (a) side A and (b) side B of a 2" diameter $LaAlO_3$ wafer. The inset figures compare the resistive and inductive transitions.

was determined at the temperature the resistance goes to zero while the inductive $T_c$ was determined by the transition midpoint. Microwave surface resistances are measured using a parallel plate resonator following a previously developed technique.[5] The sample geometry consists of two quarter-inch × half-inch samples separated by 0.0005" teflon film. The RF leads are loosely coupled to the resonator so that the loaded and unloaded Qs can be assumed equal. Values of $R_s$ are normalized from the resonant frequency of 8.5 GHz to 10 GHz assuming an $f^2$ dependence for the surface resistance.

## Experimental Results

YBCO films deposited on $LaAlO_3$ substrates are highly C-axis oriented. A very small A-axis component is observed, as shown in Figure 2, where the X-ray diffraction patterns of the front and back surfaces of a double-sided film are compared.

Resistive and inductive transition temperatures have been measured on double-sided films. The results are shown in Figure 3. The inductive transition follows very closely the resistive transition. Resistive $T_c$ (R = 0) values > 90°K are obtained for both sides of this wafer. A series of $T_c$ measurements were made spanning the diameter of a 2" wafer. The results are shown in Figure 4. The uniformity of $T_c$ varies between 89°K and 91°K over the wafer diameter.

Of particular importance for the passive microwave components that are being fabricated from these wafers is the surface resistance at microwave frequencies. $R_s$ values, at 77°K and normalized to 10 GHz, have been measured on quarter-inch × half-inch test chips, which surround microwave device patterns in the center of the 2" diameter wafer. The location of test chips is shown in Figure 5. The two sets of measured test chips showed $R_S$ values of 0.3 and 0.4 mΩ, respectively. On the antenna wafer, $R_s$ values averaged 0.65 mΩ for the front surface and 0.7 mΩ for the back surface. The specific pairs of chips measured and the results obtained for $R_s$ are listed in Table 1.

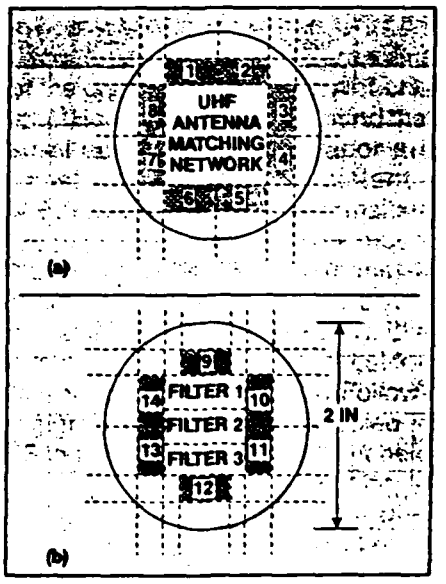


Fig. 5 Location of test chips used to determine surface resistance for (a) an antenna wafer and (b) a filter wafer.

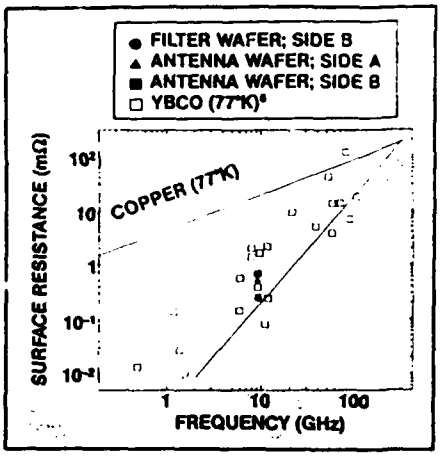


Fig. 6 Comparison of surface resistance measurements of double-sided films. The surface resistance of copper is shown for comparison.

The $R_s$ data are shown in Figure 6 superimposed on a curve summarizing $R_s$ measurements from a number of laboratories.[5] The $R_s$ values for these double-sided films fall within the scatter of the data summarized.

## Conclusion

The deposition of YBCO thin films by in-situ off-axis sputtering on both sides of 2" diameter $LaAlO_3$ substrates has been demonstrated. $T_c > 90°K$ is obtained for both sides of these films. Surface resistances of 0.65 and 0.7 mΩ at 77°K and normalized to 10 GHz have been measured for side A and side B deposited, respectively. Moreover, $R_s$ as low as 0.3 mΩ has been measured on side B of a double-sided wafer that had undergone a complete microwave device processing cycle. The reported results compare favorably with previous work on smaller area single-sided films.

## Acknowledgment

This article is part of a previously published book, *Advances in Cryogenic Engineering: Materials-Volume 38*, Plenum Publishing Co.

The technical assistance of J.H. Uphoff for $T_c$ measurements, A.M. Stewart for X-ray diffraction and G.B. Draper for $R_s$ characterization is gratefully acknowledged. The assistance of S.H. Talisa in establishing the $R_s$ measurement techniques is most appreciated. ■

## References

1. J. Talvacchio and G.R. Wagner, "High-$T_c$ Film Development for Electronic Applications," Superconductivity Applications for Infrared and Microwave Devices Proc., Vol. 1292, K.B. Bhasin and V.O. Heinen, (eds.), SPIE, Bellingham, WA, 1990, pp. 2-12.
2. J. Talvacchio, M.G. Forrester, J.R. Gavaler and T.T. Braggins, "Large-Area YBCO Films for Microwave Applications," IEEE Trans., Vol 27, No. 2, 1991, p. 978.
3. J.R. Gavaler, J. Talvacchio, T.T. Braggins, M.G. Forrester and J. Greggi, "Critical Parameters in the Single-Target Sputtering of YBCO," submitted to *J. Appl. Phys.*, 1991.
4. R.C. Taber, "A Parallel Plate Resonator Technique for Microwave Loss Measurements on Superconductors," *Rev. Sci. Instrum.*, Vol. 61, No. 8, 1990, p. 2200.
5. H. Piel and G. Muller, "The Microwave Surface Impedance of High-$T_c$ Superconductors," IEEE Trans., Vol. 27, No. 2, 1991, p. 854.

**Timothy T. Braggins** *received his B.S. and PhD in physics from Syracuse University. Currently, he is a fellow scientist at the Westinghouse Science and Technology Center. Since joining STC in 1975, Braggins has been involved with the growth and characterization of extrinsic silicon infrared detectors, bulk silicon crystals for VHSIC and bulk semi-insulating GaAs. Most recently, he has been studying thin-film growth of high $T_c$ superconductors. He is a member of the American Physical Society.*

**John Gavaler** *received his BS in chemistry from St. Francis College and did graduate work in inorganic chemistry at the University of Pittsburgh. Currently, he is a staff member of the Electronics, Information & Sciences Division at the Westinghouse Science and Technology Center. His research has been primarily in the growth and characterization of thin films of semiconducting and superconducting materials for use in electronics. Gavaler is a member of the American Physical Society and the Materials Research Group.*

**John Talvacchio** *received his BS degree in physics from Case Western Reserve University in 1977 and his PhD in applied physics from Stanford University in 1982. Since 1982, he has worked at the Westinghouse Science and Technology Center, in the areas of materials for superconducting electronics. Talvacchio is a member of the American Physical Society and the Materials Research Society.*

Presented at the Conference on Superconductivity and Its Applications (Buffalo, NY 1992)
and submitted for publication in the American Institute of Physics Conference Proceedings (New York, 1993)

# FEMTOSECOND SPECTROSCOPY OF Y-Ba-Cu-O THIN FILMS

T. Gong, L. X. Zheng, W. Xiong, W. Kula,+ R. Sobolewski,+
and P. M. Fauchet
Laboratory for Laser Energetics and Department of Electrical Engineering
University of Rochester, Rochester, NY 14627

J. P. Zheng and H. S. Kwok
New York State Institute on Superconductivity
State University of New York at Buffalo, Amherst, NY 14260

J. R. Gavaler
Westinghouse Science and Technology Center, Pittsburgh, PA 15235

## ABSTRACT

We have performed a series of ~100 fs time-resolved measurements on YBCO thin films. The dependence of the transient optical properties on probing laser frequency, pumping laser intensity, sample thickness, and ambient film temperature is discussed. Our results are compared to existing models and provide new insights on nonequilibrium properties of YBCO.

## I. INTRODUCTION

Femtosecond spectroscopy has recently been used to investigate transient nonequilibrium properties of high-temperature superconducting (HTS) materials. Femtosecond time-resolved differential reflectivity ($\Delta R/R$) measurements were performed by several groups on various YBCO films at room temperature. The dependence of the sign of $\Delta R/R$ on the oxygen [1] or Pr [2] content in YBCO compounds indicates different positions of the Fermi level ($E_F$). The correlation of the sign change of $\Delta R/R$ measured at 2 eV on optically thick YBCO films with the onset of superconductivity has been observed under relatively weak laser excitation ($<5\ \mu J/cm^2$) [3], and the picosecond response of $\Delta R/R$ has been interpreted as a direct indication of the dynamics of quasi-particles [3] and/or superconductor order parameter [4]. While most of the models assumed that the picosecond response measured at optical frequency and low temperature is mainly electric in nature, recent results of Reitze *et al.* [5] imply that a detailed energy band structure also has to be taken into account if any physical significance is to be assigned to the measured relaxation rates.

In this paper, we report a series of femtosecond spectroscopic measurements performed on YBCO films. The dependence of the transient optical properties on probing laser frequency, pumping laser intensity, sample thickness, and temperature is discussed.

## II. EXPERIMENTAL CONSIDERATIONS

A number of epitaxial YBCO films with thicknesses from 80 to 280 nm have been used in our measurements. Sample YBCO-I (200-nm thick, $T_c \sim 87.5$ K) was fabricated on a $SrTiO_3$ substrate using the technique of laser ablation [6]. Sample

YBCO-II (280-nm thick, $T_c \sim 89.5$ K) was fabricated on a $LaAlO_3$ substrate using the technique of single target sputtering samples [7]. YBCO-III (80-nm thick, $T_c \sim 83$ K) and YBCO-IV (200-nm, $T_c \sim 87$ K) were deposited on $SrTiO_3$ substrates by *in-situ* rf magnetron sputtering [8]. All the films exhibited critical current densities, $J_c$, greater than $10^6$ A/cm$^2$ at liquid nitrogen temperature. A partially oxygen depleted YBCO sample (YBCO-V) was also fabricated. The film was deposited together with YBCO-IV, but after the deposition it was furnace annealed at 500°C for 20 min in pure Ar atmosphere. As a result, its $T_c$ was lowered to 27 K, consistent with a decrease of the oxygen content to about 6.45.

The time-resolved optical experiments have been performed using a CPM laser system. Depending on the amplification arrangement, the laser system provides a pulse train either at high repetition rate (~100 MHz) and low energy per pulse (~0.1 nJ), or at moderate repetition rate (~8.5 KHz) and high energy per pulse (>1 μJ). This allows us to change the pump laser intensity ($I_p$) by more than 3 orders of magnitude and also to probe with different wavelengths selected from a white light continuum. Time-resolved differential reflectivity ($\Delta R/R$) and transmission ($\Delta T/T$) measurements have been performed with a temporal resolution of 100±20 fs using a conventional pump-probe arrangement. The polarization of a weak probe beam was rotated by 90° relative to that of the pump beam to reduce the coherent artifact. Measurements have been performed in a temperature range between 300 K and 12 K, using an optical Dewar with the temperature-controlled cold finger.

For our thin YBCO samples (grown on non-index-matched substrates), the typical penetration depth ($\lambda_p$) of the 2-eV laser beam into YBCO is ~90 nm. The dependence of $\Delta R/R$ and $\Delta T/T$ on the change of the refractive index ($\Delta n$) and absorption coefficient ($\Delta\alpha = 4\pi\Delta k/\lambda$, where k is the imaginary part of refractive index, and $\lambda$ is the laser wavelength) can be simply summarized as follows. For optically thick films (d > 150 nm), $\Delta R/R \sim 0.12\Delta n + 0.11\Delta k$ [9]; while for optically thin films (d < 150 nm), $\Delta T/T$ is primarily proportional to $-\Delta\alpha$, and $\Delta R/R$ is more strongly governed by the thin film effect [10]. In particular, if $\Delta n >> \Delta k$, $\Delta R/R$ measured on a thin film can have the opposite sign of that measured on a thick film.

## III. RESULTS AND DISCUSSIONS

### III.1. Room Temperature Measurements

Figure 1 illustrates $\Delta R/R$ measured from 1.91 to 2.17 eV on the YBCO-I sample at room temperature. The 2-eV pump intensity is kept around 10 μJ/cm$^2$. At all probe photon energies (up to 2.25 eV [11]), $\Delta R/R$ exhibits the same behavior—a pulse-width-limited rise (positive change) followed by a fast decrease, and then a long-lasting (several nanoseconds) plateau. A very similar temporal and spectral response is also obtained for the YBCO-IV sample. For all our samples with thicknesses from 80 nm to 300 nm, $\Delta R/R$ at 2 eV is positive and the temporal response of the signal has little dependence on the pump intensity from 0.3 to 100 μJ/cm$^2$. In addition, $\Delta T/T$ measured on a thin YBCO-II sample (see Fig. 2) has a temporal response that is very similar to that of $-\Delta R/R$ [12]. These results indicate that at room temperature, the change of optical properties for 2-eV-photoexcited YBCO is mainly dominated by $\Delta\alpha$, a result similar to earlier results obtained on d-band metals.

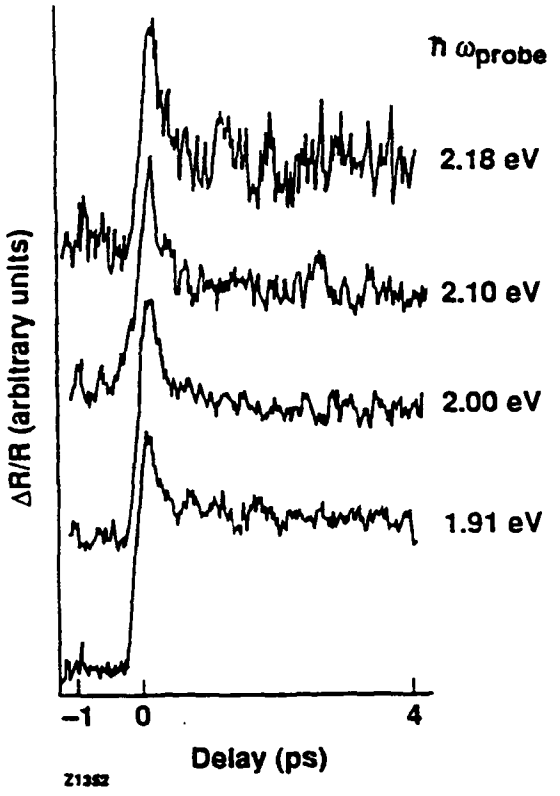


Fig. 1. Normalized $\Delta R/R$ ($\sim 10^{-4}$) measured on the YBCO-I sample at room temperature using the probe photon energies indicated in the figure. The pump intensity is ~10 $\mu J/cm^2$.

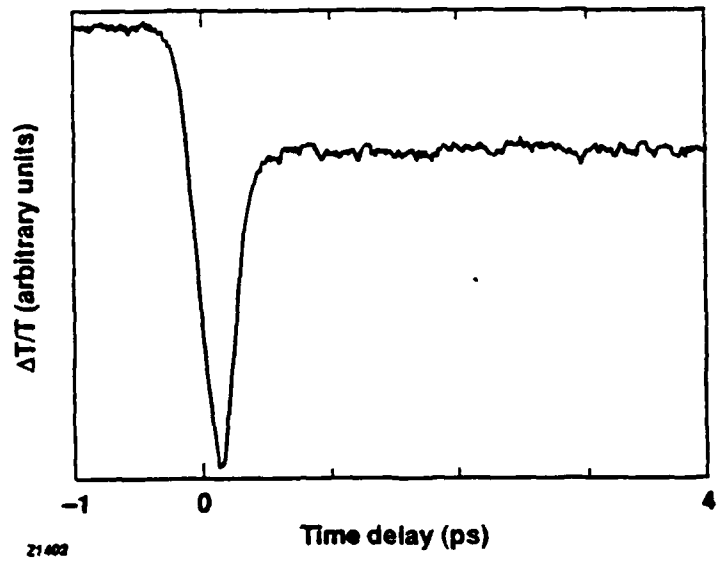


Fig. 2. $\Delta T/T$ measured on the YBCO-II sample at room temperature using 2-eV probe photon energy. The pump intensity is ~10 $\mu J/cm^2$.

Such a "bolometric" response at 2 eV can be explained by a thermomodulation model [1,2,13]. The carriers excited out of the Fermi sea by the pump pulse thermalize with all of the other carriers on a time scale typically shorter than the pulse width, because carrier-carrier scattering time is extremely fast in metals or HTS materials. Therefore, following the pump excitation, the carriers have established a temperature ($T_h$) that is much higher than the ambient film temperature ($T_L$), and the electronic occupancy near $E_F$ is modified. This "smearing" decreases (increases) the occupancy of states below (above) $E_F$. Thus, a probe monitoring the interband transition from the filled d-band to the p-states below (above) $E_F$ measures a positive (negative) $\Delta\alpha$. Since in YBCO $\Delta\alpha$ is always positive from 1.91 eV to 2.25 eV, $E_F$ for oxygen-rich YBCO must lie in the oxygen-p-band at least 2.25 eV above the copper-$d^9/d^{10}$-band. The fast decay following the pulse-width limited rise, illustrated in Fig. 1 and 2, is attributed to phonon emission, which reduces the effective carrier temperature. Afterwards, the long-lasting plateau is caused by a heat diffusion, which can be a nanosecond-time-scale process. In summary, $\Delta\alpha = a\Delta T_h + b\Delta T_L$, where the sign of a depends on probing frequency with respect to $E_F$ and is positive around 2 eV for oxygen-rich YBCO, and b is also positive for YBCO. The usual meaning of "bolometric" applies only to $b\Delta T_L$, which is the most important part of $\Delta\alpha$.

By contrast, $\Delta R/R$ measured at room temperature on the partially deoxygenated YBCO-V sample (Fig. 3) is negative at 2 eV. A similar sign change at 2 eV for oxygen-poor YBCO films was previously measured by Brorson *et al.* [1], and explained in the framework of the Fermi smearing model. The sign change was attributed to a shift of $E_F$, associated with a drastic change in the free-carrier concentration between the oxygen-rich and oxygen-poor films. Following again the Fermi smearing model, our results imply that in YBCO $E_F$ shifts down (using the hole picture) by at least 250 meV when the sample oxygen content decreases from above 6.9 to about 6.45.

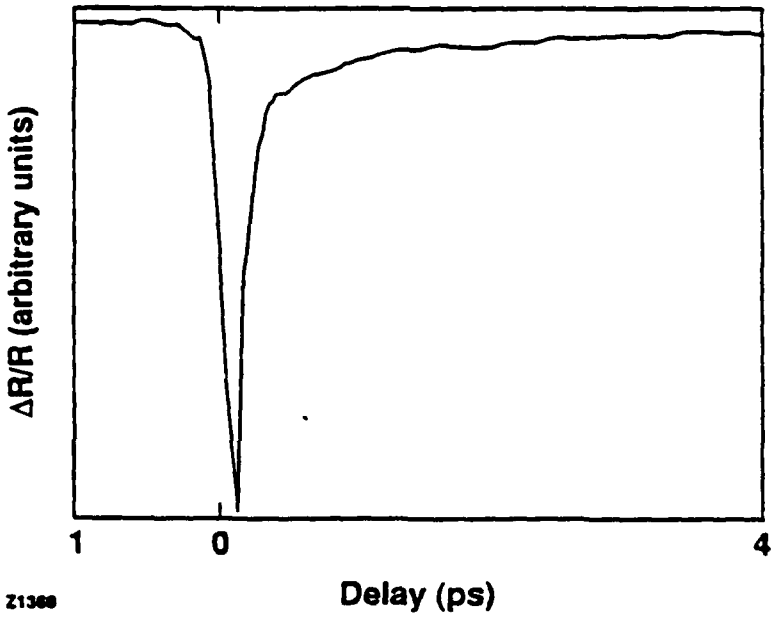


Fig. 3. $\Delta R/R$ measured on the YBCO-V (partially oxygen depleted) sample at room temperature using a 2 eV probe photon energy. The pump intensity is ~10 $\mu J/cm^2$.

III.2. Low Temperature Measurements

When the temperature is cooled down below $T_c$, the electronic density of states is strongly modified, as a result of the opening of the superconducting energy gap. The much larger density of states occupied by Cooper pairs just below $E_F$ is expected to change the Fermi smearing [14,15]. For $0 < T < T_c$, Cooper pairs and quasi-particles coexist in thermal equilibrium. The two-fluid model has been successful in explaining most of the equilibrium properties of superconductors. The absorption of a single 2-eV photon in YBCO creates, through cascading processes of carrier-carrier and carrier-phonon scattering, more than 100 quasi-particles with energies widely distributed in a continuum of states above the energy gap. Thus, a highly nonequilibrium Cooper pair/quasi-particle distribution is established following short-pulse excitation. Afterwards the system relaxes back towards equilibrium as all nonequilibrium quasi-particles recombine into Cooper pairs. When a simple two-fluid model is adopted, we have

$$\alpha = (1-f_C)\alpha_D + f_C\alpha_C + \alpha_{d-p}$$
$$n = (1-f_C)n_D + f_C n_C + n_{d-p}$$

where symbols D, C, and d–p represent contributions from the (Drude) quasi-particles, Cooper pairs, and d–p interband transitions, respectively, and $f_C$ is the fraction of the Cooper pairs at a given temperature.

Figure 4(a) and (b) present $\Delta R/R$ at 2 eV obtained at T = 12 K for the YBCO-IV sample under relatively intense excitation ($I_p$ = 20 μJ/cm$^2$ and $I_p$ = 100 μJ/cm$^2$). The temporal response is very similar to that observed at room temperature (see Fig. 1). It is worth stressing that for pump intensities ranging from ~15 μJ/cm$^2$ up to 100 μJ/cm$^2$, the same bolometric temporal response is observed for all optically thin and thick YBCO samples over the entire temperature range (from well below $T_c$ up to room temperature). However, the magnitude of the signal at $T < T_c$ is much larger than that at room temperature.

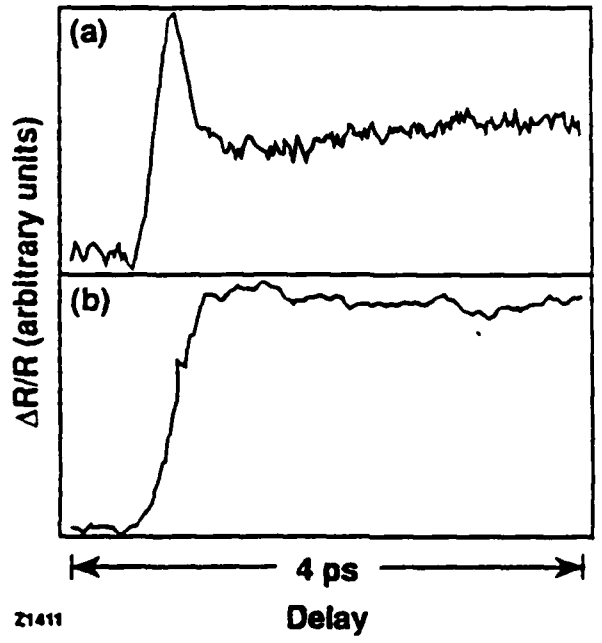


Fig. 4. $\Delta R/R$ (~$10^{-3}$) measured on the YBCO-I sample at T = 12 K using a 2 eV probe photon energy. The pump intensity is (a) ~20 μJ/cm$^2$ and (b) ~100 μJ/cm$^2$.

We believe that at high excitation levels, the density of photoexcited quasi-particles ($\delta N_Q$) is ~$10^{21}$ $cm^{-3}$, which is comparable to the total free carrier concentration in YBCO. Thus, the sample undergoes a transition to the normal state. After the pump pulse induces such a transition optically and all the Cooper pairs are destroyed, only the $\Delta\alpha_D$ and $\Delta\alpha_{d-p}$ contributions to the measured $\Delta R/R$ remain. It is clear that the magnitude of $\Delta\alpha_{d-p}$, which is directly related to the amount of smearing, is not expected to have an abrupt change over a relatively small range of ambient film temperature. Therefore, the abrupt increase in the magnitude of the signal with the onset of superconductivity implies an additional contribution from $\Delta\alpha_D$, in other words, from photoexcited nonequilibrium quasi-particles. On the other hand, the long-lasting plateau in the $\Delta R/R$ transient is a signature of a bolometric, heat-diffusion determined response. This result is also consistent with the nanosecond response of photovoltage signals measured for similar laser intensities [16].

When the pump laser intensity is reduced below a certain level (5±2.5 $\mu J/cm^2$), the transient properties of YBCO at $T < T_c$ are completely different from those either measured at room temperature or measured at $T < T_c$ but under intense excitation. Figure 5(a) shows $\Delta R/R$ at 2 eV measured on the YBCO-III (optically thick sample) at T ~ 25 K, when a weak $I_p$ (~1 $\mu J/cm^2$) is used. The decrease of the reflectivity, followed by a fast (several picoseconds) recovery, is very similar to what has been obtained by others [3–5]. By contrast, a positive $\Delta R/R$ with a similar temporal response is observed under similar experimental conditions on the YBCO-II (optically thin sample), as shown in Fig. 5(b). We believe that such a sign reversal of $\Delta R/R$ between optically thick and thin samples, which is not observed at room temperature, is due to a thin film effect.

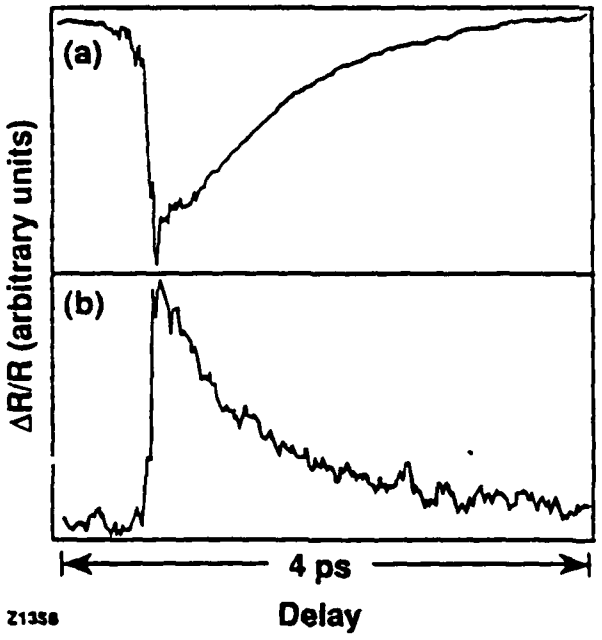


Fig. 5. The normalized $\Delta R/R$ measured on (a) YBCO-III and (b) YBCO-II samples at T = 25 K using a 2 eV probe photon energy. The pump intensity is ~1 $\mu J/cm^2$.

This interpretation is further supported by $\Delta T/T$ measurements. Both Chwalek *et al.* [14] and we [17] have observed that the sign of $\Delta T/T$ (or $\Delta\alpha$) does not change

when the ambient film temperature drops below $T_c$. This result clearly contradicts the speculation that the sign reversal of $\Delta R/R$ measured on an optically thick YBCO is related to $\Delta\alpha$. Therefore, at $T < T_c$ and under a weak excitation, it is $\Delta n$ instead of $\Delta\alpha$ that dominates $\Delta R/R$ at 2 eV. The correct sign of $\Delta n$ can be only obtained from experiments on our optically thick film, and it is indeed negative under the above experimental conditions.

Reitze *et al.* [5] stressed that the experimentally observed $\Delta R/R$ is about two orders of magnitude larger than the estimated $\Delta n_D$ (Drude component only). In fact, at $I_p = 1\ \mu J/cm^2$, the estimated $\delta N_Q$ is $\sim 4 \times 10^{19}\ cm^{-3}$, which appears to be only a small fraction of the total density of carriers (quasi-particle and Cooper pairs). Under such a weak excitation, the superconducting film may not be completely driven to the normal state, and the contribution from $\Delta n_C$ cannot be neglected. However, breaking of a fraction of Cooper pairs will cause a reduction of $\sigma_2$ (the imaginary part of conductivity), leading to a positive $\Delta n$, a fact again inconsistent with the observed negative $\Delta n$. These considerations indicate that the measured $\Delta R/R$ cannot be explained by a simple two-fluid model; the picosecond relaxation time obtained from the temporal response of $\Delta R/R$ at 2 eV is not a direct measure of the quasi-particle relaxation time [3,5,18].

This puzzling behavior may be associated with the existence of the intermediate state [19,20]. In this state the film is composed of normal and superconducting domains, which can be smaller than the excited region. Therefore, the optically measured signal consists of a mixed response resulting from both the superconducting state and the normal state. More investigations are currently being carried out, from which a comprehensive picture will emerge.

Finally, it is worth noting three other important experimental findings, which still await an explanation. First, the negative picosecond response of $\Delta R/R$ can be also obtained on some thick YBCO films when the temperature is within 20 K above $T_c$. Second, when a thick sample undergoes a constant illumination over half an hour, the sign of the measured $\Delta R/R$ can become positive, and then will never be reversed. Third, the positive picosecond response can also be obtained on thick YBCO samples of inferior quality that have a wider (>2 K, 10% to 90%) resistive superconducting transition.

## IV. CONCLUSIONS

Our results obtained at room temperature provide quantitative information on the position of the Fermi level in YBCO with different oxygen contents. We have found that in superconducting YBCO, $E_F$ must be at least 2.25 eV above the Cu-$d^9/d^{10}$ band. Simultaneously, there is a large, >250 meV, energy difference between the positions of $E_F$ in the oxygen-rich and oxygen-poor samples. These observations are a direct consequence of the Fermi smearing model, which has been generally accepted to explain experimental data for d-band metals, as well as for HTS materials at room temperature.

Systematic measurements performed at temperatures below $T_c$ indicate that in YBCO the optical response associated with nonequilibrium properties of quasi-particles and Cooper pairs is strongly dependent on the intensity of optical excitation. Under strong excitation the temporal dependence of the $\Delta R/R$ is essentially the same in optically thin and thick films and follows that measured at room temperature. In both cases $\Delta R/R$ is dominated by $\Delta\alpha$ and the response is primarily bolometric. A completely

different behavior is observed for weakly excited films. The $\Delta R/R$ signal exhibits a picosecond temporal response, but its sign depends on the film thickness and is negative for optically thick samples. The thickness-dependent sign change of $\Delta R/R$ below $T_c$ indicate that $\Delta R/R$ is dominated by $\Delta n$. However, the sign and magnitude measured on optically thick samples cannot be explained by the simple two-fluid model. Therefore, more advanced models, based on a detailed material band structure and nonequilibrium quasi-particle/Cooper pair dynamics should be developed.

## ACKNOWLEDGMENTS

The work in Rochester is supported by the ARO grant DAAL03-92-G-0202, the NYSIS grant PO #R12762, and the Laser Fusion Feasibility Project at the Laboratory for Laser Energetics. The work in Buffalo is supported by the NSF grant ECS9017053. The work at the Westinghouse Science and Technology Center is supported by the AFOSR grant F49620-91-C-0034.

## REFERENCES

+ Also at the Institute of Physics, Polish Academy of Sciences, Al. Lotników 32/46, PL-02668 Warszawa, Poland.

1. S. D. Brorson, A. Kazeroonian, D. W. Face, T. K. Cheng, G. L. Doll, M. S. Dresselhaus, G. Dresselhaus, E. P. Ippen, T. Venkatesan, X. D. Wu, and A. Inam, Solid State Comm. 74, 1305 (1990).
2. A. S. Kazeroonian, T. K. Cheng, S. D. Brorson, Q. Li, E. P. Ippen, X. D. Wu, T. Venkatesan, S. Etemad, M. S. Dresselhaus, and G. Dresselhaus, Solid State Comm. 78, 95 (1991).
3. S. G. Han, Z. V. Vardeny, K. S. Wong, and O. G. Symko, and G. Koren, Phys. Rev. Lett. 65, 2708 (1990); 67, 1053 (1991).
4. G. L. Eesley, J. Heremans, M. S. Meyer, G. L. Doll, and S. H. Liou, Phys. Rev. Lett. 65, 3445 (1990); 67, 1504 (1991).
5. D. H. Reitze, A. M. Weiner, A. Inam, and S. Etemad, to be published in Phys. Rev. B (Rapid Commun.).
6. S. Witanachchi, H. S. Kwok, X. W. Wang, and D. T. Shaw, Appl. Phys. Lett. 53, 234 (1988).
7. J. R. Gavaler, J. Talvacchio, T. T. Braggins, M. G. Forrester, and J. Greggi, J. Appl. Phys. 70, 4383 (1991).
8. P. H. Ballentine, A. M. Kadin, and D. S. Mallory, IEEE Trans. Magn. MAG-27, 997 (1991).
9. Values 0.12 and 0.11 are calculated from the unperturbed optical constants at 2 eV. See: D. E. Aspnes and M. K. Kelly, J. Quantum Electron. 25, 2380 (1989).
10. The thin film effect can also strongly affect $\Delta T$ measurements for ultrathin YBCO films ($d < 500$ Å). However, for $d \sim \lambda_p$, $\Delta T/T$ is primarily determined by $-\Delta\alpha$.
11. $\Delta R/R$ is also measured at 2.25 eV, but not displayed in Fig. 1.
12. The magnitude of $\Delta T$ is significantly larger than that of $\Delta R$ measured on the same film.
13. G. L. Eesley, Phys. Rev. B 33, 2144 (1986).

14. J. M. Chwalek, C. Uher, J. F. Whitaker, G. A. Mourou, J. Agostinelli, and M. Lelental, Appl. Phys. Lett. **57**, 1696 (1990).
15. R. Rosei, F. Antonangeli, and U. M. Grassano, Surf. Sci. **37**, 689 (1973).
16. A. D. Semenov, G. N. Gol'tsman, I. G. Gogidxe, A. V. Sergeev, E. M. Gershenzon, P. T. Lang, and K. F. Renk, Appl. Phys. Lett. 60, 903 (1992).
17. L. X. Zheng, T. Gong, R. Sobolewski, and P. M. Fauchet, unpublished.
18. T. Gong, L. X. Zheng, W. Xiong, W. Kula, R. Sobolewski, and P. M. Fauchet, submitted to Phy. Rev. B.
19. R. Sobolewski, D. P. Butler, T. Y. Hsiang, C. V. Stancampiano, and G. A. Mourou, Phys. Rev. B **33**, 4604 (1986).
20. V. F. Elesin and Yu. V. Kopaev, Usp. Fiz. Nauk **133**, 259 (1981) [Sov. Phys. –Usp. **24**, 116 (1981)].

# DYNAMICS OF VORTEX - ANTI-VORTEX PAIRS AT MICROWAVE FREQUENCIES IN $Y_1Ba_2Cu_3O_{7-\delta}$ FILMS

H-J. Chen and S. Sridhar,

Physics Department, Northeastern University, Boston, MA 02115

and

J.Talvacchio,

Westinghouse R & D Center, Pittsburgh, PA 15201

(P.A.C.S. #'s 74.30.Gn, 74.60.Ge, 74.40.+k, 74.75.+t)

*Abstract*

New phenomena are observed in a narrow window ($T_c$ - T $\leq$ 1K) in $Y_1Ba_2Cu_3O_{7-\delta}$ films in measurements of the microwave surface impedance $Z_s = R_s + i X_s$ and the field derivative ($dR_s/dH$), carried out using a specially developed modulated microwave impedance technique. These are an unexpected negative peak in ($dR_s/dH$), accompanied by a bump in the reactance $X_s$ , both of which are quenched by small magnetic fields ( $\leq$ 250 Oe). A positive peak observed at lower temperatures can be understood in terms of conventional dynamics of free vortices. The anomalies can only be explained in terms of the dynamics of vortex-antivortex pairs *above* a Kosterlitz-Thouless transition.

The superconducting transition in the high $T_c$ cuprates continues to present fundamental theoretical challenges[1]. An important piece of information would be the dimensionality of the transition, particularly in view of the very large anisotropy present. In 2-D, phase fluctuations play an important role, leading to a Kosterlitz-Thouless transition which is well documented in low $T_c$ superconducting thin films[2], and has been suggested to occur by some experiments, principally low frequency penetration depth[3] and I-V characteristics[4,5], in the high $T_c$ superconductors also.

In this paper, we present new phenomena at very low fields ( $< 250$ Oe) occurring near the superconducting transition in $Y_1Ba_2Cu_3O_{7-\delta}$ films. The observation of these phenomena is due to the implementation of a new experiment, modulated microwave surface impedance. An unexpected decrease of the impedance ($dZ_s/dH < 0$), accompanied by a bump in the reactance $X_s$, occurring in the same narrow temperature window ($T_c$ - $T < 1$K), are observed. Both effects are quenched by low applied magnetic fields ( $\leq 250$ Oe). The observed phenomenology is shown to be consistent with a picture in which phase fluctuations in the form of thermally excited vortex-antivortex pairs play an important role in the microwave impedance very near $T_c$.

Besides leading to new phenomenology of importance to the superconducting transition in $Y_1Ba_2Cu_3O_{7-\delta}$, our results also represent new physics associated with the Kosterlitz-Thouless (K-T) transition not observed previously. Our experiments show that in a very narrow region near $T_c$, the zero- and low-field transport properties are dominated by thermally generated vortex-antivortex pairs. This is followed by a crossover from 2D to 3D behavior at a temperature we call $T_{KT}$. The experiments show an "island" determined by a quenching field $H_{c+}(T)$ in the H-T plane ($H < 250$ Oe, $T_c$ - $T < 1$K), in which the pairs dominate, and at higher fields is replaced by a vortex plasma. The experiments provide access to the vortex-pair dielectric constant $\epsilon_{vb}$ and

the correlation length $\xi_+$ *above* $T_{KT}$, both of which were inaccessible in the low $T_c$ superconductors, but are of central importance in K-T theory.

The microwave (10 GHz) experiments employ a standard cylindrical cavity technique with the film as end plate, along with specially developed circuitry which enable us to measure ($dR_s/dH$) very accurately and $R_s$ and $X_s$ simultaneously. $R_s$ can be measured[6] *absolutely* from the cavity Q, and changes $\Delta X_s$ from the resonant frequency. To measure ($dR_s/dH$) we apply a modulation field $H_m$ ( $\sim$ 15 Oe at $\sim$ 100 Hz) besides a static field H (H, $H_m \parallel \hat{c}$), and have developed[7] a self-lock circuitry and employed modulation and lock-in techniques. The circuitry has two crucial features. First, it can always lock the microwave source frequency to the cavity resonance frequency. This enables us to measure frequency and hence reactance very accurately over narrow temperature windows. Secondly, it guarantees that the output is proportional to the loaded Q, and the field modulated signal is a measure of ($dR_s/dH$). In contrast, in off-resonance modulated absorption experiments[8], one measures ($dP/dH$), from which it is difficult to deconvolve the material parameter ($dZ_s/dH$). For this reason, previous modulation experiments have been difficult to interpret[9]. Another advantage of this experiment is the ability to sweep T at fixed H, which enables us to study phenomena very near $T_c$ more accurately than done previously. All of these features are essential for observation of the phenomena reported here.

High quality YBCO films, 5000 to 6000 Å thick, were sputtered onto $LaAlO_3$ substrates. The films had sharp transitions, critical currents $J_c(77K) > 10^6$ A/cm$^2$, and have been extensively characterized regarding both microwave[6] and other properties[10]. $R_s(T,H=0)$ vs. T is shown in the inset to Fig.1. It is now well-known that electrodynamic properties of high quality YBCO samples can be well parametrized over a substantial range of temperature ( $\sim 0.6 - 0.98T_c$) in terms of mean-field behavior[11,12],

such as BCS. The present films are in agreement over this observation. In this paper, we focus on a narrow temperature regions ($T_c$ - T $\sim$1K) where unexpected new phenomena are observed.

The principal results of this paper are shown in Fig.1, 2 and 3. In Fig.1, $(dR_s/dH)/R_n$ vs. T in different representative H from 30 Oe to 250 Oe is shown. (Data were also taken at several other fields). 2 peaks are observed below $T_c$ ($\sim$89.7K) - a positive one at about 87.9K and a negative peak closer to $T_c$ at about 89.2K. It is striking that $(dR_s/dH)$ is negative, since that implies that $R_s$ *decreases with increasing H.* Also the negative effect disappears at a relatively low field of 250 Oe, while the positive effect exists for all fields upto at least 3000 Oe.

Since the negative effect in $(dR_s/dH)$ is unexpected, we have carried out many checks to make sure that the data are not spurious. We measured the modulation phase, and obtained one constant $\phi_1 = 0$ for the T-range where $(dR_s/dH) > 0$, and another $\phi_2 = \pi$ where $dR_s/dH < 0$. This ruled out the possibility of the negative peak arising from a gradually changing phase shift. Another check was done by flipping the static field. This produced a relative phase shift of $\pi$ between the modulated output and the reference signal. The whole curve for $(dR_s/dH)$ in Fig.1 was flipped exactly upside-down and no asymmetry was detectable. This confirmed not only that our data is entirely the field response of the YBCO sample, but also that it is indeed the derivative with respect to the magnetic field.

Fig.2 which presents the data for $X_s$ vs. T, shows a close correlation with the $(dR_s/dH)$ data. (We have used[11] $\lambda(0) = 1400$ Å for the display, but this value is not at all crucial for the present discussion). Remarkably there is a bump in $X_s$ in the same temperature window (88.7K - 89.7K) as the negative peak in $(dR_s/dH)$, and the bump decreases with increasing field and disappears at the same fields ($\leq$ 250 Oe) as the

negative effect. Furthermore, the $X_s(T,H)$ data can be used to obtain the derivative $(\Delta X_s/\Delta H)$. It is important to note that this looks the same as $(dR_s/dH)$ within a T-dependent prefactor, i.e. with a negative peak at high T and a positive peak at low T, although the magnitudes are different. This shows that $(dR_s/dH) \propto (dX_s/dH)$. Also this data was obtained without the modulation field, and hence further rules out the same artifact being present in the two very different measuring techniques.

As is apparent from Fig.1 & 2, the unexpected effects are quenched by small magnetic fields. The temperature dependence of the quenching field $H_{c+}$ is shown in Fig.3. This field was obtained from the definition that at $H = H_{c+}$, $(dR_s/dH) = 0$ and changes sign. The noteworthy aspect of Fig.3(a) is that, unlike typical field scales such as $H_{c1}$, $H_{c2}$ or $H^*$, the present field scale $H_{c+}$ *decreases with decreasing T*. A quantitative explanation of $H_{c+}(T)$ in Fig.3, and also of the data in Fig.1 & 2 is discussed next.

The peak in $X_s(H=0,T)$ is extremely suggestive of the peak present in detailed calculations based upon both the two-fluid and BCS theories of superconductivity, and arising from the buildup of the superfluid. However two points argue against such an identification of the peak : (1) the peak should be completely insensitive to fields $\sim 250$ Oe, since the only field scale in these models is $H_{c2} >> 250$ Oe, (2) in all these theories, $(dR_s/dH)$ and $(dX_s/dH) > 0$ always, and hence the negative effect associated with the peak cannot be explained.

We next examine the $H \neq 0$ results in the context of conventional dynamics of free vortices. Because of the demagnetization ratio for the thin films, it is expected that vortices are present at all $H \neq 0$. If one considers the vortex response as $\eta \dot{x} + \alpha x = \phi_0 J_\omega$ , then expressions have been obtained for the surface impedance by Coffey and Clem[13] : $Z_s = i\mu_0\omega\tilde{\lambda}$, where $\tilde{\lambda}^2 = (\lambda_L^2 - i/2\ \delta_v^2)/(1+ i\ 2\lambda_L^2/\delta_n^2)$, where the background

condensate contribution is included in terms of the London penetration depth $\lambda_L$ and the normal skin depth $\delta_n$, and the vortex contribution is the complex skin depth $\delta_v$. We have carried out detailed calculations using this model and it always yields a single *positive* peak for $(dR_s/dH)$ near $T_c$. Thus the conventional response of free vortices is unable to explain the present negative effect, although it appears to describe the positive effect well.

We also note two other important experimental observations. Experiments on a 5000Å NbN film showed only a positive peak in $(dR_s/dH)$, consistent with simple expectations. Also the negative effect is suppressed by weak links present in poor quality YBCO films with very broad transitions, and hence is an intrinsic property of high quality YBCO films such as those studied here.

In the absence of an explanation in terms of conventional excitations such as quasiparticles and vortices, we have found that a consistent explanation of both the $H = 0$ and $H \neq 0$ data can be obtained in terms of ***vortex-antivortex pairs above a K-T transition.*** We first see how vortex-antivortex pairs contribute to the impedance in the present high-frequency experiments. In contrast, previous experiments which probe the Kosterlitz-Thouless transition were carried out at low frequencies for $T < T_{KT}$. We generalize earlier expressions[14], and including the normal fluid, obtain :

$$Z_s = (\tilde{\epsilon}_{vb}(H,T,\omega) - i\,2\pi\sigma_v/\omega\,)\,(R_{s0} + i\,X_{s0}) \qquad (1)$$

The impedance $Z_{s0} = R_{s0} + i\,X_{s0}$ represents the "background" impedance due to the superfluid and quasiparticles, such as may be described by a two-fluid model, and represents the impedance un-renormalized by vortices. We first note that this term does not contribute to the field dependence in the present experiment, since it changes only on field scales $\sim H_{c2}$. Thus all the very low field results reported here are described by the first term, where $\tilde{\epsilon}_{vb}$ is the vortex pair dielectric constant, and $\sigma_v$ the vortex

conductivity.

Detailed analysis shows that for the present experiment the prefactor in eqn.(1) is essentially real. The most compelling reason for this is suggested by the experimental observation that $(dR_s/dH) \propto (dX_s/dH)$, except for a T-dependent factor. Furthermore the conductivity term due to free vortices is suppressed by the high measuring frequency. Also the imaginary part of $\tilde{\epsilon}_{vb}$ comes essentially from those vortex-antivortex pairs with large separations which behave essentially like free vortices and are similarly suppressed due to large $\omega$. Thus for the present experiment, in the narrow region near $T_c$, we can write :

$$Z_s = \epsilon_{vb}(H,T,\omega)\,(R_{s0} + i\,X_{s0}) \qquad (2)$$

where $\epsilon_{vb}(H,T,\omega)$ represents the real part of $\tilde{\epsilon}_{vb}$. We argue below that the principal features observed, viz. $(dR_s/dH) < 0$, the bump in $X_s$ and the field scale $H_{c+}(T)$ are understandable in terms of the T- and H- behavior of $\epsilon_{vb}$.

On general grounds, we expect that $\epsilon_{vb} > 1$ always, approaching 1 for $T >> $ and $T << T_{KT}$. (Of course $\epsilon_{vb} = 1$ at $T_c$). Thus $\epsilon_{vb}$ must go through a maximum, just as the $X_s(T,0)$ data in Fig.2 does. Eqn.(2) suggests that $[\epsilon_{vb}(T,H=0) - 1]$ should correspond to $[X_s(T,H=0)/X_s(T,H=250Oe) - 1]$ for $T > T_{KT}$. We reason that $X_s(T,H = 250Oe)$ is the reactance in the absence of v-$\bar{v}$ pairs whose contribution is quenched by the magnetic field (see below). we have calculated $\epsilon_{vb}$ using[15,16] $\tilde{\epsilon}_{vb} = 1 + \int_{\xi_{GL}}^{\xi^+} dr\,(d\hat{\epsilon}/dr)\,[(14D/r^2)/(14D/r^2 - i\omega)]$, where $\xi_{GL} = \xi_0/\sqrt{1-T/T_c}$ with $\xi_0 = 15\text{Å}$, and the correlation length[15] $\xi^+ = \xi_{GL}(T)\exp[b(T/T_{KT} - 1)^{-1/2}]$, where $\xi_{GL}$ is the Ginzburg-Landau coherence length, and b is a non-universal constant of order unity (b = 0.125, see later). We obtain $\hat{\epsilon}$ from the K-T recursion relations[17] with values of $D(T_{KT}) = 6 \times 10^{-8}$ $m^2/s$, $\epsilon_c = 4.6$(ref.3). The resultant calculation (Fig.4 inset) has a "bump" above $T_{KT}$, which is similar to that observed in the data. As shown in Fig.4, the

correspondence between data and the calculation is excellent. Thus the zero-field bump in $X_s(0,T)$ is a high frequency manifestation *above* $T_{KT}$ of the renormalized penetration depth which has been observed in low $T_c$ superconductors for $T < T_{KT}$ only as $\lambda^{-2} = \lambda_0^{-2} / \epsilon_\infty$.

In this picture, the negative peak in $(dR_s/dH)$ can be understood in terms of the H-dependence of $\epsilon_{vb}$, because $d\epsilon_{vb}/dH < 0$. This can be seen by considering the relevant length scales. One is the correlation length $\xi_+(T)$ of thermally excited v-$\tilde{v}$ pairs. The other is the separation between field-induced vortices $r_H = (\phi_0/H)^{1/2}$. (A third length $r_\omega = (D/\omega)^{1/2} \sim 10\text{Å}$ is << both $\xi_+$ and $r_H$). At low fields pairs with separation > $r_H$ will behave more like free vortices and will not contribute to $Re\tilde{\epsilon}_{vb}$, which will therefore be reduced as H is increased. Thus $[d(Re\ \tilde{\epsilon}_{vb})/dH] < 0$ . This occurs over a field scale $H_{c+}$ ( $\sim 250$ Oe as we show below). In contrast the free vortex contribution in the unified expression can be shown to be $\delta_v^2/\lambda^2 = (\delta_n^2/\lambda^2)(H/H_{c2})$ in the pure flux flow limit, which would increase $R_s$ but occurs over a field scale $\sim H_{c2}$ and the corresponding increase is negligible.

*Temperature dependence of the quenching field $H_{c+}(T)$.* A natural field scale occurs when $r_H \approx \xi_+(T)$ which is a measure of the average separation or pairs. This leads to a so-called quenching field $H_{c+}(T) = \phi_0/2\pi\xi_+^2$, above which most pairs will behave like free vortices and will not contribute to $\epsilon_{vb}$. Using the previous expression for $\xi_+$ then yields :

$$H_{c+}(T) = H_{c2}(T)\ \exp[-b'(T/T_{KT} - 1)^{-1/2}] \qquad (3)$$

where $b' = 2b$, and we use $H_{c2}(T) = H_{c2}(0)\ (1\text{-}T/T_c)$, $T_c = 89.7$K and $T_{KT} = 88.7$K . The experimental data are compared with the above expression in Fig.3. Excellent agreement is seen - the scaled form in Fig. 3(b) is plotted to further emphasize this. The least square fit parameters are $b' = 0.25$ and $H_{c2}(0) = 107$T, consistent with a similar

comparison[3] *below* $T_{KT}$. The "island" defined by the $H_{c+}(T)$ curve in Fig.3(a) may be regarded as the region over which v-$\bar{v}$ pairs contribute. At higher fields, when $H > H_{c+}(T)$, the pairs are more appropriately treated as a vortex plasma. The $H_{c+}(T)$ data are only available over the left side of the maximum, i.e. for $(dH_{c+}/dT) > 0$. The other side is really the mean field superconducting transition at $H_{c2}(T)$, which is a vertical line on the scale of Fig. 3(b).

The present experiment suggests $T_c - T_{KT} \sim 1K$ in YBCO, which is substantially larger than predicted by simple estimates ($\sim 0.03K$) based[2] upon the film thickness and resistivity ($80\mu\Omega$-cm.), even after corrections for the high $\epsilon_c = 4.6$. Other estimates using completely different experimental techniques range from 1K in YBCO films[3], 0.15 K in single crystal YBCO[4] and 2.1K in single crystal BSCCO[5]. Recent measurements[18] on one unit-cell thick film and YBCO/PBCO superlattices suggested that the KT transition is an intrinsic property of $CuO_2$ layers, but occurs around 30K. The evidence suggests that interlayer coupling[19] moves the KT transition to values near $T_c$, which is consistent with the larger $T_c - T_{KT}$ values[5,20] in "bulk" BSCCO and TBCCO which are more anisotropic.

In conclusion, a new experiment has led to the observation of new phenomenology at very low fields near $T_c$ in $Y_1Ba_2Cu_3O_{7-\delta}$ films. The observed phenomenology closely resembles that associated with the KT transition in an ideal 2-D superconductor. The present work involves new physics associated with $\tilde{\epsilon}_{vb}$ above $T_{KT}$ not observed in more conventional studies of the KT transition. Furthermore, the present work poses new challenges to our theoretical understanding of the superconducting transition in $Y_1Ba_2Cu_3O_{7-\delta}$.

We thank R.S.Markiewicz and J.V.Jose for useful discussions. This work was supported by Rome Labs, USAF.

REFERENCES


1. B.Batlogg, Physics Today, 44, No.6, 44 (1991), P.W.Anderson and R.Schrieffer, Physics Today, 44, No.6, 54 (1991).

2. M. R. Beasley, J.Mooij and T.Orlando, Phys. Rev. Lett. 42, 1165 (1979)

3. A. T. Fiory et al. Phys. Rev. Lett. 61, 1419 (1988)

4. N. C. Yeh and C. C. Tseui, Phys. Rev. B 38, 2847 (1988)

5. S.Martin, et. al., Phys. Rev. Lett., 62, 677 (1989).

6. J.Owlieaei, S.Sridhar and J.Talvacchio, Phys. Rev Lett., (1992).

7. H.J.Chen and S.Sridhar (unpublished).

8. S. H. Glarum, L. F. Schneemeyer, and J. V. Waszczak, Phys. Rev. B 41, 1837 (1990), K. W. Blazey et al., Europhys. Lett. 6, 457 (1988), K. Kish, S. Tyagi, and C. Krafft, Phys. Rev. B 44, 225 (1991).

9. S. V. Bhat, V. V. Srinivasu and N. Kumar, Phys. Rev. B 44, 10121 (1991), A. Dulcic et al, Phys. Rev. B 42,2155 (1990)

10. S. Sridhar, D. H. Wu, and W. Kennedy, Phys. Rev. Lett. 63, 1873 (1989).

11. S. M. Anlage et al, Phys. Rev. B 44, 9764 (1991).

12. J. F. Annett, N. Goldenfeld, and S. R. Renn, Phys. Rev. B 43, 2778 (1991).

13. M. W. Coffey and J. R. Clem, Phys. Rev. Lett. 67, 386 (1991).

14. A. F. Hebard and A. T. Fiory Physica 109&110B 1637 (1982).

15. B. I. Halperin and David R. Nelson J. Low Temp. Phys. 36, 599 (1979).

16. L. C. Davis, M. R. Beasley and D. J. Scalapino, Phys. Rev. B 42, 99 (1990).

17. J. M. Kosterlitz and D. J. Thouless, J. Phys. C 6, 1181 (1973).

18. Y.Matsuda et al. Phys. Res. Lett. 69, 3228 (1992).

19. P. Minnhagen and P. Olsson, Phys. Rev. Lett. 67, 1039 (1991).

20. D. H. Kim et al. Phys. Rev. B 40,8834 (1989).

## FIGURE CAPTIONS

Fig.1. Data for $(dR_s/dH)$ vs. T at 3 fields. Note the negative peak near $T_c$, followed by a positive peak at lower T. The inset shows $R_s/R_n$ vs. T.

Fig.2. $X_s(T,H)/X_n$ vs. T for different H fields. Note the bump near $T_c$.

Fig.3. Quenching field $H_{c+}$ vs. T. (a) Linear scale. The dashed line represents $H_{c2}(T)$. (b) Scaled plot to emphasize the comparison with theory. The solid lines represent calculations based on the KT theory.

Fig.4. The ratio $[X_s(T,H)/X_s(T,H=250\ Oe)\ -1]$ for 3 different magnetic fields, and $T > T_{KT}$. Inset. Theoretical calculation of $\epsilon_{vb}$ - 1 vs. T. Note the qualititative agreement with the data in the main figure for H = 0.

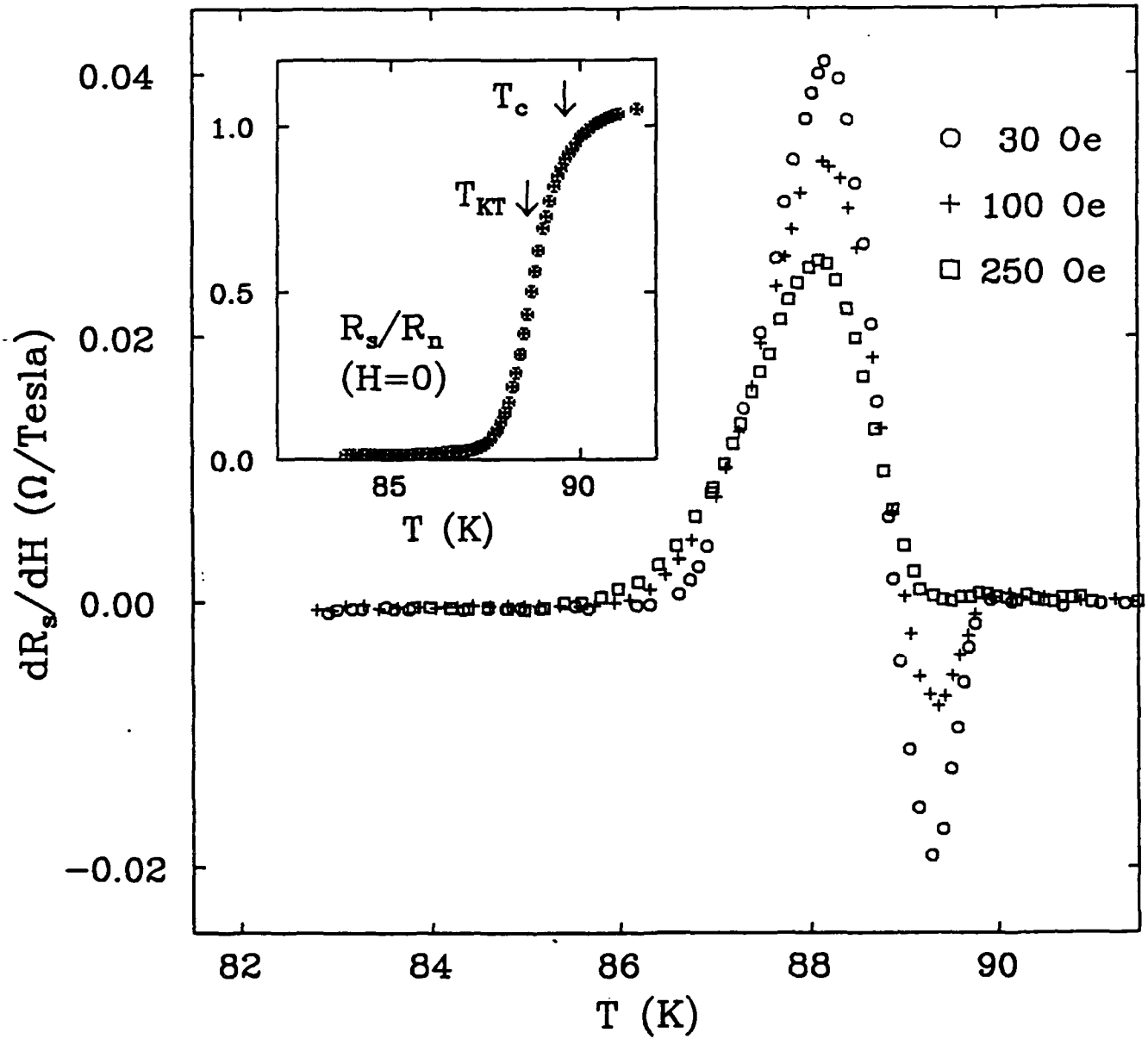
0.04
0.02
0.00
−0.02
dR_s/dH (Ω/Tesla)
82
84
86
88
90
T (K)
30 Oe
100 Oe
250 Oe
T_c
T_KT
R_s/R_n
(H=0)
1.0
0.5
0.0
85
90
T (K)

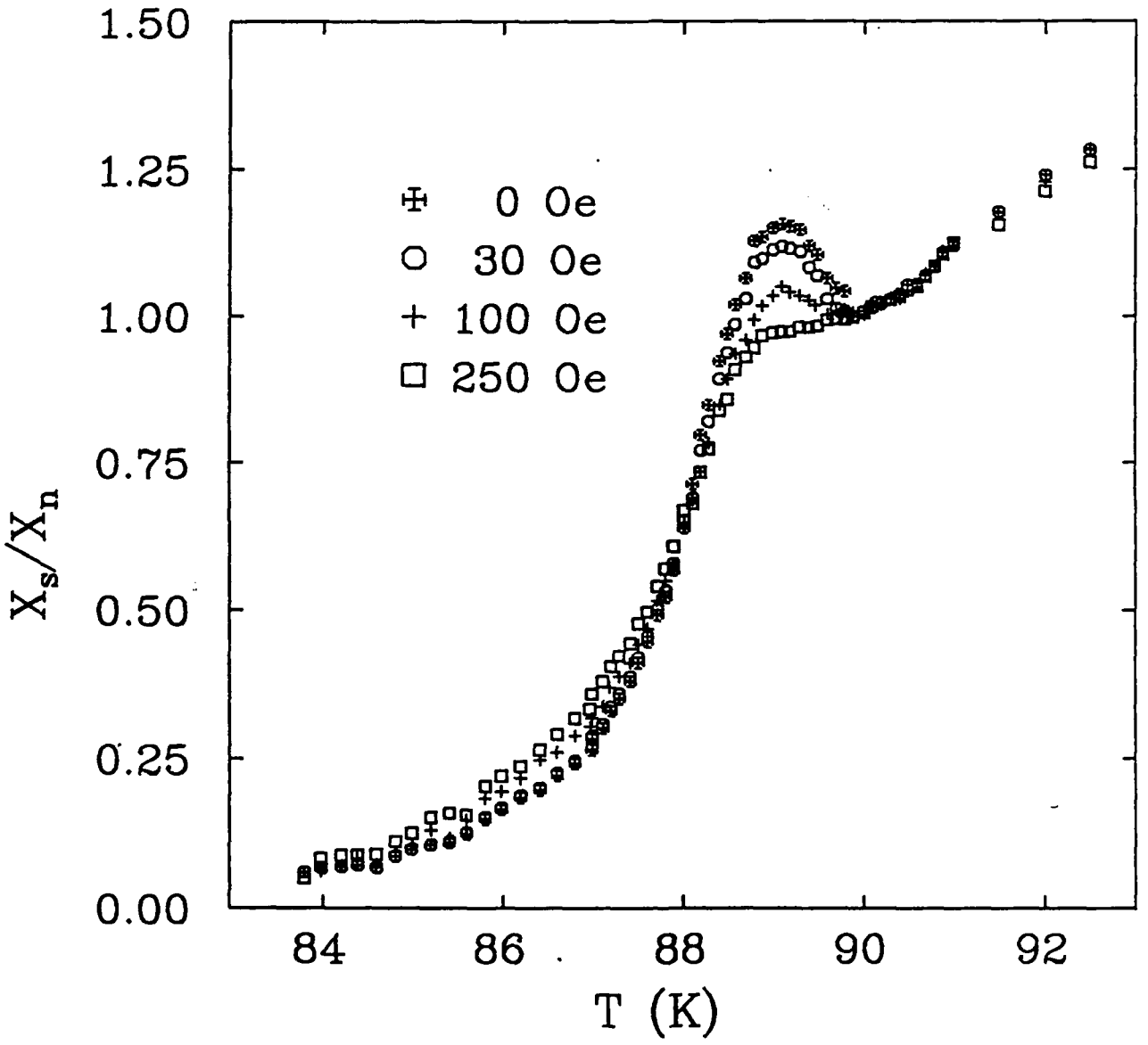
1.50
1.25
1.00
0.75
0.50
0.25
0.00
$X_s/X_n$
0 Oe
30 Oe
100 Oe
250 Oe
84
86
88
90
92
T (K)

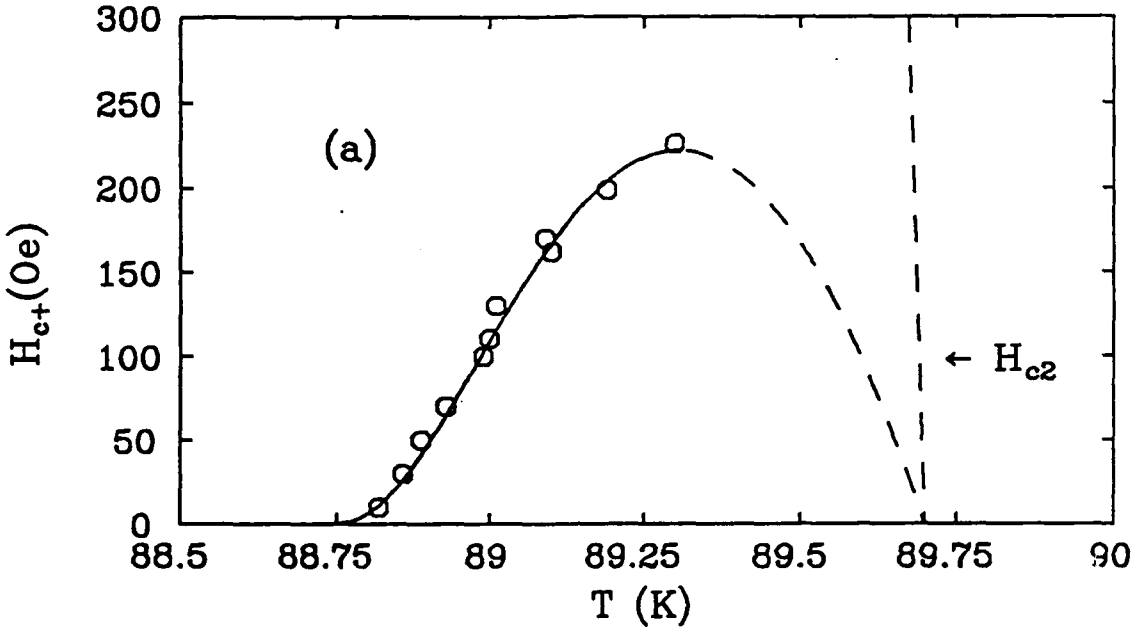
300
250
200
150
100
50
0
88.5
88.75
89
89.25
89.5
89.75
90
(a)
$H_{c+}$(Oe)
T (K)
← $H_{c2}$

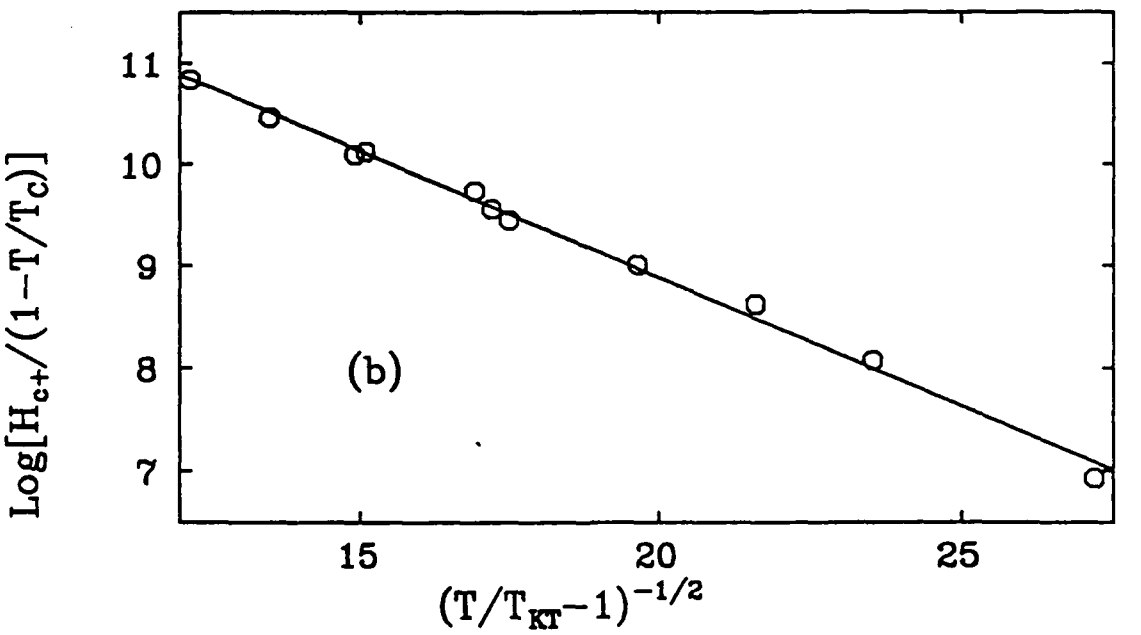
11
10
9
8
7
15
20
25
(b)
Log[$H_{c+}$/(1−T/$T_c$)]
$(T/T_{KT}-1)^{-1/2}$

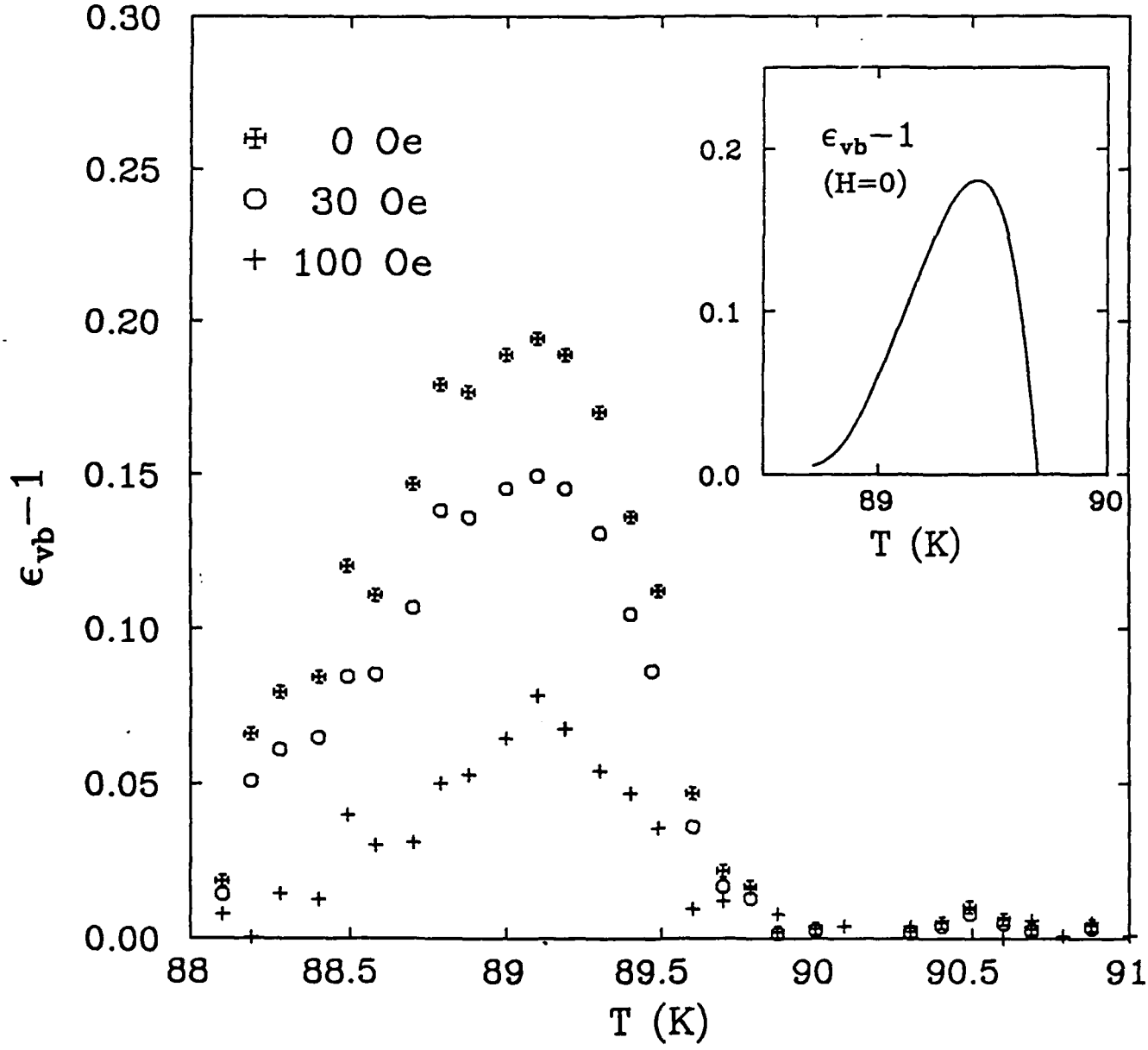
0.30
0.25
0.20
0.15
0.10
0.05
0.00
$\epsilon_{vb}-1$
0 Oe
30 Oe
100 Oe
88
88.5
89
89.5
90
90.5
91
T (K)
$\epsilon_{vb}-1$
(H=0)
0.2
0.1
0.0
89
90
T (K)

Presented at the Conference on Superconductivity and Its Applications (Buffalo, NY 1992)
and submitted for publication in the American Institute of Physics Conference Proceedings (New York, 1993)

# SUPERCONDUCTING PROPERTIES OF LASER-ANNEALED LINES FABRICATED IN OXYGEN DEFICIENT Y-Ba-Cu-O THIN FILMS

**APPENDIX 22**

Wei Xiong, Witold Kula,* and Roman Sobolewski*
Department of Electrical Engineering and Laboratory for Laser Energetics
University of Rochester, Rochester, NY 14627
and
John R. Gavaler
Westinghouse Science and Technology Center, Pittsburgh, PA 15235

## ABSTRACT

We report our studies on the laser annealing of superconducting patterns in semiconducting (oxygen-poor) $YBa_2Cu_3O_{6+x}$ thin films. The films were epitaxially grown on MgO, $SrTiO_3$, and $LaAlO_3$ single crystals in a standard, *in-situ* rf magnetron sputtering process and subsequently annealed at 450°C in pure Ar to become semiconducting at 300 K and insulating at low temperatures. Then the superconductivity was locally restored by placing the films in an oxygen atmosphere and heating up selected areas by a focused *cw* Ar-ion laser beam. A number of 6-μm-wide to 400-μm-wide and up to few-mm-long test structures have been fabricated and measured. The best lines exhibited 0.5-K-wide superconducting transition, $T_{c0}$ = 89.5 K, and $J_c$ above $10^5$ A/cm$^2$. Our results show that laser annealing is a promising technique for fabrication of planar YBCO circuits with few-μm-wide features.

## I. INTRODUCTION

Planar patterning of $YBa_2Cu_3O_{7-x}$ (YBCO) thin films is one of the key technological issues, which must be resolved before successful fabrication of even moderately complex high-$T_c$ superconducting electronic and optoelectronic circuits will be possible.[1,2] Several techniques suitable for patterning of YBCO films such as wet chemical and plasma etching, ion milling, and laser ablation, have been developed. However, they still lack the maturity achieved in metallic superconductors, and often produce structures with contaminated ($T_c$-suppressed) surfaces and fuzzy edges. The above techniques are also intrinsically nonplanar and, in the case of a multiple-layer YBCO patterning, result in a large number of highly undesirable step-like grain boundary weak-links.

Recently a new method of laser processing of YBCO films has been demonstrated.[3–7] The technique is based on the observation that YBCO electrical and optical properties are very sensitive to its oxygen content, which can be easily changed by focused laser beam heating of the material, either in the presence or the absence of an oxygen atmosphere. Local heating of YBCO enables oxygen to diffuse into the laser-annealed lines and form oxygen-rich (superconducting) regions next to depleted (semiconducting) ones, in a manner similar to *n*- and *p*-type diffusion regions in semiconductors. The process is noninvasive, does not require a patterning mask, and does not contaminate the surface of patterned films.

In this work we report our studies on fabrication and superconducting properties of the test structures, laser annealed in intentionally oxygen-depleted (semiconducting) YBCO films.

---

*Also at the Institute of Physics, Polish Academy of Sciences, PL-02668 Warszawa, Poland.

## II. THIN-FILM FABRICATION

Our fabrication procedure started with superconducting YBCO films, epitaxially grown in the *in-situ* fabrication process. A number of films with the thickness from 80 to 200 nm have been deposited on MgO and $SrTiO_3$ substrates by rf magnetron sputtering.[8] The films exhibited about a 1.5-K-wide (10% to 90%) resistive superconducting transition, $\Delta T$, with the zero-resistance temperature, $T_{c0}$, ranging from 83 K to 87 K. In addition, we used 280-nm-thick films grown on $LaAlO_3$ by single target sputtering.[9] The latter films were characterized by excellent superconducting properties ($\Delta T \leq 0.5$ K and $T_{c0} \geq 89.5$ K). All the films were *c*-axis oriented and exhibited critical current densities, $J_c$, greater than $10^6$ A/cm$^2$ at 77 K.

The superconducting films were, subsequently, intentionally deoxidized by furnace annealing at 450°C in pure argon atmosphere. The duration of the deoxidization process was varied from 60 min to 120 min, depending on the film thickness and the desired final oxygen content. Figures 1 and 2 demonstrate resistive behaviors for oxygen-depleted YBCO films deposited on $SrTiO_3$ (Fig. 1) and $LaAlO_3$ (Fig. 2), and annealed for 90 min and 180 min, respectively. We note that in both cases [see Figs. 1(a) and 2(a)] the film resistance rapidly increased at low temperatures and showed no signs of the superconducting transition. At 4.2 K both films were insulating. The observed resistance versus temperature dependence, R(T), is typical for a semiconducting material with thermally activated transport. This latter observation is demonstrated in Figs. 1(b) and 2(b), where the ln[R(T)/R(300 K)] dependence is plotted as a function of inverse temperature. We note that in the high-to-moderate temperature range, experimental points follow a straight line, which corresponds to the $\exp(E_a/kT)$ formula, where $E_a$ is the activation energy and k is the Boltzmann constant. In Figs. 1(b) and 2(b) the fitting lines are plotted for $E_a$ = 73 meV and $E_a$ = 30 meV, respectively. At low temperatures, the film resistance increased slower than expected from the simple exponential behavior, which we interpret as a contribution from the remnant metallic-like transport.

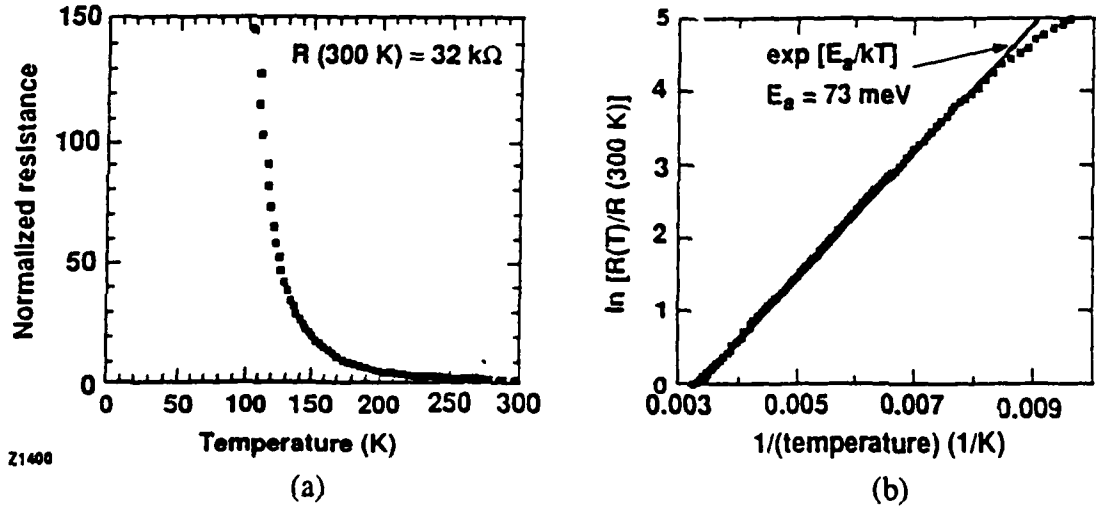


Fig. 1. Resistive behavior of an oxygen-poor 80-nm-thick YBCO-on-$SrTiO_3$ film. (a) linear R(T)/R(300 K) dependence. (b) logarithmic R(T)/R(300 K) dependence.

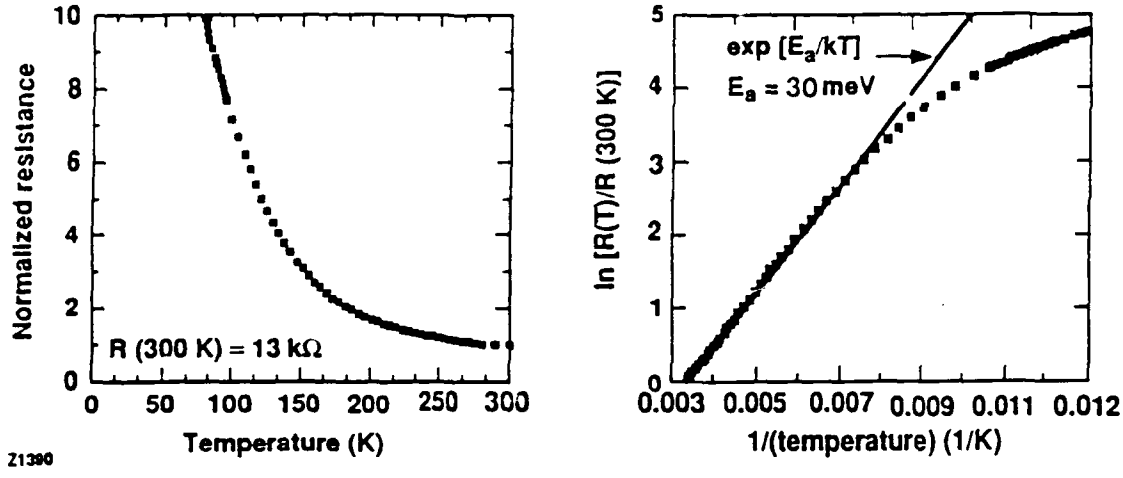


(a) (b)

Fig. 2. Resistive behavior of an oxygen-poor 280-nm-thick YBCO-on-$LaAlO_3$ film. (a) linear R(T)/R(300 K) dependence. (b) logarithmic R(T)/R(300 K) dependence.

## III. LASER ANNEALING

The optical part of our laser annealing apparatus consisted of an Ar-ion *cw* laser ($\lambda = 0.514$ μm), beam shutter, and 20× optical microscope objective. The YBCO sample was located inside a gas chamber attached to a computer-controlled X-Y translational stage. The chamber atmosphere was flowing pure oxygen. After the initial search for optimal annealing conditions,[7] we realized that for all our films the best quality superconducting lines could be obtained in a single/double-sweep laser-annealing process with the very low (0.5–2.0 μm/s) translational stage speed. The optimal laser power density was in the 0.2–1.0 mW/μm$^2$ range.

The described above annealing arrangement allowed us to write two-dimensional, few millimeters in size patterns with the line dimensions varying from 5 μm to 400 μm. Figures 3(a) and 3(b) present optical transmission micrographs of the superconducting structures (dark lines) oxygen annealed in semiconducting YBCO films deposited on $LaAlO_3$ and $SrTiO_3$, respectively. Figure 3(a) shows the example of a 60-μm-wide line, uniformly annealed by a 50-μm-diam laser beam. We note that the interface between the oxygen-rich and oxygen-poor phases is very well defined and is extremely clean. For comparison, Fig. 4(b) presents a wide line fabricated using multiple, 20-μm-wide laser paths. In this case, the line was not completely uniform and its "multiple-path structure" is clearly visible. The multiple-path method also led to a dramatic increase in the patterning time.

## IV. SUPERCONDUCTING PROPERTIES OF LASER-ANNEALED LINES

The electrical measurements of the laser-annealed lines were performed in the standard four-probe geometry using a temperature-controlled, computer-driven station. The sample electrical contacts were wire-bonded to 300-nm-thick silver contact pads evaporated directly on the top of the annealed lines. Figure 4 shows the superconducting transitions for the structures presented in Fig. 3. We note that in both cases, superconducting properties of the laser-annealed lines are the same as those of

the original superconducting films. Thus, somewhat depressed $T_c$, observed in our films fabricated by *rf* magnetron sputtering, should not be associated with oxygen deficiency and is apparently due to the film nonoptimal Y:Ba:Cu cation ratio. The R(100 K)/R(300 K) ratios for the both samples shown in Fig. 4 are relatively large,

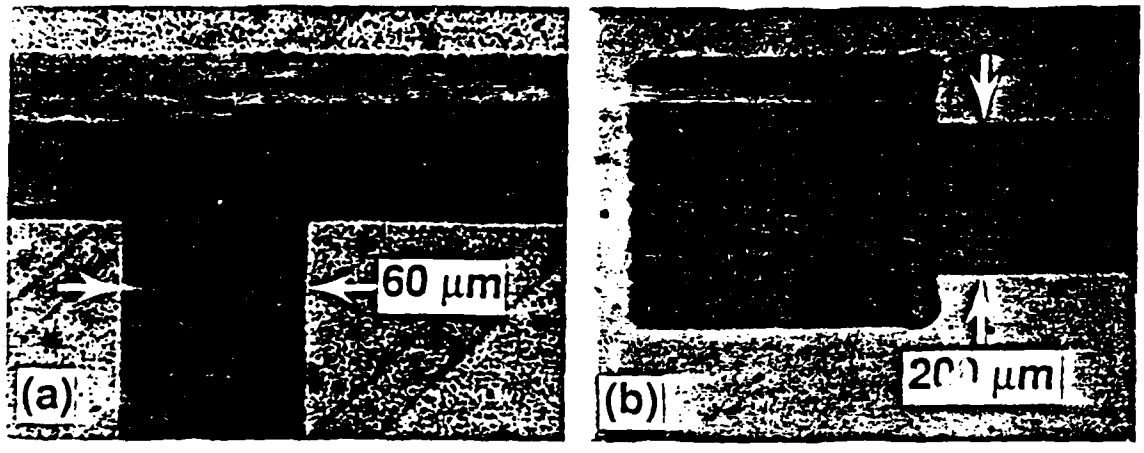


Fig. 3. Optical transmission micrographs of oxygen-rich (superconducting) structures, laser annealed in oxygen deficient YBCO films. (a) 60-μm-wide structure annealed by the single-path method. (b) 200-μm-wide line and ~400-μm-wide contact pad annealed by the multiple-path method.

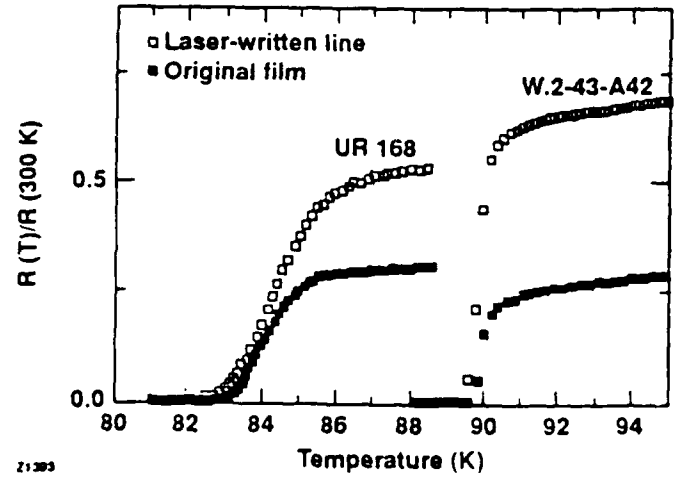


Fig. 4. Comparison between the superconducting transitions of the oxygen-annealed lines presented in Fig. 3 and original superconducting films. UR168 denotes the 80-nm-thick film deposited on $SrTiO_3$, while the label W.2-43-A4 corresponds to the 280-nm YBCO-on-$LaAlO_3$ film.

but we must remember that the actual R(T) measurements were taken in a configuration, which represented a parallel connection of the laser-annealed test structure and its semiconducting surrounding. The critical current density, $J_c$, measurements preformed on the sample W.2-43-A4 showed that $J_c$ was above $10^5$ A/cm$^2$ at 77 K, but we believe it can be increased to the $>10^6$ A/cm$^2$ level by further optimization of the laser-annealing process.

## V. CONCLUSIONS

We have demonstrated that the annealing process, performed in oxygen with the help of a focus laser beam, is a useful technique for patterning of YBCO thin films. The method produces well-defined lines with undamaged crystalline structure and very sharp interfaces. The annealing is fully reversible and the patterns can be either erased by furnace annealing, or rewritten by subsequent laser writing. Most importantly, the patterns are completely planar, free of surface contamination, and they are characterized by superconducting properties, which are as good as those of the original superconducting films.

We strongly believe that the presented laser-annealing procedure can be successfully implemented in fabricating practical electronic and optoelectronic high-$T_c$ devices. The technique is especially promising in YBCO optoelectronics, since in this compound both electrical and optical properties are very sensitive to the sample's oxygen content. Several devices, such as coplanar transmission lines, traveling-wave optical modulators, oxygen-poor photoconductive switches, and field-effect transistors have been already proposed.[2] All structures are completely monolithic and can be fabricated using laser patterning and writing methods.

## ACKNOWLEDGMENTS

The authors would like to thank M. Warmuth for his help in designing the computer-controlled writing system. This work was supported the AFOSR grants: F49620-92-J-0075 (Rochester) and F49620-91-C-0034 (Westinghouse). Additional support was provided by the sponsors of the Laser Fusion Feasibility Project at the Laboratory for Laser Energetics.

## REFERENCES

1. See, e.g., M. R. Beasley, Proc. IEEE 77, 1155 (1989).
2. R. Sobolewski, in Superconductivity and Its Applications, AIP Conference Proceedings 251, edited by Y. H. Kao, A. E. Kaloyeros, and H. S. Kwok (American Institute of Physics, New York, 1992), pp. 659–670.
3. M. Rothschild, J. H. C. Sedlacek, J. G. Black, and D. J. Ehrlich, Appl. Phys. Lett. 52, 404 (1988).
4. R. R. Krchnavek, S.-W. Chan, C. T. Rogers, F. De Rosa, M. K. Kelly, P. F. Miceli, and S. J. Allen, J. Appl. Phys. 65, 1802 (1989).
5. R. C. Dye, R. E. Muenchausen, N. S. Nogar, A. Mukherjee, and S. R. J. Brueck, Appl. Phys. Lett. 57, 1149 (1990).
6. Y. Q. Shen, T. Freltoft, and P. Vase, Appl. Phys. Lett. 59, 1365 (1991).
7. R. Sobolewski, W. Xiong, and W. Kula, to appear in IEEE Trans. on Appl. Supercond. (1993).
8. P. H. Ballentine, A. M. Kadin, and D. S. Mallory, IEEE Trans. Magn. 27, 997 (1991).
9. J. R. Gavaler, J. Talvacchio, T. T. Braggins, M. G. Forrester, and J. Greggi, J. Appl. Phys. 70, 4383 (1991).

# $SrTiO_3$ buffer layers and tunnel barriers for Ba-K-Bi-O junctions

B. A. Baumert
*Department of Materials Science and Engineering, Carnegie Mellon University, Pittsburgh, Pennsylvania 15213*

**APPENDIX 23**

J. Talvacchio and M. G. Forrester
*Westinghouse Science and Technology Center, Pittsburgh, Pennsylvania 15235*

(Received 30 November 1992; accepted for publication 1 March 1993)

Epitaxial $SrTiO_3$ films were used as buffer layers and tunnel barriers for $Ba_{0.6}K_{0.4}BiO_3$ (BKBO) films and tunnel junctions, respectively. In contrast to BKBO films grown directly on $LaAlO_3$, films grown on $SrTiO_3$ (001) buffer layers on $LaAlO_3$ had a single (001) growth orientation, with $T_c$'s of 26 K and $\Delta\omega=0.7°$. These values are both equal to those obtained for growth on a $SrTiO_3$ single crystal. A similar improvement was obtained for BKBO grown on $SrTiO_3$-buffered $NdGaO_3$ substrates. Tunnel junctions consisting of BKBO(001)/$SrTiO_3$/BKBO layers had substantial contributions to the gap voltage from both the base and top BKBO electrodes.

BKBO has a superconducting transition temperature of 30 K[1] and, unlike the higher $T_c$ oxide superconductors, which contain two-dimensional Cu-O planes, BKBO is isotropic[2] and has a relatively long coherence length of 35–50 Å.[3–5] Josephson junctions made from this material can be operated at temperatures which allow the use of closed-cycle helium refrigeration. All-BKBO tunnel junctions have already been fabricated using $KNbO_3$[6] and $BaBi_2O_y$[7] barrier layers. We have found $SrTiO_3$, however, to be the most promising substrate material for reproducibly depositing higher $T_c$, single-orientation films.[8] Consequently, this material was not only studied as a buffer layer for growing BKBO films on more technologically useful substrates such as $LaAlO_3$ and $NdGaO_3$ but was also utilized as the barrier layer in SIS junctions.

A $Ba_{0.6}K_{0.6}BiO_x$ target was used to deposit superconducting BKBO films by rf magnetron sputtering in an off-axis configuration. These were grown on $SrTiO_3$ (001), $LaAlO_3$(001), $NdGaO_3$ (110), and on the latter two with $SrTiO_3$ (001) buffer layers. Details of the depositions and fabrication of the junctions, which were grown on $NdGaO_3$ (001), have been given previously.[8] Resulting films had a composition of $\sim Ba_{0.6}K_{0.4}BiO_{3-x}$ with a lattice parameter of 4.280 Å.

Resistive transitions of BKBO grown on $SrTiO_3$, $LaAlO_3$, and $SrTiO_3$ (001) buffer layers on $LaAlO_3$, all during the same run, are shown in Fig. 1. Room-temperature resistivity measured on a film on $SrTiO_3$ was $\sim 200\ \mu\Omega$ cm. The films were metallic with $\rho(300\text{ K})/\rho(25\text{ K})=2.1$. It can be seen that BKBO films grown directly on $LaAlO_3$ had lower $T_c$'s than those on $SrTiO_3$ substrates, but when $SrTiO_3$ buffer layers were used on the $LaAlO_3$, the $T_c$'s of the BKBO films were equal to those of films grown directly on $SrTiO_3$ and actually had sharper transitions. An improvement of approximately 3 K was obtained as well in the BKBO by using $SrTiO_3$ buffer layers on $NdGaO_3$. Measurements of ac susceptibility showed inductive transitions to increase for films grown on buffer layers by 5–6 K for both $LaAlO_3$ and $NdGaO_3$.

The higher $T_c$'s and sharper transitions correspond directly to the presence of a single-orientation film. Figure 2 shows a comparison of the BKBO (022) and (003) peaks, which are theoretically located at $2\theta$ values of 61.22° and 65.37°, respectively, using Cu $K\alpha$ radiation and assuming a lattice parameter of 4.283 Å.[2] No (022) peak was seen either for films grown on $SrTiO_3$ (001) substrates or buffer layers on $LaAlO_3$, whereas a very large (003) peak was seen in each case, indicating predominantly (001) growth. Although (011) growth on $NdGaO_3$ was greatly diminished by the use of $SrTiO_3$ buffer layers, a fraction ($\sim$2%) of the grains still had an (011) orientation. A mixture of

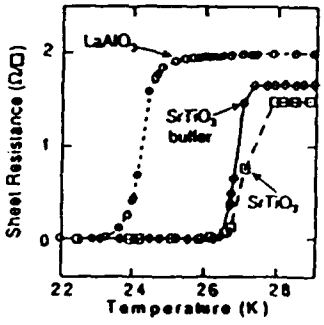


FIG. 1. A comparison of resistive transitions for BKBO films grown on $LaAlO_3$, $SrTiO_3$-buffer $LaAlO_3$, and $SrTiO_3$.

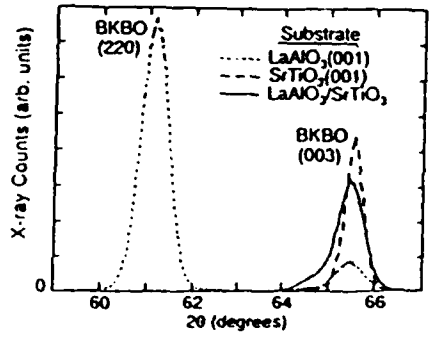


FIG. 2. X-ray $2\theta$ scans showing a comparison of (011) BKBO growth to (001) growth on various substrates.

 0003-6951/93/172137-03$06.00 © 1993 American Institute of Physics 

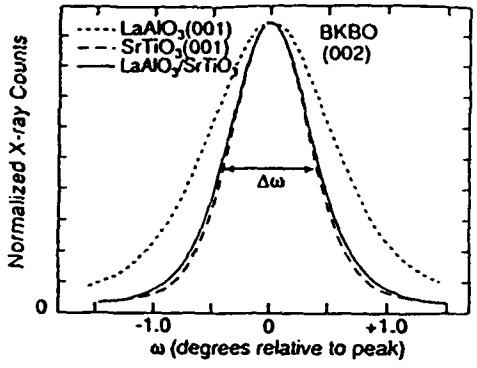


FIG. 3. Mosaic spread of misaligned grains for the (001) growth direction of BKBO films on various substrates.

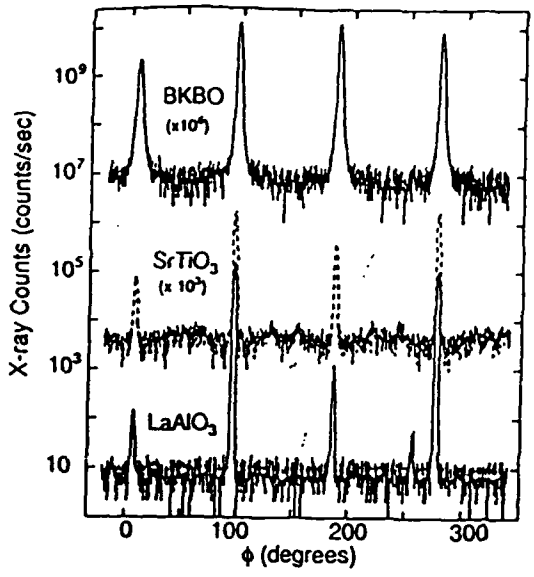


FIG. 4. The in-plane orientation of a BKBO (001) film grown on $SrTiO_3$-buffered $LaAlO_3$. This $\phi$ scan is of the BKBO, $SrTiO_3$, and $LaAlO_3$ {033} x-ray diffraction peaks.

orientations of BKBO was obtained on the $NdGaO_3$ substrates used for BKBO/$SrTiO_3$/BKBO junctions, as well, although the fraction of (011) growth was much lower than for most films grown directly on $NdGaO_3$. This may have been due to the difference in substrate miscut of various wafers.

Typical rocking curve data ($\Delta\omega_1$) for the BKBO (002) diffraction peak are shown in Fig. 3. This shows the mosaic spread in the growth direction and clearly indicates a decrease (from 1.3° to 0.7°) in the spread when a $SrTiO_3$ (001) buffer layer is used on $LaAlO_3$. The BKBO (002) peak is the same width for films grown on $SrTiO_3$ buffer layers as it is for films grown directly on $SrTiO_3$ substrates.

Not only were films grown on buffer layers well-oriented in the growth direction but in the plane of the film as well. Values of $\Delta\omega_2$, which indicate an average of mosaic spreads in the growth direction and in the plane of the film, were decreased from 1.2° for films grown directly on $LaAlO_3$ to 0.5° for films grown on $SrTiO_3$ buffer layers. To obtain the rocking curve widths defined as $\Delta\omega_2$, the BKBO (303) peaks were measured with $\omega \approx 2\theta/2$ and $\Psi = 45°$. Epitaxy is also indicated by the alignment of substrate, buffer layer, and BKBO peaks shown in the $\phi$ scans in Fig. 4.

An important consideration in the growth of trilayer junctions is whether the counterelectrode will grow epitaxially on the barrier layer. Results obtained for growth of BKBO on $SrTiO_3$ (001) substrates[8] as well as on $SrTiO_3$ buffer layers verify that BKBO does indeed grow epitaxially on $SrTiO_3$, therefore indicating the latter to be a favorable material for artificial barriers. It was found that BKBO/$SrTiO_3$/BKBO trilayers grown directly on $NdGaO_3$ (001) grew epitaxially with a predominantly (001) orientation.

Tunneling results for a BKBO/$SrTiO_3$/BKBO junction are shown in Fig. 5. Although a gap voltage cannot be unambiguously determined from the $dV/dI$ curves, the scale of the part of the curves which exhibit a strong temperature dependence in the range of 4–20 K is 7–10 mV. From previous measurements of SIN junctions with BKBO base electrodes,[8] and in agreement with others,[9] a value of $2\Delta/kT_c = 4.3$ was determined for the energy gap of BKBO, $\Delta(T \ll T_c)$. Based on this ratio, a voltage gap, $(\Delta_{base} + \Delta_{top})/e$, of approximately 7 mV would be expected if the contributions to the gap voltage from both the base and top electrodes were consistent with the $T_c$ of the bulk of this particular film. The general agreement between the expected gap voltage and the voltage scale of the structure visible in Fig. 5 is an indication that the initially-deposited BKBO layer in the top electrode, approximately a coherence length thick, was of high quality.

The effective thickness and height of the $SrTiO_3$ barrier for this junction were calculated using a rectangular-barrier model.[10] The width was ~60 Å and the height was between 220 and 360 mV at 4.2 and 14.2 K, respectively. The junctions were highly resistive, which may be why no critical current was observed at zero voltage. The nominal deposited barrier thickness was 200 Å, in disagreement with the calculated thickness of 60 Å. This implies that the barrier grew nonuniformly, with leakage occurring through the thinner parts (thus the shape of the $I$-$V$

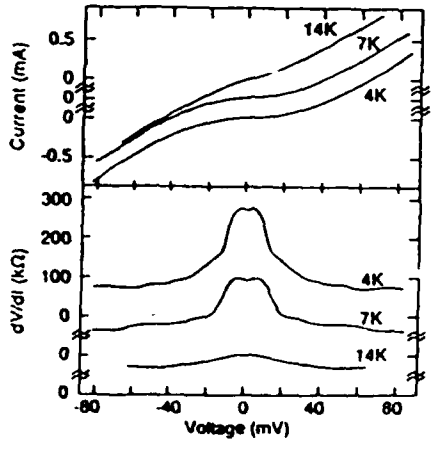


FIG. 5. Tunneling data for an epitaxial BKBO/$SrTiO_3$/BKBO trilayer junction at various temperatures below $T_c$.

curves) or that defects present in the barrier led to increased tunneling probabilities.

Attempts to use thinner $SrTiO_3$ barriers resulted in superconducting shorts, probably due to pinholes in the barrier.[8] The large junction areas used in this work, $\approx 3$ $mm^2$, contributed to the likelihood of a pinhole occurring in the junction area.

In summary, we have shown that $SrTiO_3$ (001) films are useful as both buffer layers for obtaining high-quality, single-orientation BKBO films and as barrier layers in BKBO epitaxial SIS junctions.

The authors would like to acknowledge B. A. Baumert's thesis advisor, M. E. McHenry, and are grateful to A. M. Stewart, J. H. Uphoff, and S. J. Pieseski for technical assistance as well as to A. H. Worsham, R. Hu, S. M. Garrison, R. L. Fink, and E. S. Hellman for helpful discussions. This work is supported by the Air Force Office of Scientific Research under Contract Nos. F 49620-92-J-0415 and F49620-92-C-0039.

[1] R. J. Cava, B. Batlogg, J. J. Krajewski, R. Farrow, L. W. Rupp, Jr., A. E. White, K. Short, W. F. Peck, and T. Kometani, Nature 332, 814 (1988).
[2] S. Pei, J. D. Jorgensen, B. Dabrowski, D. G. Hinks, D. R. Richards, A. W. Mitchell, J. M. Newsam, S. K. Sinha, D. Vaknin, and A. J. Jacobson, Phys. Rev. B 41, 4126 (1990).
[3] U. Welp, W. K. Kwok, G. W. Crabtree, H. Claus, K. G. Vandervoort, B. Dabrowski, A. W. Mitchell, D. R. Richards, D. T. Marx, and D. G. Hinks, Physica C 156, 27 (1988).
[4] B. Batlogg, R. J. Cava, L. F. Schneemeyer, and G. P. Espinosa, IBM J. Res. Dev. 33, 208 (1989).
[5] W. K. Kwok, U. Welp, G. W. Crabtree, K. G. Vandervoort, R. Hulscher, Y. Zheng, B. Dabrowski, and D. G. Hinks, Phys. Rev. B 40, 9400 (1989).
[6] R. L. Fink, M. Thompson, C. Hilbert, and H. Kroger, IEEE Trans. Appl. Supercond. 3, 2219 (1993).
[7] E. S. Hellman, S. Martin, E. H. Hartford, D. J. Werder, G. M. Roesler, and P. M. Tedrow, Physica C 201, 166 (1992).
[8] B. A. Baumert and J. Talvacchio, IEEE Trans. Appl. Supercond. 3, 1567 (1993).
[9] B. M. Moon, C. E. Platt, R. A. Schweinfurth, and D. J. Van Harlingen, Appl. Phys. Lett. 59, 1905 (1991).
[10] J. G. Simmons, J. Appl. Phys. 34, 238 (1963).

# Laser patterning of Y-Ba-Cu-O thin-film devices and circuits

APPENDIX 24

Roman Sobolewski, W. Xiong, and W. Kula[a)]
*Department of Electrical Engineering and Laboratory for Laser Energetics, University of Rochester, Rochester, New York 14627*

J. R. Gavaler
*Westinghouse Science and Technology Center, Pittsburgh, Pennsylvania 15235*

(Received 2 July 1993; accepted for publication 15 November 1993)

We report our studies on electrical properties of Y-Ba-Cu-O test devices and circuits fabricated using a laser-writing patterning technique. The patterning procedure is noninvasive, does not require a patterning mask, and does not contaminate nor damage the surface of patterned films. Our laser-written, oxygen-rich lines (typically 4–100 $\mu$m wide) possess excellent superconducting properties with zero resistivity at 89.5 K and critical current densities of above 2 MA/cm$^2$ at 77 K. On the other hand, oxygen-poor regions are semiconducting and exhibit thermally activated transport, well described by a three-dimensional, variable-length hopping process. Their resistance below 100 K is above 10 MΩ/square. A number of test structures patterned by laser writing, such as a microbridge, coplanar transmission line, open-ended microwave resonator, photoconductive switch, and Y-Ba-Cu-O field-effect transistor, have been presented.

Planar patterning of $YBa_2Cu_3O_{7-x}$ (YBCO) thin films is one of the key technological issues that must be resolved before successful fabrication of even moderately complex, high-$T_c$ superconducting circuits will be possible.[1] YBCO is a multielement material with highly anisotropic crystalline structure that makes the etching process difficult and often results in patterns with fuzzy edges and a degraded (e.g., oxygen deficient) chemical composition. In addition, the YBCO surface is extremely sensitive to contamination by chemicals used in standard patterning procedures.

Recently, a new laser method for patterning YBCO circuits has been developed.[2–6] The technique is based on the observation that YBCO electrical and optical properties are very sensitive to the material's oxygen content. Oxygen can be diffused in or out of the YBCO film by heating the sample in either the presence or the absence of an oxygen atmosphere. The heating can be done locally with a focused laser beam. Thus, an intentionally oxygen-depleted (insulating at low temperatures) YBCO film can be patterned by embedding in it oxygen-rich (superconducting) lines or vice versa. The writing is fully reversible, and the patterns can be either erased by furnace annealing or rewritten by subsequent laser writing. Most importantly, the technique is noninvasive, does not require a patterning mask, and results in completely planar structures, free of surface contamination or edge degradation.

The aim of this article is to demonstrate that the laser-writing method is a reliable and practical technique, perfectly suited for patterning even complicated YBCO thin-film devices and circuits. We examine several laser-written test devices and show that they exhibit very good superconducting properties and can survive, without degradation, longterm storage in air at room temperature. Some of them also combine in a new and unique way the superconducting and dielectric properties of the oxygen-rich and oxygen-poor YBCO phases. These latter structures are, in our opinion, prime candidates for the proposed high-$T_c$ superconducting optoelectronics.[7]

Our laser-patterning apparatus consisted of an Ar-ion continuous-wave laser ($\lambda$=0.514 $\mu$m), shutter, focusing microscope, and computer-controlled $X$-$Y$ translational stage with a gas chamber and sample holder. The sample ambient atmosphere was either pure nitrogen or oxygen. Contrary to our previous arrangement,[6] the substrate of the YBCO film was not in a direct heat contact with the metallic substrate holder, but it was suspended on a thin thermal insulator. This change allowed us to reproducibly write two-dimensional patterns not only on YBCO-on-$LaAlO_3$ films but also on films deposited on MgO and $SrTiO_3$. Typical line dimensions of our patterns varied from <5 to 100 $\mu$m. Laser-power intensity applied to the film was kept between 0.2 and 5 mW/$\mu$m$^2$, and a translational stage speed was in the range of 0.5–5 $\mu$m/s for writing oxygen-rich lines and ~50 $\mu$m/s for (written in $N_2$) oxygen-poor structures.

The test structures were laser patterned on about 80- to 300-nm-thick epitaxial YBCO films grown on $LaAlO_3$ and $SrTiO_3$ substrates using a single-target rf sputtering technique.[8] The best as-deposited films exhibited about 0.5-K-wide (10%–90%) superconducting transition $\Delta T_c$ with the zero resistivity $T_{c0}$ at 89.5 K, and the critical current density $J_c$ of above 2 MA/cm$^2$ at 77 K. The films have been intentionally deoxygenated by radiative heating for 60 min in 15 mT of argon at 680 °C to become nonsuperconducting. Indeed, after the argon annealing, the film resistance vs temperature $R(T)$ curve was a rapidly increasing function of the temperature decrease with no signs of the superconducting transition. The film sheet resistance below 100 K was above 10 MΩ/square, which corresponded to the upper limit of our resistance-measurement apparatus.

Optical transmission micrographs of a superconducting microbridge, oxygen-poor YBCO gap, coplanar microwave structure, and YBCO electric-field device—the four laser-written test structures presented in this letter—are shown in

[a)]Also at the Institute of Physics, Polish Academy of Sciences, PL-02668 Warszawa, Poland.

 0003-6951/94/64(5)/643/3/$6.00 © 1994 American Institute of Physics 

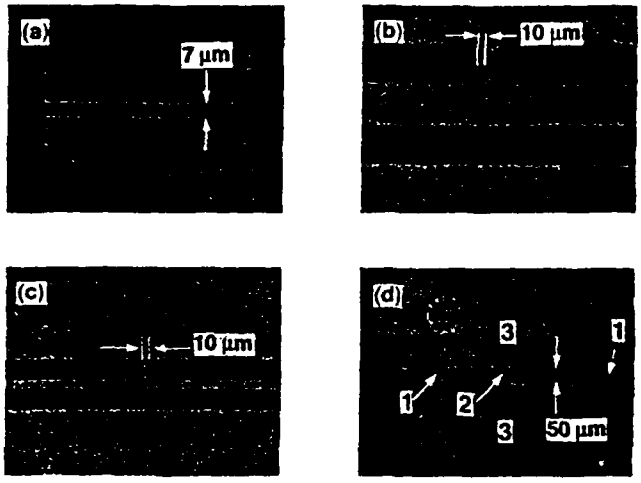


FIG. 1. Optical transmission micrographs of oxygen-rich (dark) test structures, laser written in oxygen-depleted (light-gray) YBCO films. (a) 7-$\mu$m-wide and 160-$\mu$m-long superconducting microbridge; (b) 10-$\mu$m-wide oxygen-poor YBCO gap incorporated into a superconducting transmission line; (c) left end of an open-ended coplanar microwave resonator; and (d) field-effect test structure prepared in a single YBCO film.

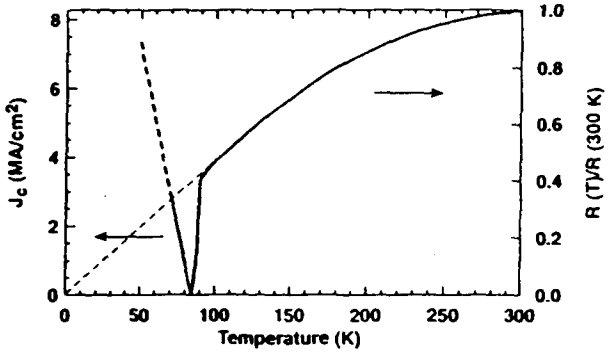


FIG. 2. Resistance and critical current density dependence on temperature for the microbridge shown in Fig. 1(a).

Figs. 1(a)–1(d), respectively. All patterns exhibit very sharp (less than 1 $\mu$m wide) superconducting-semiconducting interfaces with linear current-voltage characteristics.[9] The devices presented in Figs. 1(a)–1(c) were patterned by writing oxygen-rich (superconducting) lines in fully oxygen-depleted YBCO films. A reverse procedure, based on overwriting oxygen-rich lines in $N_2$ atmosphere, was implemented for patterning the two, 10-$\mu$m-wide coupling slits in the coplanar resonator [one slit is shown in Fig. 1(c)]. In the case of a field-effect transistor structure [Fig. 1(d)], we started the fabrication process with a partially deoxygenated film ($T_c$ between 10 and 60 K, depending on the design) and patterned in $O_2$ atmosphere fully oxygenated drain and source electrodes (the two dark regions). Next, we changed the sample's ambient atmosphere from $O_2$ to $N_2$ and produced oxygen-depleted areas (the light-gray regions) above and below the electrodes, completely insulating the transistor structure from the rest of the film. As a result, we obtained at the center of the device a 1-mm-long and 60-$\mu$m-wide, partially deoxygenated transistor's channel.

Figure 2 shows the $R(T)$ and $J_c(T)$ curves measured for the 7-$\mu$m-wide microbridge presented in Fig. 1(a). We note a sharp superconducting transition of our laser-patterned line. A somewhat unconventional shape of the normal-state $R(T)$ curve is due to the fact that at high temperatures a test current also flows through the oxygen-poor YBCO, which is parallel to the microbridge [see Fig. 1(a)]. At low temperatures (below 150 K), $R(T)$ decreases linearly, since in this temperature range, the resistivity of the oxygen-poor material is extremely high. The low temperature extrapolation of the $R(T)$ curve crosses the resistance axis at the axis origin. The $J_c(T)$ dependence is almost linear, and $J_c$ increases at the rate of about 0.2 MA/cm$^2$/K, reaching above 2 MA/cm$^2$ at 77 K.

Figure 3 shows in detail the resistive transition presented in Fig. 2 (sample A, open squares), together with the transition from the original, as-deposited film (sample A, closed squares) and the traces (sample A, closed and open circles) measured on the same sample, but two and eight months after the original patterning. We see that instead of expected degradation in the sample's superconducting properties, the laser-written structures actually exhibit slightly *enhanced* $T_{c0}$'s and improved $R(100\text{ K})/R(300\text{ K})$ ratios. We associate these effects with a slow process of longterm oxygen ordering, which should lead to the film's "self-improvement." The room-temperature storage in air also did not degrade physical appearance of our samples nor their superconducting-semiconducting interfaces. Figure 3 also presents the two superconducting transitions (sample B, open and closed squares) for a laser-written microbridge patterned in a magnetron-sputtered YBCO-on-$SrTiO_3$ film. Comparing the sets of curves for the A and B samples, we note that in both cases the laser-patterned lines and the original films exhibit the same $\Delta T_c$ and $T_{c0}$. Thus, a depressed $T_c$, observed in the B sample, should not be associated with oxygen deficiency or improper patterning but is, apparently, due to the film's nonoptimal Y:Ba:Cu cation ratio, or large concentration of defects.

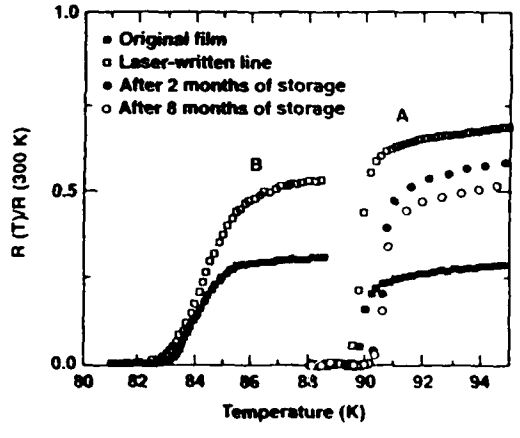


FIG. 3. Comparison between the superconducting transitions of laser-written, oxygen-rich lines and the original, as-deposited superconducting films. "*A*" denotes the 280-nm-thick, YBCO-on-$LaAlO_3$ film, while "*B*" corresponds to the 80-nm-thick film deposited on $SrTiO_3$.

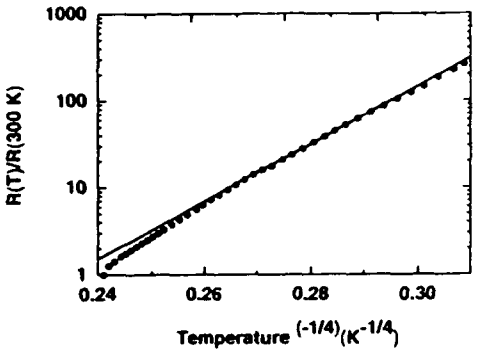


FIG. 4. Logarithmic $R(T)/R(300\ \mathrm{K})$ dependence vs the fourth root of the inverse temperature for the oxygen-poor YBCO gap shown in Fig. 1(b).

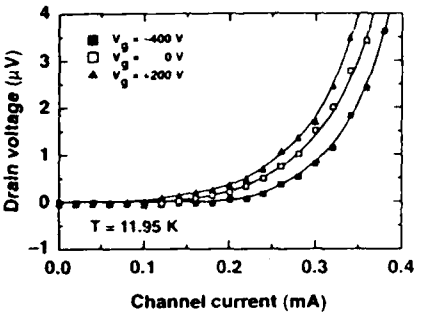


FIG. 5. Drain voltage vs channel current characteristics of the sample of Fig. 1(d), registered at 11.95 K for three different values of $V_g$.

Resistive measurements of the oxygen-poor YBCO were performed on the sample shown in Fig. 1(b). We observed a thermally activated transport, which is characteristic for disordered semiconductors. This latter fact is illustrated in Fig. 4, where the $\ln[R(T)/R(300\ \mathrm{K})]$ dependence is plotted as a function of the fourth root of the inverse temperature. We note that most of our experimental data points follow a straight line, demonstrating that the low-temperature transport in oxygen-poor YBCO is controlled by three-dimensional, variable-length hopping. We also note that the complete structure presented in Fig. 1(b)—a gap incorporated in a transmission line—is very similar to that of a GaAs photoconductive switch (so-called "Auston switch"), routinely used in generating ultrafast electrical transients.[10] Indeed, we fabricated the above structure with the intention to study the dynamics of the optical electron-hole pair generation in semiconducting YBCO.

Figure 1(c) shows one end of a coplanar microwave resonator. The entire resonator is 7.5 mm long and is incorporated into an oxygen-rich coplanar transmission line. A resonator structure identical to that shown in Fig. 1(c) but with the line separation of 285 $\mu$m has been tested and has shown very good microwave properties. Its quality factor measured at 24 K was about 5000 at 6.5 GHz. We also studied a 50 $\Omega$ coplanar transmission line, laser written in the same process as the resonator. The measurements were performed in the frequency range of 1–15 GHz, and we observed more than 60 dB improvement in the line-transmitted power $S_{21}$, as the temperature was lowered from 300 K to that below $T_c$. At all temperatures below $T_c$, the $S_{21}$ was practically constant and near 0 dB, indicating low microwave losses of the oxygen-poor YBCO.

A top view of a YBCO field-effect transistor with a partially deoxygenated channel is presented in Fig. 1(d). The homogeneous regions with three different levels of gray, visible in this figure, correspond to (1) highly oxygenated ($T_c \sim 90$ K) drain and source electrodes, (2) partially deoxygenated ($T_c \sim 25$ K) channel, and (3) oxygen-poor (insulating) transistor borders. The structure was patterned in a 100-nm-thick YBCO-on-$SrTiO_3$ film, with the film substrate serving as the device's gate dielectric. Figure 5 presents the drain voltage vs the channel current characteristics for an as-fabricated device, operated in a common-source mode at 12 K. We note that the positive gate voltage, $V_g$, caused suppression of $J_c$, while the negative $V_g$ enhanced $J_c$. We observed up to 43% $J_c$ enhancement in our best sample, and even higher $J_c$ increase is expected, since we applied to the gate, electric fields which were about an order of magnitude lower than those typically applied by the other groups. We need to stress, however, that the $J_c$ changes observed by us were partially irreversible and samples measured more than one week after their fabrication did not exhibit any measurable field effect. The above observation, as well as the magnitude and the sign of the $J_c$ modulation, leads us to believe that the field effect in oxygen-depleted YBCO is of a chemical nature and is related to the electric-field-induced modification of the oxygen order in YBCO, exactly as it has been predicted by Chandrasekar *et al.*[11] Detailed studies on the physics of the charging effect in oxygen-deficient YBCO thin films will be presented elsewhere.[12]

The authors would like to thank Professor Donald P. Butler for providing us with the microwave data. This work was supported by the Air Force Office for Scientific Research Grants F49620-92-J-0075 (Rochester) and F49620-91-C-0034 (Westinghouse). W.X. also acknowledges support from the Frank Horton Graduate Fellowship Program.

[1] See, e.g., A. I. Braginski, in *Superconducting Devices and Their Applications*, edited by H. Koch and H. Lübbig, Springer Proceedings in Physics (Springer, Berlin, 1992), Vol. 64, pp. 3–18.
[2] M. Rothschild, J. H. C. Sedlacek, J. G. Black, and D. J. Ehrlich, Appl. Phys. Lett. 52, 404 (1988).
[3] R. R. Krchnavek, S.-W. Chan, C. T. Rogers, F. De Rosa, M. K. Kelly, P. F. Miceli, and S. J. Allen, J. Appl. Phys. 65, 1802 (1989).
[4] R. C. Dye, R. E. Muenchausen, N. S. Nogar, A. Mukherjee, and S. R. J. Brueck, Appl. Phys. Lett. 57, 1149 (1990).
[5] Y. Q. Shen, T. Freltoft, and P. Vase, Appl. Phys. Lett. 59, 1365 (1991).
[6] R. Sobolewski, W. Xiong, and W. Kula, IEEE Trans. Appl. Supercond. 3, 2986 (1993).
[7] R. Sobolewski, AIP Conf. Proc. 251, 659 (1992).
[8] J. R. Gavaler, J. Talvacchio, T. T. Braggins, M. G. Forrester, and J. Greggi, J. Appl. Phys. 70, 4383 (1991).
[9] R. Sobolewski, W. Xiong, W. Kula, and B. McIntyre, Physica B (to be published).
[10] D. H. Auston, Appl. Phys. Lett. 26, 101 (1975).
[11] N. Chandrasekhar, Oriol T. Valls, and A. M. Goldman, Phys. Rev. Lett. 71, 1079 (1993).
[12] W. Kula and R. Sobolewski (unpublished).

# Superconductive Electronics with High Transition Temperature Films

A. Davidson, J. Talvacchio, M.G. Forrester, and J.R. Gavaler

Westinghouse Science and Technology Center
1310 Beulah Road
Pittsburgh, PA 15235

## ABSTRACT

Electronics based on high transition temperature superconductive thin film materials is presently viable in some important niches, particularly in passive microwave circuits. Applications requiring Josephson junctions are impeded by the lack of reproducible junctions, but the junctions that can be produced are good candidates for the new Rapid Single Flux Quantum class of extremely fast digital circuits. Other devices that take advantage of the weak fluxoid pinning of some films are also promising, particularly the flux flow transistor. The availability of both Josephson and flux flow devices at 77K invites exploration of hybrid technologies using HTS multi-chip modules supporting silicon CMOS chips and superconductive chips at the same time. The superconductive contribution to the emerging applications can result in significant performance advantages, particularly in remote sensing and communications.

## INTRODUCTION

The Rapid Single Flux Quantum[1] (RSFQ) Josephson junction family of digital circuits was invented before the discovery of high temperature superconductivity. The flux flow transistor[2] (FFT) was developed using classic helium temperature superconductive materials. Superconductive microwave devices[3] are also not new. CMOS semiconductors have been developed for reasons having nothing at all to do with competition from superconductive devices. But all of these independent advances are now linking up with one another as a result of the discovery and unique material properties of high temperature superconductivity (HTS) oxides, and the steady improvement of HTS thin films and structures. Applications in radar and communication using passive devices[4] are most imminent, because the structures are simple, and the improvement over the normal-state equivalent is large. Signal processing and data switching circuits are also under development, but will require a lot more materials understanding to be equally advantageous. This paper reviews the progress that has been made in depositing high

quality HTS films on appropriate substrates, and relates this progress to device and circuit properties needed for various applications.

## FILMS

Many other papers in this conference deal with the details and complexities of film deposition. Here we list two of the major techniques used now, with some comments on the relative merits. Despite a lot of early work using coevaporation[5], the presently preferred methods are sputtering[6] and laser ablation[7]. These work in similar ways. They both involve transport of material from a stoichiometric target to a heated substrate. In ablation this transport is accomplished by focusing a nanosecond scale laser pulse of sufficient energy onto the target. The pulse heats the target immediately under the surface, vaporizing it, and causing an explosive discharge of material perpendicular to the target surface. Some of the ejected material is energetic enough to be in the form of a plasma; some is apparently in the form of particles and droplets. A heated substrate a few centimeters away collects the material to build up a film. Laser ablated films are typically of high quality, with excellent stoichiometry, and good supercondcutive parameters.Work is progressing to improve surface roughness, and to handle larger (>5 cm) wafers. The deposition rate for small wafers, however is fairly rapid, typically a few Angstroms per second.

The sputtering method is in many ways complementary to laser ablation. It is slow, often in the range of 0.1 Angstroms per second. It is easy to scale up to large wafers, with 5 cm diameters common, and 10 cm under development. The most common kind of sputtering is with rf magnetron systems, using an off-axis geometry. In the off-axis arrangement, the substrates are orthogonal to the target, and usually off to the side, to avoid direct bombardment by negative ions. These are ionized oxygen atoms, which can come from either the sputter gas or the target itself, and which are energetically emitted from the target. Under conditions which minimize resputtering from hot surfaces in the vicinity of the substrate, sputtered YBCO films were the first to be grown without the presence of CuO precipitates. Smooth films resulting from the elimination of CuO particles have also been produced by laser ablation by employing an off-axis configuration[8]. The off-axis configuration reduces the high-deposition-rate advantage of laser ablation compared to sputtering. The ultimate importance of uniform deposition on large wafers should be emphasized. For this purpose other deposition techniques such as MOCVD[9] may prove to be the best technique. For now, however, ablation and sputtering produce the best films.

Choice of substrate is extremely important to the successful completion of useful circuits. $SrTiO_3$ substrate[10] can be used to grow very high quality films, but with an extraordinarily high dielectric constant, which rules it out for any high speed applications. $LaAlO_3$[11] has a much lower dielectric constant, approximately 24, and has been used successfully for single layer applications, such as microstrip or co-planar microwave filters and delay lines. It has not worked so well for multi-layer circuits, however, because of motion of twin boundaries[12] when the wafer is heated for application of new HTS layers. The moving twins can shift the bottom film layers by several microns over the width of even a one centimeter chip, making alignment of subsequent layers impossible. At the moment, $NdGaO_3$[13] appears to be the substrate of choice for multilayer circuits. It has a low dielectric constant, similar to $LaAlO_3$, but without the shifting twins.

Consideration of multi-layer structures also determines the choice of HTS film material. The materials with the highest $T_c$'s are TBCCO,and, recently, HgBCCO[14], but their lack of stability means that for now there is no way to produce multiple levels. YBCO has proven to have the best combination of transition temperature and superconductive properties, and with enough stability so that subsequent layers can be formed without degradation of prior layers.

In addition to superconducting films, epitaxial insulating films are required in multilayer superconducting circuits for isolation of ground planes, crossovers, lumped-element capacitors and inductors, and flux transformers. Epitaxial growth is not necessarily required to obtain desired properties for the insulator but is necessary to support growth of subsequent high-quality superconducting film layers. The obvious candidate materials for epitaxial insulators are the same ones that work well as substrates. Other oxide and fluoride compounds which, for example, cannot oe grown as large single crystals, but have a good lattice match to YBCO have been tested. Figure 1 summarizes the dielectric loss properties of various thin-film dielectrics studied at Westinghouse in comparison with minimum requirements estimated for several applications. The loss tangent is based on data from bulk samples and the dc resistivity at 77K was measured on parallel-plate capacitor structures with YBCO on the bottom or on both sides. Both the $SrTiO_3$ and $Sr_2AlTaO_6$ (SAT)[15] grew as pinhole-free films but SAT is the better choice for most applications based on lower values of both the real and imaginary parts of its dielectric constant.

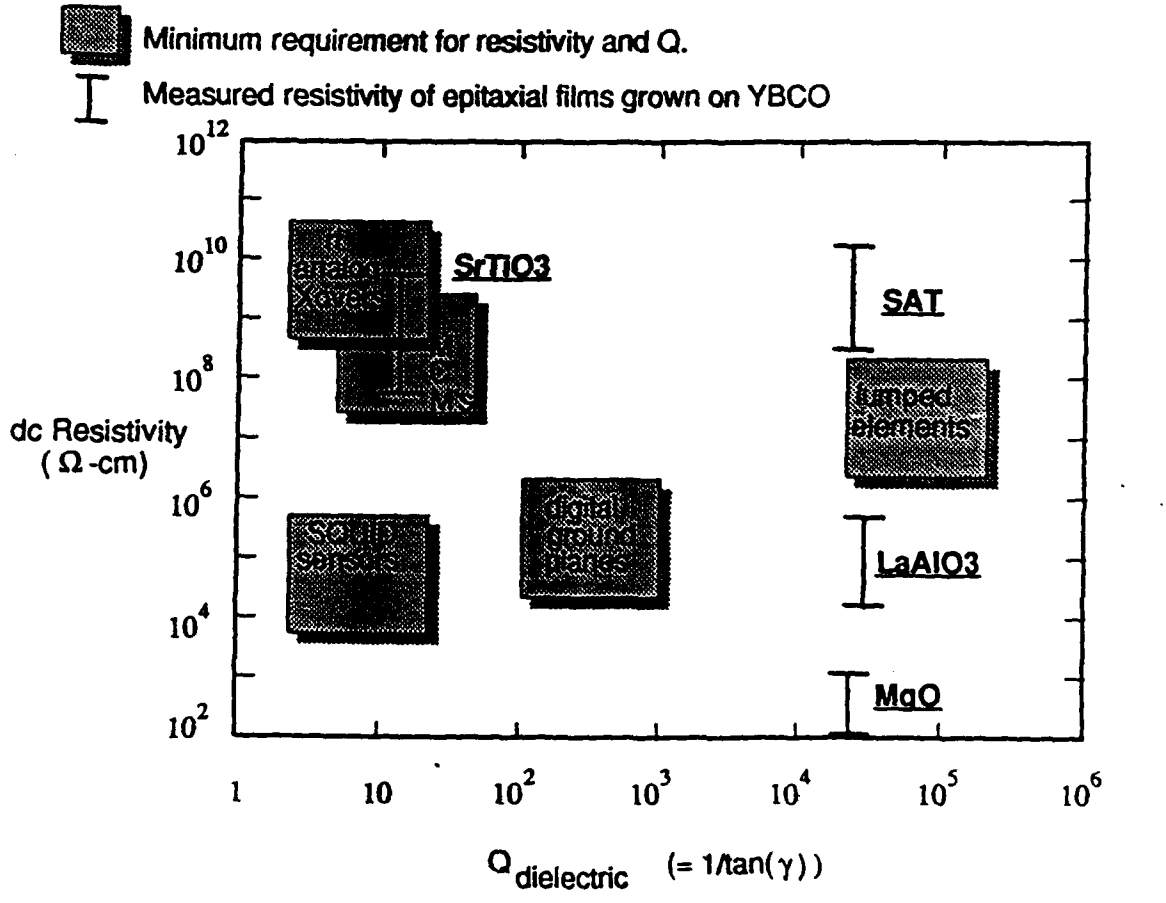


Fig. 1. Requirements for HTS dielectrics, and the performance of some known examples. These films grow epitaxially on appropriate substrates, and support epitaxial growth of YBCO.

It is possible to find substrate materials that are compatible with both HTS films and ordinary semiconductor devices, so that hybrid circuits for use in liquid nitrogen can be produced monolithically[16]. For example, a layer of silicon can be grown epitaxially on

is known as Silicon on Sapphire, or SOS. After the transistors are formed, areas for the HTS devices can be stripped down to the substrate, and with appropriate buffer films, good YBCO layers can be grown as well. The 750 C temperature will not hurt the transistors, particularly if the HTS deposition is quick, as in laser ablation.

## HTS Applications

We can expect commercial and military use of HTS films for microwave passive components, such as filters or delay lines, in the near future; and as ground planes and interconnection wires on multi-chip modules further out in time. Passive microwave devices using HTS films are particularly attractive because they combine very low insertion loss with small size and low weight. In fact, even including the necessary refrigeration, use of such devices still saves space and weight, and provides a performance edge[17]. A prototype Westinghouse X-band filter is shown in Fig. 1, and the measured performance of a prototype bank of four filters[18] is shown in Fig. 2.

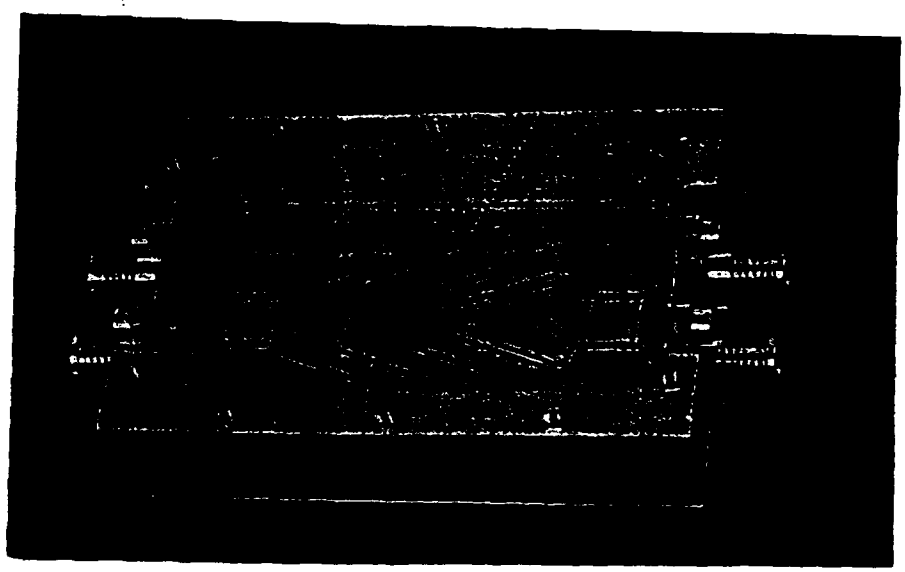

Fig. 2. A Westinghouse 4 GHz HTS filter. The wafer is approximately 5 cm long. Such filters will outperform normal components with dimensions of 30 or more cm, and weighing many kilograms.

In the longer term, HTS film structures can be expected to play a key role in the interconnection of semiconductor chips[19]. CMOS silicon devices work better at 77K than at room temperature. The operating voltage is lower, there is less dissipation, and switching is faster. By putting low temperature silicon chips on a HTS board, this speed advantage

can be increased because of the nearly lossless characteristics of HTS microstrip transmission lines. The advantage could be increased even further if hybrid CMOS HTS circuits are developed to drive these transmission lines.

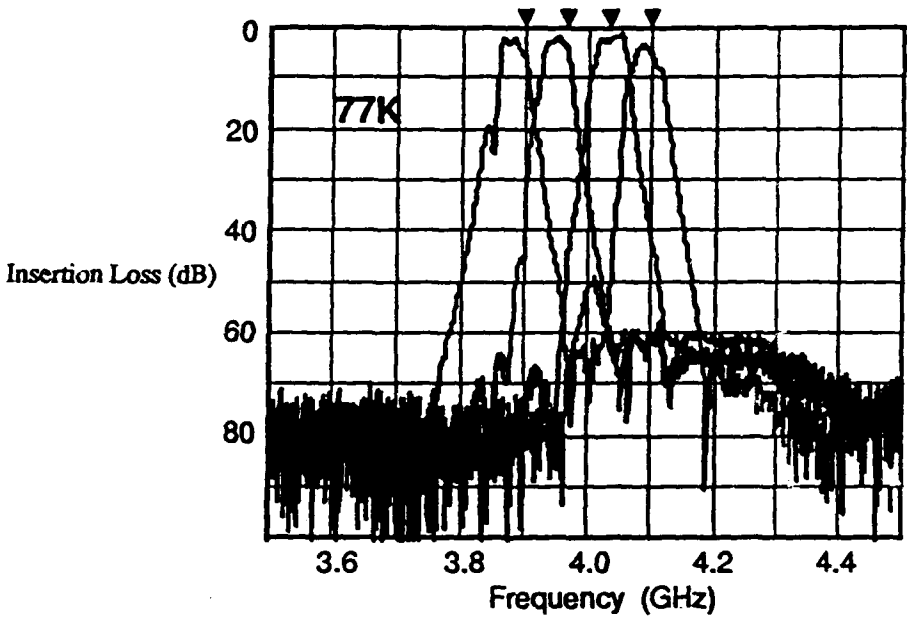


**Fig. 3.** Measured characteristics of the Westinghouse prototype filter bank. The four triangles at the top mark the intended center frequencies.

## HTS Active Devices

The classical superconductive active device is the Josephson junction, in one form or another. Several other types of active devices have also been developed in classical technology, including FET-like and bipolar-like devices[20], and also a rather successful group of devices which control the movement of magnetic flux, or flux-flow devices. In HTS technology at present, two types have achieved some success, the Josephson junction and the flux flow devices. However, the relative success of these two are reversed, relative to classical superconductive technology. The flux flow devices in many ways take advantage of some natural properties of HTS material, whereas Josephson junctions have to fight against them.

### Josephson junctions

It is very difficult to make the exact analog of a classical Josephson junction out of HTS materials. The trouble stems from a combination of extreme anisotropy due to the layered nature of HTS superconductors, and their very short coherence lengths (roughly 3 to 30 Angstroms). This means that superconductivity, and hence the Josephson effects, are suppressed at almost all interfaces of these materials. Usable junctions, however, have been made in some clever ways.

For electronics the most successful methods so far involve "edge junctions[21]," where some property or configuration is altered where a film goes up over an edge of an underlying film, usually an insulator. In some cases, a thin normal metal at the edge provides the coupling between films, in others a deposited oxide is used. Fig. 4 shows a typical step-edge geometry where gold couples to HTS films across a small (100 nm) gap.

Josephson junction. Where parasitic capacitance has been large, hysteresis has also been observed but never with a true gap structure. Therefore these junctions are not suited for many of the classical superconductive circuit families that require hysteresis or a sharp gap.

There is one class of digital circuits which require just what HTS edge Josephson junctions seem to deliver, and that is the Rapid Single Flux Quantum[1,22] (RSFQ) type of circuit. RSFQ circuits do not use voltage or current levels to represent ones and zeroes, as all transistor and most superconducticive circuits do. Rather, bits are represented by the presence or absence of quantized fluxoids in different parts of the circuits.

Quantization of magnetic flux is an integral part of superconductive circuits, where the magnetic flux enclosed by a superconductive path is forced to take on a value corresponding to an integral multiple of $\Phi_0 = 2.07 \times 10^{-15}$ Webers. It is relatively simple, by controling inductance and critical current values, to control the motion of single flux quanta, or fluxons, in superconductive circuits using Josephson junctions. Fig. 5 below compares a simple RSFQ circuit for transmitting fluxons to a mechanical analog. The marble clearly corresponds to the fluxon, and the spring loaded gates are roughly analagous to Josephson

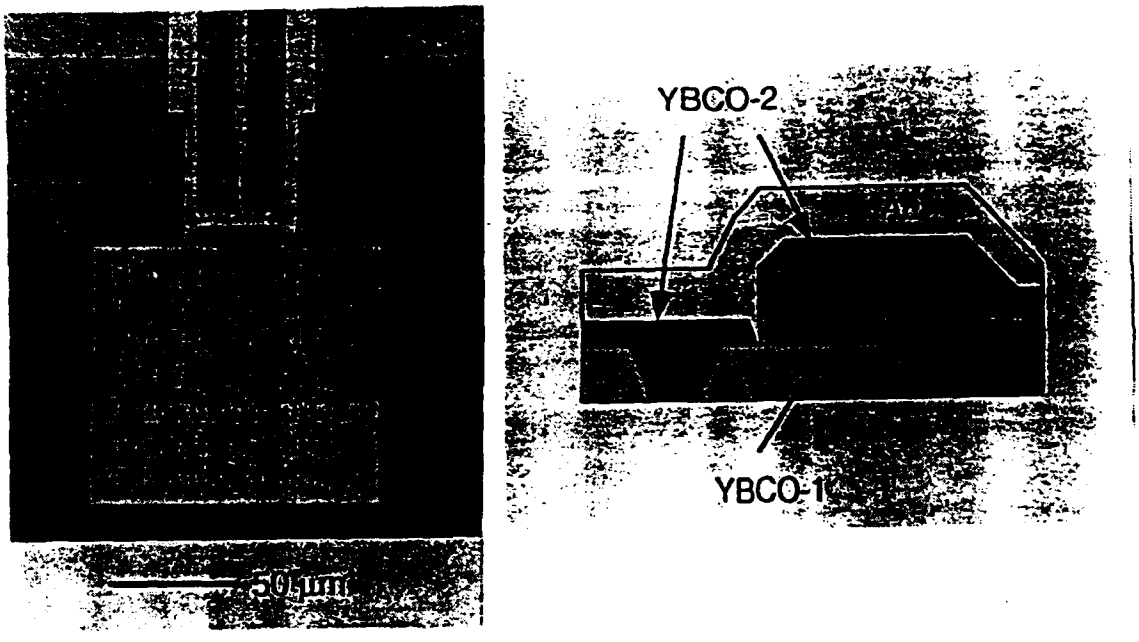


**Fig. 4. Configuration of an HTS step-edge Josephson junction. On the right is a schematic cross section, showing the two layers of YBCO, the insulating step, and the gold layer that provides the Josephson coupling. On the left is a top view of a device fabricated at Westinghouse using this structure.**

junctions. The bias current exerts a force on the fluxon, via the Lorentz force, as gravity applies a force to the marble. It is possible to achieve any logic function using some fluxons to control the motion of other fluxons through their interaction with the Josephson junctions. In this approach it is necessary to use some Josephson junctions to allow surplus fluxons to escape from the circuit, as one could use spring loaded gates in the mechanical analog as trap doors to dispose of excess marbles.

The focus of research on edge junctions is to find ways to minimize the spread in critical current values. At present it is common for junctions on the same chip to have a critical curent spread of 50% or more, though some have been produced with spreads of only about 20%. This magnitude of variation is sufficient for only the smallest digital

circuits, with at most a few dozen junctions. To fulfill the potential of RSFQ circuits with thousands of junctions, critical current spreads of at most a per cent or two will have to be developed. At the moment, a certain type of nanobridge junction[23] is much better than the edge geometry for minimizing current spread, but these junctions have critical currents too low for reliable operation at liquid nitrogen temperature, and are not amenable to higher currents.

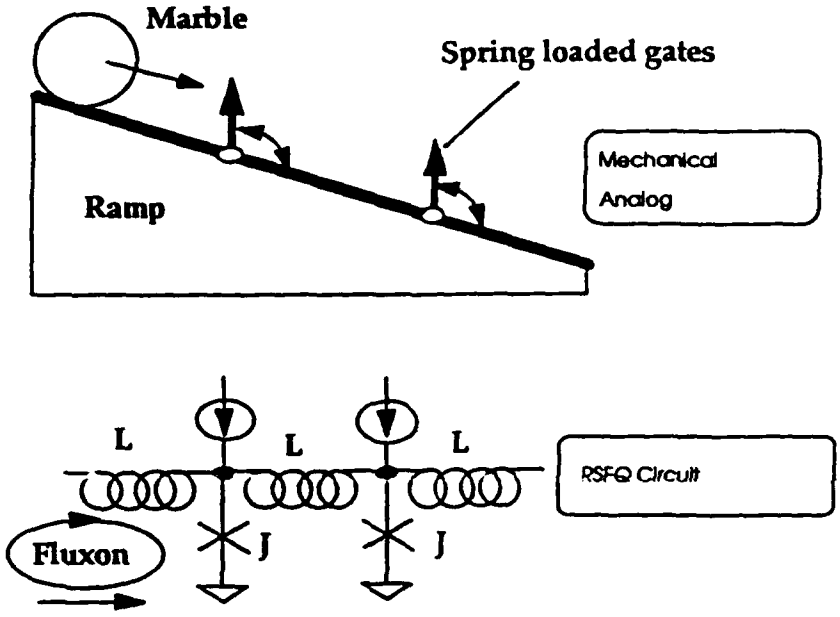


**Fig. 5. Comparison of simple RSFQ circuit to a mechanical analog. The Josephson circuit treats the fluxon as conserved particle, forced through the circuit by bias currents, like the marble forced down the ramp by gravity. The Josephson junctions, labeled with J's, act like the spring loaded gates that interact with the marble on the ramp.**

## Flux Flow Transistors

HTS thin films, particularly those based on thallium compounds, allow fluxons to flow relatively freely through them. This property is referred to as "weak pinning," and is the basis for the Flux Flow Transistor (FFT), a true three-terminal superconductive device[24]. Figure 5 schematically compares the control of flux motion in an FFT to charge motion in an FET. Figure 6 shows the IV curve of a large scale FFT a few millimeters on a side, made from a piece of bulk ceramic YBCO, with a coil wound around it. For a load of a few milliohms, it is apparent that this device has both current and voltage gain. Smaller devices fabricated with thin films have produced similar gain or transimpedance, with much smaller currents and higher voltage.

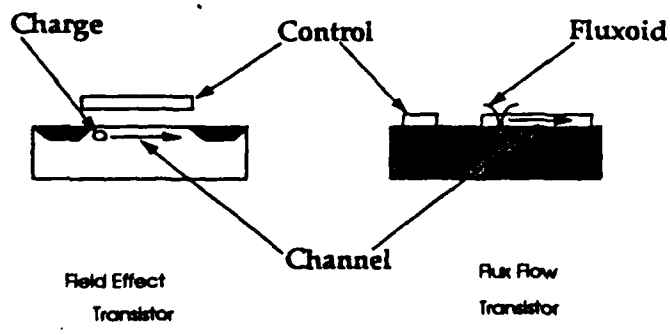


**Fig. 6. Analogy between charge transport in the channel of an FET and magnetic flux transport in the channel (HTS thin film) of an FFT.**

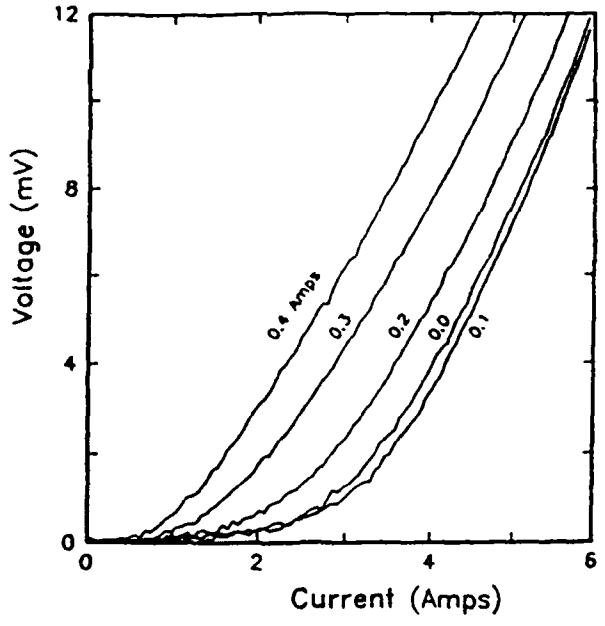


**Fig. 7. Current-voltage characteristics of HTS bulk FFT device. Veteran engineers will note the similarity to vacuum triode characteristics.**

Martens[24] has shown many circuits using these devices, including microwave amplifiers, oscillators, and digital logic and memory. From a circuit view point, the main problem with these devices is that they are so far pretty leaky. That is, the high resistance state is still a fairly low resistance, generally a few ohms. Strongly in their favor is that they can be made from a a single HTS film deposition, and they have been reported to have very high effective $I_cR_n$ products, sometimes over 10 millivolts. They are therefore a natural for interfacing to semiconductors.

There are opportunities to use flux flow superconductive devices as amplifiers in significant military and civilian applications. These opportunities have to do with the interconnection of fast but very low voltage Josephson junction devices with the semiconducting devices, such as CMOS circuits. This type of interconnection could take at least two forms. In the first form, the CMOS circuits are the ultimate destination of the outputs of the Josephson circuits. For example, in communications, a Josephson signal processor in a cryogenic environment is of no value unless there is a way of reading the cryogenic output bytes into conventional computing equipment.

The other type of interconnection would be between Josephson circuits and CMOS circuits all in the dewar. There is at least one proposal[25], for example, to use Josephson devices as output drivers for FET memory cells. In the processor, where the memory bytes are received, another superconductive circuit would be used to pick up the low level signal, and deliver it to another semiconductor.

## Multi-Chip Modules

A natural application for HTS thin films is in multi-chip-module[19] (MCM) technology. Here the idea is to eliminate one level of packaging for chips. In present desk-top computers, for example, chips are mounted in epoxy packages with multiple pins sticking out, to be plugged into sockets or soldered directly to printed circuit boards. MCMs eliminate the epoxy package. Bare chips are mounted to the board by various techniques, including wire bonding, and flip-chip soldering. If the printed circuit board

were constructed of HTS thin films and appropriate dielectrics, several advantages could accrue. Because resistance is eliminated, the wiring channels could be put on a much finer pitch, which could greatly simplify the construction of the boards. Power and ground planes would be more ideal, helping to eliminate cross talk and power dips. It should be possible to build high quality transmission line structures, with either strip line or coplanar geometries. If terminations can be used, these lines could be charged up by one-way transmission of the signal, and so HTS MCMs could also be significantly faster than normal metal boards, which rely on multiple reflections to transfer data. The challenge here is to find ways to grow high quality HTS films in multiple layers with compatible insulators, and to do this with materials having an acceptable thermal expansion match to the chips and connectors. Also needed are stable and reliable interface materials for all the connections, and some means of modification and repair.

## ACKNOWLEDGEMENTS

We wish to express our gratitude for data, and helpful consultation to Salvador Talisa, John X. Przybysz, Mike Janocko, Don Miller, Dan Meier, Joon-Hee Kang, Hodge Worsham, and George Wagner. This work was supported in part by ONR/ARPA Contract No. N00014-91-C-0112, AFOSR Contract No. F49620-91-C-0034, and NRL Contract No. N00014-92-C-2043.

## REFERENCES

1. K.K. Likharev, O.A. Mukhanov, and V.K. Semenov, "Resistive Single Flux Quantum Logic for Josephson Junction Technology," in SQUID'85, Berlin, Germany: W. de Gruyter, 1985, pp.1103-1108.
2. D.P. McGinnis, J.E. Nordman, and J.B. Beyer, "Optimization of Circuit Parameters for the Vortex Flow Transistor," IEEE Trans. Mag., MAG-23, 699 (1987).
3. R.A. Davidheiser, "Superconducting Microstrip Filters," AIP Conference Proceedings No. 14, Future Trends in Superconducting Electronics, Edited by B.S. Deaver, C.M. Falco, J.H. Harris, and S.A. Wolf, AIP, New York, 1978, pp. 219-222.
4. M. Nisenoff, J.C. Ritter, G. Price, and S.A. Wolf, "The High Temperature Superconductivity Space Experiment," IEEE Trans. Appl. Supercond. Vol. 3, 2885 (1993).
5. J. M. Phillips, M. P. Siegal, C. L. Perry, and J. H. Marshall," Comparison of Ba2YCu3O7-d Films on NdGaO3 and LaAlO3," IEEE Trans. Magn. 27 (2), 1006 (1991).
6. J. R. Gavaler, J. Talvacchio, T. T. Braggins, M. G. Forrester, and J. Greggi, "Critical Parameters in the Single-Target Sputtering of YBa2Cu3O7," J. Appl. Phys. 70(8), 4383 (1991).
7. T. Venkatesan, X. Wu, A. Inam C. C. Chang, M. S. Hegde, and B. Dutta, "Laser Processing of High-Tc Superconducting Thin Films," IEEE J. Quantum Elec. 25(11), 2388 (1989).
8. Robin J. Kennedy, " A New Geometry for Laser Ablation for the Production of Smooth single Layer YBCO/PBCO Multilayer Films," Adv. in Cryo. Eng. (Materials) Vol. 138, 1005. Edited by F.R. Fickett and R.P. Reed, Plenum Press, New York, 1992.
9. A. Erbil, K. Zhang, B. S. Kwak, and E. P. Boyd, "Review of Metalorganic

Chemical Vapor Deposition of High-Temperature Superconducting ThinFilms," in Processing of Films for HTS Electronics, edited by T. Venkatesan (SPIE 1187, Bellingham, WA, 1990) pp. 104.

10. P. Chaudhari, R. H. Koch, R. B. Laibowitz, T. R. McGuire, and R. J. Gambino, Critical Current Measurements in Epitaxial Films of $YBa_2Cu_3O_{7-x}$," Phys. Rev. Lett. 58, 2684 (1987).
11. R.W. Simon, "Substrates for HTS Films," in Processing of Films for HTS Electronics, edited by T. Venkatesan (SPIE1187, Bellingham, WA, 1990) pp. 2.
12. Gong-Da-Yao, Shang-Yun Hou, M. Dudley, and J.M. Phillips, " Synchrotron X-Ray Topography Studies of Twin Structures in Lanthanum Aluminate Single Crystals," J. Mater. Res. 7, 1847 (1992).
13. M. Sasaura, S. Miyazawa, and M. Mukaida, "Thermal Expansion Coefficients of High-Tc Superconductor Substrate $NdGaO_3$ Single Crystal," J. Appl. Phys. 68(7), 3643 (1990).
14. A. Schilling, M. Cantoni, J.D. Guo, and H.R. Ott, "Superconductivity above 130K in the Hg-Ba-Cu-O System," Nature 30, 56 (1993).
15. A.T. Findikoglu, C. doughty, S. Bhattacharya, Qi Li, X.X. Xi, T. Venkatesan, R.E. Fahey, A.J. Strauss, and Julia M. Phillips, "Sr2AlTaO6 Films for Multilayer High-Temperature Superconducting Device Applications," Appl. Phys. Lett. 61, 1718 (1993).
16. M.J. Burns, P.R. de la Houssaye, S.D. Russell, G.A. Garcia, S.R. Clayton, W.S. Ruby, and L.P. Lee, "Demonstration of YBCO and Complementary Metal Oxide Semiconductor Device Fabrication on the same Sapphire Substrate," to be published, Appl. Phys. Lett. 63 (1993).
17. Invited presentations at the "High Tc Superconductivity in Microwave Systems: A Technology Assessment," Workshop, 1993 International Microwave Symposium, Atlanta, GA, June, 1993. R.R. Bonetti, M. Nisenoff, NRL, COMSAT Laboratories, D.L. Johnson, JPL.
18. Data kindly provided prior to publication by S. Talisa and M. Janocko, Westinghouse STC, Pittsburgh, PA 15235.
19. M.J. Burns, K. char, B.F. Cole, W.S. Ruby and S.A. Sachtjenh, "Multichip Module using Multilayer $YBa_2Cu_3O_7$ Interconnects, Appl. Phys. Lett., 62, 1435 (1993).
20. D.J. Frank and A. Davidson, "Prospects for High-Tc supercondcutor/Semiconductor transistor like devices", 5th International Workshop on Future Electron Devices, Miyagi, Japan, June 1988
21. R.P. Robertazzi, R.H. Koch, R.B. Laibowitz, and W.J. Gallagher, "$Y_1Ba_2Cu_3O_7/MgO/Y_1Ba_2Cu_3O_7$ " Appl. Phys. Lett. 61, 711 (1992).
22. K.K. Likharev and V.K. Semenov, "RSFQ Logic/Memory Family," IEEE Trans. Appl. Supercond. 1, 3 (1991).
23. J.R. Wenot, J.S. Martens, C.I:H. Ashby, T.A. Plut, V.M. Hietala, Cc.P. Tigges, D.S. Ginley, M.P. Siegal, J,M, Phillips and G.K.G. Hohenwarter, "YBCO Nanobridges Fabricated by Direct-Write Electron Beam Lithography," Appl. Phys. Lett. 61, 1597 (1992).
24. J. S. Martens, V.M. Hietala, T.A. Plut, D.S. Ginley, G.A. Vawter, C.P. Tigges, M.P. Siegal, Julia M. Phillips, and S.Y. Hou, "Flux Flow Microelectronics," IEEE Trans. Appl. Supercond., vol. 3, 2295 (1993).
25. Harry Kroger and Uttam Ghoshal, "Can Superconductive digital Systems Compete with Semiconductor Systems?" IEEE Trans. Supercond., Vol. 3, 2307 (1993).

# Inductance Measurements in Mulitlevel High-$T_c$ Step-Edge Grain Boundary SQUIDs

M. G. Forrester, A. Davidson, J. Talvacchio, and J. R. Gavaler

Westinghouse Science and Technology Center, Pittsburgh, PA 15235

We report the fabrication and electrical characterization of multilevel high-$T_c$ SQUIDs, designed for digital circuit applications. The devices feature a $YBa_2Cu_3O_{7-\delta}$ (YBCO) ground plane, an epitaxial $SrTiO_3$ insulator, and a YBCO active layer. Junctions are formed by the step-edge grain boundary process, with a ground plane contact for the "low" side of each junction, using only isotropic sputtering and milling techniques. Control current is directly injected in a microstrip segment of the SQUID loop, allowing us to measure the microstrip inductance, and thus to infer the magnetic penetration depth of the YBCO. The SQUIDs are operational above 77K, at which temperature we infer a penetration depth of 330 nm. The temperature dependence of the penetration depth is found to be in reasonable agreement with the Gorter-Casimir form.

*First draft, 3/23/94*

We report the first demonstration of multilayer high temperature superconducting (HTS) SQUIDs, in a configuration suitable for digital circuit applications, with critical currents of a magnitude useful for circuit operation in the 65 to 77 K temperature range. Further, our process features isotropic film deposition and etching techniques, with no favored direction for the junctions, and thus is potentially extendible to complex circuits.

The development of a high temperature superconducting (HTS) digital circuit process requires the development of reproducible Josephson junctions, and the integration of these junctions into an epitaxial, multilayer process. Such layers would include superconductors, epitaxial insulators, and probably epitaxial resistors. Of particular importance is the use of a superconducting ground plane, in order to keep circuit inductances values both low and well defined.

A previous report by Missert et al. described the fabrication of step-edge superconductor-normal-superconductor (SNS) junctions over a ground plane, using directional deposition of the YBCO to ensure a discontinuity in the YBCO over a step in a deposited insulator, with a noble metal deposited as the normal barrier.[1] These devices operated as SQUIDs only up to 20 K, preventing the measurement of inductance as a function of temperature up to the more useful 65 to 77 K temperature range.

We have fabricated step-edge grain boundary junctions over a YBCO ground plane, using a process which is designed from the outset to allow junctions to be fabricated in four directions, for flexibility in circuit layout. Since the fabricated devices operate to above 77 K, we have measured the inductance of a microstrip portion of the SQUID loop as a function of temperature, and have inferred the temperature dependent magnetic penetration depth for our YBCO films.

Our fabrication process uses off-axis RF magnetron sputtering for both YBCO and $SrTiO_3$ films, with YBCO sputtered in oxygen, argon, and water,[2] and $SrTiO_3$ in oxygen and argon. Typical deposition temperatures were in the 670-700 C range for both materials. Substrates were silver pasted to a nickel block, which rotated during

deposition to ensure uniformity and edge coverage. Patterning of each layer was by argon ion milling with a 20 cm diameter RF ion source, with beam energies of 150 and 300 eV for the YBCO and $SrTiO_3$, respectively. Samples were clamped to a water cooled, rotating sample table. The choice of a higher voltage for the $SrTiO_3$ is dictated by the need for a well collimated beam for etching of sharp steps in this layer, while the slightly more divergent beam obtained at 150 eV is more suitable for milling tapered edges in the YBCO layers. An end-point detector based on Secondary Ion Mass Spectroscopy was used to determine when to terminate each etch step.

A 200 nm YBCO ground plane was deposited first on a single crystal $NdGaO_3$ substrate, and its pattern defined with photoresist, with a process designed to give tapered photoresist sidewalls. The film was etched by ion milling at a shallow angle, which, in combination with the tapered resist, ensured that the edges of the YBCO should be tapered to ensure good contact with the second YBCO layer and good coverage by the $SrTiO_3$. After ion milling the photoresist was stripped using a combination of RF oxygen plasma, and soaking in acetone. We have found from XPS observation that this process leaves the surface of the YBCO relatively free of both hydrocarbons and carbonates.

After deposition of a 200 nm $SrTiO_3$ layer, another photoresist process, this one designed to produce a steep resist profile, was used to define its pattern. Ion milling at close to normal incidence was then used to etch the $SrTiO_3$ film, producing sidewalls with angles thought to be between zero and twenty degrees from vertical, based on the observation of test samples, viewed in cross section in an SEM. After the resist clean-up a second 200 nm layer of YBCO was deposited, followed by approximately 30 nm of Au, in-situ. This bilayer was then patterned by photolithography and ion milling, with no particular precautions taken in defining the profile of the etched material for this last layer. The Au was left on both to provide low resistance contacts and to protect the grain boundary junctions from processing damage, which we have observed in "uncovered" junctions.

It is worth noting that we have not found it necessary to use a deposited milling mask, such as Nb [3,4] or diamond-like carbon [5] to produce sharp steps in our deposited $SrTiO_3$, a significant process simplification. This is also in contrast to our own work in making junctions on a step etched into the $NdGaO_3$ substrate, where a metal mask was required to obtain sharp steps. This is an example of the often significant differences in the etching properties of the various materials being employed in HTS process development.

Figure 1 shows the geometry of the fabricated SQUIDs, in cross section and plan views. The SQUIDs incorporate microstrip inductors, $L_\mu$, of various lengths, into which a control current, $I_{cont}$ can be directly injected to provide a flux, $\Phi = L_\mu I_{cont}$. The junctions, of width 6 or 10 μm, contact the ground plane in a region which contains a grid of holes, allowing both c-axis and a-b-axis contact between the two YBCO layers.

The current-voltage characteristic of a typical device is shown in Fig. 2(a), and exhibits generally an "RSJ-like" behavior, with the expected downward curvature. The voltage onset is actually somewhat *sharper* than expected from the zero-capacitance RSJ model, possible due to the capacitance associated with the high dielectric constant (several hundred) of the $SrTiO_3$.

Figure 2(b) shows SQUID voltage versus control current, for various values of the SQUID bias current, $I_S$, at 77 K. The period of this modulation is determined by the inductance of the microstrip portion of the loop, $L_\mu$, including any parasitic inductance associated with the center tap and the ends, through

$$\Delta I_{cont} = \frac{\Phi_o}{L_\mu}, \qquad (1)$$

where $\Phi_0$ is the superconducting flux quantum. By measuring this period, directly from oscilloscope traces, as a function of temperature we determine the inductance as a

function of temperature. This is shown in Fig. 3 for a 50 μm long, 10 μm wide microstrip inductor.

To infer an effective penetration depth, λ, for our YBCO films we assume that the two films are identical, and use the following expression for the inductance per square of a superconducting strip over an infinite ground plane:[6]

$$L = \frac{\mu_o d\kappa}{w}\left(1+\frac{2\lambda}{d}\coth\left(\frac{b}{\lambda}\right)\right), \qquad (2)$$

where, $d$ is the insulator thickness, $w$ the microstrip width, $b$ the superconductor thickness, and $\kappa$ is a factor which determines the field strength at the center of the finite width microstrip. Using our nominal values, $d = b = 200$ nm, w=10 μm, and $\kappa$=?, and measured values of $L_\mu$ for a 50 μm long microstrip, we solve Eqn. 2 to determine λ. The result is shown in Fig. 4 as a function of temperature. The magnitude of the inferred penetration depth is in good agreement with measurements by other techniques (? reference?). The solid line in Fig 4. is a fit to the Gorter-Casimire form for the temperature dependence of the penetration depth: $\lambda(T) = \lambda_o/[1-(T/T_c)^4]^{1/2}$, using the measured zero-resistance transition temperature of 86 K.

In summary, we have fabricated HTS step-edge grain boundary SQUIDs incorporating an HTS ground plane, using a process which allows junctions to face in all four directions. These SQUIDs have critical currents of a magnitude useful for digital circuit operation in the 65 to 77 K temperature range, and exhibit good Josephson behavior. Measurements of the inductance of the microstrip portion of the SQUID loop have allowed us to infer a penetration depth for our YBCO films, whose magnitude and temperature dependence are consistent with other measurements, and with the requirements of low-inductance interconnects in digital circuits. Further work is required to determine the reproducibility of the process, especially that of junction critical current.

The authors wish to acknowledge the assistance of G. J. Faychak in sample fabrication. This work was supported in part by the Air Force Office of Scientific Research, Contract F49620-94-C-0021.

## REFERENCES

1) N. Missert, T. E. Harvey, R. H. Ono, and C. D. Reintsema, Appl. Phys. Lett. **63** (12), 1690 (1993).

2) J. R. Gavaler, J. Talvacchio, T. T. Braggins, M. G. Forrester, and J. Greggi, J. Appl. Phys. **70** (8), 4383 (1991).

3) K. Herrmann, Y. Zhang, H. M. Muck, J. Schubert, W. Zander, and A. I. Braginski, Supercond. Sci. Technol. **4**, 583 (1991).

4) J. Luine, J. Bulman, J. Burch, K. Daly, A. Lee, C. Pettiette-Hall, S. Schwarzbek, and D. Miller, Appl. Phyus. Lett. **61** (9), 1128 (1992).

5) J. Z. Sun, W. J. Gallagher, A. C. Callegari, V. Foglietti, and R. H. Koch, Appl. Phys. Lett **63**, 1561 (1993).

6) T. Van Duzer and C. W. Turner, *Principles of Sueprconductive Devices and Circuits* (Elsevier, New York, 1981), page 114.

7) [Something on penetration depth]

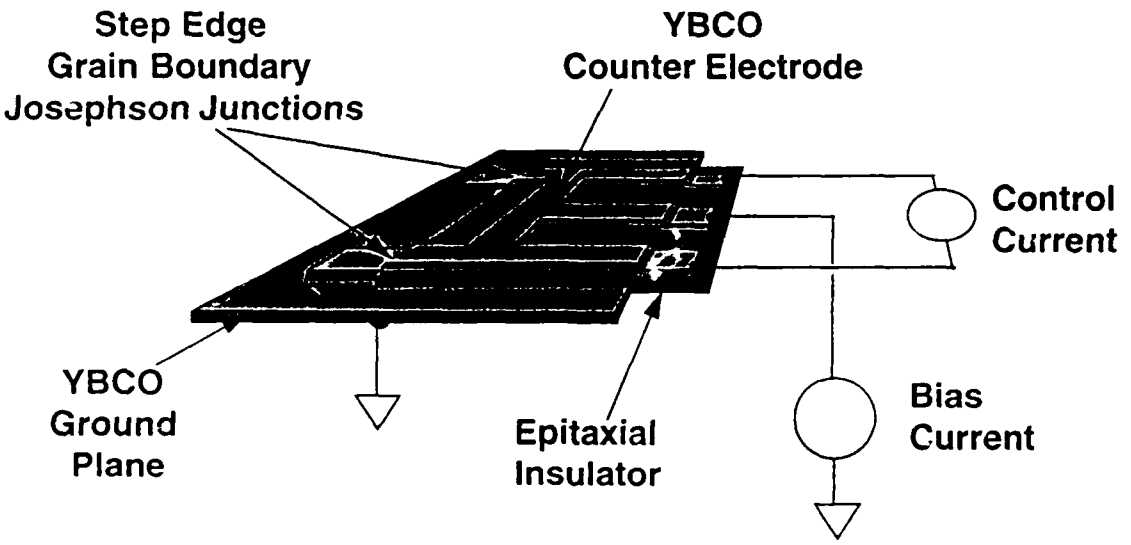


Figure 3 - SQUID inductance plotted as a function of temperature. The solid line simply connects the data points.

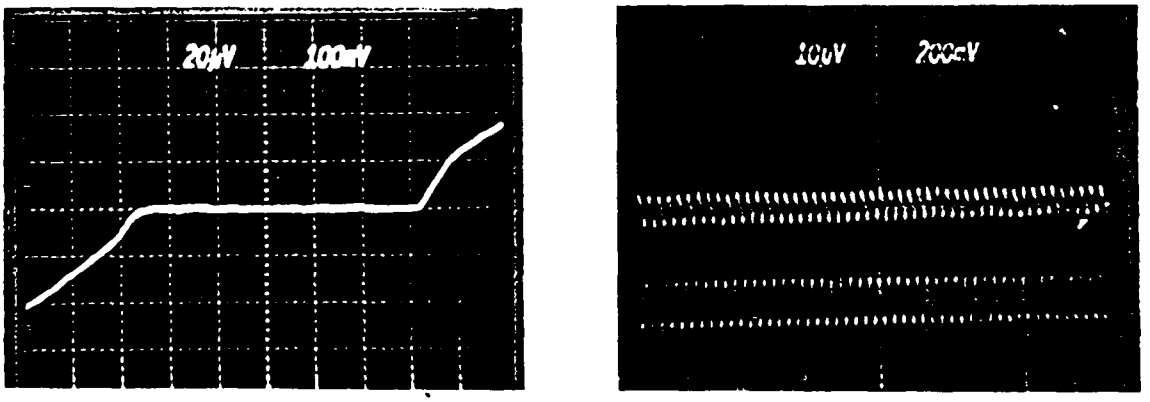

Figure 4 - Magnetic penetration depth normalized to $\lambda_o = 0.2\ \mu m$ plotted as a function of temperature. The solid line is a fit to the Gorter-Casimir form of the temperature dependence.

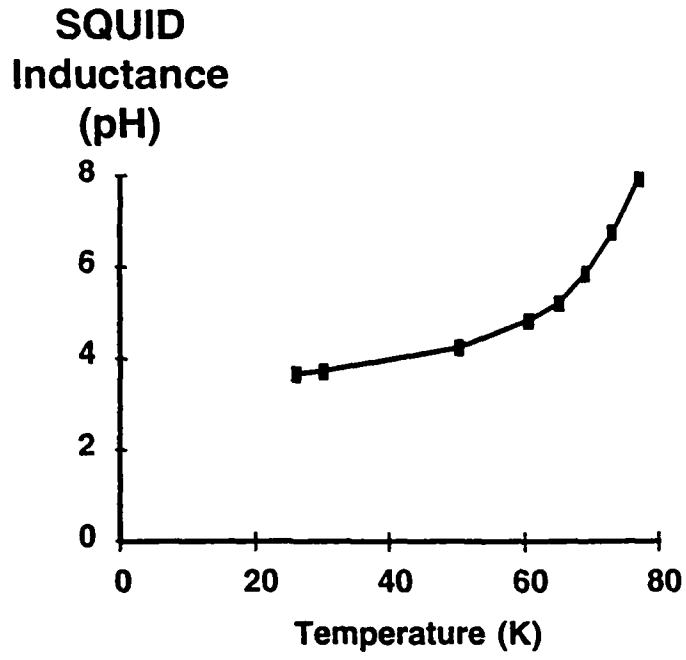


Figure 1 - Schematic view of the multilayer SQUID structure and measurement configuration.

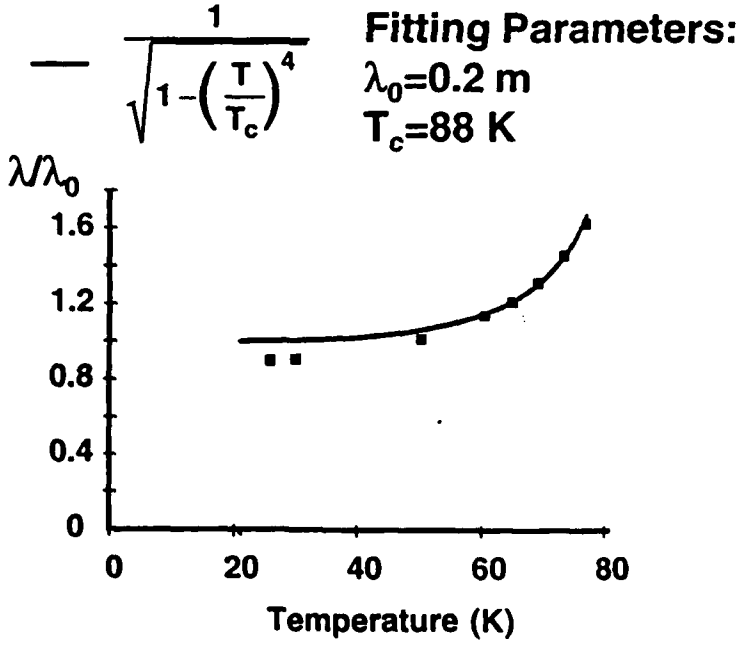


Figure 2 - (a) I-V and (b) V-Φ characteristics at 67K for a multilayer SQUID. The scales are 20 μV and 100 μA / div in (a) and 10 μV / div in (b).

# 1994 ASC Abstract

**Effect of Oxygen Over-Doping on Properties of $YBa_2Cu_3O_x$ Films*** J. R. GAVALER, J. TALVACCHIO, and R. W. WEINERT, Westinghouse STC, Pittsburgh, PA. USA --Data on bulk $YBa_2Cu_3O_x$ have shown that optimum superconductivity is obtained in material that has less than the maximum (stoichiometric) oxygen content, x=7. By controlling temperature, time, and oxygen pressure we have prepared films of $YBa_2Cu_3O_x$ that were over-doped with oxygen, and have measured their properties. In extreme cases $T_c$'s were degraded in these films to ~85K and $R_s$'s to >10 mΩ (at 77K and 10 GHz). Re-annealing at 450°C to optimize oxygen content raised $T_c$ significantly but only had a marginal effect on $R_s$. Larger improvements in $R_s$ values were obtained by annealing at higher (>700°C) temperatures. Using a proper annealing schedule, $T_c$ and $R_s$ of the over-doped films could be restored to $T_c$>90K and $R_s$<0.5 mΩ. The procedures for optimally annealing $YBa_2Cu_3O_x$ films and interpretations for their efficacy are presented as well as structural data comparing oxygen over-doped with stoichiometric films.

*Supported in part by AFOSR Contract F49620-94-C-0021.

# 1994 Applied Superconductivity Conference Abstract

**Laser Patterning of $YBa_2Cu_3O_x$ Thin Films Protected by In-Situ Grown $SrTiO_3$ Cap Layers,*** W. KULA,# R. SOBOLEWSKI, and V. LOH, University of Rochester, Rochester, NY USA, and J. TALVACCHIO, Westinghouse Science and Technology Center, Pittsburgh, PA USA — We report our studies on a non-invasive laser technique suitable for patterning $YBa_2Cu_3O_x$ (YBCO) films through a $SrTiO_3$ (STO) top layer of the YBCO-STO bilayer thin-film structure. The structures were deposited in-situ on $LaAlO_3$ substrates and consisted of 200-nm-thick YBCO films with 100-nm-thick single-crystalline STO cap layers. The patterning was achieved by changing YBCO oxygen content and was done locally, on a micrometer scale, by heating up the structures with a focused cw Ar-ion laser beam in a controlled, oxygen or oxygen-free atmosphere. We found that oxygen easily migrated through the STO layer, allowing us to reversibly convert the underlying YBCO film between the superconducting and semiconducting (virtually insulating at low temperatures) phases. We were also able to create in a single YBCO film, well-defined regions of various electrical properties. A number of planar test structures, including microbridges and superconducting field-effect devices, were fabricated and measured. Our studies show that selective, laser-enhanced diffusion of oxygen through the STO cap layer can be successfully implemented as a practical method of patterning and/or electrical trimming of multilayered YBCO layer circuits.

* This work was supported by the AFOSR grant No. F49620-94-1-0094 (UR) and AFOSR Contract No. F49620-94-C-0021 (Westinghouse).

# Also at the Institute of Physics, Polish Academy of Sciences, Warszawa, Poland.

# 1994 ASC Abstract

**Multilayer HTS SQUIDs for Digital Circuit Applications***
M.G. FORRESTER, A. DAVIDSON, J. TALVACCHIO and J.R. GAVALER, Westinghouse STC, Pittsburgh, PA USA — We are developing a simple multilayer HTS digital circuit process, based on two layers of YBCO, and one epitaxial insulating layer of either $SrTiO_3$ or $Sr_2AlTaO_6$. Step-edge grain boundary junctions are fabricated at either a step in the $NdGaO_3$ substrate, or a step etched partially or completely through the deposited insulator, allowing junctions to be either grounded or floating. Each epitaxial layer is patterned separately by ion milling, using a SIMS probe for end-point detection, with particular attention paid to proper cleaning of each layer before the subsequent high temperature deposition. Our initial multilayer SQUIDs, fabricated with a $SrTiO_3$ insulator, have allowed the measurement of the temperature dependent inductance of a YBCO microstrip inductor to above 77 K, from which we have inferred the penetration depth of YBCO as a function of temperature. Simple circuits, such as shift registers, have also been fabricated and are currently being tested.

* Supported in part by AFOSR Contract F49620-94-C-0021

# 1994 Applied Superconductivity Conference Abstract

**Properties of Passive Structures for Multilayer HTS Digital Circuits*** J. TALVACCHIO, M. G. FORRESTER, D. L. MEIER, and J. R. GAVALER, Westinghouse STC, Pittsburgh. PA, USA — The passive structures required for HTS digital circuits that must be formed at high temperature (650-750°C) were evaluated by fabricating crossovers, vias, YBCO/YBCO contacts, and multiple coverage of steps with trilayer structures of YBCO / epitaxial insulator / YBCO. Two insulator materials were used, high-ε $SrTiO_3$ and relatively low-ε $Sr_2AlTaO_6$ (SAT). The deposition conditions for both insulators had to be optimized to simultaneously obtain smooth surfaces, sufficiently high oxygen diffusion rates to re-oxidize underlying YBCO, and resistivities in planar capacitor structures of $> 10^9$ Ω-cm at 77K. The particular process used to clean film surfaces after photolithography and Ar ion milling was also critical in obtaining smooth surfaces for a subsequently deposited film layer. For the non-planar capacitor structures formed at crossovers, the effective resistivity of insulators decreased as a function of linewidth, particularly for lines less than 10 μm wide. However, even for narrow lines patterned in the top YBCO layer, critical current densities, $J_c$(77K), exceeded $10^6$ A/cm$^2$.

* Supported in part by AFOSR Contract F49620-94-C-0021 and ONR Contract N00014-91-C-0112.